ANTHRAQUINONE BASED ANTICANCER DRUG MITOXANTRONE AND ITS COMPLEX WITH DNA

A THESIS

Submitted in partial fulfilment of the requirements for the award of the degree of

DOCTOR OF PHILOSOPHY

in

BIOTECHNOLOGY

by

DURAIRAJ R.

DEPARTMENT OF BIOTECHNOLOGY
INDIAN INSTITUTE OF TECHNOLOGY ROORKEE
ROORKEE - 247 667 (INDIA)

JULY, 2008

INDIAN INSTITUTE OF TECHNOLOGY ROORKEE
ROORKEE

CANDIDATE'S DECLARATION

I hereby certify that the work which is being presented in the thesis entitled, **ANTHRAQUINONE BASED ANTICANCER DRUG MITOXANTRONE AND ITS COMPLEX WITH DNA** in partial fulfilment of the requirements for the award of the Degree of Doctor of Philosophy and submitted in the Department of Biotechnology of the Indian Institute of Technology Roorkee, Roorkee is an authentic record of my own work carried out during a period from July 2003 to July 2008 under the supervision of Prof. Ritu Barthwal, Department of Biotechnology and co-supervision of Late Dr. S. K. Barthwal, Department of Physics, Indian Institute of Technology Roorkee, Roorkee.

The matter presented in this thesis has not been submitted by me for the award of any other degree of this or any other Institute.

(DURAIRAJ R.)

This is to certify that the above statement made by the candidate is correct to the best of my knowledge.

(Ritu Barthwal)
Supervisor

Dated: 28.07.2008

The Ph.D. Viva-Voce Examination of **Mr. Durairaj R.**, Research Scholar has been held on 24/X/08.....

Signature of Supervisor

24.10.08

Signature of External Examiner

24/X/08

ACKNOWLEDGEMENTS

It would not have been possible to complete this thesis without the help and guidance of numerous people and herein I would like to thank them all.

I am grateful to my supervisors, Professor Ritu Barthwal and Late Dr. S. K. Barthwal, for giving an opportunity to start my scientific career in their expert guidance. In particular, I wish to express my gratitude to my supervisor Prof. Ritu Barthwal for her continued encouragement and invaluable suggestions.

I wish to express my special thanks to Prof. A. N. Tripathi for taking intense academic interest in this study as well as providing valuable suggestions.

I would like to extend my thanks to Prof. Sudha Mahajan Cowsik for accepting me for six months as a member of her research team at Jawaharlal Nehru University, New Delhi.

I am also thankful to the faculty members and staff of the Department of Biotechnology, IIT Roorkee for their support and help.

This thesis would not be in its present state without timely help of my labmates and friends Lata, Kushuma, Amit, Asif, Maya, Sulaxana, Viswanath and Deepankar. Special thanks to Lata for helping me to submit in time. I am thankful for valuable inputs from my seniors Prashansa, Manpreet and Monica.

I recall my friends Chandan, Deva and Lenin for their unconditional support during my stay in Roorkee.

Finally, I am forever grateful to my family members, whose foresight and values paved the way for a privileged education, and the support from my beloved wife Selvi. My son Maheshwar is a powerful source of inspiration and energy. My special thought is devoted to my parents for a never ending support.

The resources provided by the Central NMR Facility, Indian Institute of Technology Roorkee are acknowledged.

I am thankful to Ministry of human Resources and Development, Govt. of India for financial assistance during my Ph. D.

ABSTRACT

Mitoxantrone belong to class of anthraquinone drugs, developed as an alternative to the apparently more cardiotoxic anthracycline antibiotics e.g. daunomycin and adriamycin. Mitoxantrone has shown promising perspective in patients with breast cancer, acute leukemia and non–Hodgkin's lymphoma. It affects DNA transcription as well as RNA processing. Several measurements reveal a preference for mitoxantrone binding to GC base pairs while in–vitro transcription assay has shown that the consensus sequences are 5'(A/T)CpA and 5'(A/T)CpG. It is of interest to understand the base specificity and structural factors that control chemical recognition process of mitoxantrone with DNA by direct independent evidence. Structural tools such as NMR spectroscopy and X-ray crystallography, coupled with molecular modeling techniques and theoretical studies have considerable impact in advancing our understanding of the structural selectivity and the molecular basis for drug-DNA interactions. We have used proton and phosphorus-31 Nuclear Magnetic Resonance spectroscopy followed by restrained Molecular Dynamics simulations to study conformation of mitoxantrone–DNA complexes with DNA hexamer sequences, d–$(TGATCA)_2$, d–$(CGTACG)_2$ and d–$(TGTACA)_2$.

The Ph.D. thesis work has been reported in the form of seven chapters.

Chapter 1 contains introduction of the subject, a comprehensive review of the literature and scope of thesis.

Chapter 2 deals with the materials and methods used. The details of Nuclear Magnetic Resonance Spectroscopy methods used for the proton and phosphorus assignment are discussed. The strategies used for restrained molecular dynamics simulations and quantum chemical calculations are also discussed.

Chapter 3 deals with quantum chemical calculations and restrained Molecular Dynamics simulation of Mitoxantrone. Structural and electronic properties of

mitoxantrone have been studied using Density Functional Theory (DFT) employing B3LYP exchange correlation. The geometry of mitoxantrone is fully optimized without any constraints at the B3LYP/6-31G+(d,p) and B3LYP/6-31G(d,p) levels in vacuum, water and DMSO environments. Percentage variation of the difference between measured data and calculated results were 8.2 % and 4.6 % for ^{1}H and ^{13}C chemical shifts respectively. The calculated bond lengths and bond angles compare reasonably well with the experimental structure and the crystal structure data reported in literature. The geometrical parameters are relatively less influenced by the solvent effect but a noticeable change is seen in the values of the chemical shift due to inclusion of solvent. An overall analysis show that the B3LYP/6-31G+(d,p) level of theory predicts results which are in good agreement with the experiment.

Chapter 4 to 6 deals with ^{31}P and ^{1}H NMR and rMD studies on binding of mitoxantrone with DNA hexamer sequences d–$(TGATCA)_2$, d–$(CGTACG)_2$ and d–$(TGTACA)_2$, respectively. The following experiments were performed on mitoxantrone-DNA complexes studied. ^{1}H and ^{31}P NMR titration studies at various drug (D)/DNA duplex (N) ratios of upto 2.0 at 275 K and 298 K in 90% water and 10% D_2O. Temperature dependence of ^{31}P and ^{1}H NMR of the mitoxantrone-d–$(TGATCA)_2$ complex having D/N = 0.5, 1.0, 1.5 and 2.0 in the range of 275 - 328 K. 2D ^{31}P - ^{31}P exchange spectra of drug-DNA complex by a phase-sensitive NOESY using mixing time of 150ms and 200 ms at 275 K for D/N = 0.5, 1.0 and 2.0. 2D ^{1}H - ^{1}H NOESY at D/N = 0.5, 1.0, 1.5, 2.0 using mixing time τ_m = 100, 200, 300 ms at 275 K in 90% H_2O and 10% D_2O. Diffusion Ordered Spectroscopy (DOSY) experiments of complex of mitoxantrone-d–$(TGATCA)_2$ and uncomplexed mitoxantrone in D_2O. Restrained molecular dynamics studies of the solution structure for the complexes of mitoxantrone-DNA using inter-proton connectivity obtained from 2D NOESY as restraints.

Binding of mitoxantrone with d–$(TGATCA)_2$ shows, the ring protons of mitoxantrone 2H/3H, 6H/7H, and protons adjacent to aromatic ring i.e., 11NH, $11CH_2$ are shifted upfield up to 0.7 ppm due to binding. ^{31}P NMR titration studies show absence of large downfield shifts in phosphate resonances. The T1pG2 resonance shifts downfield by ~0.3 ppm at 278K. Intermolecular NOE connectivity observed between drug and DNA protons (2H/3H-T1CH_3, 2H/3H-T1H6, 2H/3H-A6H8, 6H/7H-T1CH_3, 6H/7H-T1H2", $11CH_2$-T1CH_3, $11CH_2$-A6H8, 11NH-T1CH_3) show proximity of drug chromophore to terminal T1.A6 base pair. Conformational analysis of the final rMD structure shows DNA hexamer in complexed state adopts a conformation close to that of canonical B–DNA structure. These observations point towards external binding mode of mitoxantrone to d–$(TGATCA)_2$. Preferably with mitoxantrone stacked between two molecules of DNA.

2D ^{31}P NMR exchange spectrum of mitoxantrone complexed with d–$(CGTACG)_2$ shows strong exchange correlation between bound and free C1pG2 resonance at stoichometric ratio of 0.2, 0.5 and 1.0. The bound C1pG2 resonance is 0.40 ppm downfield shifted with respect to its free resonance. Absence of large downfield shift in ^{31}P NMR spectra suggest that there is no characteristic unwinding of the DNA helix due to change in backbone torsional angle ζ , C3'–O3'–P–O5' from gauche$^-$ to trans as observed with intercalators. There is a slow exchange on NMR time scale between free and bound species as exhibited by separate bound and free resonance for DNA protons – T3NH, G6NH, G2NH, T3CH_3 and 11NH of mitoxantrone. Mitoxantrone protons $11NH^b$, 1OH/4OH, $12CH_2$ / $13CH_2$ and $14CH_2$ are simultaneously close to C1 and G6 residue protons, which are located on opposite sides of C1.G6 base pair. This is not possible if mitoxantrone aromatic chromophore intercalates between base pairs of DNA. The presence of intra base pair, sequential inter base pair and all sequential intramolecular

NOE connectivities, show that all base pairs in d-$(CGTACG)_2$ are intact on drug binding. Mitoxantrone binds externally to d-$(CGTACG)_2$ and the aromatic chromophore stacking with C1.G6 base pairs leading to large upfield shifts in 6H/7H, 2H/3H and particularly 11NH protons ($\Delta\delta \sim 0.95$ ppm upfield).

On addition of mitoxantrone to d–$(TGTACA)_2$, G2NH and T3NH resonances, gives rise to new set of broad signals upfield at the expense of the intensities of their free resonances. 2D ^{31}P NMR exchange spectrum shows strong exchange correlation between bound and free T1pG2 resonance at stoichometric ratio of 0.5. The bound T1pG2 resonance is 1.15 ppm downfield shifted with respect to its free resonance. The significantly large downfield shift may be attributed to local drug–induced distortions at T1pG2 step leading to change in phosphate backbone conformation from gauche, gauche (α = -60°, ζ = -90°) to gauche, trans (α = -60°, ζ = -180°). The existence of bound and free resonance for G2NH, T3NH and 11NH (drug) clearly demonstrates that the drug indeed binds to the DNA hexamer and there is exchange of free and bound DNA on NMR time scale at 275 K. Several intermolecular contacts observed are close to T1.A6 base pair. $11NH^b$ gives close contacts with $T1CH_3$, T1H6, A6H2, A6H8, T1H1' and A6H1'. 2H/3H is close to A6H8 as well as with T1H1' and T1H4'. Similarly $12/13CH_2$ gives close contacts with $T1CH_3$, A6H8 and T1H1'. Such NOE connectivities are possible only if mitoxantrone aromatic chromophore binds externally to the terminal base pairs of DNA. The aromatic chromophore of mitoxantrone stacks with T1.A6 base pairs leading to large upfield shifts in 6H/7H, 2H/3H and particularly 11NH protons ($\Delta\delta \sim 0.78$ ppm upfield).

Chapter 7 compares the binding of mitoxantrone with d–$(TGATCA)_2$, d–$(CGTACG)_2$ and d–$(TGTACA)_2$ and its implications in understanding molecular basis of action of mitoxantrone.

LIST OF PUBLICATIONS

Conference/Symposium Presentation
International

1. XXI International Conference on Magnetic Resonance in Biological Systems, Hyderabad, Andhra Pradesh, India (XXIst ICMRBS-2005) January 16 - 21, 2005, entitled 'Structure of antitumor agent mitoxantrone with DNA hexamer d-$(ATCGAT)_2$ by ^{1}H and ^{31}P NMR' **R. Durairaj**, Prashansa Agrawal, S. K. Barthwal, Ritu Barthwal.
2. Joint Meeting of the Biophysical Society 52nd Annual Meeting & 16th International Biophysics Congress at Long Beach, California, USA, February 2 - 6, 2008, entitled '^{31}P and ^{1}H NMR Spectroscopy of Binding of Anticancer Drugs Mitoxantrone, Adriamycin and 4'-Epiadriamycin to DNA Hexamer Sequences - A Comparative Study of Intercalating and Non-intercalating (external binding) Drugs' Ritu Barthwal, Manpreet Kaur, Prashansa Agrawal and **R. Durairaj**.
3. XXIII International Conference on Magnetic Resonance in Biological Systems, San Diego, California, USA. August 24-29, 2008. ^{31}P and ^{1}H NMR Spectroscopy of binding of anticancer drug Mitoxantrone with 5'(A/T)CpA and 5'(A/T)CpG containing DNA hexamer sequences. Ritu Barthwal, Manpreet Kaur, and **R. Durairaj**. Abstract submitted

National

1. National Symposium on Cellular and Molecular Biophysics, NIMHANS, Bangalore, (NSCMB-2004) entitled, 'Studies on DNA binding of Camptothecin and /or its analog using Spectroscopy and Molecular Modeling Techniques' **Durairaj R.** Prashansa Agrawal and Ritu Barthwal.

2. National Symposium on Cellular and Molecular Biophysics, NIMHANS, Bangalore, (NSCMB-2004) entitled, 'Direct DNA binding of Camptothecin analog using molecular modeling Studies' Prashansa Agrawal, **Durairaj R** and Ritu Barthwal.
3. National symposium on Biophysics: Trends in Biomedical research', February 13-15, 2007, New Delhi, India entitled 'Structure of antitumor agent mitoxantrone with DNA hexamer d- $(TGATCA)_2$ by ^{1}H and ^{31}P NMR' **Durairaj R**, S. K. Barthwal and Ritu Barthwal.
4. 14th annual symposium (NMRS-2008) on 'Advanced MR Applications' at Institute of Nuclear Medicine & Allied Sciences, New Delhi, INDIA, January 16-19, 2008, entitled 'Quantum Chemical and Nuclear Magnetic Resonance Studies on Molecular Properties and Electronic Structure of Mitoxantrone' **Durairaj R**, A N Tripathi, Ritu Barthwal.

Manuscripts

1. Quantum chemical and Nuclear Magnetic Resonance studies on molecular properties and electronic structure of mitoxantrone. Ritu Barthwal, Durairaj R and A.N. Tripathi
2. Structure of antitumor agent mitoxantrone in complex with DNA hexamer d-$(TGATCA)_2$ by ^{1}H and ^{31}P NMR. Ritu Barthwal and Durairaj R.
3. Structure of antitumor agent mitoxantrone in complex with DNA hexamer d- $(CGTACG)_2$ by ^{1}H and ^{31}P NMR. Ritu Barthwal and Durairaj R.
4. Structure of antitumor agent mitoxantrone in complex with DNA hexamer d- $(TGTACA)_2$ by ^{1}H and ^{31}P NMR. Ritu Barthwal and Durairaj R.

CONTENTS

		Page No.
CHAPTER 1		
	INTRODUCTION	**1-47**
1.1	General	1
1.2	Drug-DNA Interaction	2
1.3	Forces involved in drug-DNA interaction	7
1.4	Structure of Nucleic Acids	8
1.5	Literature Review	17
1.6	Scope of Thesis	45
CHAPTER 2		
	MATERIALS AND METHODS	**48-84**
2.1	Materials	48
2.2	Sample Preparation for NMR	48
2.3	Methodology	52
2.4	Two Dimensional NMR Techniques	58
2.5	Experimental Parameters	65
2.6	Determination of Three-Dimensional Structure	67
2.7	Estimation of Interproton Distances	72
2.8	Restrained Molecular Dynamics and Simulated Annealing	75
2.9	Defining DNA Structure	81
2.10	Quantum Mechanical Calculations	83
CHAPTER 3		
	QUANTUM CHEMICAL AND NUCLEAR MAGNETIC RESONANCE STUDIES ON MOLECULAR PROPERTIES AND ELECTRONIC STRUCTURE OF MITOXANTRONE	**85-104**
3.1	Results and discussion	86
3.1.1	Resonance Assignment of Mitoxantrone in Water and DMSO	86
3.1.2	Chemical Shift and Coupling Constant	90
3.1.3	Conformational Studies of Mitoxantrone	95
3.2	Conclusions	104
CHAPTER 4		
	STUDIES ON COMPLEX OF MITOXANTRONE WITH d-$(TGATCA)_2$ BY PHOSPHOROUS-31, PROTON NUCLEAR MAGNETIC RESONANCE SPECTROSCOPY AND RESTRAINED MOLECULAR DYNAMICS APPROACH	**105-176**
4.1	Results and discussion	106
4.1.1	Phosphorous-31 NMR studies of Mitoxantrone-d-$(TGATCA)_2$ Complex	106
4.1.2	Proton NMR studies of Mitoxantrone-d-$(TGATCA)_2$ Complex	128
4.1.3	Restrained Molecular Dynamics Studies	164
4.2	Conclusions	175

CHAPTER 5

STUDIES ON COMPLEX OF MITOXANTRONE WITH d–$(CGTACG)_2$ BY PHOSPHOROUS-31, PROTON NUCLEAR MAGNETIC RESONANCE SPECTROSCOPY AND RESTRAINED MOLECULAR DYNAMICS APPROACH 177-235

5. 1 Results and discussion 178
- 5.1.1 Phosphorous-31 NMR studies of Mitoxantrone-d-$(CGTACG)_2$ Complex 178
- 5.1.2 Proton NMR studies of Mitoxantrone-d-$(CGTACG)_2$ Complex 190
- 5.1.3 Restrained Molecular Dynamics Studies 225

5. 2 Conclusions 234

CHAPTER 6

STUDIES ON COMPLEX OF MITOXANTRONE WITH d–$(TGTACA)_2$ BY PHOSPHOROUS-31, PROTON NUCLEAR MAGNETIC RESONANCE SPECTROSCOPY AND RESTRAINED MOLECULAR DYNAMICS APPROACH 236-293

5. 1 Results and Discussion 237
- 6.1.1 Phosphorus-31 NMR Studies of Mitoxantrone-d-$(CGTACG)_2$ Complex 237
- 6.1.2 Proton NMR Studies of Mitoxantrone-d-$(CGTACG)_2$ Complex 249
- 6.1.3 Restrained Molecular Dynamics Studies 281

6.2 Conclusions 292

CHAPTER 7

COMPARATIVE RESULTS OF MITOXANTRONE COMPLEXED WITH d-$(TGATCA)_2$, d-$(CGTACG)_2$ AND d-$(TGTACA)_2$ 294-297

REFERENCES i-xviii

Chapter 1

Introduction

1.1 GENERAL

Cancer is defined as the uncontrolled growth of cells, with loss of differentiation and commonly with metastasis, spread of the cancer to other tissues and organs. Although there are many new ideas and treatments being studied every day, chemotherapy and radiation are still the most widely used treatments for the majority of cancers. Anticancer or antineoplastic drugs are used to treat malignancies and cancerous growths. These are naturally occurring or synthetic chemical agents employed in treatment of cancer. DNA, as carrier of genetic information is a major target for chemotherapy because of the ability to interfere with transcription and replication, major steps in cell growth and division. The three principally different ways of drug binding to DNA are: first, through control of transcription factors and polymerases. Here, the drugs interact with the proteins that bind to DNA. Secondly, through RNA binding to DNA, forming DNA-RNA hybrids, which may interfere with transcriptional activity. Third, small ligand molecules that bind to DNA double helical structures by (i) intercalating between stacked base pairs thereby distorting the DNA backbone conformation and interfering with DNA-protein interaction or (ii) the groove binders. Both work through non-covalent interactions but the latter cause little distortion of the DNA backbone. Critical to the understanding of the function of such molecules is the characterization of their binding modes, which are usually investigated through ensemble measurements. Understanding how DNA-ligand interaction affects both the structural and mechanical properties of DNA is an important step towards understanding the functional mechanism of binding agents.

Structural tools such as X-ray crystallography and NMR spectroscopy, coupled with molecular modeling techniques and theoretical studies have considerable impact in advancing our understanding of the structural selectivity and the molecular basis for drug-DNA interactions and may also provide a key to more rational drug design.

1.2 DRUG-DNA INTERACTION

Drugs can directly damage DNA by binding covalently or non–covalently. They can alkylate the DNA or intercalate between the base pairs as well as bind to the major or minor groove of DNA.

1.2.1 Covalent DNA Binding Drugs

Drugs that interfere with DNA function by chemically modifying specific nucleotides. These drugs damage DNA. There are two types of alkylating agents: mono–functional (one reactive group) which cause single–strand breaks in DNA or damage bases and bi–functional (two reactive groups) which form cross–links. A large number of first generations of anti– cancer drugs were designed to combine a simple alkylating function. Their common feature is that they form an initial physical complex with DNA before covalently bonding to it. Many of them have also shown selective anti–tumor activity, this can be attributed to DNA binding specificity or to preferential metabolic activation by tumour cells. The mechanism of action of these anticancer agents is by alkyl group transfer and they cause alkylation of DNA at N7 or N2 position of guanine (other sites as well) and interaction may involve single strands or both strands. Anthramycin is an anti–tumor antibiotic that binds covalently to N–2 of guanine located in the minor groove of DNA. Cisplatin is a transition metal complex *cis–diamine–dichloro–platinum* and clinically used as anticancer drug. The effect of the drug is due to the ability to platinate the N–7 of guanine on the major groove site of DNA double helix. Other interactions involve the reaction of these

drugs with amino, hydroxyl and phosphate groups of other cellular constituents. These drugs usually form a reactive intermediate ethyleneimonium ion.

Poly functional alkylating drugs offer resistance against cancer by increased ability to repair DNA defects, decreased cellular permeability to the drug, increased glutathione synthesis, which inactivates alkylating agents through conjugation reactions. Mitomycin C is a well characterized anti–tumor antibiotic, which forms a covalent interaction with DNA after enzymatic reductive activation of its quinone to alkylate DNA. The activated antibiotic forms a cross–linking structure between guanine bases on adjacent strands of DNA thereby inhibiting single strand formation which is essential for m–RNA transcription and DNA replication.

1.2.2 Noncovalent DNA Binding Drugs

1.2.2.1 Intercalators

Intercalators are the most important group of compounds that interact reversibly with the DNA double helix. These are clinically useful anticancer antibiotics, which are primarily derived from *Streptomyces peucetius*. Some of them are valuable anticancer drugs currently used for the treatment of ovarian and breast cancers and acute leukemia, while many others are in different phases of clinical trials. Intercalating agents share common structural features such as the presence of planar polyaromatic systems, which bind by insertion between DNA base–pairs, termed as intercalation (Lerman, 1961). Binding of peptides to polynucleotides by Intercalation are also reported (Rajeshwari, 1996)

Nowadays it is well accepted that the anti–tumor activity of intercalators is closely related to the ability of these compounds to stabilize the DNA–intercalator–topoisomerase II ternary complex. Majority of these drugs have shown marked preference for 5'–pyrimidine–purine–3' steps. The chromophores are linked to basic

chains that might also play an important role in the affinity and selectivity shown by these compounds. Bis–intercalators have two potential intercalating ring systems connected by linkers, which can vary in length and rigidity. They also alter membrane fluidity and ion transport. One potential mechanism is based on the ability of these agents to participate in electron–transfer processes, with the subsequent generation of free radicals. The property results from the presence of two very different types of redox–active groups, namely the quinone and hydroquinone moieties on daunomycin, adriamycin. Quinone moiety of daunomycin undergo one–electron reduction to a semiquinone radical, which in the presence of oxygen gives rise to superoxide and other reactive oxygen species. The first crystal structure with a mono–intercalator and oligonucleotide was obtained by Wang and co–workers (Wang et al, 1987) for a complex of antibiotic daunomycin and d–$(CGTACG)_2$.

1.2.2.2 Groove Binding Molecules

The major and minor groove differs significantly in electrostatic potential, hydrogen bonding characteristics, steric effects and hydration. Typically minor groove binding molecules have several simple aromatic rings connected by bond with torsional freedom. This creates compounds, which with the appropriate twist, can fit into the helical curve of the minor groove with displacement of water from the groove and forming Van der Waalls contacts with the helical chains which define the walls of the groove. Additional specificity in the binding comes from contacts between the bound molecule and the edges of the base pairs on the 'floor' of the groove. Thus, the aromatic rings of many groove binding molecules form close contact with AH2 protons in the minor grooves of DNA. Pullman and coworkers have shown that the negative electrostatic potential is greater in the A.T minor groove than G.C rich regions, and this provides an additional important source for A.T specific minor

groove binding of cations. Examples of minor groove binding drugs are netropsin and distamycin.

1.2.3 Other Anticancer Agents

1.2.3.1 Antimetabolites - Nucleic Acid Synthesis Inhibition

Purine antagonists like mercaptopurine act by hypoxanthine–guanine phosphoribosyl transferase (HGPRT) to form 6–thioinosinic acid, which inhibits enzymes involved in purine metabolism. Thioguanine which acts as inhibitor of purine nucleotide pathway is an enzyme which decreases intracellular concentration of guanine nucleotides and inhibit glycoprotein synthesis, finally blocking DNA / RNA synthesis.

1.2.3.2 Topoisomerase Targeting Drugs

Chromosomal DNA is extensively twisted and topoisomerases permit selected regions of DNA to untangle so as to allow transcription and replication. These enzymes temporarily break DNA, allowing for topological changes, and then reseal the breaks. Topoisomerase targeting drugs like etoposide stabilizes the topoisomerase II–DNA complex preventing it from making a topological change. This results in an irreversible double strand break, which is lethal to cells in S and G2 phases. Six anti–neoplastic drugs targeting topoisomerase II, i.e., doxorubicin, daunorubicin, idarubicin, mitoxantrone, etoposide and teniposide are currently approved for clinical use in the United States. Synthetic topoisomerase inhibitory analogs are also stuidied (Singh, et al., 1992).

DNA topoisomerase II is a ubiquitous enzyme that is essential for the survival of all eukaryotic organisms and plays critical roles in virtually every aspect of DNA metabolism. The enzyme unknots and untangles DNA by passing an intact helix through a transient double–stranded break that it generates in a separate helix. Beyond

its physiological functions, topoisomerase II is the target for some of the most active and widely prescribed anticancer drugs currently utilized for the treatment of human cancers. DNA is an extremely important target for drug action, with a wide range of biological activities (anti-tumor, antiviral and antimicrobial) arising from the ability of compounds to bind sequence specifically to DNA and interfere with DNA topoisomerases or with transcription binding factor (Lancelot et al, 2003). These antibiotics act by intercalating between base pairs of DNA causing lengthening of the double helix and a decrease in the helical twist on unwinding, inducing mediated strand scission. These drugs act in an insidious fashion and kill cells by increasing levels of covalent topoisomerase II–cleaved DNA complexes that are normally fleeting intermediates in the catalytic cycle of the enzyme. The anti–tumor topoisomerase II inhibitors presently used in the clinic, poison the enzyme by stabilizing cleavable complexes, presumably by increasing the rate of forwards reaction i.e. more rate of DNA cleavage or by decreasing the rate of backward reaction i.e. slow rate of religation of cleaved DNA (Fig. 1.1). Thus synthesis of DNA and RNA is blocked.

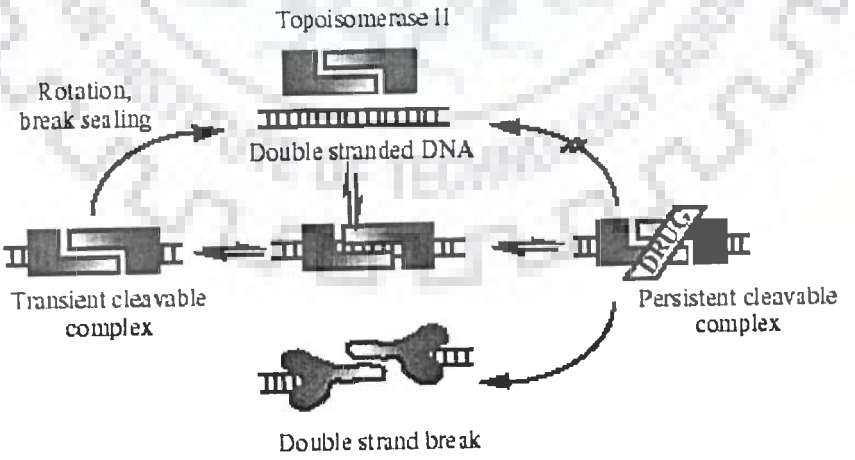

Figure 1.1: DNA damage induced by inhibition of Topoisomerase II.

1.2.3.3 Microtubule Inhibitors

Microtubules are protein polymers involved in cellular movement and morphology. Microtubules occur in equilibrium between polymerized and free tubulin dimers. Inhibitor drugs disrupt this equilibrium. Vinca alkaloids (vinblastine, vincristine) are examples of this type of drugs.

1.3 FORCES INVOLVED IN DRUG-DNA INTERACTION

1.3.1 Hydrogen Bonding

The phosphate group, sugar, bases in nucleic acids and hydrophilic groups in drug participate in hydrogen bonding with water. Since all linear hydrogen bonds have similar free energies, they make little net contribution to the favorable free energy change when drug and nucleic acid interact in solution. By contrast, formation of poorly aligned hydrogen bonds, or absence of some of them on the complex formation, carries a free energy penalty of about 4 KJ mol^{-1}. Thus hydrogen bonds are one of the most important means of making sequence specific interaction of nucleic acid with drug.

1.3.2 Electrostatic Forces: Salt Bridges

Salt bridges are electrostatic interactions between groups of opposite charge. They typically provide about 40 KJ mol^{-1} of stabilization per salt bridge. In drug–DNA complexes, strength of salt bridges decreases with the increase in concentration of the salt. They are much stronger when there are no water molecules between the ionized groups because water has a high dielectric constant. These are relatively long–range forces.

1.3.3 Entropic Forces: The Hydrophobic Effect

The hydrophobic effect is due to the behavior of water at an interface. Any molecule in water creates a sharply curved interface and so orders a layer of water

molecules around itself. When molecules aggregate, the ordered water molecules at the interface are released and become part of the disordered bulk water, thus stabilizing the aggregate by increasing the entropy of the system.

Polar surfaces, where the enthalpy loss tends to offset the entropy gain or desolvation are less likely to aggregate than non–polar ones. Molecules of water left at the interface between the drug and the nucleic acid obviously decrease the entropy of the system. Therefore, the surface of the non–planar aromatic chromophore of drug tends to be exactly complementarily so that no unnecessary water molecules remain when the complex forms.

1.3.4 Base Stacking: Dispersion Forces

Base stacking is caused by two kinds of interaction: the hydrophobic effect mentioned above and dispersion forces. Molecules with no net dipole moment can attract each other by a transient dipole–induced–dipole interaction. Such dispersion forces decreases with the inverse sixth power of the distance separating the two dipoles, and so are very sensitive to the thermal motion of the molecules involved. Despite their extreme distance dependence, dispersion forces are clearly important in maintaining the structure of double stranded nucleic acids because they help to cause base stacking. Besides they allow aromatic ring of the drug to intercalate between bases and stabilize it by base stacking.

1.4 STRUCTURE OF NUCLEIC ACIDS

1.4.1 Nucleotide Bases

1.4.1.1 Purines: Adenine and Guanine

Two different heterocyclic aromatic bases with a purine ring (composed of carbon and nitrogen) are found in DNA (Fig. 1.2a). Adenine has an amino group (–NH_2) on the C6 position of the purine ring. Guanine has an amino group at the C2

position and a carbonyl group at the C6 position. Besides these, minor bases like inosine, 7–methyl guanosine, etc. are also found as components of nucleic acids.

1.4.1.2 Pyrimidines: Thymine, Cytosine and Uracil

Thymine contains a methyl group at the C5 position with the carbonyl group at C4 and C2 positions. Cytosine contains a hydrogen atom at the C5 position and an amino group at C4 (Fig. 1.2b). In RNA thymine is replaced by uracil.

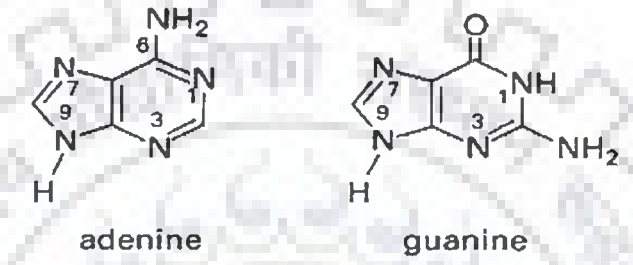

(a) Purines

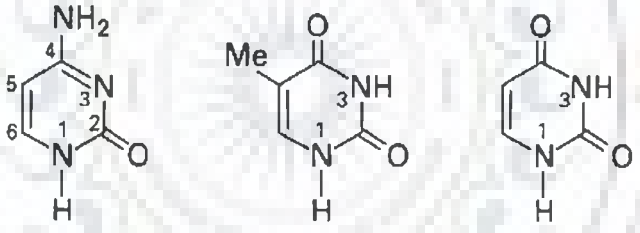

(b) Pyrimidines

Figure 1.2: (a) Structural formulae of purines and (b) pyrimidines.

1.4.2 Sugar Ring

Ribose sugar is found in all RNA molecules while a slightly different sugar, β-D-2-deoxyribose is found in DNA. This is a derivative of β–D–ribose in which the hydroxyl (–) the 2' position is replaced by hydrogen (–OH) (Fig. 1.3). The sugar moiety of DNA is one of the more flexible and dynamic parts of the molecule. The

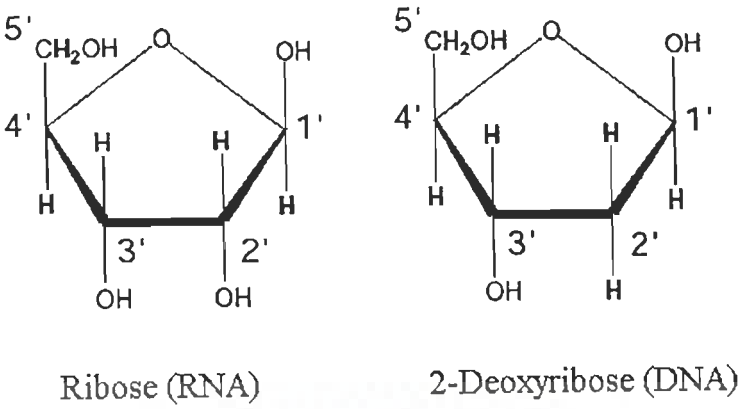

Figure 1.3: Five membered furanose ring of deoxyribose and ribose sugar

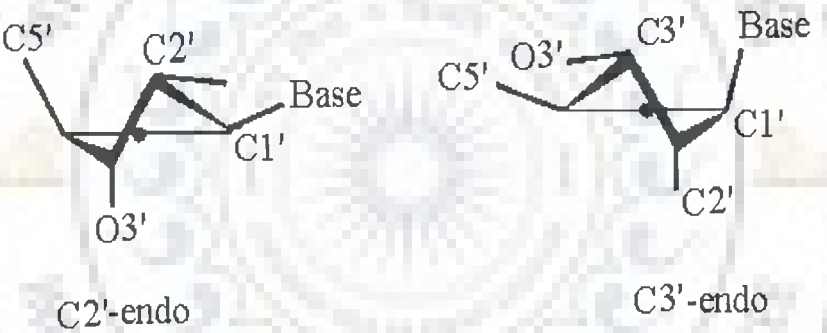

Figure 1.4: Preferred conformations C2'–endo and C3'–endo of sugar pucker

sugar base combination is called nucleoside unit. A nucleotide is a nucleoside phosphorylated at one of the free sugar hydroxyls.

1.4.3 Sugar Pucker

Usually all complexes have purine sugar at the 5' position in C3'–endo pucker. In most of them, the pyrimidine sugar at the 3' end is C2'–endo with only few cases of C3'–endo are found (Fig.1.4). Upon intercalation both χ and β increase by over 50°, χ being pushed into high anti range. Model building studies suggested that

the unwinding angle is dependent on a combination of small variations in the backbone torsion angles and base–pair geometry expressed as bend and twist, and not just on sugar puckering. It is clear that a correlation exists between unwinding angle and shape of intercalator agent.

1.4.4 Endocyclic Torsional Angles: Furanose Sugar Ring

The sugar ring occupies a pivotal position in the nucleotide unit because it is part of both the backbone and the side chain. In order to provide a complete description of the ring conformation, it is necessary to specify the endocyclic torsion angles for the ring as well as the bond lengths and bond angles. The five endocyclic torsion angles (Fig. 1.5a) for the bonds O4'–C1', C1'–C2', C2'–C3', C3'–C4' and C4'–O4' are denoted by the symbols, υ_0, υ_1, υ_2, υ_3 and υ_4 respectively.

1.4.5 The Phosphodiester Bond

In DNA and RNA the individual nucleotides are joined by a 3'–5' phosphodiester bond. The nucleotides are joined from the 3' sugar carbon of one nucleotide, through the phosphate to the 5' sugar carbon of adjacent nucleotide. This is termed as 3'–5' phosphodiester bond (Fig. 1.5b). The primary sequence of nucleic acids is determined by the sequence of bases along the nucleotide chain and the function of acids namely replication, transcription and translation are governed by this sequence. The three–dimensional back bone conformation of nucleic acids is governed by a number of torsion. The sequential numbering of atoms $_{(n-1)}$P—O5'—C5'—C4'—C3'—O3'——P——O5'$_{(n+1)}$ is defined by torsion angles α, β, γ, ε and ζ as shown in Fig. 1.5b.

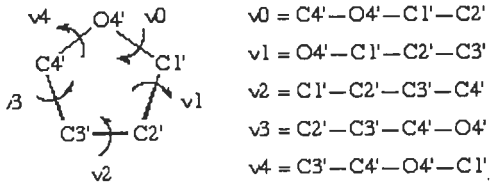

(a)

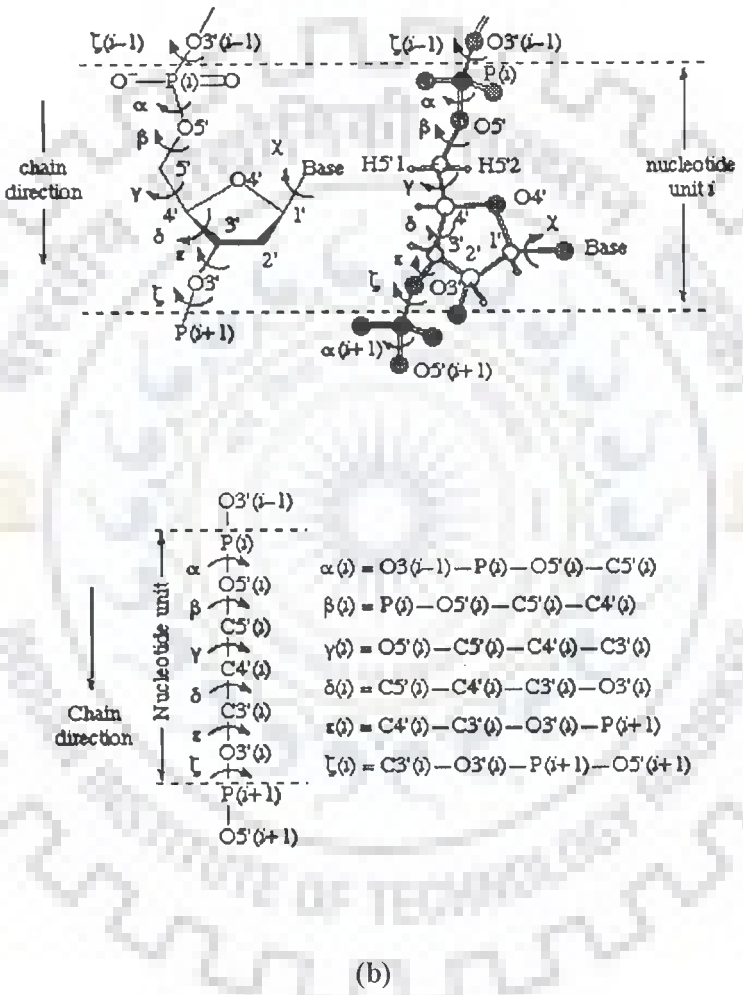

(b)

Figure 1.5 : (a) A ribose unit showing atomic numbering and definition of torsion angles, ν0, ν1 , ν2, ν3 and ν4 (b) Section of a polynucleotide backbone showing the atom numbering and the notation for torsion angles α, β, γ, δ, ε, and ζ

Duplex DNA is a right-handed helix formed by two individual DNA strands aligned in anti–parallel fashion. The two strands are held together by hydrogen bonds between individual bases as shown in Fig. 1.6. The bases are stacked near the center of the cylindrical helix. The hydrophobic interactions provide stability to the helix. A common feature of all the double helices is base stacking. Although the geometry of adjacent base pair varies, in each case the distance between neighbouring base pair plane is about 3.4 Å. This is equal to Van der Waals radius of planar aromatic compound. It was shown that purines cause large upfield chemical shift due to stacking as compared to pyrimidines. The sugar and phosphate groups are at the outer side of the helix and forms a backbone of the helix. In a double helix, complementary base pairing connects the two-polynucleotide chains. Adenine always forms base pair with thymine and cytosine forms base pair with guanine according to Watson and Crick base pairing scheme (Fig. 1.6). Although right handed DNA is presumed to be the predominant conformation *in vivo* but under different conditions of salt and humidity DNA shows structural polymorphism i.e. it exists in alternative conformations like A and Z DNA. The main features of A, B and Z–DNA are listed in

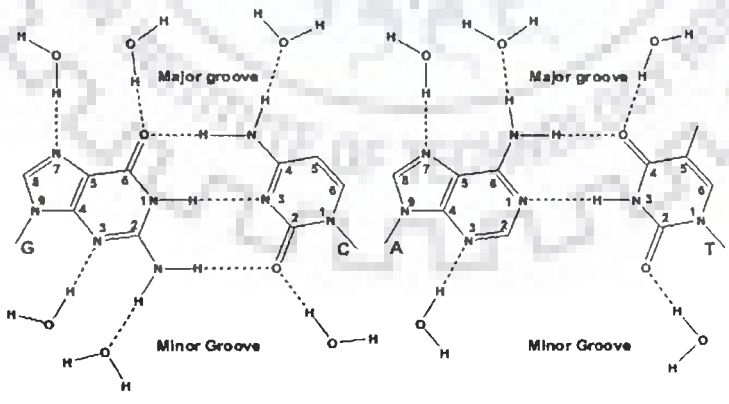

Figure 1.6: Watson and Crick base pairs showing the hydrogen bonding arrangements in the double helical DNA

Table 1.1. The structure of DNA can be described by number of helicoidal parameters like rise, pitch, tilt, roll, twist, no. of bases per turn, etc. These different types of DNA differ from each other in their helicoidal parameters, which define the helix of DNA. At high temperature, the secondary structure of DNA is lost and random coils are generated. Each conformation of the furanose ring can be unequivocally described by two pseudorotational parameters: the phase angle of pseudorotation, *P*, and the degree of pucker, ψ_{max}.

In nucleotides, the pseudorotation phase angle P is calculated from the endocyclic sugar torsion angles Fig. 1.7 (Altona et al, 1972).

$$\tan P = \frac{(\nu_4 + \nu_1) - (\nu_3 + \nu_0)}{2.\nu_2 (\sin 36° + \sin 72°)}$$

Given the phase angle P, the five torsional angles are related by

$$\nu_j = \nu_{max} . \cos (P + j. \psi)$$

where j = 0 to 4 and $\psi = 720° / 5 = 144°$. The maximum torsion angle, ν_{max} is derived by setting j = 0

$$\nu_{max} = \nu_0 / \text{Cos } P$$

At every phase angle P, the sum of the positive torsional angles is equal to the sum of the negative torsional angles, i.e. the sum of the five angles is zero.

$$\nu_0 + \nu_1 + \nu_2 + \nu_3 + \nu_4 = 0$$

Standard conformation (P=0°) is defined with a maximally positive C1'–C2'–C3'–C4' torsion angle [i.e. the symmetrical $^3T_2$ form], and P has value 0–360°. Conformations in the upper or northern half of the circle (P = 0–90°) are denoted *N* and those in the

Table 1.1: Structural characteristics of A, B and Z type of double helices

Characteristics	A	B	Z
Helix sense	Right handed	Right-handed	Left handed
Repeating unit	1 bp	1bp	2 bp
Rotation/bp	33.6°	35.9°	60°/ 2
Mean bp/turn	10.7	10.0	12
Inclination of bp to axis	+19°	-1.2°	-9°
Rise/bp along axis	2.3Å	3.32Å	3.8Å
Pitch/turn of helix	24.6Å	33.2Å	45.6Å
Mean propeller twist	+18°	+16°	0°
Glycosyl angle	Anti	anti	C: anti, G: syn
Sugar pucker	C3'–endo	C2'–endo	C: C2–endo, G: C2'–exo
Diameter	26Å	20Å	18Å

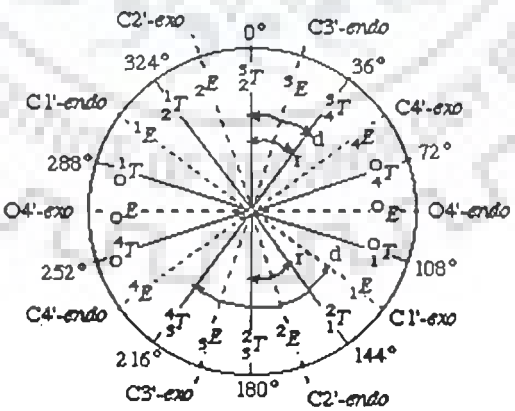

Figure 1.7: Pseudorotation cycle of furanose ring in nucleosides (Altona et al, 1972)

southern half of the circle (P = 180 / 90°) are denoted *S* conformation. The relationship between *P* and the *endo / exo* and *T / E* notations is illustrated in. It may be seen that the symmetrical twist (*T*) conformations arise at even multiples of 18° of *P* and the symmetrical envelope (*E*) conformations arise at odd multiples of 18° of *P*. The symbols 'r' and 'd' represent the usual range of *P* values for *N* and *S* conformations of ribo–(r) and 2'–deoxyribo–(d) furanose rings of –D–nucleosides and nucleotides. In B–DNA two ranges of pseudorotation phase angles are preferred C3' endo at $0° \leq P \leq 36°$ (N conformer) and C2' endo at $144° \leq P \leq 180°$ (S– conformer).

1.4.6 Glycosyl Torsion Angle (χ)

The glycosyl torsion (χ) angle define the orientation of the purine and pyrimidine bases relative to sugar ring. For pyrimidine nucleoside, χ is defined as torsion angle O4'–C1'–N1–C2 and for purines χ is O4'–C1'–N9–C4. Relative to the sugar moiety the base can adopt two main orientations about the glycosyl C1'–N link, called *syn* and *anti* (Fig. 1.8). Rotamers with *chi* values between -90° and +90° are called *syn* whereas *anti* refers to *chi* values from +90° to +270°.In Watson-Crick double helices both bases of base pairs are in *anti* conformation. Bases in *syn* conformation indicate a distortion of the double helix due to base pair opening or mismatched base pairs. The *syn* conformation is also found with guanines in left-handed Z–DNA (zig-zag helix). In *anti*, the bulk of heterocyclic atoms i.e., the six-membered pyrimidine ring in purines and O_2 in pyrimidines is pointing away from the sugar, and in *syn*, pyrimidine is over and toward the sugar. An *anti* conformation is located near $\chi = 0°$, whereas in *syn* domain is around 210°. There is also a high *anti* which denotes a torsion angle lower than *anti*.

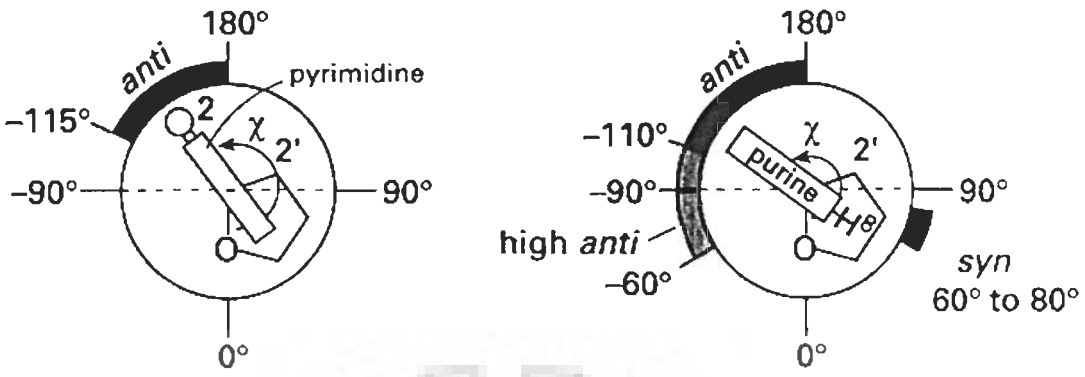

Figure 1.8: Anti high, anti and syn orientations about the glycosidic bond in pyrimidine and purines.

1.5 LITERATURE REVIEW

1.5.1 Mitoxantrone

Mitoxantrone (MTX), 1,4-dihydroxy-5,8-bis[[2-[(2-hydroxyethyl)amino] ethyl]amino]-9,10-anthracenedione (Fig. 1.9) is synthetic analogue of the anthracycline antibiotic synthesized by independent group of workers (Murdock et al, 1979; Cheng, et al, 1983; Zee–Cheng et al, 1987). Structurally similar to anthracyclines, mitoxantrone was developed as replacement for doxorubicin (adriamycin) to circumvent the cardio toxic effects (irreversible damage to heart muscles) after extended use of chemotherapy by anthracyclines. The benefit of mitoxantrone is that not only is its antitumor activity more efficient than adriamycin, doxorubicin and daunomycin, but more importantly, it shows considerably reduced dose – related cardiotoxic effects over the other anthracycline (Bonnadonna et al, 1969; Smith et al, 1983).

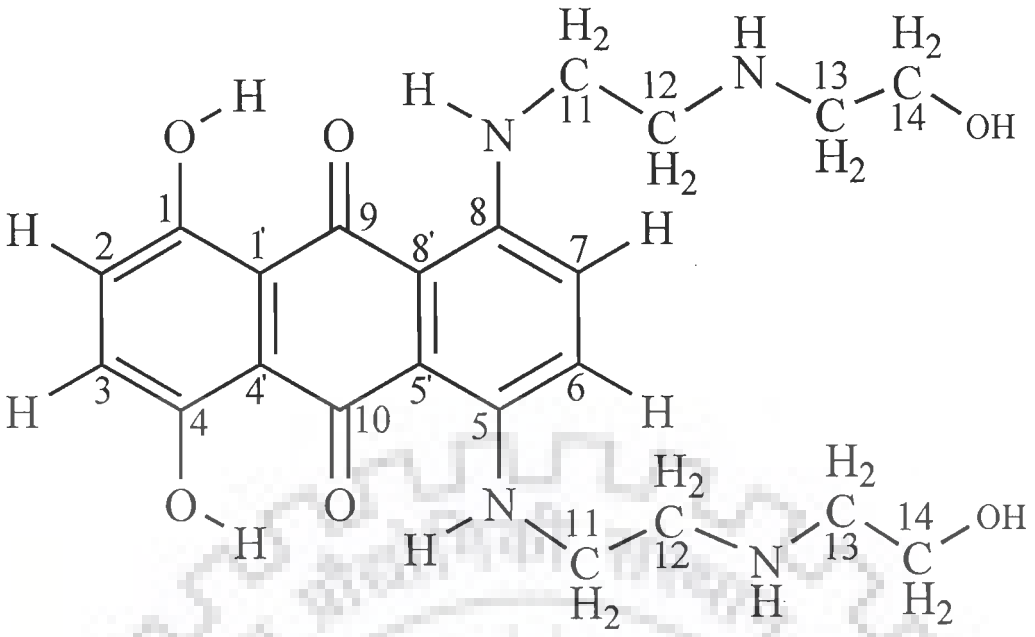

Figure 1.9: Molecular structure of Mitoxantrone.

1.5.2 Spectroscopic Studies

1.5.2.1 Nuclear Magnetic Resonance Spectroscopic Studies:

(a) Uncomplexed drug

^{1}H NMR of mitoxantrone (Lown et al, 1985a) indicated symmetrical nature of the drug. They reported that all the methylene protons; namely, $11CH_2$, $12CH_2$, $13CH_2$ and $14CH_2$ lie in the region 3–4 ppm where as the 6H / 7H and 2H / 3H protons are observed around 6–7 ppm. They assigned 2H / 3H downfield with respect to the 6H / 7H protons, which was contradicted by the studies carried out later (Davies et al, 2001a; Davies et al, 2001b; Birlirakis et al, 1992). Concentration dependent NMR experiments (Birlirakis et al, 1992) revealed a down field shift of the proton resonances upon dilution, attributable to the self–association due to π–π^* transitions. The 1D NOE experiments indicated proximity between 2H / 3H and 6H / 7H indicatives of the head to tail dimer formations. The 6H / 7H protons of mitoxantrone showed strong cross peaks with $11CH_2$ and $12CH_2$ hence confirming their assignment

(Davies et al, 2001a) reported that since the mitoxantrone has plane of symmetry and so chemical equivalence is found for resonances of 2H / 3H and 6H / 7H and the protons of the two amino alkyl side chains. The 2D ROESY spectrum of the mitoxantrone solution at initial drug concentration 1.01 mM exhibits an intermolecular contact between 2H / 3H and $11CH_2$ of the antibiotic, provided the unambiguous evidence of the inverse (head to tail) orientation of the antibiotic chromophore in the aggregate. The self association constant of mitoxantrone was found to be 12400 ($\pm$ 4000) l mol $^{-1}$ (Davies et al, 2001b). The concentration dependent experiment showed the shift of proton chemical shifts to lower frequencies at higher concentrations, which result from intermolecular stacked complex of aromatic drug molecule in solution (Davies et al, 1996; Martin 1996). The structure of mitoxantrone monomer obtained theoretically by energy minimization showed significant overlap of the aromatic chromophore and amino alkyl side chains. Hydrogen bond may be formed between the side chain secondary amino 11NH and hydroxyl groups (1OH / 4OH) of the antibiotic chromophore. Indirect conformation of the assumption of intermolecular hydrogen bonding were shown by optical investigation of ametantrone (lacking 1OH / 4OH) was characterized by five times smaller dimerization constant as compared to mitoxantrone. They also proposed that mitoxantrone dimer in solution by excition model (Martin, 1996) is unlikely to be correct, resembles the head to tail orientation but the orientation of the planes of the chromophore is much higher (~ 0.62 nm) because at such large separation between the chromphores the magnetic shielding of the drug protons in the aggregate, as well as changes of proton chemical shifts with concentration and temperature should be negligible (Giessner–Prettre et al, 1976). They also proposed relatively high negative value of enthalpy of self–association of mitoxantrone is determined by dispersive

interaction between the aromatic chromophore and possible formation of intermolecular H–bonds in the antibiotic aggregated.

(b) Binding studies of drug with DNA

Complete assignment of the stochiometric 1: 1 complex of mitoxantrone with d–$(CGCG)_2$ tetranucleotide sequence (Lown et al, 1985b) was made by 2D–COSY, 1D NOE and 2D–HH–INADEQUTE techniques. Upfield shifts of 0.22 ppm and 0.19 ppm for C1H5 and C3H5 protons respectively, substantial line broadening for G2H8 and C3H5 suggested their closeness to the binding site and hence the observed shifts. Sugar protons of the tetramer, H1', H2' H2" and H4' showed large shifts, indicating that they lie with in the immediate vicinity of the ring current due to the aromatic chromophore of mitoxantrone while the H3' showed intermediate change in the chemical shift whereas H5' and H5" showed negligible shifts suggesting they are remote from the binding site. These results were in accord with the intercalated chromophore (Lown et al, 1983) rather than one externally bound to duplex (Frederick et al, 1990; Kapuscinski et al, 1981) since the H3', H5' and H5" protons for links to the sugar phosphate backbone on the outside edges of the miniature double helix. On intercalation largest upfield shift was observed for the 11NH followed by the aromatic protons, namely 2H/3H and 6H/7H respectively with in the drug molecule. The effect diminishes along the side chain to terminal 14OH group. Several intermolecular NOEs (Nuclear Overhauser Effect) connectivities between the drug and DNA i.e, 14OH–C1H6, 14OH–C3H6, and $11CH_2$–G4H8 (weak NOEs) were observed. Intramolecular NOEs with in the drug (d_i) were also observed between $11CH_2$–$12CH_2$ and $11CH_2$–$13CH_2$. This indicated that 14OH, 11NH and 12NH bind to the neighbouring base pairs from the intercalation site and in major groove and also to the central phosphate backbone as was also evident from the ^{31}P studies.

The ^{13}C and ^{31}P NMR signals showed that neither the tetramer nor the 1:1 complex showed doubling of signals, signifying no loss of symmetry on complexation, thus compatible with intercalation of the mitoxantrone is in the center of the tetramer i.e. between G2 and C3 i.e. G2pC3 base pair step. ^{31}P studies suggested that terminal 14OH of the side chains binds to central phosphates such that the methylene groups are proximate to the C1H6, C3H6 and G4H8 all in the major groove, suggesting that side chain bind at the intercalation site from the major groove. This was in accordance with the GC preference for binding from spectroscopic and electron microscopic data (Lown et al, 1985b).

^{1}H and ^{31}P NMR studies of the hexanucleotide d–$(CGATCG)_2$ and mitoxantrone (Kotovych et al, 1986) was carried out in H_2O solvent with particular attention to the imino protons and ^{31}P assignments of the oligonucleotide. The detection of only three signals for imino protons was consistent with the anticipated two–fold symmetry of the duplex. The ^{31}P–^{1}H shift correlation contours were implied in ^{31}P assignments and confirming ^{1}H assignments of the duplex.

Further, titrimetric addition of mitoxantrone resulted in selective and progressive chemical shifts with critical changes at stoichiometric of 1:1 and 2:1 drug / DNA. The addition of the drug did not cause the hexanucleotide ^{1}H and ^{31}P to drift continuously, instead it gives rise to new set of broad signals at the expense of the intensity of the originals one. Consequently, the complex formation formed was regarded as the non–liable one with respect to the NMR time scale and point towards "slow exchange". The finite stoichiometry and the non–liability of the complex imply binding site–selectivity at the hexanucleotide duplex. Since, there was only one set of new signals observed in both proton and phosphorus studies it lead to the possibilities either the binding process is (a) fully co–operative at both binding sites or (b) the

binding is symmetrical and remote from each other such that at one site will not influence binding at other site. Assumption (a) was ruled out as it would lead to combine ring effect of the two drug molecule resulting in upfield shift ~1 ppm of imino protons as well as that of thymine and methyl protons which was not observed. The results were thus simply interpreted as that the drug preferably binds at CG base pairs at the both end of the duplex. Same conclusion that binding was CG base pair selective was lead by other assumption.

Kinetic study of the SDS (sodium dodecyl sulphate) driven dissociation of mitoxantrone from DNA, poly $d(G–C)_2$ and poly $d(A–T)_2$ (Krishnamoorty et al, 1986) reported two rate components differing by factor of four which was consistent with assumption (a), though the mitoxantrone has much slower dissociation rate from poly $d(G–C)_2$ than poly $d(A–T)_2$. Independent electron microscopic studies (Lown et al, 1983) and equilibrium binding studies of mitoxantrone to natural and synthetic studies revealed GC base pair specificity. The results were in accord with the previous studies that mitoxantrone intercalates into DNA prefentially at CG sites (Foye et al, 1982, Lown et al, 1985a, 1985b). Best fit model for the drug at the intercalation site with the chromophore approximately perpendicular to the base pair axis and with the side chain extending into the major groove (Islam et al, 1985) was obtained by computer graphics.

The interaction of (2S)–2–morpholinodoxorubicin and morpholinodoxorubicin with hexanucleotides $d–(CGATCG)_2$ and $d–(CGTACG)_2$ by ^{1}H and ^{31}P NMR spectroscopy was investigated (Ragg et al, 1988). In all the complexes the aglycon was shown to be located in the middle of the double helix, orthogonally oriented with respect to the base pairs, with ring D out of helix, extending out of the helix on the major groove and ring A, with $^{9}H_8$ conformation, between guanine G2 and G12. The

variation of ^{31}P chemical shifts was interpreted in terms of the conformational equilibrium leading to different populations of conformers. Alpha (α) and zeta (ζ) torsional angles monitored during the molecular dynamics simulations indicate a relevant population of terms of ζ and also α angles for C5pG6 and G2pT3 (G2pA3) units while the other phosphates exist in $\alpha\,\zeta$ gauche gauche conformation. The assignments for phosphate groups of the oligomers were done at low drug / DNA ratio. They reported intensity of the C5pG6 signal in bound state as a function of ratio R = (drug / DNA) gave a stoichiometry ratio of two drugs per molecule. The second molecule of the drug intercalates at the symmetrically located C5pG6 site of opposite strand. The decrease of K_{off} of (2S)–2–morpholinodoxorubicin corresponding to 10 fold increase of the residential time of the drug in the intercalation site, was in line with the higher activity found for this component.

1D and 2D homonuclear NMR spectroscopy was combined with simulated annealing / rMD to characterize the interaction of 2-(pyrido[1,2]-purin-4-yl) with d-$(CGATCG)_2$ (Favier et al, 2001). Intercalation occurs at the C1pG2 step. Pyridopurine derivative rings were not exactly perpendicular to the helix. C1 was not involved in the intercalation process and does not stack with its upper base G2. There was a weak, stacking interaction between the intercalated ligand and the DNA bases; however, the drug / DNA affinity was enhanced by a hydrogen bond between the hydroxyl group at the end of the intercalator (drug) side chain and amide group of G6. The structure of the intercalated complex enabled insight into the structure activity relationship.

Interaction of (2S)-2-methoxymorphlino doxorubicin and morpholino doxorubicin with hexanucleotide $d(CGATCG)_2$ and $d(CGTACG)_2$ by 2D ^1H NMR and ^{31}PNMR coupled with molecular dynamics techniques is reported by Mazzini et al (Mazzini et al, 1998). The results of above study were compared with doxorubicin

and daunorubicin. On intercalation of drug, deformation was noticed in DNA as torsional angle α and ζ changes from value of gauche gauche (as found in B-DNA) to gauche trans values. The change is associated with downfield shift of phosphorus. Different nucleotide sequences do not affect the dissociation rate constants of the drug from the DNA. As a consequence it appeared that structural modifications at a level of ring A and amino sugar in the anthracycline molecule are important and the methoxymorpholino moiety plays a significant role in stabilizing the complex.

(c) Heteroassociation of drug

Inclusion of the mitoxantrone (Birlirakis et al, 1992) in cyclomaltooligosachharides was studied by ^{1}H NMR investigations. The presence of the cross peak between 2H / 3H of mitoxantrone and H–3 of sugar indicates the presence of the inclusion complexes. Cross peak was not observed between the 2H / 3H of the drug and H5 of the cyclomaltooctaose (sugar) implying that the guest molecule enters into the sugar from the large hole. Factors affecting the stability of the inclusion complexes were explained by formation of hydrogen bonding between guest's polar and primary and secondary hydroxyl groups of cyclomaltooligosaccharides. Studies of mitoxantrone with sugar counterparts possessing no hydroxyl groups indicated the absence of the inclusion complexes indicating no inclusion took place in encapsulated in both cyclomaltooligosccharides and thus could be used for adjusting release rate, and also enhancing the solubility of other analogues.

Hetero–association of mitoxantrone (Davies et al, 2001a) with caeffine was reported and comparison of the concentration dependence chemical shifts of mitoxantrone with and without CAF in solutions showed that presence of CAF in solution shifts proton resonances of mitoxantrone to higher frequencies (low field)

due to hetero–association between mitoxantrone and caffeine molecules. This was explained by smaller shielding effects by caffeine molecules on the protons of mitoxantrone molecules in the hetero–complexes compared with that of the mitoxantrone in self–association aggregates. Association constant obtained for complexation of caffeine with mitoxantrone was intermediate between values of self–association constants of self–association constants of the interacting aromatic drug molecules, as found for systems studied previously (Davies et al, 1996).

Equilibrium constant of hetero–association is consistent is somewhat higher than other drug– caffeine systems. Hydrophobic interactions between methyl group and alkyl side chains of mitoxantrone impart stabilization to the complex. The calculated 1:1 hetero–association proposed that planes of chromophores of mitoxantrone and caffeine in 1:1 are parallel to each other at distance of 0.34 Å. The structure of the mitoxantrone – caffeine complex was consistent with that obtained using molecular modeling from which it was concluded that "rotation of caffeine by 180°" relative to the DNA intercalation ring system does not significantly alter the relative binding.

Solution study of the complex between 4'6–diamidino–2–phenylindole (DAPI) and DNA oligomer d–$(CGATCG)_2$ at 2:1 drug / duplex was studied (Trotta et al, 1996). Structure perturbations, and resonance shifts induced by binding provide evidence that DAPI interacts with DNA hexamer by two different binding mechanisms, in fast exchange on the NMR time scale, without any significant distortion of the B–type conformation of DNA hexamer. The results indicate that the ligand binds into the dimer groove of central 5'–ATC–3' region of the hexamer and on the oligomer by $\pi - \pi$ stacking interaction with the terminal C1: G6 base pairs. A model for both binding mechanisms that accounts for all experimental data was

generated by molecular mechanics and dynamics calculations based on experimental NOEs. In the minor groove binding, N2 amino group of G2 precludes a deep insertion of phenyl ring of DAPI into the groove. Position and orientation of the drug in the external stacking interaction resemble those suggested for intercalation of DAPI between C: G base pairs.

1.5.2.2 UV–Visible, Fluorescence, Vibrational Spectroscopy and Circular Dichroism studies

(a) Uncomplexed mitoxantrone and analogues

For the uncomplexed mitoxantrone, (Kapuscinski et al, 1981) four distinct peaks λ_A, = 242; λ_B = 276; λ_C = 610 and λ_D = 662 peaks were observed in the UV region. The amplitude of these peaks varied on drug concentration and pH, and to lesser extent on ionic strength. The molar absorption of D peak was particular sensitive to drug concentration. Beer–Lambert law was obeyed between the concentrations between 1μM to 50 μM at isobestic point of 682 nm. It is also, reported that mitoxantrone has three absorption bands in the UV region one around 200 nm and the others around 243 and 279 nm with extinction coefficient of the later two being 26,700 and 11,000 cm^{-1} M^{-1}, respectively (Rao et al, 1989).

UV–Vis absorption studies of the uncomplexed drug (mitoxantrone) have been done in different solvents namely, acetone, water, methanol and chloroform, (Lee et al, 1989). Four absorption bands at 225 nm, 243 nm, 240 nm and 380 were observed in the aqueous media (H_2O) and these bands were assigned readily to the band characterized by four π–π^* transition in UV region. The fifth band in the visible region was characterized by electron donating substituents on the anthraquinone ring by amino and hydroxyl groups and several interpretations for this group was postulated for this band such as interchange in position of bands of anthraquinones

due to H–bonding and charge transfer from the substituent to the carbonyl group to the ring or the intramolecularly H–bonded carbonyl chelate ring. It had also been assigned due to imino 11NH and 12NH to ring charge transfer transition with red shift and conjugation due the phenolic groups as compared to the $-NH_2$ substituents. This band was shifted to lower frequencies, presumably due to increased electron donating ability.

Major influence of the solvent was found to be dominant as solvents appear to be shifting of the absorption peaks at the higher wavelengths as the solvent polarity decreases and the energy transitions were found to occur at 660, 680, 677 and 665 nm in H_2O, CH_3OH, CH_3COCH_3 and $CHCl_3$, respectively. It was further supported by observed red shift with decreasing solvent polarity is contrast to generally observed blue shifts in the emission spectra. As mirror image relationship was absent, it showed difference in the geometry of the ground and excited states. The opposite trend of mitoxantrone indicated that the ground electrostatic state of the solute is stabilized by bonding of the phenolic–OH (1OH / 4OH) groups with polar solvent molecules.

Fluorescence of mitoxantrone was found to be sensitive to pH and exhibited decrease in intensity at pH levels above 7.8 reflecting the ionization state of the hydroxyl groups. The extinction coefficient of the 608 nm bands was determined to be 14,000 cm^{-1} M^{-1} in the SSC buffer. They also reported the peaks at 608 nm and 657 nm in the visible spectra (Bell, 1989).

The properties of mitoxantrone in aqueous and water-dioxane solutions have been investigated by steady-state and time-resolved fluorescence by Askirka et al (Askirka et al, 2004). Two fluorescing forms of the molecule have been proposed for mitoxantrone in low-polar and polar solvents.

(b) Binding studies of Mitoxantrone and its analogues with DNA

Absorption studies (Lown et al, 1985b) indicated shift of λ_{max} values of mitoxantrone of 612 nm and 660 nm to 660 and 674 nm, respectively, on binding with d–$(CGCG)_2$ compared with those resulting from intercalation of ethidium from 492 to 528 nm. Thus it was proposed that the intercalation mechanism exist for mitoxantrone on binding with DNA as red shift was observed.

Preliminary studies of CT–DNA–mitoxantrone complex (Bell, 1989) showed that on increase in amount of DNA indicated increase in fluorescence polarization at maximum value at 25 μg / ml DNA. Fluorescence polarization increased due to the binding of mitoxantrone with DNA due to restricted mobility of drug. Further addition showed decrease in polarization due to aggregation of the resultant complex, which leaves only those molecules free in solution detected by the instruments optics. Authors reported that shifts in the excitation and emission spectra with in the molecule were suggestive of the intercalative mechanism. On binding with DNA the absorption studies showed red shift suggestive of the fact these substituents are unable to form H–bond with the solvent water molecule. Both absorption and emission spectra were found to be dependent on the concentration of the drug.

Kapunsciski et al, 1981 reported that both A–DNA and B–DNA structures form intercalation complexes with mitoxantrone although electrostatic interaction also plays part in the binding. Interaction with the polymers containing A–T base pairs were somewhat weaker than with other polymers, and alternating polymers exhibited stronger affinity than did homopolymers pairs.

Interaction with natural nucleic acids showed large red shift in the C and D band (λ_C = 610 and λ_D = 662 nm peaks) as well as increase in relative absorption of D and C band i.e. ε_D / ε_C. . The titration with calf thymus–DNA showed that absorption

complex. The intrinsic constant of the drug (K_i) was found to be 1.8 x 10^{6} M^{-1}, binding site size (n) = 5 and the unwinding angle (φ) was 26.5°.

Interaction of mitoxantrone with synthetic nuclei duplexes indicated the shift in the D band replicates the red shift characteristic of drug intercalation, unwinding of the closed, circular, double stranded DNA by mitoxantrone. The earlier studies had suggested intercalative mode of binding of DNA as evident by the characteristics of C and D bands. However, it was also postulated that long chains at 1, 4–position could hinder intercalation. The value for unwinding angle (φ) of mitoxantrone was found to be 21.5°.

Interaction of mitoxantrone and AME with natural and synthethic DNA (Kapuscinski et al, 1985) by spectroscopic method was studied in order to establish the monomeric and dimeric form of ligands (uncomplexed drug) and their complex with DNA at low drug / phosphate ratios (D / P) or drug / nucleotide ratio (D / N). The spectra of the complexes were red shifted and had lower amplitude compared with spectra of the free ligands monomer. This observation was consistent with the already well–established intercalative mode of drug–nucleic acid interaction.

At higher D / N ratio, a secondary mode of binding was detected by both spectroscopic and light microscopy. Homo–polymers pairs containing the dI and dC were especially susceptible to the secondary type of binding. It was reported that both mitoxantrone and ametantrone are strong intercalators (Kapuscinski et al, 1986) and their intercalative modes of binding are most plausible explanation for their pharmacological activity. No significant differences were explained on the basis of their intercalative properties, but the ability to condense nucleic acid is twice as much for mitoxantrone than ametantrone. The condensation was found to be base and

sugar–specific and the long purine sequences of single stranded RNA were found to be most sensitive.

Sodium sulphate driven dissociation of mitoxantrone, daunomycin and ametantrone and related compounds with calf thymus DNA, poly[(G–C)].poly[(G–C)] and poly[(A–T)].poly[(A–T)] by stopped flow kinetics methods (Krishnamoorty et al, 1986) and found that all the four compounds exhibit biphasic dissociation reactions. Daunomycin exhibited similarity with mitoxantrone in similar dissociation rate constant, effect of temperature and ionic strength. Rate constant of these two drugs were suggestive that both of the drugs involve formation of the initial outside complex followed by intercalation where as dissociation in ametantrone follows single–phase kinetics.

Mitoxantrone followed biphasic kinetics for both poly [(G–C)].poly [(G–C)], poly[(A–T)].poly[(A–T)] but rate constant for poly[(G–C)].poly[(G–C)] are approximately 10 times lower than poly[(A–T)].poly[(A–T)]. This behavior, which is unique to the mitoxantrone, was suggestive of the selective binding and dissociation from the alternating polymer intercalation sites / and or dual mode of binding, modes of intercalation with both the side chains in the same groove or one side in each groove.

It was reported (Rao et al, 1989) that circular dichroism (CD) spectra of the poly [d (G–C)] had a maximum at ($[\theta]_{275}$= 6,500 deg cm^2 d mol^{-1} of nucleotide) with distinct shoulder at 285 nm and negative band at 250 nm ($[\theta]_{250}$= -16,600 deg cm^2 d mol^{-1}. On increasing the concentration of mitoxantrone the intensity of the long wavelength increased steeply, the 285 nm shoulder lost its identity increased steeply and resulting band was centered on 278 nm. At drug / nucleotide (D / N) ratio of 0.2 a saturation in the ellipticity was observed, with limiting value of ($[\theta]_{278}$= 37,100 deg

cm^2 d mol^{-1}) i.e. approximately six fold rise. Reversal of the 250 nm band to positive 251 nm band had ellipticity value of 28,300 deg mol^{-1} cm^{-1}, was not reported for daunomycin, actinomycin etc. The indication of the CD in the visible region showed that band decreased in the two stages at maxima centered at 688 nm, one below the D / N ratio of 0.11 and other above this ratio. At the D / N < 0.11 enhancement in ellipticity was slow but at D / N > 0.11 is sharp and apparently cooperative growth in the ellipticity reaching $[\theta]_{688}$= 48,000 at D/N= 0.22. Ellipticity changes at 251 nm and 278 nm to reveal that interaction of the drug occurs at D / N = 0.12 and other above this value. The induction of the intense circular dichorism in the 250 and 278 nm regions, apart from that in the visible region for mitoxantrone–poly [(d(C–G)] system suggested that mode of intercalation is different from that of ethidium and acridine orange.

Babayan et al reported increase in DNA concentration at constant mitoxantrone resulted in hypochroism red shift and absence of isobestic point at 676 nm (Babayan et al, 1998). At low concentration, it was observed that DNA concentration in the solution changes such that interaction of mitoxantrone with double stranded nucleic acids depends upon the solution's ionic strength. With increase in mitoxantrone concentration (at constant DNA concentration) the CD spectra changes and the isobestic point at 265 nm was observed. Thermal denaturation studies of the poly [d(A–T)]–poly[d(A–T)] at high ionic strength (0.11) showed that the shape of the melting curves does not change with increase in temperature, but range of melting temperature remains the same, whereas at the ionic strength of (0.011) the curve becomes biphasic. The same pattern was observed between mitoxantrone and double stranded helical polynucleotides. On the basis of

the absorption and CD spectra it was concluded that mitoxantrone binds through intercalation at high ionic strength of 0.11 (Rao et al, 1989).

Mitoxantrone also showed specificity for different nucleotide pair and dissociation constant (K) is of almost an order of magnitude higher for binding to DNA than RNA. The values of dissociation constant (K) and binding constant (n) agreed well with data of (Lown et al, 1985a). The value of ΔH was found to be negative for binding with mitoxantrone with M. lysodiklius DNA and poly (G). Poly(C) and ΔS are positive for both. The value of ΔH is positive for compounds, which do not intercalate into DNA. This anomalous behaviour for mitoxantrone was explained as besides, intercalation interaction of the side–chains in the major groove contributing towards ΔH. The value for number of binding sites (n) reported for mitoxantrone complexes with DNA, agreed well, i.e. two mitoxantrone molecules per duplex to one mitoxantrone molecule per three base pairs, that mitoxantrone binds to G–C base pairs (Kotovych et al, 1986).

Babayan (Babayan et al, 1998) studied the interaction of mitoxantrone and ametantrone with DNA as determined from the changes in the circular dichroism spectra. Their study was performed into the effect of the ionic strength and temperature of the medium on the changes in the various nucleotide compositions. The change in the circular dichorism spectra indicated transformation of the DNA helix geometry upon the interaction with geometry. The relative change in the dichroic absorption at maximum was integrated as function of the relative concentrations of C_o and C_p where C_o is the concentration of the mitoxantrone and ametantrone and C_p is the concentration of DNA and dependence were deduced at maximum and minimum in the circular dichroism spectra of the complex of mitoxantrone and AME with poly [d (G–C)] poly – [d (G–C)]. They found that the

increase in per base pair raises the $\Delta E^{(M)}_{273} / \Delta E^{(o)}_{273}$ ratio. The slope of the curve is far larger for complexes of mitoxantrone, which exhibits deviation from linearity even at low Co / Cp, and change in the helix geometry less pronounced. Similar pattern was observed for the relative change in dichroic absorption at the maximum.On interaction of mitoxantrone with DNA, the linearity of dependence of $\Delta E^{(M)} / \Delta E^{(o)}$ is retained till $C_o / C_p = 0.15$ where as in DNA– ametantrone complex formation the linearity is violated when the $C_o / C_p = 0.05$. The effect of temperature on change in the $\Delta E^{(M)}_{273} / \Delta E^{(o)}_{273}$ upon complex formation was also monitored. Pronounced changes were observed at 30° as compared to 50° i.e. helix geometry is altered more strongly at low temperatures. Raising the C_o / C_p increases $\Delta E^{(M)}_{273} / \Delta E^{(o)}_{273}$, this increase is much higher than increase upon binding that proceeds only through intercalation mode. At fairly high C_o / C_p, ΔE tend to saturation. The change in base pair geometry upon intercalation followed the order CG, AT and IC at 0.11 ionic strength. They concluded that upon interaction of mitoxantrone and ametantrone with DNA from the changes in the CD spectra one could determine the mechanism of binding of mitoxantrone and ametantrone to DNA to study the possible conformational changes in DNA upon binding.

1.5.3 Footprinting Studies: Sequence Specificity of Mitoxantrone

Transcriptional assay (Panousis et al, 1994) determined the sequence specificity of binding of mitoxantrone. Transcriptional blockages were observed dominantly prior to 5'–CpA sequences (64%) occurrence and to lesser extent 5'–CpG sequences (29%). Overall 93% of the blockages were prior to the pyrimidine (3'–5') purine sequences. An effect of flanking sequence was evident since the blockage sites contained A / T base pair prior to the consensus of the CpA and CpG intercalation sites. The location of transcriptional base pair prior to the intercalation site was

consistent with (Chen et al, 1985; Lown et al, 1985a; Lown et al 1985b) manifesting that mitoxantrone intercalates perpendicular to the base pair axis with both side chains in the major groove (Collier et al, 1988) and extending approximately to one base–pair 5' to the intercalation site, it was expected that progression of the polymerase will be halted one base prior to the intercalation site. Though it was not clear how 5'(A / T)GC and 5'(A / T)CG sequences specifically relate to drug action, it was possible that the drug is localized prefentially in the specific control regions of the genome such as transcriptional promoter enhancer regions where it could result in critical effect on the regulation of the transcriptional process.

Mitoxantrone can be activated by formaldehyde to form adduct in DNA *in vitro* and the result revealed that formaldehyde activated mitoxantrone blocked the progression about E. coli RNA polymerase and λ exonuclease in a sequence dependent manner (Parker et al, 1999; 2000; 2004). The major transcription blockages were described at CpG and CpA sites on the non–template strand of DNA. Exonuclease studies revealed that the formaldehyde activated mitoxantrone blockage were specified at CpG sites and suggested that the adducts at CpG sequences may distort the DNA helix to produce a lesion which can block the progression of exonuclease, whereas the CpA lesion does not. The proposed structure of the mitoxantrone–DNA adduct implied the likelihood of hydrogen bonding to the second DNA strand. The hydrogen bonding at CpA / TpG sequences may therefore be weaker due to absence of the guanine residue on the second strand. Although the sequence specificity occupancy of mitoxantrone suggested no significant effect of flanking sequence on adduct formation and frequency most stable adducts were detected with ACGC sequence. They also proposed if compared with adriamycin, formaldehyde activated mitoxantrone might be covalently bound to only one strand of

DNA at most likely the N2 amino group of guanine residues at CpG and CpA i.e. TpG dinucleotide. They are likely to contain an interstrand (virtual) crosslink with covalent attachment to guanine on one DNA strand. It is possible that the CA sites contain the same site of lesion that occur at the CG sites, but with difference in hydrogen bonding to the second strand due to lack of guanine (on the non covalently bound strand), resulting in reduced stabilities. The activity of mitoxantrone against myeloid and solid tumors was also consistent with the proposed mechanism of activation of mitoxantrone by formaldehyde, associated with higher levels of formaldehyde in these tumors.

Bailly and coworkers (Bailly et al, 1986) studied closely related derivatives of mitoxantrone and found that both of the derivatives were capable of intercalating into DNA as evident by their unwinding angles comparable to that of the mitoxantrone and structurally related anthraquinones. The two drugs bind prefentially to alternating purine–pyrimidine sequence containing both A–T and G–C base pairs. With the dihydroxy derivative every region is protected from DNAase I cleavage (a presumptive drug binding site). Tri nucleotide ACG or 5'(A/T) CA which is equivalent to 5'–TG (A/T), triplets are the consensus sequences as reported for mitoxantrone hence indicating that the hydroxyethyl terminal groups which distinguishes mitoxantrone from this compound are not responsible for sequence selective recognition process. However, there was rather poor correspondence between the drug–protected site and ACG but good correlation with sites containing CCA, TCA and TGT. Therefore, the results suggested the binding to 5'–(A/T) CG site is dependent on the presence of the 5, 8 hydroxyl groups on the anthracenedione where the binding to 5'–(A / T) CA sites proceed to a large extent by presence or absence of hydroxyl groups.

The most of the foot printing studies at X–CG are observed for bis hydroxylated than non–hydroxylated analogue, whereas as found to be identical with footprints of CA or TG are almost identical. The sequence recognition does not depends upon interaction with 2–amino group of guanine located in the minor groove, but is consistent with the alkyl amine chains in the major groove as found for mitoxantrone (Panousis et al, 1995).

1.5.4 X-ray studies

The binding of macrocyclic bisacridine and ametantrone to CGATCG was studied (Yang et al, 2000). Only one acridine of the bisacridine drugs binds at C5pG6 step of DNA, with the other acridine plus both linkers completely disordered. Surprisingly both terminal G.C base pairs are unreveted. The C1 nucleotide is disordered and the G2 base is bridged to its own phosphate through a hydrate Co^{+} ion, G2 swing towards the minor groove with its base stacked over the backbone. The C7 nucleotide is flipped away from the duplex part and base paired to a two-fold symmetry related to G6. The central four base pairs adopt the B-DNA conformation. An unusual intercalator platform is formed by bridging four complexes together such that the intercalator cavity is flanked by two sets of G.C base pairs (i.e., C5G8 and G6C7) on each side, joined together by G6.G8 tertiary base pair interaction. In the bisacridine–CGATCG complex, only one AME is bound. NMR titration of the bisacridine to AACGATCGTT suggests that the bisacridine prefers to bridge more than one DNA duplex by intercalating each acridine to different duplexes. The result may be relevant in understanding binding of certain intercalators to DNA structure associated with the quadruplet helix and holiday junction.

The structure of 9–amino–N–[2–(4–morpholinyl)ethyl]–4–acridinecarboxamide bound to d–$(CGATCG)_2$ has been resolve at 1.8 Å (Adams et al, 2002). The complex has been resolved at the space group P64 and the final structure has an overall R factor of 21.9%. The drug molecule intercalate between each of the CpG dinucleotide steps with the side chain lying in the major groove, and is protonated morpolino nitrogen partially occupying positions close to N1 and O6 atoms of guanine G2. The morpholino group is disordered, the major conformer adopting a twist boat conformation that makes Van der Waals contact with O4 oxygen of thymine T3. Water molecule forms bridging hydrogen bonds between the 4–carboximide NH and the phosphate group of guanine G2. Sugar rings are found in alternating C3'–exo and C2'–endo conformations except for cytosine C1 which is C3'–endo. Intercalation perturbs the helix winding throughout the hexanucleotide compared with B–DNA with CpG and GpT steps being unwound by 10° and 8° degrees, respectively while the central TpA step is overwound by 11°. An additional drug molecule lies at the end of each DNA helix linking it to next duplex to form continuous stacked structure. The protonated morpholino nitrogen of this "end stacked" drug hydrogen, bonds to the N7 atom of guanine O6 oxygen. In both drug molecules the 4–carboximide group is internally hydrogen bound to the protonated N10 atom of the acridine ring.

1.5.5 Theoretical Studies

Series of 1 and 1, 4 di–substituted anthraquinones (Collier et al, 1988) were examined in relation to their cytotoxic and anti–tumor properties as compared with mitoxantrone. The representative structure N–(9, 10)–dihydro–9, 10–dioxo–1–anthracenyl)–3–[4–3–(–hydroxypropyl)–piperazine–1–yl] ropanamide hydrochloride was taken from X–ray crystallography. Thus compound possessed hydrogen coplanar

with the anthraquinone ring and there is an intermolecular hydrogen bond between the amide hydrogen atom and the quinoid oxygen atom on the ring (NH1 --- O9) distance of 1.84 Å. For molecular modeling studies both AT and CG sites were examined. For the mono–substituted compounds the intercalation was found to occur in the both the wide major groove and narrower minor groove. The major groove was suggested to be preferred over minor groove for side chains on account of the more favorable electrostatic interactions between the phosphate groups of the di–nucleotide backbone and side chain protonated amino groups of the drugs, whereas for the di–substituted compounds the low energy intercalated geometries were produced with the side chain lying in the major groove, or in spear mode with side chains lying in each groove.

The models studied indicated that the amide groups even though they are coplanar with the anthraquinone chromophores, do not take part in the intercalative stacking interaction and thus suggesting that primary role of these groups is to diminish the flexibility of the side chain compared to their amido analogues. In mitoxantrone two carbon chain separate the nitrogen atoms immediately attached to the anthraquinone and the base side chain nitrogen atom. This short chain has unconstraint conformational flexibility and allows the terminal chain of the atoms to form favorable short range interactions with the bases specially with the nitrogen bases (Balaji et al, 1985; Islam et al, 1985) and such arrangement are not present in amido anthraquinones studies on account of their less flexible side chains. It was also apparent that changes in the nature and dimensions of the – $(CH_2)_2$ group present between amide and basic groups would be deleterious in the formation of electrostatic interactions. The predictions for the major grooves for the side chains of the di–substituted compounds on purely steric grounds was in accord with the NMR

(Kotovych et al, 1986) and kinetic studies (Krishnamoorty et al, 1986) studies on the di–substituted compounds.

The *in vivo* and *in vitro* activities of compounds have been done and found that a mark divergence of behaviour for the mono- substituted compared to the di–substituted compounds. The former ones showed little or no activity against tumour models (L120 cell lines) whereas later showed marginal to moderate activity. The clearance rate of these compounds was in marked contrast to the mitoxantrone. Thus it was found that amidoanthraquinones as a class are probably less metabolic active then amino anthraquinones as a result of liability of amide linkage.

Solutions studies on (amino alkyl) amino substituted anthraquinones, differing in the substituted pattern, namely, 1– (diethylamino)ethyl)amino] and 1,4; 1,5; and 1, 8– bis[(diethylamino)ethyl)amino] anthraquinones (Islam, 1985) were reported. The study has been correlated with the computer graphics modeling of their fit into a DNA intercalation site. Degree of unwinding with CCC–DNA was 10.6° for monosubstituted compounds and 14.2° – 14.3° for di- substituted compounds. Spectrometric titrations of drug with DNA showed order of DNA affinity as 1, 5 > 1, 4 > 1, 8 > 1–compounds.

Intercalative mode of binding of the antitumor drug mitoxantrone and ametantrone was studied (Mazerski et al, 1998), with dodecamer duplex $(CGCGAGCTCGCG)_2$ with drug molecule intercalated in the GC base pairs. Molecular simulations were carried out in water by applying GROMOS force field. Four different starting orientations namely, (S, N, E and W) for the intercalation of the drug in relation to the axis of inter–base pair 9 G6–C19) hydrogen bonds were examined. S–orientation was more favored in terms of high electrostatic energy (-2580 + 30 kJ / mol), and hydrogen bond formation between the 14OH group as well

as the aliphatic amino groups with the DNA base pairs. Both mitoxantrone and ametantrone complex exhibited similar intermolecular interactions but intermolecular topologies were significantly higher in case of the mitoxantrone complex. In mitoxantrone–complex mitoxantrone molecule observed was coplanar with the base pair axis. They suggested that the 1OH / 4OH group being at para–position enhances the width of the aromatic ring and decreases the inclination and hence better intercalation whereas ametantrone intercalate at an angle of 13° with respect to DNA base pairs though both posses identical side chains. This leads to better electrostatic interaction between mitoxantrone–DNA complexes as compared to ametantrone–DNA complex.

Theoretical calculations at the RHF 3-21G* level on mitoxantrone and its amido analogs (Zaggatto et al, 1997) with truncated side chains as adequate models show that the stereochemistry of the drug molecule is not appreciably affected when an amide group replaces the aromatic amine function. The reverse is true for electrostatic properties with the reversal of the direction of the dipole moment in the amido analogs as compared to the mitoxantrone. This may explain the absence of cleavable topoisomerase II-DNA complex for amido analogs.

The molecular geometries of MTX and the DNA bases (adenine, guanine, cytosine and thymine) were optimized with the aid of the B3LYP/ 6-31G* method (Riahi et al, 2008). The properties of the isolated intercalator and its stacking interactions with the adenine-thymine (AT) and guanine-cytosine (GC) nucleic acid base pairs were studied with the DFTB method (density functional tight-binding), an approximate version of the DFT method, that was extended to cover the London dispersion energy. The B3LYP/ 6-31G* stabilization energies of the intercalator-base pair complexes were found 10.06 kcal/mol and 21.64 kcal/mol for AT-MTX and GC-

MTX, respectively. It was concluded that the dispersion energy and the electrostatic interaction contributed to the stability of the intercalator-DNA base pair complexes. The results concluded from the comparison of the DFTB method and the Hartree-fock method point out that these methods show close results and support each other.

1.5.6 Metal Complexes of Mitoxantrone with DNA

Studies were done on the interaction of mitoxantrone, ametantrone Pd (II) complexes with DNA by means of ultraviolet and circular dichorism spectroscopy (Kolodziejczyk et al, 1987). These complexes behaved like complexes of other antitumor drugs like daunomycin, carminomycin, which bind strongly with Fe (III) and Pd (II). These complexes also exhibited higher cytoxicity as well as cardiotoxicity towards P–388 leukemia as compared to that of free drug. Mitoxantrone and ametantrone were found to be less susceptible to enzymatic reduction, therefore, appeared to be less toxic than Adriamycin and daunorubicin. However, on complexation they exhibited different biological properties in comparison to free drug. This can be explained on the basis that drugs owing to change in polarity, modifies its interaction with cell components such as membrane and nucleic acids. Both drugs formed 2:2 stoichiometry with Pd (II), i.e. the complex is formed with two molecules of drug (D1 and D2). One Pd (II) is bound to the nitrogen's of the side chains on C–5 of the molecule D1 and other to two side chains of the side chain of the C–5 of molecule D2 whereas second Pd (II) is bound to the nitrogen's of the side chains on C–8 of molecule D1 and D2. This complex formation prevents the intercalation of the drug between the base pair of DNA but preserves the ability of the drug to condense DNA. Nitrogen atoms have been proposed for most suitable candidates for complex formation to both ametantrone and mitoxantrone. Both yielded similar results, which would have been different if the 1, 4 groups had been

candidates for complexation giving rise to very stable five membered chelate on release of two protons per molecule. It was further found that both drugs exhibited decrease in intensity of absorption in the visible region, decrease in pH indicating the release of protons simultaneously with complex formation.

Mitoxantrone and its Cu (II) complexes (Yang et al, 1996) were studied by the methods of electrochemistry and fluorescence spectroscopy. On complexation it was observed that fluorescence emission was quenched completely at Cu (II) / mitoxantrone= 2:1 whereas the absorption spectra did not change. This indicates that one molecule of the drug can bind with two molecules of the Cu (II) ions. Cu (II) ions complex with nitrogen's of the side chains of mitoxantrone as similarity reported for Pd (II) complexes (Kolodziejczyk et al, 1987). Taking into steric hindrance Cu (II) complexes are usually tetra coordinate. Cu (II)–mitoxantrone complex showed stronger inhibiting ability on the DNA synthesis and hence better anti–tumor agent. Cu (II) / mitoxantrone = 1:1 is more potent than Cu (II) / mitoxantrone = 2:1. In CD study when mitoxantrone bound to calf thymus DNA the positive band at 275 nm of DNA increase greatly, and the negative band at 245 decreases rapidly indicating mitoxantrone leads to the conformational change of DNA from B to A. The transition metal ions interacted prefentially with GC by the chelation of N–7 of guanine and to phosphate residue. Thus, it was assumed that Cu (II)–mitoxantrone (side chain)–DNA is formed to cause denaturation of DNA which may be plausible action mechanism of the complex.

1.5.7 Clinical Studies

The anticancer agent mitoxantrone was found to be readily oxidized by human heam enzyme myeloperoxidase and hydrogen peroxide (Panousis et al, 1994). Intercalalation of mitoxantrone with DNA inhibited oxidation of the drug

myeloperoxidase but at physiological strength the significant oxidation was evident. The 1:1 complex (H_2O_2: MTX) was oxidized to product, which binds reversible with DNA whereas at higher 5:1 (H_2O_2: Mitoxantrone), two products were formed none of which binds reversible with DNA as indicated by absence of spectral change in the presence of DNA, indicating that further oxidation of the product at 1:1 H_2O_2: mitoxantrone by myeloperoxidase occur probably at the hydroquinone ring. Since, mitoxantrone has been shown to intercalate into DNA with chromophore perpendicular to the base pair axis, it was proposed that the oxidation of the chromophore may affect the binding of this highly oxidized form of DNA.

The binding of mitoxantrone to DNA has been found to inhibit direct oxidation of myeloperoxidase in a DNA dependent manner. Hence, when mioxantrone is intercalated into DNA the drug cannot gain access to the active site of the myeloperoxidase to unable subsequent oxidation to drug, that would therefore facilitate the access of myeloperoxidase to the drug, and unable the oxidation to occur. Thus, it was therefore likely that significant oxidation would occur both with in the cytoplasm and the nucleoplasm. Thus myeloperoxidase catalysed oxidation of mitoxantrone to products capable of interacting covalently and non–covalently with nucleic acids that may represent an important mode of action of mitoxantrone against acute leukemia since these cells (including neutrophils, monocytes and their precursors) contains certain levels of myeloperoxidase.

The cytotoxicity activity of mitoxantrone and related anthracenediones (2–aza–2aza–oxideanthracenedione) has been ascribed to the ability of these compounds to interfere with DNA top–II function resulting in DNA cleavage stimulation (Isabella et al, 1995). Their results indicated that the substitution of the pyridine ring for the deoxyphenylene ring in the planar chromphore caused a marked reduction in the

cytotoxicity and of the ability to stimulate top–II mediated DNA cleavage in the intact cell. Though all the derivatives were shown to intercalate into DNA their binding affinities were lower than that of mitoxantrone. The behaviour of 2–aza derivatives closely resembled that of the ametantrone suggesting that the potency of these agents is influenced by hydroxyl group rather than by phenylene ring. The observation that dramatic reduction of the stability of the aza derivatives to stimulate DNA cleavage was associated with marked reduction of cytotoxic potency supported a primary role of top II in the mechanism of action of this class.

Compounds containing 9, 10 anthracenediones with one or two peptide chains at 1, 4 positions with the introduction of Glycine (Gly), Lysine (Lys) and Tryptophan (Tryp) with the derivatives of the latter two in both L– and D–conformation (Gatto et al, 1996) were studied. Formation of the DNA–anthraquinone complex caused almost total quenching of the fluorescence signal for all the compounds. All the compounds exhibit remarkable affinity for DNA (K in the range of 10^5 M^{-1}) close that of ametantrone but clearly lower than that of mitoxantrone. Mono–di–triglyceral derivatives showed a distinct preference for CG–rich sequences as many anthraquinones do the most specific being the 1, 4–bis[glycyl–glycl–glycyl) amino] anthracene, 9, 10 dione (AG_3–11) and 1, 4 bis [glycyl–glycl) amino] anthracene, 9, 10 dione (AG_2–11) comparing well with the ametantrone and mitoxantrone exhibiting the clear preference for the CG steps in polynucleotide chain. Geometry of the intercalation of the peptidyl anthraquinones was similar to that of ametantrone and mitoxantrone and the induced rotational strength was negative. However, different values of induced molar ellipticity pointed to slightly different peptidyl arrangements when inserted between the base pair. Cell toxicity correlated with the nature of the amino acids in the side chains than to presence of one or two of them at positions at 1

and /or 4 of the anthraquinone ring. AG_n and 1, 4 Bis [D–tryptophnyl–glycyl0–amino) anthracene–9,10–dione [(AG_w–11)] are less effective in top II mediated cleavage show reduced cardiotoxicity than stimulate top II functions, which suggests competition between the drug and the enzyme in DNA template occupancy. Accordingly, they were found devoid of cell killing properties, which indirectly points to the importance of top II mediated mechanisms in anticancer activity. This finding was consistent with the reduced activity shown by number of mitoxantrone congeners bearing bulky substituents and additional bulky charges in the side chains (Cheng et al, 1983).

The physiological, cytotoxic and pharmacological properties of 2, 3 diazaanthracene diones (Isabella et al, 1995) studied by spectroscopic and voltametric measurements. In comparison with mitoxantrone and ametantrone they were characterized by less negative reduction potential, lower affinity for DNA and modified geometry of intercalation. The biological effects of the new compounds were not affected by the biosteric N or C replacement. Stimulation of Topoisomerse II mediated DNA cleavage was not observed, whereas the other mechanism of cell cytotoxicity, possibly involving oxidative DNA damage, appeared to be operative. The inability to generate the protein associated DNA breaks was explained by unfavorable orientation of the drug in the intercalation complex rather than reduced binding to DNA. DNA damaging pathway of 2, 3 di-aza substituted derivatives which could produce radical species to a remarkably greater extent than carbocyclic parent drug.

1.6 SCOPE OF THESIS

Interactions of small molecules with DNA have been studied for several decades in the hope of learning design principles for the targeting of specific DNA

sequences in order to control gene expression. Many small molecules that bind to DNA are clinically proven therapeutic agents although their exact mode of action remains incompletely defined. There is a renewed focus on the use of small molecules as therapeutic agents. This renewed interest arises, in part, as a result of several advantages of small molecules as potential drugs, including the economics of their synthesis and their effective delivery to cells. The results of binding studies are correlated with biological (antitumor) efficiency of the compounds tested with the aim to exploit these data for design of new cytostatics with better therapeutic properties as compared to the drugs already used in the clinic. Therefore, these studies are aimed in particular at the development of new anticancer drugs whose antitumor efficacy is associated with their interactions with DNA, i.e. for which DNA is the main target inside tumor cells. The facilities of this laboratory make it possible to accquire the knowledge, which is needed for design of new cytostatics and suggestions for structure requirements for pharmacological activity. Understanding structure-function directed macromolecule-target interactions of anticancer drugs, and further rational design of improved anticancer agents are the long-term research goals of our laboratory. This thesis deals with (i) the typical procedure for studying the molecular and electronic properties of small molecules using quantum chemical calculations (ii) structural studies of the anticancer drug complexed with different hexanucleotides (iii) to investigate the relationship between the structure and biological activity of the drug

The Ph.D thesis work has been reported in the form of seven chapters. Chapter 1 contains introduction as of the subject as well as review of literature. Chapter 2 deals with the materials and methods used. In chapter 3, the molecular and electronic properties of mitoxantrone are discussed using quantum chemical calculations in water and DMSO. Chapter 4, 5 and 6 deals with Phosphorus–31 NMR,

Proton and rMD studies on binding of mitoxantrone with DNA hexamer sequence d–(TGATCA)$_2$, d–(CGTACG)$_2$ and d–(TGTACA)$_2$, respectively. ^{1}H and ^{31}P NMR titration studies were used to study the change in chemical shifts on binding. 2D ^{31}P - ^{31}P exchange spectra of drug-DNA complex gives direct evidence for binding and conformation of the DNA backbone. 2D ^{1}H - ^{1}H NOESY studies provide detailed information on the close intermolecular contacts between the drug and DNA molecule in the complex. Restrained molecular dynamics studies using inter-proton distances obtained from 2D NOESY as restraints, provide understanding of the conformational and helical parameters of the drug-DNA complexes in solution. Chapter 7 compares the results of mtioxantrone binding to three different hexamer DNA. These studies reveal structural tools such as NMR spectroscopy, coupled with molecular modeling techniques have considerable impact in advancing our understanding of the structural selectivity and the molecular basis for drug-DNA interactions. Understanding the physicochemical properties of the drug as well as the mechanism by which it interacts with DNA, would ultimately lead to rational design of novel anti-cancer drugs.

Chapter 2

Materials and Methods

2.1 MATERIALS

The deoxyribonucleic acid sequences d-$(TGATCA)_2$, d-$(CGTACG)_2$, d-$(TGTACA)_2$, and dimethyl sulphoxide (DMSO) with isotopic purity 99.96% were purchased from Sigma-Aldrich Chemicals, Ltd. Mitoxantrone Hydrochoride was obtained from Sigma-Aldrich and Calbiochem Ltd. 3 - (Trimethylsilyl) propionic-2, 2, 3, 3-d_4 acid sodium salt (TSP) was added to sample as an internal NMR reference. HPLC grade solvents and reagents like Na_2HPO_4 and NaH_2PO_4 used for buffer preparation were purchased from Qualigens Fine Chemicals India Ltd. Drug samples were used without further purification but nucleotide sample was purified by dialysis using benzoylated dialysis tubing from Sigma-Aldrich Co. USA.

2.2 SAMPLE PREPARATION FOR NMR

2.2.1 Purification by Dialysis

The sample was further purified by dialysis using benzoylated dialysis tubing. The tube of 6 cm length was cut and activated by boiling it in large volume of 2% (w/v) sodium bicarbonate and 1 mM EDTA (pH = 8.0) for 10 minutes followed by thorough rinsing in distilled water. Dialysis membrane was then again boiled for 10 minutes in 1 mM EDTA (pH = 8.0). The sample was then put into the tubing, sealed with holders and dialyzed against 4 M NaCl for 12 hours followed by dialysis against distilled water for 12 hours twice. Sample was then taken out, lyophilized and dissolved in 20 mM phosphate buffer. The purified oligonucleotide was annealed by heating it in a computer aided Cary 100 Biospectrophotometer equipped with a thermoelectric control unit (peltier unit) upto 80°C at the rate of 1°C per minute with

hold time of 10 minutes and then slowly cooled it to the room temperature to get oligonucleotide in duplex state.

2.2.2 Preparation of Complex

Solution of mitoxantrone (25 mM / 36 mM) was prepared by dissolving a known quantity of sample in 20 mM Phosphate buffer (pH = 7.0) having 70 mM NaCl concentration. The final concentration was checked by absorbance measurements at wavelength of 682 nm using Cary 100 Bio Spectrophotometer. The extinction coefficient (ε) value used for mitoxantrone was $\varepsilon = 8300\ M^{-1}\ cm^{-1}$. Solution of deoxyoligonucleotide, d-$(TGATCA)_2$ (2.76 mM duplex concentration), d-$(CGTACG)_2$ (2.76 mM duplex concentration) and d-$(TGTACA)_2$ (4.0 mM duplex concentration) were prepared by dissolving a known quantity of sample in 90% water and 10% D_2O phosphate buffer (20 mM) of pH = 7.0 having 70 mM Na salt and their concentrations were determined by absorbance measurements at 260 nm using the extinction coefficient (ε) value, 61400 $M^{-1}cm^{-1}$ for d-$(TGATCA)_2$, 57200 $M^{-1}cm^{-1}$ for d-$(CGTACG)_2$ and 61400 $M^{-1}cm^{-1}$ for d-$(TGTACA)_2$. Ethylene diamine tetra acetic acid (EDTA), 0.1 mM, was added to suppress paramagnetic impurity, which may cause line broadening during NMR measurements. Typically 1µl of 0.1 M solution of 3-(Trimethylsilyl) propionic-2, 2, 3, 3-d_4 acid sodium salt (TSP) was added to the samples as an internal reference.

(i) d-$(TGATCA)_2$ and mitoxantrone complex: A complex of d-$(TGATCA)_2$ and mitoxantrone was prepared by titration. 100 µl of 25 mM mitoxantrone was added in steps to 0.45 ml of 2.76 mM d-$(TGATCA)_2$ sample during titration in order to make 2:1 complex of mitoxantrone: d-$(TGATCA)_2$. The concentration of d-$(TGATCA)_2$ (N_1) in total volume of 0.46 ml is determined as follows:

$$N_1V_1 = N_2V_2$$

$$N_1 \times 0.46 = 2.76 \times 0.45$$

$$N_1 = 2.70 \text{ mM}$$

The concentration of mitoxantrone in this solution is determined as follows:

$$N_3V_3 = N_4V_4$$

$$N_3 \times 0.46 = 25 \text{ mM} \times 0.01$$

$$N_3 = 0.54 \text{ mM}$$

Like wise other mitoxantrone-d $(TGATCA)_2$ complexes of different drug / nucleotide (D/N)) ratios were prepared. The concentration of mitoxantrone (D), d-$(TGATCA)_2$ (N) and drug/ nucleotide (D/N) ratio are shown in Table 2.1a.

Table 2.1a: Various concentration ratios (D/N) for the complex formed between mitoxantrone and d-$(TGATCA)_2$

Nucleotide Concentration (mM) = N	Drug Concentration (mM) = D	D/N
2.76	0.00	-
2.70	0.54	0.20
2.66	0.94	0.35
2.61	1.32	0.50
2.57	1.68	0.65
2.53	2.04	0.80
2.48	2.50	1.00
2.43	2.94	1.21
2.40	3.26	1.36
2.37	3.57	1.51
2.31	4.07	1.76
2.26	4.54	2.01

(ii) d-$(CGTACG)_2$ with mitoxantrone complex: The complex of d-$(CGTACG)_2$ and mitoxantrone was prepared by titration. 69 µl of 36 mM mitoxantrone was added in steps to 0.45 ml of 2.76 mM d-$(CGTACG)_2$ sample during titration in order to make 2:1 complex of mitoxantrone: d-$(CGATCG)_2$. The calculations for this complex are

same as mentioned above. Like wise other mitoxantrone-d $(CGTACG)_2$ complexes of different drug / nucleotide (D/N)) ratios were prepared. The concentration of mitoxantrone (D), d-$(CGTACG)_2$ (N) and drug/ nucleotide (D/N) ratio are shown in Table 2.1b.

Table 2.1b: Various concentration ratios (D/N) for the complex formed between mitoxantrone and d-$(CGTACG)_2$

Nucleotide Concentration (mM) = N	Drug Concentration (mM) = D	D/N
2.76	0.00	-
2.73	0.28	0.10
2.72	0.55	0.20
2.70	0.82	0.30
2.67	1.08	0.40
2.65	1.35	0.50
2.64	1.60	0.61
2.62	1.86	0.71
2.60	2.11	0.81
2.58	2.35	0.91
2.56	2.60	1.00
2.52	3.07	1.21
2.50	3.40	1.36
2.47	3.73	1.50
2.45	4.05	1.65
2.42	4.36	1.80
2.39	4.78	2.00

(iii) d-$(TGTACA)_2$ with mitoxantrone complex: The complex of d-$(TGTACA)_2$ and mitoxantrone was prepared by titration. 100 µl of 36 mM mitoxantrone was added in steps to 0.45 ml of 4 mM d-$(TGTACA)_2$ sample during titration in order to make 2:1 complex of mitoxantrone: d-$(TGTACA)_2$. The concentration of mitoxantrone (D), d-$(TGTACA)_2$ (N) and drug/ nucleotide (D/N) ratio are shown in Table 2.1c.

Table 2.1c: Various concentration ratios (D/N) for the complex formed between mitoxantrone and d-$(TGTACA)_2$

Nucleotide Concentration (mM) = N	Drug Concentration (mM) = D	D/N
4.00	0.00	-
3.95	0.39	0.10
3.91	0.78	0.20
3.87	1.16	0.30
3.83	1.53	0.40
3.79	1.89	0.50
3.75	2.25	0.61
3.71	2.60	0.70
3.67	2.94	0.80
3.64	3.27	0.90
3.60	3.60	1.00
3.53	4.23	1.20
3.48	4.69	1.35
3.43	5.14	1.50
3.38	5.58	1.65
3.33	6.00	1.80
3.27	6.54	2.00

2.3 METHODOLOGY

2.3.1 NMR Spectroscopy

Nuclear Magnetic Resonance (NMR) spectroscopy is a powerful spectroscopic technique that provides information about the structural and chemical properties of synthetic, biomolecules (Wuthrich, 1986), liquid crystals (Khetrapal, 1975), etc. NMR exploits the behaviour of certain atoms when they are placed in a very strong magnetic field and many of the spectral parameters can be interpreted directly in terms of conformation or dynamics. As ^{1}H, ^{13}C, ^{15}N and ^{31}P are all present in nucleic acids, there are large number of signals present that can report on structure, dynamics and the effect of ligand binding.

2.3.1.1 The Phenomenon of NMR

Subatomic particles (electrons, protons and neutrons) spin on their axis. A nucleus (of spin 1/2) when placed in a static magnetic field behaves like a small magnet. This nucleus is in the lower energy level (i.e. its magnetic moment does not oppose the applied field). In the absence of an external magnetic field, these orientations are of equal energy. Each level is given a magnetic quantum number, m, characterizing Z component of spin, I. On interaction with magnetic field, nuclei with spin I >1/2 distributes themselves among 2I + 1 energy level with the separation by:

$$\Delta E = h \gamma B_0$$

The overall spin, I, is important. A nucleus with spin 1/2 will have 2 possible orientations (Fig. 2.1a). These spins are capable of interacting with a beam of electromagnetic radiation. These energy levels correspond to the spins aligned along and against the applied magnetic field, B_0. The spin oriented to oppose B_0 has higher energy. These spin do not align perfectly along B_0 and this give rise to a permanent torque. The nucleus also has the property of angular momentum because of its spin and as a result the nuclei precess (Fig. 2.1b), with frequency of precession given by:

$$\omega_0 = \gamma B_0$$

where, γ is proportionality constant, ω_0 is the Larmor frequency in radians/second and B_0 is the magnitude of the applied magnetic field. When the frequency of the beam is same as that of precessing spin then absorption of energy takes place, which causes the nuclei to flip from a lower energy state to a higher energy state by a process termed resonance (Fig 2.1c). In an NMR sample there are many molecules, each with its spin precessing about B_0 at same frequency and result in a net magnetization of M_z oriented along the Z-axis. On application of a rotating radio frequency field with frequency at or near $\omega_0 = \gamma B_0$, the spins resonate giving rise to net M_{xy} component which is phase coherent.

The following are the spectral parameters in NMR:

2.3.1.2 Chemical Shift

The magnetic field at the nucleus is not equal to the applied magnetic field, B_0; electrons around the nucleus shield it from the applied field. The difference between the applied magnetic field and the field at the nucleus is termed the nuclear shielding. The induced field is directly proportional to B_0. This is represented by the equation:

$$B_{eff} = B_0 (1-\sigma)$$

where, σ is the shielding constant which depends on the nature of electrons around the nucleus. Chemical shift is a function of the nucleus and its environment. It is measured relative to a reference compound. For ^1H NMR, the reference is usually tetramethylsilane, $Si(CH_3)_4$. Chemical shift is expressed in parts per million (ppm) is given as:

$$\delta = 10^6 \times \left(\frac{\delta_{ref} - \delta_{obs}}{\delta_{ref}} \right)$$

where, δ_{ref} is the position observed for a reference compound and δ_{obs} is the position of the signal of interest. There are useful general conclusions that can be drawn from specific chemical shift value, or changes due to the binding of the ligand.

2.3.1.3 Spin-Spin Coupling Constant (J)

Nuclei experiencing the same chemical environment or chemical shift are called equivalent. Those nuclei experiencing different environment or having different shifts are nonequivalent. Nuclei, which are close to one another, exert an influence on each other's effective magnetic field. This effect shows up in the NMR spectrum when the nuclei are nonequivalent. If the coupling between non-equivalent nuclei is less

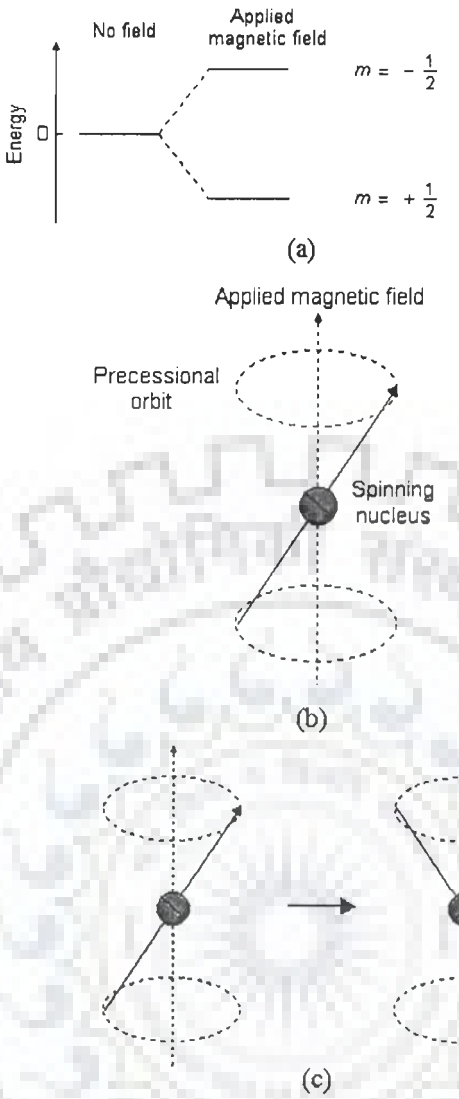

Figure 2.1: (a) Energy levels for a nucleus with spin quantum number ½ (b) Precessional motion by the nucleus spinning on its axis in presence of the external magnetic field (c) Flipping of the magnetic moment on absorption of the radiations

than or equal to three bond lengths, this effect is observable. This effect is called spin-spin coupling or J coupling and is expressed in Hertz (Hz). This coupling causes splitting of lines. The appearance of multiplet patterns depends on relative magnitude of δ and J for coupled nuclei. Vicinal couplings (^{3}J) display a characteristic

dependence upon the involved dihedral angle (Fig. 2.2a) according to the relation dihedral couplings;

$$^3J = 8.5 \cos^2\theta - 2.8$$

$$^3J = 9.5 \cos^2\theta - 2.8$$

This relationship is known as the Karplus relation. Fig. 2.2a and 2.2b shows the definition of dihedral angle and relationship between J couplings and dihedrals.

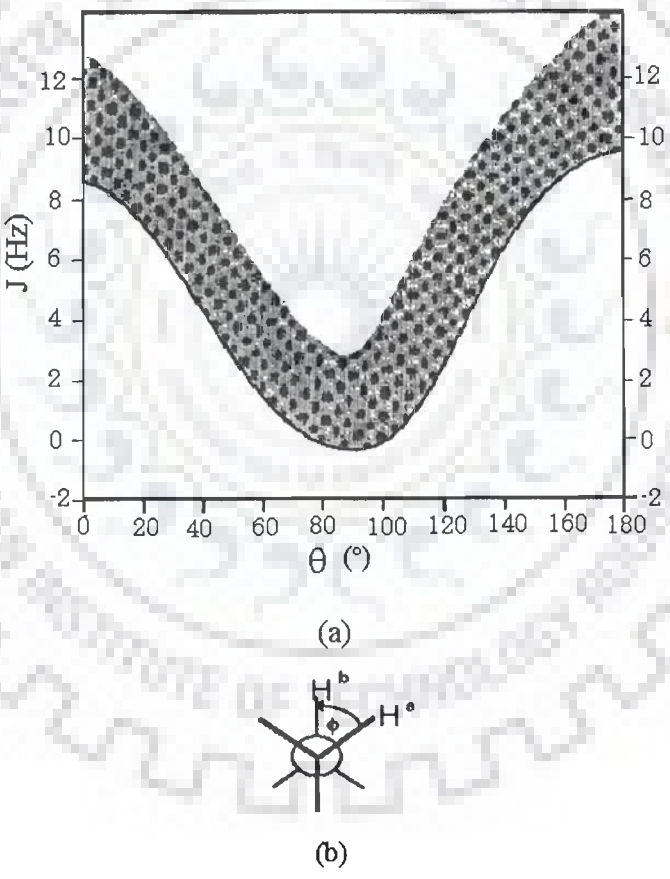

Figure 2.2: (a) Karplus curve showing relationship between J couplings and dihedral angle (b) definition of the dihedral angle

2.3.1.4 Relaxation Process

The magnetization does not precess infinitely in the transverse plane but turns back to the equilibrium state. This process is called relaxation. Two different time-constants describe this behaviour. The importance of these phenomena is in the Nuclear Overhauser Effect (NOE), which can be used to probe internuclear distances in a molecule. There are two major relaxation processes namely, spin-lattice (longitudinal) relaxation (T_1) and spin-spin (transverse) relaxation (T_2). The relaxation time T_1 represents the "lifetime" of the first order rate process that returns the magnetization to the Boltzman equilibrium along the +Z axis. The components of the lattice field can interact with nuclei in the higher energy state, and cause them to lose energy (returning to the lower state). The energy that a nucleus loses increases the amount of vibration and rotation within the lattice. The relaxation time, T_1 depends on the motion of the molecule. As mobility increases, the vibrational and rotational frequencies increase, making it more likely for a component of the lattice field to be able to interact with excited nuclei. T_1 spin-lattice relaxation rate is then measured by plotting magnetization M as a function of τ:

$$M(\tau) = Mo\,(1 - 2\exp^{-(\tau / T1)})$$

T_2 represents the lifetime of the signal in the transverse plane (XY plane) and it is this relaxation time that is responsible for the line width. In solution NMR, very often T_2 and T_1 are equal. The very fast spin-spin relaxation time provides very broad signals. The transverse relaxation constant T_2 is related to the linewidth of the signals. The width of the signal at half height is given by:

$$(\Delta\omega)_{1/2} = 1 / \pi\, T_2$$

Fast decay leads to broad signals, slow decay to sharper lines. The transverse relaxation constant T_2 of spin I=1/2 nuclei is mainly governed by the homogeneity of

the magnetic field and the strength of the dipolar interaction with other I=1/2 nuclei depending on the number and the distance of neighbouring nuclei and the overall tumbling time of the molecule, which is related to its size. Transverse relaxation (T_2) is faster than longitudinal relaxation. T_2 spin-spin relaxation rate is measured by plotting M as a function of τ:

$$M(\tau) = Mo^{(-\exp(\tau/T2))}$$

2.4 TWO-DIMENSIONAL (2D) NMR TECHNIQUES

In one-dimensional pulsed Fourier transform NMR the signal is recorded as a function of one time variable and then Fourier transformed to give a spectrum, which is a function of one frequency variable. In two-dimensional NMR the signal is recorded as a function of two time variables, t_1 and t_2, and the resulting data Fourier transformed twice to yield a spectrum, which is a function of two frequency variables. The two-dimensional signal is recorded in the following way. First, t_1 is set to zero, the pulse sequence is executed and the resulting free induction decay recorded. Then the nuclear spins are allowed to return to equilibrium, t_1 is then set to $\Delta 1$, the sampling interval in t_1, the sequence is repeated and free induction decay is recorded and stored separately from the first. Again the spins are allowed to equilibrate, t_1 is set to $2\Delta 1$, the pulse sequence repeated and a free induction decay recorded and stored. The free induction decay can be processed by tools like topspin and NMRLAB (Gunther, 2000). The whole process is repeated again for $t_1 = 3\Delta 1, 4\Delta 1$ and so on until sufficient data is recorded, typically 50 to 500 increments of t_1. Thus recording a two-dimensional data set involves repeating a pulse sequence for increasing values of t_1 and recording free induction decay as a function of t_2 for each value of t_1. The general scheme for two-dimensional spectroscopy is shown in Fig. 2.3.

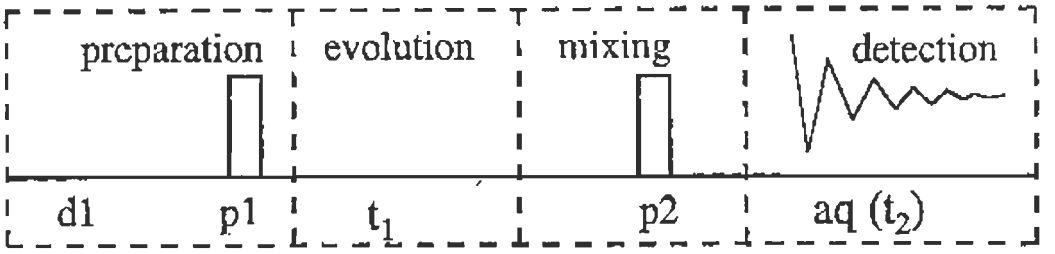

Figure 2.3: Four different time segments of a 2D NMR experiment namely (i) preparation period (ii) evolution period (t_1) (iii) mixing period (τ_m) (iv) detection period (t_2)

***Preparation time (d1)*:** The sample is excited by one or more pulse. This consists of a delay time or a sequence of pulses separated by fixed time intervals saturation sequences. Thermal equilibrium is attained during this period.

***Evolution Period (t_1)*:** The resulting magnetization is allowed to evolve for the first time period, t_1. The evolution period is the pulse sequence element that enables frequency labeling in the indirect dimension. Further, one or several radiofrequency pulses may be applied to create coherence.

***Mixing time (τ_m)*:** During this period coherence is transferred between spins. Mixing sequences utilize two mechanisms for magnetization transfer: scalar coupling or dipolar interaction (NOE). After the mixing period the signal is recorded as a function of the second time variable, t_2. This sequence of events is called a pulse sequence.

***Detection Period (t2)*:** The signal is recorded during the time t_2 at the end of the sequence, detection, often called direct evolution time; during this time the magnetization is labelled with the chemical shift of the second nucleus. The data is recorded at regularly spaced intervals in both t_1 and t_2.

Gradient enhanced NMR: It is a method for obtaining high resolution NMR spectra without the need for *phase cycling*. Gradient methodology is used extensively for two purposes, either rephasing (selection) or dephasing (elimination) of a particular

magnetization transfer pathway. It includes the application of magnetic field gradient pulses to select specific coherences. By using actively shielded gradients, a gradient pulse is applied during the evolution period of the selected coherence to dephase the transverse magnetization and another gradient pulse refocuses the desired coherences remaining during the acquisition period.

2.4.1 Two – Dimensional Correlation Spectroscopy (2D-COSY)

The COSY experiment is used in determining those atoms which are connected through bonds. The basis of COSY experiment whose pulse sequence is shown in Fig. 2.4a is the classical Jeener sequence (Jeener, 1971). After the preparation period of 90° pulse constitutes brief mixing period whose effect is to mix single quantum coherence into a whole range of orders of coherence. However, only the single quantum coherence will give rise to any measurable signal during the detection period. The mixing process interchanges orders of coherence, mixes coherence among the transitions associated with a given spin and exchanges coherence between spins having a mutual scalar coupling. Thus a magnetization, initially associated with the A spin of an A-X spin system, may be transferred to spin X through the scalar coupling, J_{ax}. Therefore the A magnetization in the X-Y plane will also depend upon the Larmor frequency ωx and the 2D COSY will show signals with frequency coordinates (ωA, ωX) and (ωX, ωA) as well as (ωA, ωA). The former are the characteristic cross peaks of COSY spectrum and the latter, the diagonal peaks, which corresponds to 1D spectrum. COSY experiment can be carried out with special phase cycling and data processing to change the 2D line shape into pure 2D absorption mode, allowing the use of phase-sensitive display. There are two different methods in use, the first requires the results of two complete COSY experiments with different phase cycling to be added (States et al, 1982) and the second known as TPPI

(Time proportional phase incrementation) method uses a single experiment with phase cycling which changes with t_1 increment (Bodhenhausen et al, 1977; Keeler and Neuhaus, 1985; Marion and Wuthrich, 1983; Redfield et al, 1975). The phase sensitive COSY spectra have cross peaks in antiphase. The antiphase multiplet structure of a cross peak only occurs in the active coupling giving rise to cross peak. Extra splitting present in multiplet but which do not give rise to cross peaks are called passive couplings and appear in phase. Thus, the advantage of phase sensitive COSY is that the phase relation between peaks can be used for accurate assignment and calculation of coupling constants.

2.4.2 Phase Sensitive COSY: Double Quantum Filtered COSY (DQF-COSY)

The experiment uses a pulse sequence 90_ϕ-t_1-90_φ-90_ζ-t_2 where ϕ, φ and ζ are the appropriate phase cycles (Piantini et al, 1982). In double quantum filter COSY experiment, (Fig. 2.4a) the resonance from a COSY experiment is passed through a double quantum filter, thereby removing methyl and other singlets from the final spectrum. The short delays, Δ, immediately before and after the final pulse, are of order of microseconds. Twice as many transients are needed in these experiments to achieve the same signal to noise ratio than in conventional COSY. Another advantage of DQF COSY is that it converts the phase of COSY diagonal signals from dispersive antiphase to absorptive antiphase. These signals then do not interfere with the cross peaks. So, the cross peaks lying close to diagonal can be observed in double quantum filtered phase-sensitive COSY. Double filter COSY can be used to determine the coupling constants (Celda et al, 1989; Gochin et al, 1990).

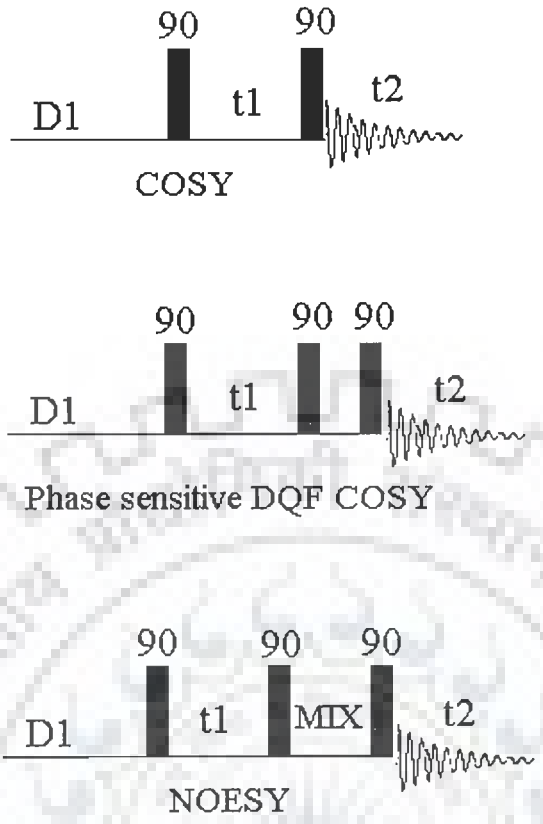

Figure 2.4a: Pulse schemes of various 2D NMR techniques

2.4.3 Total Correlated Spectroscopy (TOCSY)

During this pulse sequence, after the evolution period t_1, the magnetization is spin-locked. During this mixing time, the magnetization exchange through scalar coupling. During this spin-lock period, the magnetization behaves as a strongly coupled spin system and evolves under the influence of a "collective spin-mode". In that collective mode, coherence transfer is possible between all coupled nuclei in a spin system, (even if they are not directly coupled). This essentially gives the same information as that of COSY, except that COSY gives information only on the directly coupled spins, whereas TOCSY gives the complete spin-coupling network

2.4.4 Nuclear Overhauser Effect Spectroscopy (NOESY)

NOESY is one of the most useful techniques as it allows correlating nuclei through space (distance smaller than 5Å). By measuring cross peak intensity, distance information can be extracted. The pulse sequence starts as usual with a 90° pulse followed by an evolution time t_1 (Fig. 2.4a). This delay is varied systematically as usual to provide chemical shift information in the F1 domain. Then 90° pulse transmits some of the magnetization to the Z-axis and during the following mixing period, the non-equilibria Z component will exchange magnetization through relaxation (dipole-dipole mechanism). This exchange of magnetization is known as Nuclear Overhauser Effect (NOE). After some time (shorter than the relaxation time T1), the transverse magnetization is restored and detected. If relaxation exchange (or chemical exchange) has taken place during the mixing time, cross peaks will be observed in the spectra. The phase cycling ensures proper detection of NOESY signal.

2.4.5 Hetero – Nuclear Multiple Bonded Correlation Spectroscopy (HMBC)

Long-range hetero-nuclear correlation can yield signals for these nuclei while suppressing one-bond correlations. The most common application of this technique is for ^{1}H-^{13}C and ^{1}H-^{31}P. Δ_1 is set to 1/ (2J one-bond) and Δ_2 to 1/ (2J long- range). The phase is strongly dependent on the long range and hetero-nuclear proton coupling constant so each multiplet peak pattern has a different phase with an extreme first order component. The correlation experiment does not contain a diagonal. Each proton signal may be correlated with one or more carbon signals. Those signals in the 1D spectrum that do not correlate with carbons do not appear in the 2D spectrum (Fig. 2.4 b).

Nucleus bound to H	Ratio of 1st and 3rd gradient	J (one-bond)
^{13}C	3.98	145 Hz
^{31}P	12.0	8 Hz

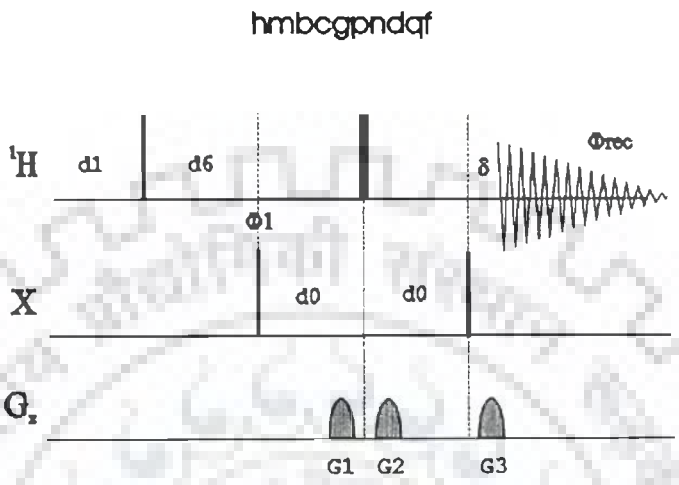

Figure 2.4b: Pulse sequence for HMBC

2.4.6 Diffusion Ordered Spectroscopy (DOSY)

The DOSY experiment is the measure of diffusion coefficients by NMR. In DOSY spectra, chemical shift is detected along the F2 axis and diffusion coefficient is along the F1 axis. The method developed by Stejskal and Tanner which relies on two gradient pulses surrounding the 180° pulse in the spin echo was used. The first gradient dephases, the transverse magnetization in a spatially dependent manner along the z-axis and the second gradient then rephases the magnetization. The relation between translational self-diffusion and the measurable NMR parameters (Stejskal and Tanner, 1965) is:

$$A/A_0 = -\exp\left[D_t\gamma_H^2\delta^2G_z^{\,2}(\Delta - \delta/3)\right]$$

where A is the measured peak intensity (or volume), A_0 is the maximum peak intensity, D_t is the translational diffusion constant (in cm^2/s), γ_H is the gyromagnetic

ratio of a proton (2.675197 x 10^4 G^{-1} s^{-1}), δ is the duration of the gradient, Δ is the time between gradients and G_z is the strength of the gradient (in G/cm). Data can be plotted as -ln (A/A_0) versus $\gamma_H^2\delta^2G_z^2$ ($\Delta-\delta/3$). The slope of the line gives the value of D_t. The pulse program used is Pulsed gradient spin echo (stimulated echo sequence incorporating bipolar gradients) sequence modified with binomial water suppression (Fig: 2.4c). The gradient strengths were incremented as a square dependence in the range from 1 to 32 G cm^{-1}. It has been developed in order to facilitate the complex mixture analysis without physical separation. This experiment will monitor any modification of the solvent or of the solutes, and molecular events such as molecular interactions or associations.

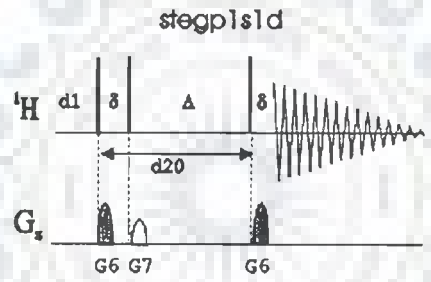

Figure 2.4c: Pulse sequence for DOSY

2.5 EXPERIMENTAL PARAMETERS

All NMR experiments were recorded on Bruker Avance 500 MHz FT-NMR spectrometer at Central NMR Facility located at Indian Institute of Technology Roorkee.

2.5.1 Study of Mitroxantrone–DNA Complex

^{31}P and ^1H NMR experiments were recorded for d-$(TGATCA)_2$, d-$(CGTACG)_2$ and d-$(TGTACA)_2$ and its complexes with mitoxantrone on successive addition of drug (Table 2.1a-c) at 278 K / 275 K in $H_2O + D_2O$ solvent.

The parameters were as follows:

1D ^{1}H NMR experiments were acquired with 64 K data points; number of scans = 64–128 and digital resolution = 0.15–0.3 Hz / point. Receiver gain was optimized in each instance to obtain the best signal to noise ratio.

1D ^{31}P NMR experiments were acquired with 64 K data points, number of scan = 128 and digital resolution 0.12 Hz / point.

$^{1}H - ^{31}P$ HMBC experiment were recorded with 2048 data points along t_2 dimension; 400 induction decays in t_1 dimension; no. of scans = 64 digital resolution 3.09 Hz / point in t_1 dimension and relaxation delay of 2.0 secs. τ value was optimized for 8 Hz coupling constants.

$^{1}H - ^{1}H$ 2D NOESY experiment were recorded with variable mixing times (τ_m) 200, 300 and 350ms at 278 / 275 K. Number of data points = 2048 data points along t_2 dimension; 256 induction decays in t_1 dimension; no. of scans = 48-64 digital resolution 1.495 Hz / point in t_1 dimension and relaxation delay of 2.0 secs. Mixing time (τ_m) = 100, 200 and 300 ms were used for D / N= 0.5, 1.0, 1.5 and 2.0 complex.

$^{31}P - ^{31}P$ 2D NOESY experiments for D / N = 0.2, 0.5, 1.0 and 2.0 at 275 K were recorded with mixing time of 150 / 200 ms; 4096 data points along t_2 dimension; 300 free–induction decays in t_1 dimension; no. of scans = 128; digital resolution 1.495 Hz / point in t_1 dimension and relaxation delay of 2.0 secs.

DOSY experiments were recorded with diffusion time (Δ) of 100 ms and the duration of the magnetic field gradients (δ) 6 ms, respectively in D_2O. Other parameters include a sweep width of 6000 Hz, 64 K data points, 16 transients, digital resolution 0.30 Hz / point and relaxation delay of 10 s.

2.6 DETERMINATION OF THREE-DIMENSIONAL STRUCTURE

2.6.1 Resonance Assignments in Nucleic Acids

Resonance assignment is the first endeavour in the structural determination of DNA. From the NMR point of view, the protons can be grouped into four categories; (i) exchangeable NH and NH_2 protons of the bases and non-exchangeable base protons between 7-15 ppm (ii) non-exchangeable sugar protons between 2-6.5 ppm (iii) methyl protons of thymine between 0.5-2 ppm. In order to observe NH and NH_2, protons, experiments have been carried out in water whereas the other protons were observed in D_2O solution. The strategy for resonance assignment consists of two steps. In the first stage, the J correlated spectra are used to identify network of coupled spins. In the second stage, the spin systems so identified are assigned to particular nucleotides along the sequence of the molecule by making use of the NOESY spectrum as described below. The sugar protons H1', H2', H2", H3', H4', H5' and H5" form a complex J correlated network (Fig. 2.5). The various cross peaks observed in the 2D J-correlated between these protons was used in identification of spin system within individual nucleotide units. The H1' proton shows a cross peak with H2', H2" sugar protons. The H2' and H2" protons are further coupled to H3' proton. We have used phase sensitive DQF-COSY spectra to identify the various J-coupled cross peaks. In the second phase sequential assignment is carried out using NOESY spectrum. Short internucleotide distances between adjacent nucleotide units are used as shown in Figure 2.5. In right handed DNA with sugars in C3'-endo/C2'-endo/O1'-endo pucker and glycosidic angle in anti domain, a convenient strategy for sequential assignment is

$$(H6/H8)_n \qquad (H2',H2'')_{n-1}$$

$$(H6/H8)_n \longrightarrow (H1')_{n-1}$$

$$(H6/H8)_n \longrightarrow (H6/H8)_{n-1}$$

where, n stands for nth residue in 5'-3' oligonucleotide sequence. In case of Z-DNA, where the repeating unit is a dinucleotide, the internucleotide pathway is Base (2n–1) …. H5' (2n–1) …. Base (2n) …. H1' (2n) …. H2' (2n) and H2" (2n) …. Base (2n+1).

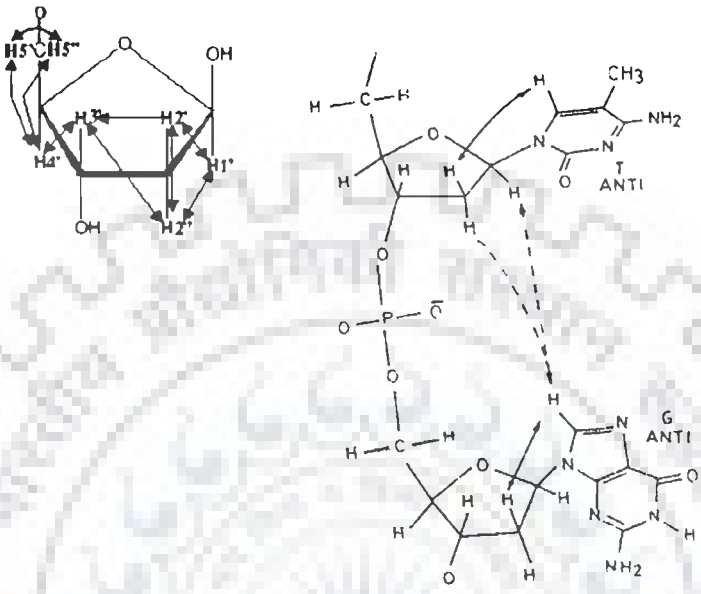

Figure 2.5: Schematic representation of sugar J connectivities and short interproton distances between adjacent nucleotides units in right handed DNA.

2.6.2 Pseudorotation

Because of the r^{-6} dependence of the pre-steady state NOE, the relative magnitude of the NOEs provide a sensitive probe which can be used to obtain a qualitative view of the solution structures of short oligonucleotides. The glycosidic and sugar pucker conformations can be assessed qualitatively on the basis of the relative magnitudes of the intranucleotide sugar-base NOEs. The flexible five-membered sugar ring plays a pivotal role in nucleic acid structure and dynamic behaviour. In B-DNA family sugar responds to its surroundings (e.g. base stacking pattern) by an appropriate adaptation of its geometry. X-ray studies have now shown that P values usually occur in two distinct ranges. In a conformational wheel (Fig. 1.8

of Chapter 1) one range of form occupies the "Northern" half of the circle (N-type, P_N 0° ± 90°); the second range occupies the "Southern" hemisphere (S-type, P_S 180 ± 90°). To a good approximation (0.4-0.7°) the torsion angles can be reproduced by a two-parameter pseudorotation equation:

$$\nu_j = \phi_m \cos [P + 0.8\pi (j-2)]$$

for j equals 0-4 and ϕ_m is amplitude of pucker. In crystal structures nucleotides usually a single pure N- or S-type conformer is found, but not necessarily the one that is predominant in aqueous solution. In some cases both N and S forms reside side by side in the same unit cell. Statistical analyses of X-ray data make it clear that details of sugar geometry of monomers are influenced by anisotropic crystal packing forces. The situation appears to be different in the helical oligomers, where stacking forces may play a more predominant role. NMR investigations in solution have demonstrated that N (C3'-endo) and S (C2'-endo) type conformations are in rapid equilibrium. If the interconversion rate between conformers is sufficiently rapid then observed couplings represent weighted average of couplings in individual conformers. Generally, in deoxyribose sugar, a trend to a larger proportions of C2'-endo pucker sugar is observed. A phase sensitive DQF-COSY spectrum allows J-coupling patterns to be delineated from the well-resolved cross peaks. In general, the relation between ^3J and φ takes the form of the semi empirical Karplus equation:

$$^3J = A \cos^2 (\varphi) + B \cos (\varphi) + C$$

The constants A, B and C have to be determined from ^3J values measured for compounds for which the value of φ, in solution, is known. There are five ^3J values in deoxyribose sugar, H1'-H2', H1'-H2", H2'-H3', H2"-H3' and H3'-H4', which are related to the relevant H-C-C-H dihedral angle, φ, according to the relation:

$$J = 10.2 \cos^2\varphi - 0.8 \cos \varphi$$

The above dihedral angles are inter-dependent and their values can be calculated in terms of the two pesudorotation parameters, P and φ_m, where φ_m is a constant for deoxyribose and thus various geometries can be expressed in terms of P. Fig. 2.6 (Hosur et al, 1986) shows the plots of five coupling constants in a deoxyribose ring as a function of P, (T_m = 38°). It is clear from the curves that the value of coupling constants ^3J (H1'-H2") and ^3J (H2'-H3') vary within a narrow range of 6-10 Hz and are comparatively insensitive to the sugar geometry. On the other hand, values of ^3J (H2"-H3'), ^3J (H3'-H4') and ^3J (H1'-H2') coupling constants vary in the range 0-10 Hz and can be utilized with greater advantage in fixing the domains of sugar geometry. ^2J (H2'-H2") is a geminal coupling which does not show significant conformational dependent variation. ^3J (H1'-H2'), ^3J (H1'-H2"), ^3J (H2'-H3'), ^3J (H2"-H3') and ^3J (H3'-H4') are vicinal coupling which show a strong dependence on the conformation of the deoxyribose ring (Hosur et al, 1986). The approach used for determination of sugar geometry is based on interpretation of intra-sugar proton-proton distances.

2.6.3 Conformation about the Glycosidic Bond

A large body of crystallographic data for nucleotides clearly establishes that the torsional angle, χ_{CN}, defining the orientation of base ring falls into two relatively narrow ranges designated as syn and anti conformation (Sundaralignam, 1969).

$$\chi \begin{cases} \text{O4'-C1'-N9-C4 (Purines)} \\ \text{O4'-C1'-N1-C2 (Pyrimidines)} \end{cases}$$

The relative magnitudes of the intranucleotide and internucleotide (H8/H6)-H1' and (H8/H6)-(H2', H2") cross peaks in NOESY spectra at different mixing times can be

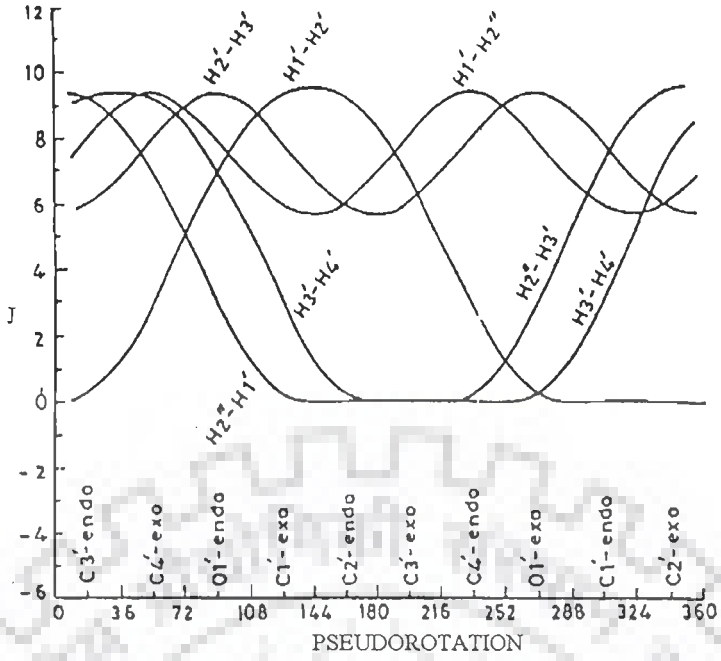

Figure 2.6: Variation of the vicinal coupling constants in the deoxyribose ring as a function of the ring geometry.

used to establish the domains of glycosidic dihedral angles of individual nucleotide unit (Hosur et al, 1985; Roche et al, 1994). Below the spin diffusion limit, the intensity patterns of the cross peak look similar at all mixing times although the absolute intensity may vary with the mixing time. The expected intensity patterns for the above mentioned cross peaks for different glycosidic dihedral angles are given below:

1. For the syn conformation, a strong NOE between base H8/H6 and H1' protons should be observed. At the same time, the NOEs from base to H2' and H2" protons will be relatively weak and will have different intensities.
2. In the anti conformation, the NOE from base H8/H6 to H2' is stronger than the NOE from base H8/H6 to H2". Also, for right handed structures the H2" proton shows a stronger NOE to the base proton of the next nucleotide.

3. In the high anti conformation, the (H8/H6)-H2' and (H8/H6)-H2" NOEs will have similar intensities for C2'-endo geometry.

The (H8/H6)-H1' distance depends only on χ while, other distances depend on both P and χ. Iso-distance contours have been calculated by Wuthrich (Wuthrich, 1986) in (P, χ) space for H8/H6-H2', H2", H3', H4' and H5' distances.

2.7 ESTIMATION OF INTERPROTON DISTANCES

If one resonance A is irradiated, an increase (positive NOE) or decrease (negative NOE) of signal intensity of other resonances such as resonance C is observed when spin C is close in space to spin A. This phenomenon is called Nuclear Overhauser Effect or NOE. The NOE effect is the method for elucidation of 3D structural features and stereochemistry using NMR together with information from scalar spin-spin couplings. The most important quantity derived from NOE cross peaks is the cross-relaxation rate between protons i and j. The cross relaxation rate σ_{ij} between two proton spins i and j is related to the distance between protons i and j in the following way:

$$\sigma_{ij} = \langle d_{ij}^{-6} \rangle f(\tau_{ij}) \qquad (1)$$

$\langle d_{ij}^{-6} \rangle$ denotes an ensemble average of molecular structures interconverting in thermal equilibrium where $f(\tau_{ij})$ is a function of correlation time τ_{ij} for the vector connecting the two spins. This function accounts for the influence of motional averaging processes on the NOE. The cross relaxation rates can be measured from buildup rates of cross peaks in 2D NOE spectra at several mixing times. According to equation (1), the measured cross relaxation rates are a function of the ensemble average properties, which are dependent on the configurational space accessible to the molecular system at the temperature and time scale. If the interconversion between conformational equilibria in the oligonucleotide is fast on NMR time scale, NOEs from several

equilibrium conformations will be observed simultaneously. This means that the derived set of distance constraints does not necessarily represent the average structure, and there may be no single conformation that is consistent with the data set. Initially the intensity of the cross peak in equation (1) varies linearly with mixing time, and therefore this condition is referred to as "linear regime", but on higher mixing times, this condition does not exist due to multispin relaxation. Interproton distances can be estimated by measuring the intensities of cross peaks in the "linear regime". Two-spin approximation is used in NOE distance measurements in which only the rate of dipolar magnetization transfer between proximal spins i and j is monitored and all other spins are ignored. For two spin approximation, the intensity I_{ij} can be written as:

$$I_{ij} = \frac{\gamma^4 \hbar^2 \tau_c \tau_m}{10 r_{ij}^{-6}} \qquad \text{when } \omega \tau_c >> 1$$

where γ is gyromagnetic ratio and $\hbar$, is Planck's constant divided by 2π. In order to determine the accurate value of τ_m for estimation of interproton distances, NOE build up curves should be obtained as a function of τ_m for several cross peaks, since spin diffusion can be different for different protons. Correlation times, τ_c, can be obtained from T2 and T1 measurements, according to the equation:

$$\tau_c = \quad 2\omega^{-1}(3T_2/T_1)^{-1/2}$$

which holds good for $\omega\tau_c >> 1$

If protons i, j, k, l have similar τ_c values and if r_{ij} is a known distance, then the unknown distance r_{kl} can be calculated by comparing the intensities I_{ij} and I_{kl} in a single spectrum. r_{ij}

$$\frac{I_{ij}}{I_{ij}} = \frac{r_{ij}^6}{r_{ij}^6}$$

The choice of known distance is important in the light of the mobility associated with different atoms in the nucleic acid. Gronenborn (Gronenborn and Clore, 1985) have expressed the opinion of using different yardsticks for NOEs involving different group of protons. The r(CH5-CH6) and r(H2'-H2") have different effective correlation times and can be used as reference depending on the cross peak being compared. The thymidine (H6-CH3) distance of 3.0 Å can be used as reference for all NOEs involving CH_3 protons, the sugar H2'-H2" protons and for the rest, cytidine H5-H6 distance of 2.45 Å can be used. Reid et al (Reid et al, 1989) examined H2'-H2" and H5-H6 cross relaxation at 15, 30, 60, 90 and 100 ms in dodecamer DNA duplexes. Results indicate that sugars and bases have the same correlation times, therefore all proton-proton distances in short DNA duplexes can be determined by scaling the initial NOE build up rate to the slope of cytosine H5-H6 cross peak, as H2'-H2" NOE cross peak are close to diagonal and are usually unresolved.

The characteristics of NMR data can be summarized as below:

1. NOEs cannot be translated into the precise distances. In practice this means that NOEs give only a number of approximate upper limits (e.g., 3 Å, 4 Å and 5 Å for strong, medium and weak NOEs). Sometimes it is not possible to make this division and only one single upper limit is used. For some proton pairs, corrections have to be applied to the upper limit value. This may arise due to stereo specific assignments (e.g., methyl group of thymine) or because of dynamic effects such as rotation of hydrogens in a methyl group and flipping of the aromatic rings.
2. Translating NOEs into reliable lower limit constraints is difficult, and it is preferable to take the sum of van der Waals radii as a lower limit to the

distance. The absence of NOEs between two assigned protons may be translated into a minimum distance of proton pair.

3. NMR data contain contributions from different molecular conformations. Not all distance constraints need to be consistent with the single conformation.
4. NOE information is limited to short distance relative to the size of the drug-DNA complex. For some part of the molecule none or only a few NOEs are observed.

2.8 RESTRAINED MOLECULAR DYNAMICS AND SIMULATED ANNEALING

When restrained energy minimization methods are used, inevitable local energy minima are encountered which can lead to inaccurate structures. To circumvent this, restrained molecular dynamics (rMD) are usually employed. This involves including NMR restraints in one of the many molecular dynamics simulation programs. Molecular dynamics solve Newton's equation of motion,

$$F_i = m_i a_i \quad (1)$$

Where F_i is the force, m_i is the mass and a_i is the acceleration of atom i. The force on atom i can be computed directly from the derivative of the potential energy V with respect to the coordinates r_i. The energy can be expressed in an explicitly differentiable form:

$$dV/dr_i = m_i d^2r_i / dt^2 \quad (2)$$

Therefore, with an adequate expression for the potential energy and the known masses, this differential equation can be solved for future positions in time t_i. In general, this can be solved only approximately, since V is usually a complex function of the coordinates of all (or many) of the atoms (i.e. $V = V(r_1, r_2, r_3, \ldots\ldots, r_N)$). The temperature can be calculated from the atomic velocities

$$3N/2\ k_B\ T = \sum_{i=1}^{N} 1/2\ m_i\ v_i^2 \quad (3)$$

where, k_B is Boltzmann's constant, m_i and v_i are the mass and velocity of atom i, and N is the number of atoms (and 3N is the number of degrees of freedom). For a simulation at constant energy, the temperature fluctuates due to the interconversion of kinetic and potential energy. If the temperature is held constant then the atomic velocities can be adjusted accordingly. If the pressure is held constant, the volume is allowed to fluctuate by rescaling the interatomic distances.

The total potential energy V_{total} is usually defined as the sum of a number of terms:

$$V_{total} = V_{bond} + V_{angle} + V_{dihedr} + V_{vdw} + V_{coulomb} + V_{NMR} \quad (4)$$

where, V_{bond}, V_{angle} and V_{dihedr} keep bond lengths, angles, and dihedral angles at their equilibrium values. The first five terms are empirical energy terms describing the physical interactions between the atoms, whereas the last term is a means of including the NMR information, but does not correspond to any real physical force. They can be summarized as follows:

$$V_{bond} = \sum_{bond} \tfrac{1}{2}\ K_b(b-b_0)^2 \quad (5)$$

$$V_{angle} = \sum_{Angle} \tfrac{1}{2}\ K_\theta(\theta-\theta_0)^2 \quad (6)$$

$$V_{angle} = \sum_{dihedr} K_\Phi(1+\cos(n_\Phi-\delta)) \quad (7)$$

These are pseudo-harmonic potentials that constrain bond lengths (b), bond angles (θ), and the rotamer angles (ϕ, δ) for staggered and eclipsed conformations, and K is a constant. The van der Waals and electrostatic interactions are described by V_{vdw} and $V_{coulomb}$.

$$V_{vdw} = \sum_{Pairs\ (ij)} [C_{12}/\ r_{ij}^{12} - C_6/\ r_{ij}^{6}] \quad (8)$$

$$V_{coulomb} = \sum_{Pairs\ (ij)} qiqj\ /\ 4\pi\varepsilon_0\varepsilon_r\ r_{ij} \quad (9)$$

where equation (8) is the Lennard-Jones potential, containing repulsive and attractive terms (C is a constant), and equation (9) describes the coulombic interactions between two charged particles (i, j) with partial charges q that are at a distance r_{ij} apart in a dielectric medium described by $\varepsilon_o\varepsilon_r$ term. The potential V_{NMR} contains the NMR restraints, and has the effect of pulling the protons that show an NOE interaction closer to the measured distance r_{ij}. Similarly, these potentials are also pesudo-harmonic functions of similar forms to equations (5)-(7). Distance constraints which can be reasonably accurately determined may therefore be defined as follows:

$$V_{NOE} = \begin{cases} K_1(r_{ij}-r_{ij}^0)^2 & \text{if } r_{ij} > r_{ij}^0 \\ K_1(r_{ij}-r_{ij}^0)^2 & \text{if } r_{ij} < r_{ij}^0 \end{cases} \qquad (10)$$

where, r_{ij} and r^0_{ij} are the calculated and experimental interproton distances, respectively, and K_1 and K_2 are force constants given by:

$$K_1 = k_B TS/[2(\Delta^+_{ij})^2] \text{ and } K_2 = k_B TS/[2(\Delta^-_{ij})^2] \qquad (11)$$

Where k_B is Boltzmann's constant, T, absolute temperature of the simulation, S a scale factor, and Δ^+_{ij} and Δ^-_{ij} are the positive and negative error estimates, respectively, of r_{ij}. If, however, only ranges of distances can be specified, then the distance restraints are incorporated into a pseudo-square-well potential of the form:

$$V_{NOE} = \begin{cases} K_{NOE}(r_{ij}-r_{ij}^u)^2 & \text{if } r_{ij} > r_{ij}^u \\ 0 & \text{if } r_{ij} \le r_{ij} \le r_{ij}^u \\ K_{NOE}(r_{ij}-r_{ij}^l)^2 & \text{if } r_{ij} < r_{ij}^l \end{cases} \qquad (12)$$

where r^u_{ij} and r^l_{ij} are the upper and lower limits, respectively, of the target distances obtained from the experimental, and K_{NOE} is the force constant, which is typically chosen to be the order of 1000 kJ mol^{-1} nm^{-1}.

To ensure that the experimental restraints are the dominating factor in determining the conformation of the molecule, it is very important that the force constants for the restraints are set sufficiently high that the experimental data are satisfied within the precision of the measurements. At the same time, the contribution from the empirical energy function should be such that in any individual rMD structure, the deviations from ideal geometry are small, and the non-bonded interactions are good (i.e. the Lennard-Jones potential is negative). Thus convergence on the structure is guided by the requirement to minimize NOE or other restraint violations. The number of distance restraint violations N_{viol} is counted when, for example, $r_{ij} \geq r_{ij}^0 + 1$, which would for 1 Å fluctuations. Another parameters which can be minimized in addition to N_{viol} is the sum of the distances in excess of the constraints $\sum \Delta r_{viol}$, which is defined as:

$$\Sigma \Delta r_{viol} = \sum_{K=1}^{N_{viol}} (r_{ij)k} - [(r_{ij}^0)_k + 1] \qquad (13)$$

where the sum runs over all those interproton (or pseudoatom) distances for which N_{viol} is defined. Although an arbitrary structure may be used for restrained molecular dynamics calculation, in practice a starting structure obtained from distance geometry and energy minimization is often used. The rMD approach requires a relatively large amount of computation time compared to distance geometry methods. This problem can be overcome by using a simplified potential energy function, where all non-bonded contact interactions are described by a single van der Waals repulsion term. Also by using a cut off distance, in which non-bonded interactions for pairs of atoms that are separated by a distance greater than some reasonable value (e.g. 5-10 Å) are excluded, the number of non-bonded interactions is decreased considerably. Simulated annealing involves raising temperature of the system followed by slow

cooling in order to overcome local minima and locate the global minimum region of the target function. It is computationally more efficient than rMD and yield structures of similar quality. The potentials are very similar to rMD and again Newton's laws of motion are solved as a function of time. However, in implementations found in commercial programs, the non-bonded interaction potential is modified so that there is a simple van der Waals repulsion term with a variable force constant K_{rep}:

$$V_{repel} = \begin{cases} 0 & \text{if } r \geq s.\, r_{min} \\ K_{rep}\,(s^2 r^2_{min} - r^2)^2 & \text{if } r < s.\, r_{min} \end{cases} \qquad (14)$$

The values of r_{min} are given by the sum of the standard values of the van der Waals radii between two atoms as represented by the Lennard-Jones potential.

2.8.1 Strategy for Molecular Modeling

2.8.1.1 Restrained Molecular Dynamics (rMD) of Uncomplexed Drug

In Chapter 3, the conformational features of mitoxantrone obtained after rMD simulations in water and DMSO are discussed. The structure of mitoxantrone was made by using builder module in MOE (Molecular Operating Enviornment, CCG canada) module. Pseudoatoms were defined for the equivalent set of protons. $13CH_2$–$14CH_2$ peak of MTX was used as the reference using a distance = 2.40 Å. The initial structure of Mitoxantrone was energy minimized against NOE constraints using 1000 steps each of Steepest Descent and Conjugate Gradient using CFF91 force field in DISCOVER software (Accelrys Inc., San Diego, California). Conformational search was performed by using the following simulated annealing restrained molecular dynamics (rMD) protocol. The molecule was heated to a temperature of 800 K in steps of 100 K, Molecular dynamics was carried out for 25 ps at 800 K during which 25 structures were saved at regular intervals of 1 ps. Each of them was then slowly cooled to 300 K in steps of 100 K. The total number of distance restraints used in the

calculations was 16 and 34 derived from H_2O and DMSO (Chapter 3) respectively. The force constants for NOEs for strong, medium and weak peaks were held constant as 25 Kcalmole^{-1} Å^{-2}. At the end of simulated annealing all the structures were minimized by 1000 steps of Conjugate gradient until a predefined convergence limit of root mean square derivative of < 0.01 Kcal mole^{-1} Å^{-1} was reached. The average structure obtained was examined in detail.

2.8.1.2 Restrained Molecular Dynamics (rMD) of Mitoxantrone Complexed with Hexamer

In Chapter 4, 5 and 6 we have discussed the conformational features of mitoxantrone complexed with d-(TGATCA)$_2$, d-(CGTACG)$_2$ and d-(TGTACA)$_2$, respectively. Starting structure of the complex of mitoxantrone–hexamer was made using builder module in MOE. rMD studies were done using DISCOVER / MOE. Pseudo atom corrections were used for methyl and other equivalent protons of DNA and Drug. Force constants of 25 kcal mol^{-1}Å^{-2} were used for distance restraints and 40 kcal mol^{-1}Å^{-2} for hydrogen bonds throughout the simulations. The energy of the molecule was minimized using 1000 steps each of Steepest Descent and Conjugate Gradient Methods to remove any internal strain due to short contacts in starting structure using CFF91 (DISCOVER) or MMFF94 (MOE) force field. Dielectric constant was fixed as 1.0 * r (r=distance) for calculation of electro electrostatic interactions. Conformational search was performed by the following simulated annealing restrained molecular dynamics protocol: The molecule was heated to a temperature of 800K in steps of 100 K. Molecular Dynamics was carried out for 25 ps at 800K during which 25 structures were saved at regular intervals (1000 iterations steps of 1 fs each). Each of them was then slowly cooled to 300K in steps of 100 K. At each step of cooling the molecule was equilibrated for 1000 iterations steps of 1 fs

each. At the end of simulated annealing, 1000 steps of Steepest Descent minimized all the structures until a predefined convergence limit of root mean square derivative of energy with respect to atomic coordinates of <0.01 kcal $mol^{-1}Å^{-1}$ was reached. All molecular dynamics calculations have been carried out in vacuum. To gain more insight into structural details the resulting average structure obtained was examined in detail with program CURVES, version 5.1 (Lavery and Sklenar, 1988).

2.9 DEFINING DNA STRUCTURE

The structure of DNA can be described by a number of parameters (Fig. 2.7) that define the helix (Dickerson et al, 1989). Polynucleotides in helical arrangement display order which can be expressed in terms of Helical Parameters. The output from helix analysis program CURVES of Richard Lavery (Lavery and Sklenar, 1988), includes "global helical parameters" defined relative to a global helix axis and "local helical parameters" defined relative to local helix axis at each base pair. The helicoidal parameters are classified into three categories:

1. global base pair-axis parameters
2. intra-base pair or global base-base parameters
3. inter-base pair or base pair-step parameters

The global as well as the local inter base pair parameters are related to particular base pair steps. These parameters are vector quantities, which have a defined location in 3-dimensional space and with respect to the nucleic acid sequence. In contrast, the average inter base pair parameters are scalar values that are not related to any part of the structure. They characterize properties of the whole structure. Among global base pair–axis parameters, x- and y- displacement refers to the shift of bases in positive or negative x and y direction with respect to each other.

Intra–base pair or global base–base parameters comprise of the translational components as stagger, stretch and shear, and the rotational components are propeller twist, buckle, opening. Propeller twist refers to the angle between the planes of two paired bases. A base pair is rarely a perfect flat plane with each aromatic base in the same plane. Rather, each base has a slightly different roll angle with respect to the other base. This makes two bases look like an aeroplane propeller. Twist or rotation per residue refers to the angle between two adjacent base pairs. Each step from one plate to the next can be described as a combination of a translational and a rotational movement. The translational and the rotational displacements are three-dimensional vectors, which can be split into three orthogonal components.

In inter-base pair or base pair-step parameters the three translational components are rise, shift and slide. Twist, roll and tilt are the three rotational components. Rise is the distance between adjacent planar bases in the DNA double helix i.e. it is a translation in the direction of the helical axis (z-axis), and shift is orthogonal to the helical axis and directs to the major groove side. Twist is a rotation about the helical axis (z- axis). Base pair roll refers to the angle of deflection of the base pair with respect to the helix axis along a line drawn between two adjacent base pairs relative to a line drawn perpendicular to the helix axis. A positive roll indicates that there is a cleft between two stacked base pairs, which opens towards the minor groove. A negative roll is related to an opening towards the major groove. Base pair tilt refers to the angle of the planer bases with respect to the helical axis. In the B-form DNA the bases are tilted by only –6°. In the A-form DNA the base pairs are significantly tilted at an angle of 20°. The sense of the base-pair tilt is associated with sugar puckering. In double helical polynucleotides, the normal to the base pair are not exactly parallel to the helix axis but inclined to it by up to 20°. The sense of tilt is

positive in A-type and negative in B-type of helices, and hence is correlated with sugar puckering. Base tilt angle is correlated with rise per residue. If the bases in base

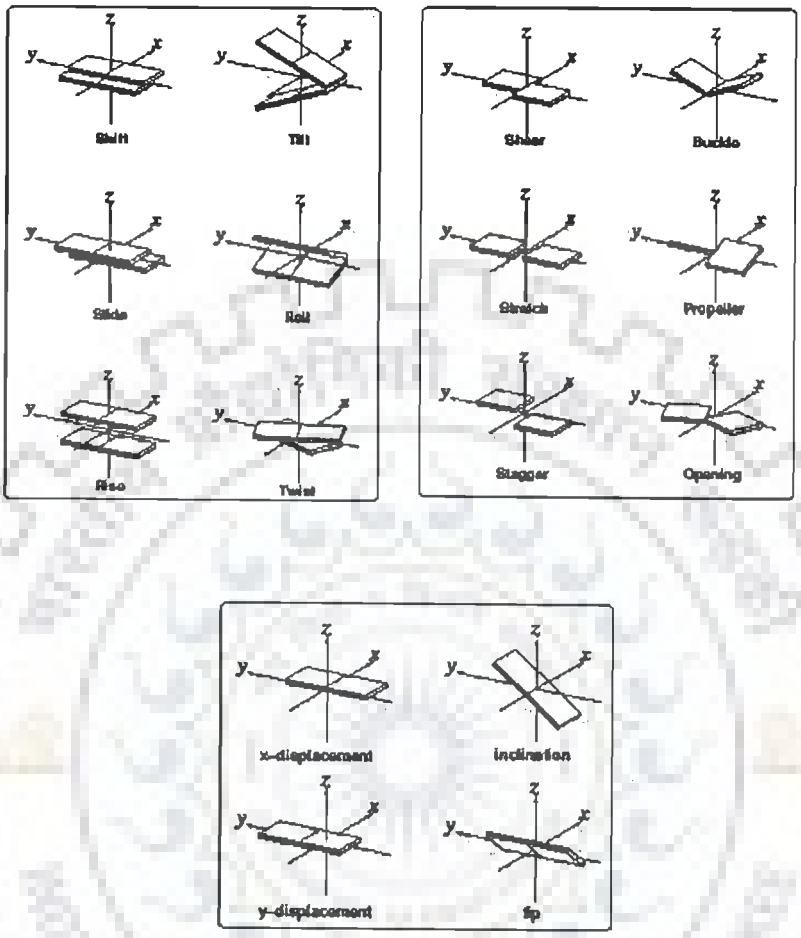

Figure 2.7: Pictorial representation of helical parameters

pairs were coplanar and the base pairs exactly perpendicular to the helix axis, the axial rise per nucleotide should correspond to the van der Waals distance, 3.4 Å.

2.10 QUANTUM MECHANICAL CALCULATIONS

The popularity of density functional methods and their applications to a broad range of problems and biochemical interest has been growing rapidly each year (Parr et al, 1989, Labauowski et al, 1991, Kohn et al, 1996). In chapter 3, the best known Hybrid B3LYP based on Becke's three parameters functional (Becke, 1993) and the

correlation functional provided by Lee, Yang and Parr's correlation energy (LYP) which includes local and non-local terms (Lee et al, 1988) of density functional theory (DFT) was used. In all of these calculations, Cartesian Gaussian type orbitals (GTO's) were used as basis function for the molecular orbitals. Although the capability of the basis functions to describe bonding deformations of the electronic density can be enhanced by increasing the number of basis functions for each orbital or including higher angular functions, yet as a thumb rule it should be able to yield results which are comparable with larger basis set while remaining computationally manageable, and thus at least a basis set of the split-valence type with polarization function should be employed. All calculations were done using the Gaussian 03 program package (Gaussian 03, 2004). Unconstrained geometry optimizations were performed using DFT with B3LYP functional methods. Basis sets 6-31G(d,p) and 6-31G+(d,p), were used for optimizing the geometry in H_2O and DMSO solvents conditions. Solvent conditions an Integral Equation Formalism) (Cances et al, 1997) Although it does not include any solvent hydrogen bonding, van der Waals or anisotrophy contributions, yet it is found one of the most successful model for incorporating the solvent effects. The molecular properties and chemical shifts were computed using the optimized structure of the molecule. The chemical shifts were calculated both in gas phase and in solvent using the Gauge Independent Atomic Orbital (GIAO) approach. This approach allows the computation of the absolute chemical shielding due to the electronic environment of the individual nuclei.

Chapter 3

Quantum Chemical and Nuclear Magnetic Resonance Studies on Molecular Properties and Electronic Structure of Mitoxantrone

Considering the fact that NMR chemical shifts are affected by the chemical environment i.e. molecular conformation and interaction with the solvent molecules. In this chapter, we report the quantum chemical calculations based on Density Functional Theory (DFT) to compute chemical shifts, structural parameters and spin-spin coupling constants for mitoxantrone in gas, water and DMSO solvent environments.

The following is presented in this chapter:

- Structural and electronic properties of mitoxantrone (Fig. 3.1) using DFT employing B3LYP exchange correlation at 6-31G+(d,p) and 6-31G(d,p) levels of basis sets in gas, water and DMSO conditions. Calculation of chemical shift of ^{1}H and ^{13}C resonances in Nuclear Magnetic Resonance (NMR) spectra of the molecule using the Gauge–Invariant Atomic Orbital (GIAO) method as implemented in Gaussian 03. The spin-spin coupling constant (J) has also been calculated from B3LYP/6-31G+(d,p) and 6-31G(d,p) levels using Gaussian 03. Besides this, bond length, bond angle and dihedral angles were computed at the same basis set level.
- Restrained Molecular Dynamics (rMD) simulations of Mitoxantrone using interproton distance constraints from 2D ROESY data (Manpreet, 2006) was performed to obtain most preferred conformations of the molecule in water and DMSO.
- Proton one dimensional NMR of Mitoxantrone, in H_2O and DMSO at 298 K at concentration of 10 mM.

3.1 RESULTS AND DISCUSSION

3.1.1. Resonance Assignment of Mitoxantrone in Water and DMSO

The proton resonance assignment at 298 K in water is shown in Fig. 3.2. The two singlets resonating at 6.83 and 6.95 ppm are due to aromatic ring protons, 2H/3H and 6H/7H. Four triplets resonating in the region 3.2–4.0 ppm (Fig. 3.2) are attributed to four sets of methylene protons. Among the spin–spin coupled pairs of methylene protons, $14CH_2$–$13CH_2$ and $11CH_2$–$12CH_2$, the $14CH_2$ and $11CH_2$ protons are expected to be downfield shifted, being attached to 14OH and 11NH protons, respectively. The amino proton coupled to $11CH_2$ protons is assigned to 11NH. All methylene protons are assigned accordingly. The resonance at 13.21 ppm has been assigned to 1OH/4OH being the maximum downfield shifted protons. The proton assignments made are in agreement with that published by Davies and coworkers (Davies *et al*, 2001, Lown *et. al,* 1985a).

The proton resonance assignment at 298 K in DMSO is shown in Fig. 3.3. The two singlets resonating at 7.21 and 7.68 ppm are assigned due to 2H/3H and 6H/7H, respectively. Four triplets resonating in 3.0–4.0 ppm are attributed to the methylene protons. Among the spin–spin coupled pairs of methylene protons $13CH_2$–$14CH_2$ and $11CH_2$–$12CH_2$, the $11CH_2$ protons is shifted downfield with respect to $14CH_2$ proton contrary to the results observed in H_2O. Some extra resonances for mitoxantrone in DMSO–d_6 have also been observed which were earlier not observed for mitoxantrone in H_2O solvent. The triplet resonating at 5.30 ppm coupled to $14CH_2$ proton is assigned to14OH. TOCSY spectra also show that broad resonances at 9.07 ppm gives relay peaks with $11CH_2$, $12CH_2$, $13CH_2$ and$14CH_2$ and hence are assigned to 12NH protons. The resonance at 13.46 ppm has been assigned to 1OH/4OH being the maximum downfield

shifted protons. The detailed strategy for the unambiguous assignment of carbon resonances of mitoxantrone in water and DMSO solvents were done by Manpreet, 2006.

The exchangeable protons which were not observed in proton spectra recorded in H_2O solvent, that is, 12NH and 14OH protons are now observed in the DMSO solvent in addition to the other protons. The hydroxyl/amino proton is shifted down-field due to strong hydrogen bonding of the X–H to the sulfoxide oxygen of DMSO, which not only deshields the proton (causing a resonance shift to lower field), but also secures it from very rapid exchange reactions. Under routine conditions, rapid intermolecular exchange of the OH/NH protons often prevents their coupling with adjacent hydrogens from being observed. Since hydrogen bonding not only causes a resonance shift to lower field, but also decreases the rate of intermolecular proton exchange, the proton remains bonded for a sufficient time to exert its spin coupling influence.

It is observed that $11CH_2$ protons in DMSO are shifted downfield with respect to the $14CH_2$ contrary to the observation made in H_2O solvent. The observed shifts can be explained in terms of the capability of 11NH to protonate the DMSO solvent owing to its basicity and lack of protons. Thus, the $11CH_2$ now in turn carries a partial double bond character where as such effect is absent at 14OH end, hence to the observed downfield shift for the $11CH_2$ as compared to$14CH_2$ protons in DMSO solvent. No such effect was observed in water, which behaves as proton donor solvent. Thus, it can be said that while in water the inductive effect predominates the resonance stabilization effect precede in the DMSO solvent and hence the $14CH_2$ protons are shifted downfield with respect to the $11CH_2$ protons in H_2O solvent.

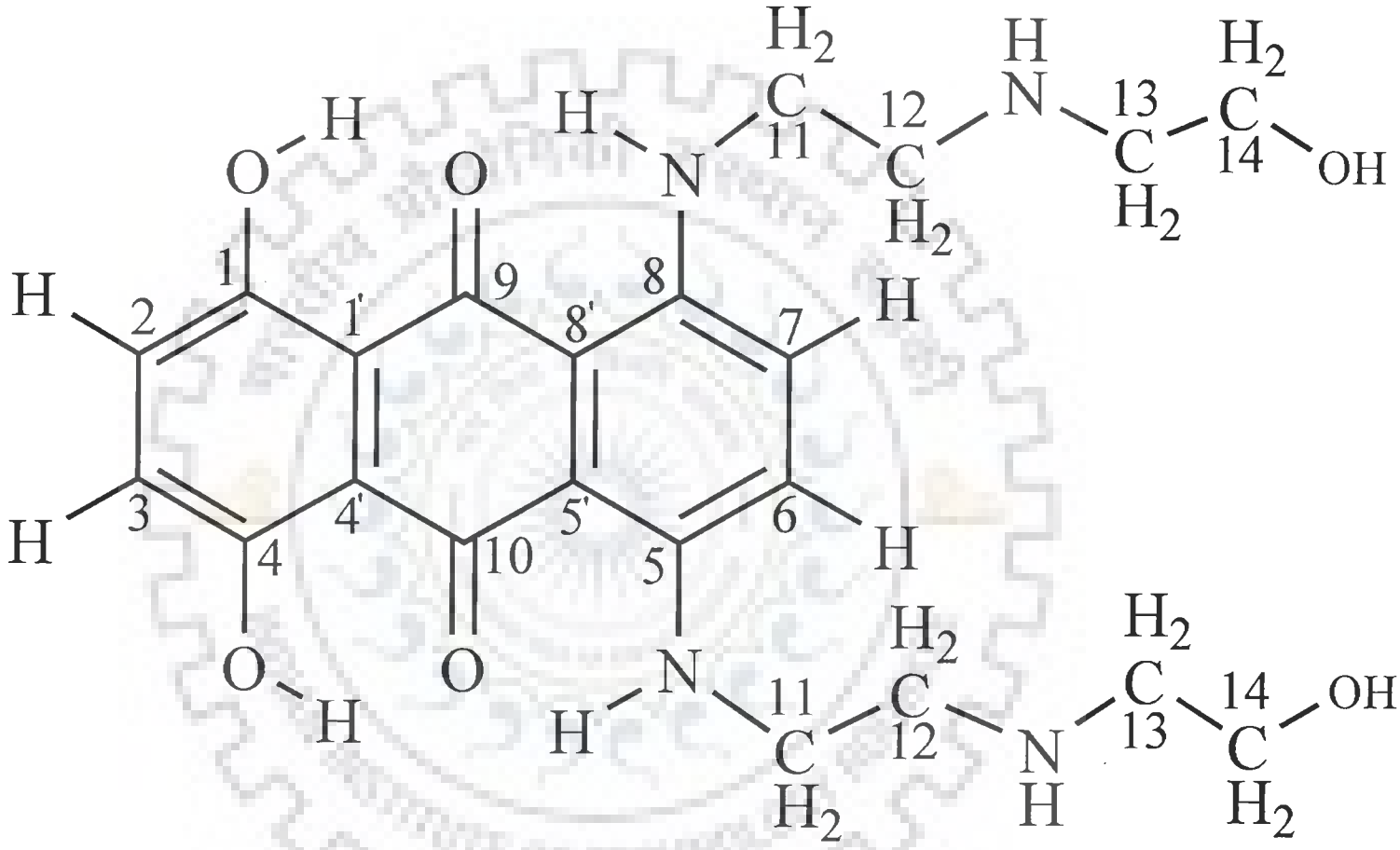

Figure 3.1: Chemical Structure of Mitoxantrone.

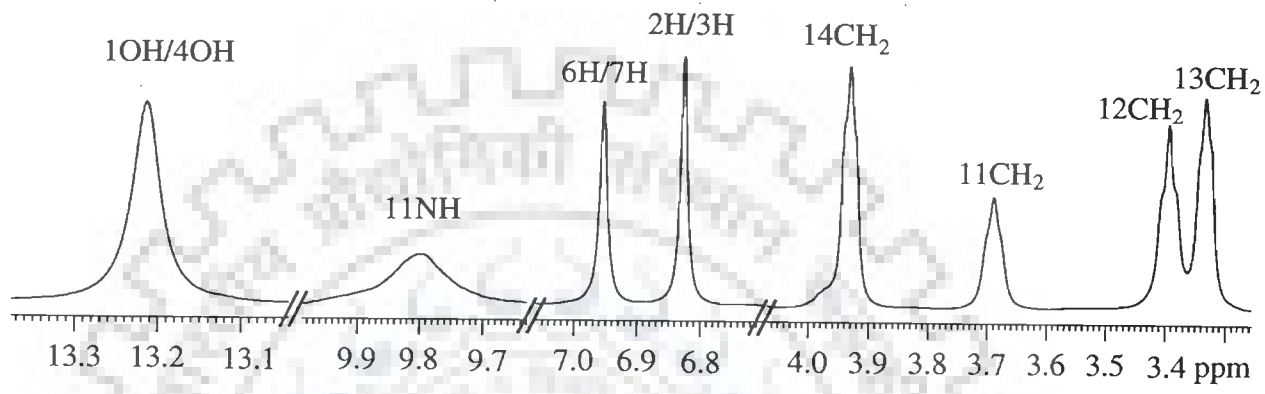

Figure 3.2: Proton NMR spectra of 10 mM mitoxantrone in H_2O at 298K at 500 MHz

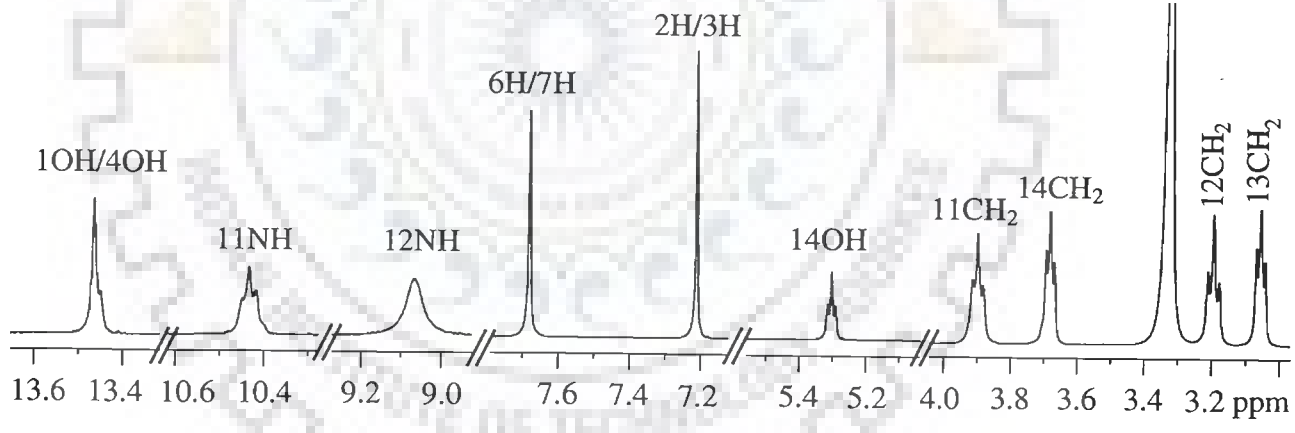

Figure 3.3: Proton NMR spectra of 10 mM mitoxantrone in DMSO–d_6 at 298 K at 500 MHz

3.1.2. Chemical Shift and Coupling Constant

The calculated ^{1}H and ^{13}C chemical shifts were referenced to those of tetra methyl silane (TMS). The absolute ^{1}H and ^{13}C isotropic shielding of TMS based on the B3LYP were calculated at the same basis set levels used in the calculation of mitoxantrone. In this way we compute isotropic shielding to chemical shifts values in ppm, by subtracting the absolute shielding value of each resonance (^{1}H and ^{13}C) from the reference value for TMS. Comparison of experimental Proton and carbon NMR chemical shifts (ppm) with calculated chemical shifts (ppm) by GIAO method using B3LYP/6-31+G (d,p) and 6-31G(d,p) wave functions for mitoxantrone in gas phase, water and DMSO at 298K is depicted in Tables 3.1 and 3.2 respectively. It is of interest, however to see, how good the correlation between experimental and calculated results is? A linear correlation between theoretical and experimental results, both for carbon and proton chemical shifts in various solvent conditions, are clearly seen from Fig. 3.4 with correlation coefficient (r) very close to 1.0 in all cases. These results show that, the dependence of the calculated solvent-induced changes of both ^{1}H and ^{13}C shielding on correlation level to be negligible. The proton and carbon chemical shifts obtained by B3LYP are in very good agreement to that obtained by our NMR measurements, except for 12NH and 14OH in DMSO, thus ascertaining the reliability of the assignment. The inclusion of 12NH and 14OH for correlation decreases correlation to a low value of 0.7. The overall observed differences in individual chemical shift between solvents may possibly be due to the ring current shifts expected for these structures. On the whole good correlation demonstrates that in general B3LYP method predicts the best NMR parameters at the basis set levels

used in our calculations. A quick look at the Tables 3.1 and 3.2 shows that the calculated chemical shifts for ^{1}H are more sensitive to the variation of basis sets as compared to that of ^{13}C. This can be rationalized by the fact that ^{1}H atoms are the smallest of all atoms and are mostly localized on periphery of the molecules therefore their chemical shifts would be more susceptible to intermolecular interactions in the aqueous solutions as compared to that for other heavier atoms. The tabulated value, show that the percentage variation of the difference between measured data and calculated results, is largest for proton than that for the carbon; it being on average 8.2 % and 4.6 % for proton and carbon, respectively. The largest difference between the experimental and calculated carbon chemical shifts is at positions 11C and 14C (Table 3.2). While for proton the difference lies at positions 12NH, 14OH, $11CH_2$ and $13CH_2$ respectively as observed in Table 3.1.

We also observe a noticeable difference in the chemical shifts calculated in the gas phase and PCM solvent conditions. Considering the fact that NMR chemical shifts are affected by the chemical environment of the atoms i.e. molecular conformation and interaction with the solvent molecules, it is seen that the overall agreement between the calculated and measured values both for ^{1}H and ^{13}C chemical shifts is satisfactory.

Further, ^{1}H-^{1}H spin-spin coupling constants (J in Hz) have been calculated using Gauge–Invariant Atomic Orbital (GIAO) method as implemented in Gaussian 03 and compared with experimental values obtained from DQF–COSY Nuclear Magnetic Resonance spectra recorded at 500 MHz in water and DMSO solvents (Table3.3). The spin-spin coupling constant is calculated using B3LYP/6-31G(d,p) and 6-31G+(d,p) levels. The calculated J values are in reasonable agreement with that obtained

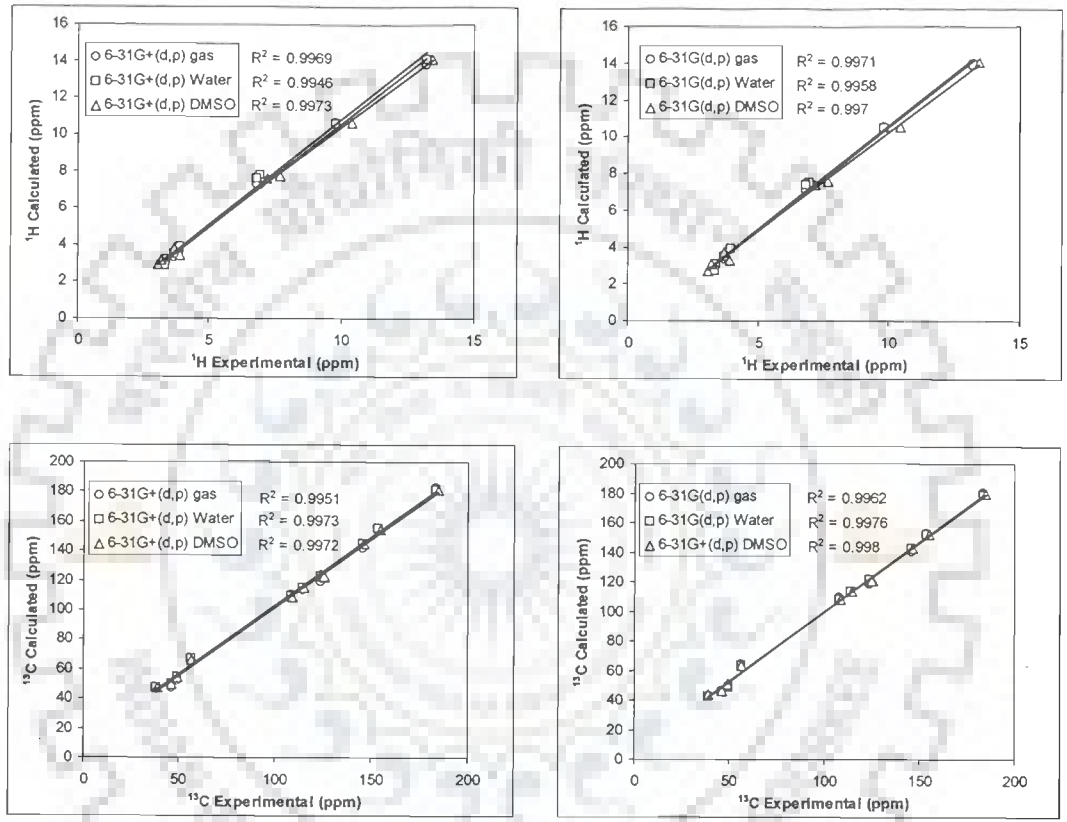

Figure 3.4: Correlation of experimental with calculated proton and carbon NMR chemical shifts of mitoxantrone in water and DMSO environments.

Table 3.1: Comparison of experimental Proton NMR chemical shifts (ppm) with calculated chemical shifts (ppm) by GIAO method using B3LYP/6-31+G(d,p) and 6-31G(d,p) wave functions for mitoxantrone in gas phase, water and DMSO at 298K.

Proton	NMR				CALCULATED						Davies *et.al.* 2001 318K	Lown *et.al.* 1985 298K
	Conc. 10 mM		Conc. 0.01 mM		6-31+G(d,p)	6-31G(d,p)	6-31+G(d,p)	6-31G(d,p)	6-31+G(d,p)	6-31G(d,p)		
	H_2O	DMSO	H_2O	DMSO	gas	gas	H_2O	H_2O	DMSO	DMSO		D_2O
6H/7H	6.95	7.68	7.39	7.61	7.12 / 7.32	6.98 / 7.64	7.75/7.83	7.39/7.60	7.77/7.68	7.52/7.57	7.68	7.02
2H/3H	6.83	7.21	7.13	7.24	7.26 / 7.25	7.04 / 7.03	7.59/7.62	7.39/7.37	7.58/7.60	7.37/7.37	7.30	7.12
11CH_2	3.69	3.90	3.75	3.86	3.27	3.32	3.47	3.44	3.44	3.30	3.96	3.78
12CH_2	3.39	3.19	3.29	3.22	3.14	2.95	3.15	3.06	3.15	3.07		3.39
13CH_2	3.33	3.06	3.10	3.07	2.87	2.75	2.87	2.73	2.88	2.69		3.28
14CH_2	3.93	3.68	3.75	3.66	3.68	3.83	3.83	3.89	3.81	3.74		3.90
11NH	9.79	10.43	10.24	10.48	10.60	10.55	10.59	10.45	10.61	10.54		
12NH	-	9.07	-	8.57	-	-	-	-	2.47	1.90		
1OH/4OH	13.21	13.46	-	13.52	13.83/13.79	13.83/13.84	14.14/14.12	13.93/13.90	14.17/14.10	14.08/14.04		
14OH	-	5.30	-	5.32	-	-	-	-	3.25	2.57		

Table 3.2: Comparison of experimental Carbon NMR chemical shifts (ppm) with calculated chemical shifts (ppm) by GIAO method using B3LYP/6-31+G (d,p) and 6-31G (d,p) wave functions for mitoxantrone in gas phase, Water and DMSO at 298K.

Carbon	NMR		CALCULATED					
	Conc. 10 mM H_2O	Conc. 10 mM DMSO	6-31+G(d,p) gas	6-31G(d,p) gas	6-31+G(d,p) water	6-31G(d,p) water	6-31+G(d,p) DMSO	6-31G(d,p) DMSO
1C/ 4C	153.95	154.94	155.39 / 154.40	152.90 / 152.77	154.90/154.95	152.16/151.91	154.97/154.38	152.13/152.08
2C/3C	124.44	125.63	123.37 / 123.14	121.36 / 121.35	122.39/122.25	121.07/120.75	122.49/122.38	121.01/120.96
5C/8C	146.00	146.64	141.99 / 142.70	140.24 / 140.76	144.91/145.42	142.40/143.02	144.83/145.26	142.44/142.64
6C/7C	123.96	125.49	118.75 / 117.65	118.39 / 117.93	123.03/122.82	121.70/121.83	123.27/121.87	121.72/120.51
9C/10 C	183.77	184.98	182.30 / 181.77	180.32 / 180.22	181.15/181.05	178.26/179.49	181.21/180.81	179.32/179.46
11C	38.67	38.79	46.69	42.12	47.15	42.74	46.87	43.80
12C	46.44	46.32	47.59	46.51	49.32	45.77	49.25	46.57
13C	49.64	49.50	52.2	48.42	54.31	48.24	54.05	50.66
14C	56.73	56.63	65.70	64.27	66.99	63.26	66.47	63.22
5'C/8'C	108.24	109.01	110.47 / 110.53	109.81 / 109.75	109.21/109.27	108.50/107.98	108.84/108.94	108.37/108.15
1'C/ 4'C	114.33	115.09	113.31 / 113.95	113.06 / 113.04	115.37/115.12	114.03/113.93	115.01/115.19	114.05/114.05

except for $14CH_2$–14OH in water and gas phase calculated at the level of theory without diffuse functions. The observed violations in experimental and calculated values for $11CH_2$–$12CH_2$ and $13CH_2$–$14CH_2$ connectivity may arise from the chemical equivalence of methylene protons.

3.1.3. Conformational Studies of Mitoxantrone

3.1.3.1. Restrained Molecular Dynamics

The inter-proton distances were calculated from the ROESY spectra by integrating the volume of cross peaks. The method of integration is based on isolated spin pair approximation in which the spin diffusion is not taken into consideration. The distance between $13CH_2$ and $14CH_2$ protons, r = 2.4 Å, is used as an internal reference to calculate the distances of other protons from the NOE intensity. Pseudo atom corrections were used for methyl and other equivalent protons. The force constants for NOEs were held constant at 25 Kcal $mole^{-1}$ $Å^{-2}$. Total of 10 and 16 distance restraints (Table 3.4) were used in the structure calculations using Restrained Molecular Dynamics in water and DMSO respectively. The connectivities and inter-proton distances (Å) from ROESY spectra of the mitoxantrone and the corresponding distances obtained from optimized rMD structure are shown in Table 3.4. rMD simulations were carried out for 25 ps to search for optimum conformation. During the final equilibrium stage, there is no significant change in either the total potential energy or restraint deviation energy. The root mean square deviation between the rMD structures is very low; this is generally taken as an indication that the convergence has been achieved. The average conformer of the 25 structures saved at a regular interval of 1 ps is used for the structural analysis.

Table 3.3: Observed ^1H-^1H coupling constants, (J in Hertz) for mitoxantrone in H_2O, D_2O and in DMSO, along with calculated spin-spin coupling using B3LYP/6-31+G(d,p) and 6-31G(d,p).

Connectivity	NMR		CALCULATED					
	H_2O	DMSO	6-31+G(d,p) gas	6-31G(d,p) gas	6-31+G(d,p) water	6-31G(d,p) water	6-31+G(d,p) DMSO	6-31G(d,p) DMSO
$11CH_2$–$12CH_2$	6.20	6.40	7.44	7.52	7.60	7.60	7.59	7.73
$13CH_2$–$14CH_2$	4.98	3.84	4.00	3.73	3.94	3.75	3.87	3.87
11NH–$11CH_2$	4.80	4.60	4.67	4.67	5.02	5.05	5.01	4.99
12NH–$12CH_2$	-	-	3.37	2.67	3.30	2.64	3.21	3.35
$14CH_2$–14OH	-	7.00	7.49	4.20	7.03	3.52	7.22	7.54

Table 3.4: The interproton distances (Å) of mitoxantrone obtained from 300ms ROESY spectra in water and DMSO recorded at 298K. $13CH_2$–$14CH_2$ = 2.4 Å is used as reference peak.

S. No.	Connectivity	NMR Distances (Å)	NMR Distances (Å)	Distance obtained from average rMD structure (Å)	
		H_2O	DMSO	H_2O	DMSO
1.	$13CH_2$–$14CH_2$	2.40	2.40	2.51	2.49
2.	$11CH_2$–$12CH_2$	2.84	2.49	2.65	2.41
3.	$12CH_2$–$14CH_2$	2.90	3.52	3.07	3.97
4.	$11CH_2$–$13CH_2$	2.94	3.13	3.12	3.40
5.	$12CH_2$–$13CH_2$	3.21	2.79	3.37	3.01
6.	$11CH_2$–$14CH_2$	-	3.36	-	3.45
7.	$11CH_2$–6H/7H	2.21	2.34	2.63	2.73
8.	$12CH_2$–6H/7H	2.65	2.76	2.83	2.80
9.	11NH–$11CH_2$	2.79	3.22	2.67	2.81
10.	11NH–$12CH_2$	3.48	3.62	3.39	3.62
11.	11NH–$13CH_2$	-	5.06	-	5.02
12.	11NH–6H/7H	4.08	4.19	3.86	3.77
13.	12NH–$12CH_2$	-	2.68	-	2.54
14.	12NH–$13CH_2$	-	3.14	-	2.79
15.	12NH–6H/7H	-	4.62	-	4.73
16.	1OH/4OH–2H/3H	-	4.06	-	3.70

Table 3.5, 3.6 and 3.7 indicates an assessment of refined average structure in terms of structural and energy parameters with respect to the atomic coordinates and compared with the structure generated from the atomic coordinates of published mitoxantrone in complex with protein kinase B (Wehenkel *et al.* 2006). The total potential energy of final structures is 173.05 Kcal $mole^{-1}$ and 170.90 Kcal $mole^{-1}$ for water and DMSO respectively is compared well with enegetics of mitoxantrone in complex with a biomolecule, 188.53 Kcal $mole^{-1}$. The forcing potential, which indicates contribution to potential energy due to violation of experimental distance, exhibit much lower values for all the final structures (3.99 Kcal $mole^{-1}$ and 7.6 Kcal $mole^{-1}$ for water and DMSO). As observed from Fig. 3.6, the aromatic anthraquinone chromphore of mitoxantrone is highly planar also evidenced by very small values for the out of plane angle for the optimized conformations. The structures maintain the hydrogen bonding formed between the side chain amino groups (11NH) and hydroxyl group (OH1/OH4) of the anthraquinone chromophore, which are situated sufficiently close to each other in space.

3.1.3.2. Quantum Chemical Calculations

The distinctive feature of mitoxantrone molecule is the presence of large number of ionizable groups (hydroxyl and amino) because of this, in aqueous solutions mitoxantrone can exist as various ionic forms and conformations. In order to establish the relevance of conformational and electronic properties of mitoxantrone to its binding with biological target mainly DNA, we performed a detailed computational study of mitoxantrone in water and DMSO solvent conditions using B3LYP functional with 6-31G(d,p) and 6-31G+(d,p) wave functions. Calculations were performed first in vacuum conditions and later with the dielectric solvent effects (ε = 78.39 for water and ε = 46.7

for DMSO) included in the calculation using PCM-IEF model, with total charge on the molecule Z = 0. Conformational parameters, bond length, bond angle and dihedral angles for the optimized structures calculated are compared against crystal structure data and NMR solution structure in Tables 3.5 and 3.6. The optimized geometries are shown in Fig. 3.5. The calculated results show that the anthracene-9, 10-dione ring system is essentially planar in all cases with the nitrogen atoms (N11) adopting a planar sp^2 conformation with ring system. The presence of hydrogen bonding between aromatic NH and the quinone carbonyl functions limits the side chain conformational freedom to an extent and makes both 11NH amino residues coplanar with the ring system. The hydroxyl groups attached to the ring chromophore OH1/OH4 also forms hygrogen bond with the quinone carbonyl group. The various solvent conditions do not change the optimized geometry significantly and hence the energy of the final optimized geometry (Fig.3.5). Infact, the presence of diffuse function in the calculations improves the energy of the optimized geometry (Table 3.5) particularly for a molecule like mitoxantrone with ionizable groups (hydroxylic and amino). Unfortunately calculations using such functions are computationally expensive and time consuming. Further, the influence of the solvent on the geometrical parameters is found very negligible as can be seen from the tabulated values in Table 3.5. It is also noticed that all the calculated bond lengths are very close to the present solution structure based on NMR experimental data and also compare reasonably well with the crystal structure data reported in the literature (Wehenkel *et al.* 2006), except the bond length of the carbonyl oxygens C9-O9 and C10-O10, which are slightly longer compared to the experimental value. Also the calculated bond angles are

close to the present experimental results and X-ray measurements (Table3.5). On comparing our calculated bond length and bond angle structural parameters with solution

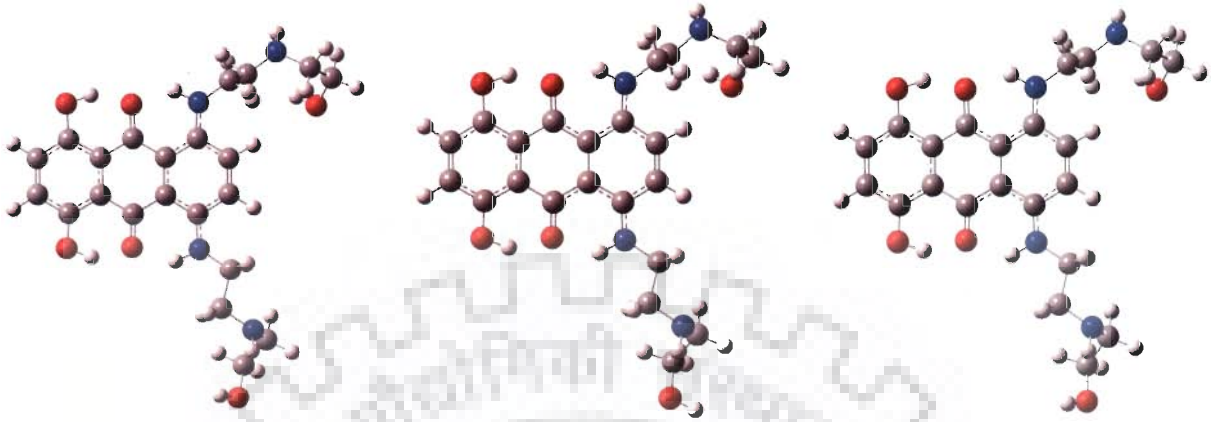

(a) (b) (c)

Figure 3.5: Gaussian optimized geometries using B3LYP/6-31+G(d,p) wave function for mitoxantrone in (a) gas phase, (b) water and (c) DMSO at 298K

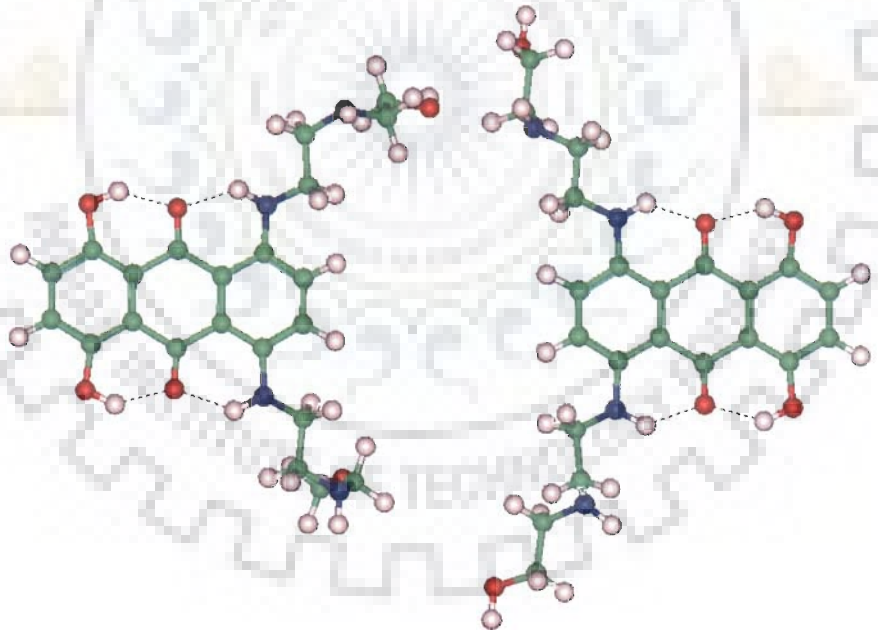

(a) (b)

Figure 3.6: NMR calculated average conformational geometry of mitoxantrone obtained during 25 ps simulation. (a) Water (b) DMSO

Table 3.5: Comparison of structural parameters for the optimized structures calculated using B3LYP/6-31+G(d,p) and 6-31G(d,p) wave functions in water and DMSO.

Parameter	6-31+G(d,p) water	6-31G(d,p) water	6-31+G(d,p) DMSO	6-31G(d,p) DMSO	6-31+G(d,p) gas	6-31G(d,p) gas	rMD H2O	rMD DMSO	X-ray [Wehenkel *et al.*2006]
Bond length (Å)									
C1-O1	1.35	1.35	1.35	1.35	1.34	1.34	1.35	1.37	1.35
C4-O4	1.35	1.35	1.35	1.35	1.34	1.34	1.35	1.37	1.35
C9-O9	1.28	1.28	1.28	1.28	1.27	1.27	1.23	1.24	1.23
C10-O10	1.28	1.28	1.28	1.28	1.28	1.27	1.23	1.24	1.23
C5-N11	1.35	1.35	1.35	1.35	1.36	1.36	1.46	1.49	1.33
C8-N11	1.36	1.35	1.35	1.36	1.36	1.36	1.46	1.50	1.33
C11-C12	1.54	1.54	1.54	1.54	1.54	1.54	1.49	1.55	1.53
C12-N12	1.46	1.46	1.46	1.46	1.46	1.46	1.45	1.46	1.47
N12-C13	1.46	1.47	1.47	1.46	1.46	1.46	1.48	1.48	1.48
C13-C14	1.53	1.53	1.53	1.53	1.53	1.53	1.52	1.52	1.54
C14-O14	1.43	1.43	1.43	1.43	1.43	1.43	1.38	1.34	1.45
N11-C11	1.46	1.45	1.46	1.45	1.45	1.45	1.45	1.50	1.46
Bond angle (deg)									
C7-C8-N11	119.53	119.41	119.56	119.80	120.01	120.01	119.62	119.35	117.31
C6-C5-N11	119.15	119.28	119.10	119.29	119.48	119.53	120.02	119.46	121.09
C8-N11-C11	127.07	126.29	127.20	126.97	126.69	126.09	118.36	124.24	120.70
C5-N11-C11	125.77	125.68	125.84	125.78	125.41	125.37	120.23	124.84	121.74
N11-C11-	112.93	113.38	113.01	113.24	113.61	113.01	115.05	114.35	110.28
C11-C12-	110.94	110.90	110.79	110.47	110.82	111.69	113.87	112.74	109.47
C12-N12-	117.06	117.62	116.56	116.32	118.87	119.05	112.24	117.15	112.83
N12-C13-	116.21	118.19	115.97	116.36	116.23	118.63	106.15	112.07	110.86
C13-C14-	114.25	111.56	113.85	114.00	114.05	113.82	112.76	110.05	112.81
C2-C1-O1	117.82	117.94	117.87	117.95	117.60	117.71	121.76	118.71	120.39
C3-C4-O4	117.84	117.95	117.87	117.97	117.65	117.77	121.32	118.67	119.20

Table 3.6: Comparison of Side chain torsional angles for the optimized structures calculated using B3LYP/6-31+G(d,p) and 6-31G(d,p) wave functions with that of structure obtained from NMR calculations and crystal structure data.

Parameter	6-31+G(d,p) water	6-31G(d,p) water	6-31+G(d,p) DMSO	6-31G(d,p) DMSO	6-31+G(d,p) gas	6-31G(d,p) gas	rMD H2O	rMD DMSO	Xray [Wehenkel *et al.* 2006]
C5-N11-C11-C12	179.16	175.70	178.75	179.91	178.33	177.26	82.63	75.01	-165.52
C8-N11-C11-C12	83.90	85.50	83.93	81.52	84.96	83.79	92.83	77.43	98.10
N11-C11-C12-N12	177.97	179.06	176.04	177.55	177.72	179.44	173.40	90.50	170.11
	176.19	176.23	177.38	175.44	176.33	177.54	-179.41	159.55	-167.27
C11-C12-N12-C13	91.86	72.44	90.82	94.23	89.02	70.50	79.78	72.50	114.17
	-87.14	-88.17	-86.96	-87.32	-87.10	-89.49	-80.55	-40.00	-109.60
C12-N12-C13-C14	90.79	60.85	91.89	82.79	89.31	64.73	81.35	114.02	90.93
	-71.55	-75.12	-71.76	-73.40	-67.09	-76.30	-80.40	-115.20	-102.42
N12-C13-C14-O14	-65.69	-76.23	-65.32	-64.86	-64.93	-73.93	176.39	-163.45	-72.50
	-61.02	-62.58	-67.25	-65.41	-60.62	-59.60	-176.04	165.66	-32.45
C7-C8-N11-C11	4.91	-2.64	3.48	7.66	-2.73	-0.30	-5.72	12.73	74.21
C6-C5-N11-C11	2.26	1.98	-0.99	-0.19	-0.13	1.28	7.08	5.55	-21.80

Data shown in duplicate corresponds to the different amino alkyl side chain of mitoxantrone

Table 3.7: Energy terms (Kcal mol^{-1}) for average rMD structure and X-ray structure.

Energy	rMD structure water	rMD structure DMSO	Xray [Wehenkel *et al.* 2006]
Total	173.05	170.90	188.53
Electrostatic	47.29	41.70	43.02
Vdw	125.75	129.20	145.51
Out of plane	0.006	0.002	-
Restraint Violation	3.99	7.60	-

Table 3.8: Calculated Dipole moment, Total, HOMO and LUMO energies of MTX in gas, water and DMSO solvents, using B3LYP/6-31+G(d,p) and 6-31G(d,p) wave functions.

Basis set	solvent	Total energy (Hartree)	HOMO (eV)	LUMO (eV)	Dipole moment (Debye)
6-31+G(d,p)	gas	-1525.6668	-7.208	-2.990	5.4085
	water	-1525.7148	-7.222	-3.039	12.0398
	DMSO	-1525.7121	-7.235	-3.054	8.7135
6-31G(d,p)	gas	-1525.6046	-6.775	-2.531	6.2241
	water	-1525.6423	-6.913	-2.699	10.3573
	DMSO	-1525.6389	-6.949	-2.732	7.6235
6-31G* Riahi *et al.* 2008	gas	-	-8.42	-1.27	4.415

parameters we found that the maximum variation in the calculated and measured values is less than 5%. The side chain $(CH_2)_2$-NH-$(CH_2)_2$-OH of mitoxantrone has a fairly flexible structure; this has made it possible to reveal a number of stable conformations for the molecule with similar potential energy terms as observed from Fig. 3.6. Systematic measure of the various side chain torsional angles of mitoxantrone are shown in comparison with our NMR calculated structure and other published data in Table 3.6. Overall the side chains adopt a similar conformation in all the Gaussian optimized structures, irrespective of the solvent conditions used (Fig.3.5). The NMR calculated structure in water more closely resembles the Gaussian optimized structures except for

the torsion N12-C13-C14-O14. This deviation could be due to lack of experimental NMR distance constraint for the terminal OH group. The side chains were more open in DMSO solution structure as compared to the conformation in water. In polar solvents, the solvation will compensate to a large measure the electrostatic interactions and will lead to stabilization of the energy levels of the conformers. It is apparent from the values of torsions C7-C8-N11-C11 and C6-C5-N11-C11 from Table 3.6 that the $11CH_2$ group adopts a position planar with the ring structure in the calculated structures. This is attributed to the presence of hydrogen bonding between aromatic NH and the quinone carbonyl functions, which limits the side chain conformational freedom to an extent and makes both NH amino residues coplanar with the ring system. Similar observation was reported in earlier theoretical studies on mitoxantrone and its analogues (Zaggato *et al.* 1997; Almond *et al.* 1983). The crystal structure of mitoxantrone with protein kinase B (Wehenkel *et al.* 2006) shows that anthraquinone chromophore adopts a planar structure but the torsions C7-C8-N8-C11 and C6-C5-N5-C11 adopt a non-coplanar angle supposedly due to binding of mitoxantrone with the biomolecule. The recent theoretical results of Riahi *et al.* 2008 report that the side chains are out of plane of the molecule and also the anthraquinone chromophore of mitoxantrone adopts a non-planar structure. This could be due to the loss of hydrogen bonding between aromatic NH and the quinone carbonyl functions. The bias could have emerged from the initial PM3 calculations used by them to optimize the geometry before optimizing using the stringent DFT approach.

Electronic transfer plays an important role in the mechanism of action of anticancer drugs. Therefore it is of interest to quantify electron affinity that is the ability of the molecule to undergo reduction by accepting an additional electron. We used

abinitio methods to predict the LUMO energy for the mitoxantrone in different solvent conditions and attempted to correlate with the biological activity of the molecule. The LUMO energy in DMSO is lower compared to that in water and gas respectively (Table 3.8). Which confirms mitoxantrone can be more easily reduced in DMSO environment than in water. Also it is known that dipole moment being the first derivative of energy with respect to an electric field is taken as a measure of symmetry of molecular charge distribution. Higher value of dipole moment gives a strong correlation for the electrostatic interaction between drug and DNA. From the Table 3.8, we find that our calculated values are higher than the values obtained by Riahi *et al.* 2008 using similar calculations.

3.2. CONLCUSIONS

The geometry of mitoxantrone is fully optimized without any constraints at the B3LYP/6-31G+(d,p) and B3LYP/6-31G(d,p) levels in gas water and DMSO environments. ^{1}H and ^{13}C chemical shifts, structural parameters and coupling constants of mitoxantrone were calculated and compared with experimental data. We found that all the calculated bond lengths and bond angles compare reasonably well with the experimental structure and the crystal structure data reported in literature. The side chains adopt a similar conformation in all the Gaussian optimized structures, irrespective of the solvent conditions used. Further, the geometrical parameters are relatively less influenced by the solvent effect but a noticeable change is seen in the values of the chemical shift due to inclusion of solvent. An overall analysis show that the B3LYP/6-31G+(d,p) level of theory predicts results which are quantitatively good and compare well with the experiment.

Chapter 4

Studies on Complex of Mitoxantrone with d-(TGATCA)$_2$ by Phosphorous-31, Proton Nuclear Magnetic Resonance Spectroscopy and Restrained Molecular Dynamics Approach

Specific intermolecular contacts between drug and DNA molecules and knowledge of detailed conformational changes at each phosphate site is important to understand the drug-DNA interactions This chapter contains the following studies of the complex of mitoxantrone-d-(TGATCA)$_2$ by one- and two-dimensional ^{31}P and ^{1}H NMR followed by restrained molecular dynamics simulations:

- 1D ^{1}H and ^{31}P NMR titration studies of mitoxantrone-d-(TGATCA)$_2$ complex at various drug (D)/DNA duplex (N) ratios of 0.2, 0.35, 0.5, 0.65, 0.8, 1.0, 1.1, 1.2, 1.3, 1.4, 1.5, 1.75, 2.0 at 278 K, 298 K and 318 K in 90% water and 10% D_2O.
- The temperature dependence of ^{31}P and ^{1}H chemical shift of 2.76 mM d-(TGATCA)$_2$ duplex in the range of 275 - 328 K.
- Temperature dependence of ^{31}P and ^{1}H NMR of the mitoxantrone-d-(TGATCA)$_2$ complex having D/N = 1.0, 1.5 and 2.0 in the range of 275 - 328 K.
- 2D ^{31}P - ^{31}P exchange spectra of drug-DNA complex by a phase-sensitive NOESY using mixing time of 200 ms at 278 K for D/N = 0.5, 1.0, 1.5 and 2.0.
- 2D NOESY ^{1}H - ^{1}H at D/N = 1.0, 1.5, 2.0 using mixing time τ_m = 100, 200, 300 ms at 278 K in 90% H_2O and 10% D_2O.
- Diffusion Ordered Spectroscopy (DOSY) experiments of complex of mitoxantrone-d-(TGATCA)$_2$ and uncomplexed mitoxantrone.

- Restrained molecular dynamics studies on the solution structure for the complex of mitoxantrone with d-$(TGATCA)_2$ using inter-proton distances obtained from 2D NOESY as restraints.
- Analysis of the converged structure in terms of time average for the various conformational and helical parameters.

4.1 RESULTS AND DISCUSSION

4.1.1 Phosphorous-31 NMR Studies of Mitoxantrone-d-$(TGATCA)_2$ Complex

For the purposes of this discussion, the positions of the bases in the hexamer are designated as follows: d–$(T1pG2pA3pT4pC5pA6)_2$. The assignment of phosphate resonances of hexamer d–$(TGATCA)_2$ were already done in our lab using ^{31}P - ^{1}H Heteronuclear Multiple Bond Correlation (HMBC) 2D NMR at 278K (Fig. 4.1). Three bond scalar coupling of ^{31}P with $(H3')_n$ and $(H5'/H5'')_{n+1}$ protons as well as four bond coupling with $(H4')_n$ and $(H4')_{n+1}$ protons are expected to manifest as cross peaks in the 2D ^{31}P - ^{1}H correlation map. Based on the proton assignments of the hexanucleotide (Barthwal et al, 2004), the assignment of ^{31}P nucleotide resonances were quite straightforward using the three bond scalar coupling of ^{31}P with $(H3')_n$ of the sugar residue. In addition ^{4}J couplings of the phosphorous to the $(H4')_{n+1}$ protons of the sugar residues are also clearly evident. Accordingly the phosphate resonances at -2.31, -2.15, -1.97, -1.94 and -1.66 were assigned as A3pT4, T4pC5, T1pG2, G2pA3 and C5pA6 respectively at 278K.

4.1.1.1. Chemical Shift

The binding of mitoxantrone to d–(TGATCA)$_2$ was investigated by titrating a known concentration of mitoxantrone (25mM) successively to a fixed hexanucleotide concentration of 2.76mM (duplex) to arrive at Drug to Nucleotide (D/N) stoichiometric ratios from 0 to 2.0. Fig. 4.2 (a-c), 4.3 (a-c), Table 4.1 and 4.2 show the change in ^{31}P chemical shift due to binding as a function of added mitoxantrone at 278K, 298K and 318K. There are only five resonances observed on the formation of the DNA-drug complex and they show a moderate shift as compared to the resonances from free hexamer, but broaden severely with increase in D/N ratio, thus indicates that there is a fast chemical exchange on the NMR time scale. It is observed that the T1pG2, G2pA3 and T4pC5 resonances shift ($\Delta\delta = \delta^b - \delta^f$) downfield by 0.16 to 0.26, 0.13 to 0.23 and 0.03 to 0.05 ppm, respectively for the complexes of D/N 1 to 2.0 at 278K. C5pA6 resonance shift upfield to a lesser extent by -0.05 ppm. All five phosphate resonances showed downfield shift in the titration experiments performed at 298K and 318K. Maximum shift were observed for T1pG2 and G2pA3 resoanances in all three temperatures. This shows that T1pG2 is more involved in binding to mitoxantrone than other bases on the hexamer and since G2pA3 is adjacent to T1pG2 thus got affected. T4pC5 and C5pA6 shows marginal shift, but comparatively in lesser extent than observed for T1pG2 and G2pA3 resonances. A3pT4 was least shifted in all three temperatures studied. This shows that the mitoxantrone is interacting with d-(TGATCA)$_2$ at the T1pG2 site and hence other sites are least affected.

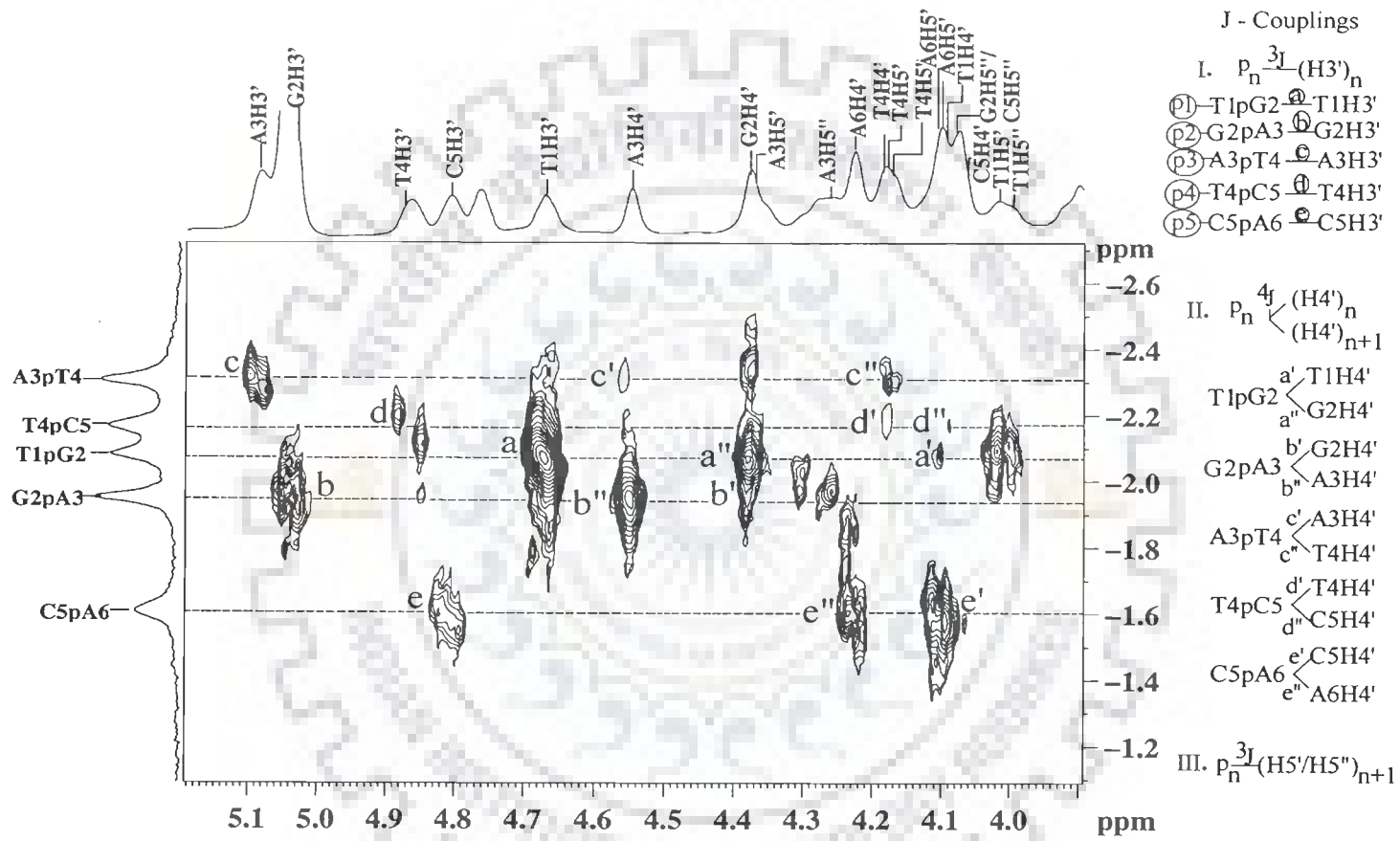

Figure 4.1: Two Dimensional $^{31}P - {}^{1}H$ Heteronuclear Multiple Bond Correlation (HMBC) spectra of d–$(TGATCA)_2$ at 278 K (reprinted from Prashansa, 2007).

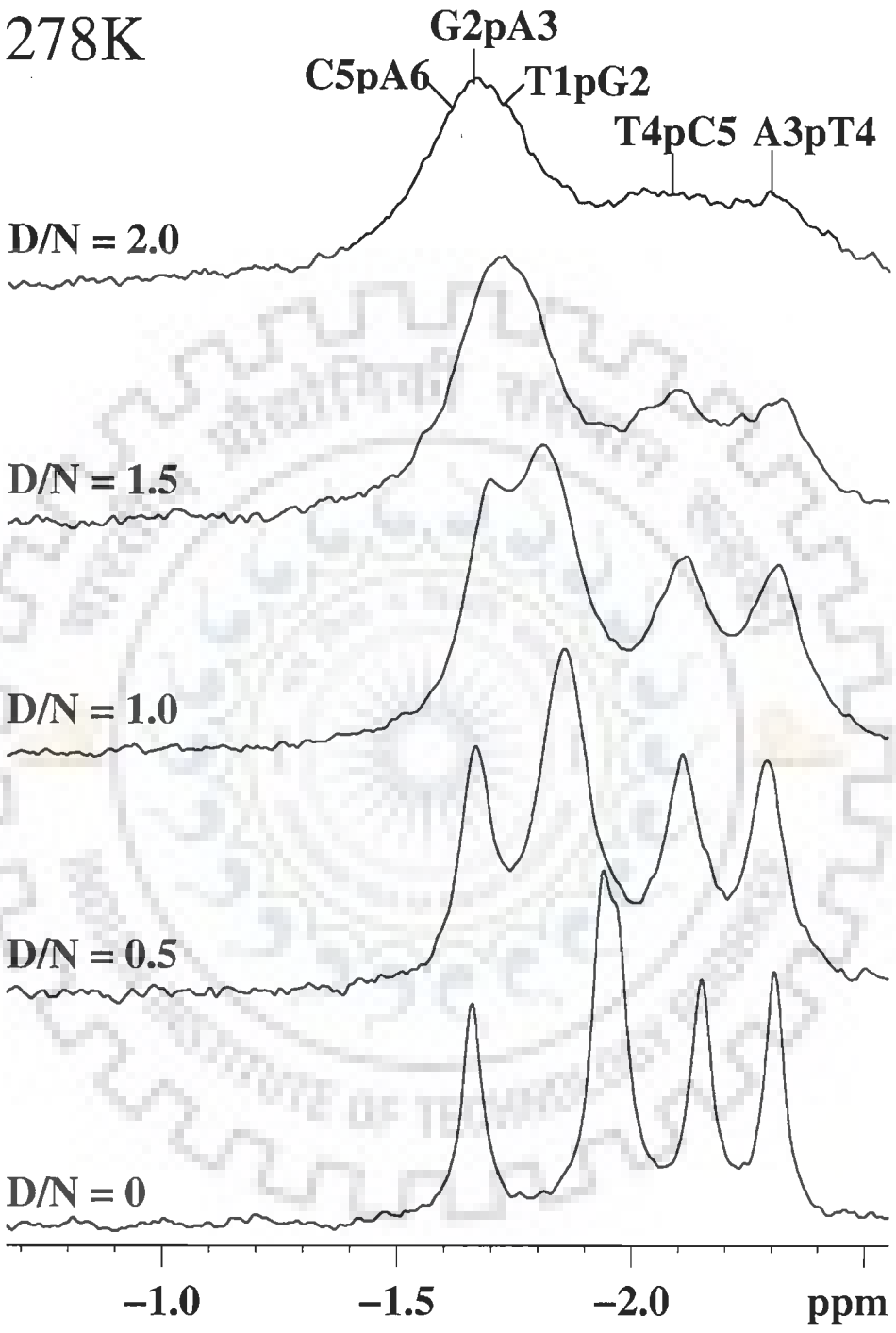

(Fig. 4.2a)

Figure 4.2 (a-c): Proton decoupled ^{31}P NMR spectra of 2.76 mM d-$(TGATCA)_2$ in uncomplexed state and complexed with mitoxantrone with increasing drug (D) to nucleic acid duplex (N) ratio, D/N, at (a) 278 K, (b) 298K and (c) 318K.

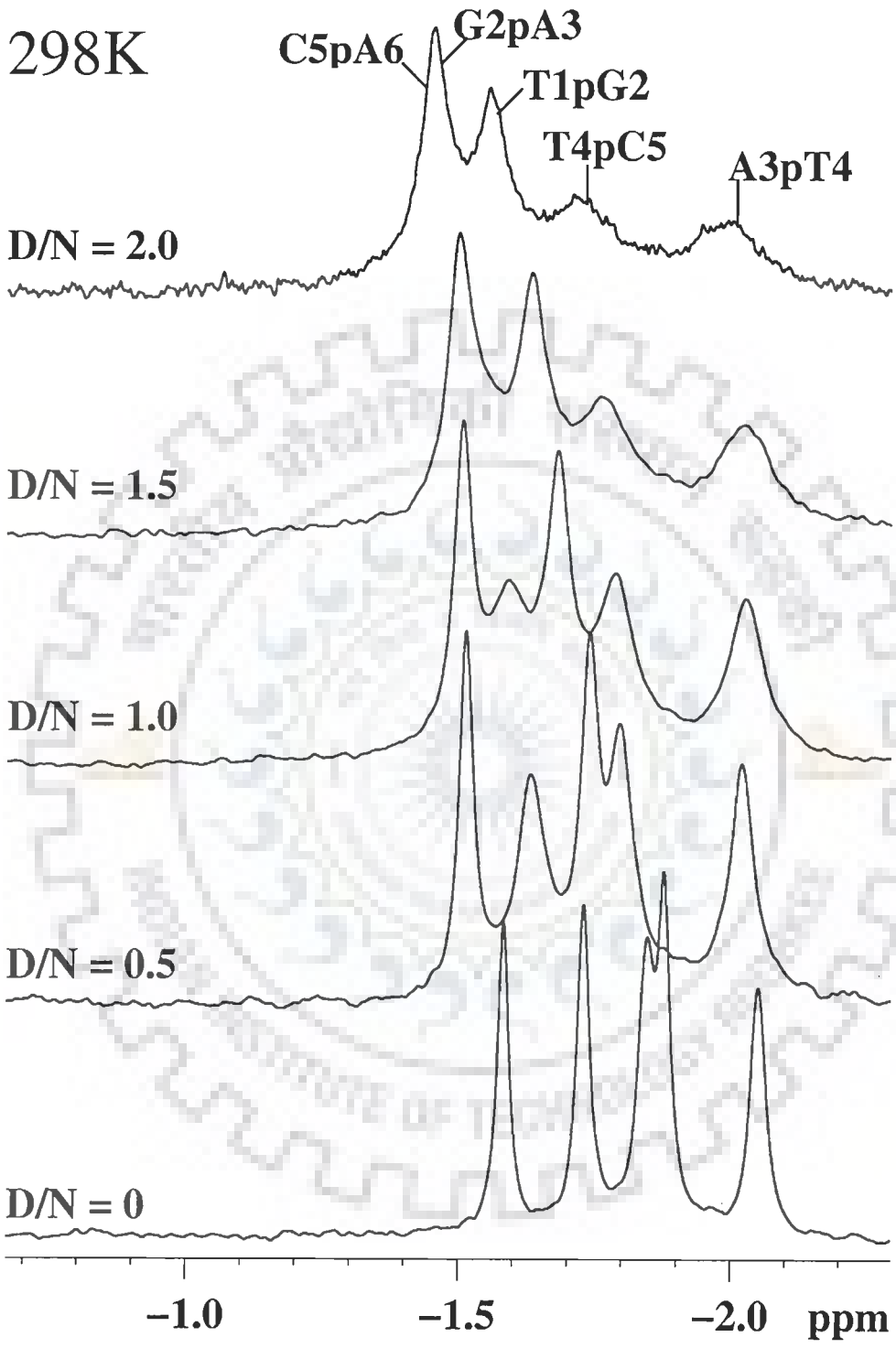
298K
C5pA6
G2pA3
T1pG2
T4pC5
A3pT4
D/N = 2.0
D/N = 1.5
D/N = 1.0
D/N = 0.5
D/N = 0
−1.0
−1.5
−2.0
ppm

(Fig. 4.2b)

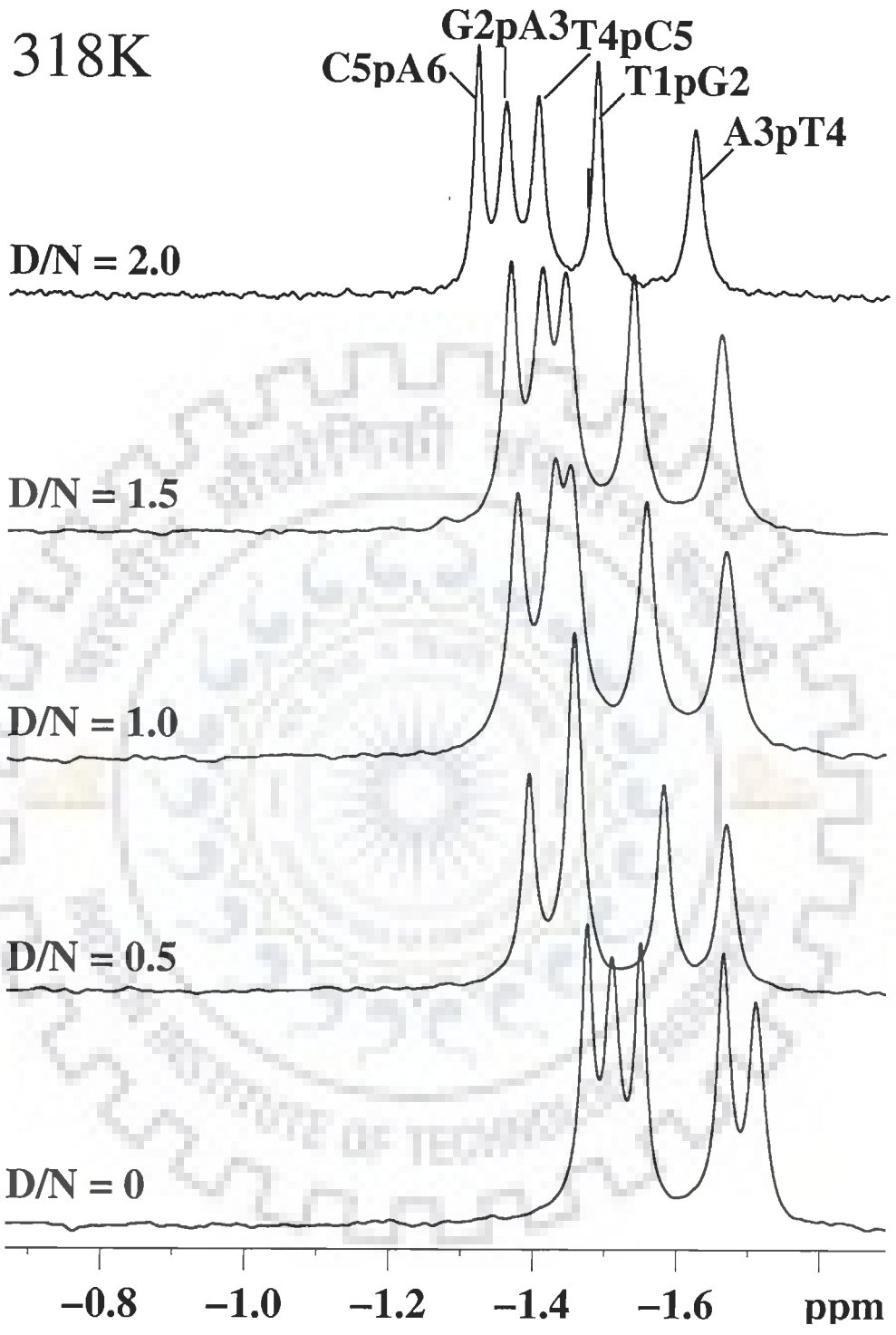
318K
G2pA3T4pC5
C5pA6
T1pG2
A3pT4
D/N = 2.0
D/N = 1.5
D/N = 1.0
D/N = 0.5
D/N = 0
−0.8
−1.0
−1.2
−1.4
−1.6
ppm

(Fig. 4.2c)

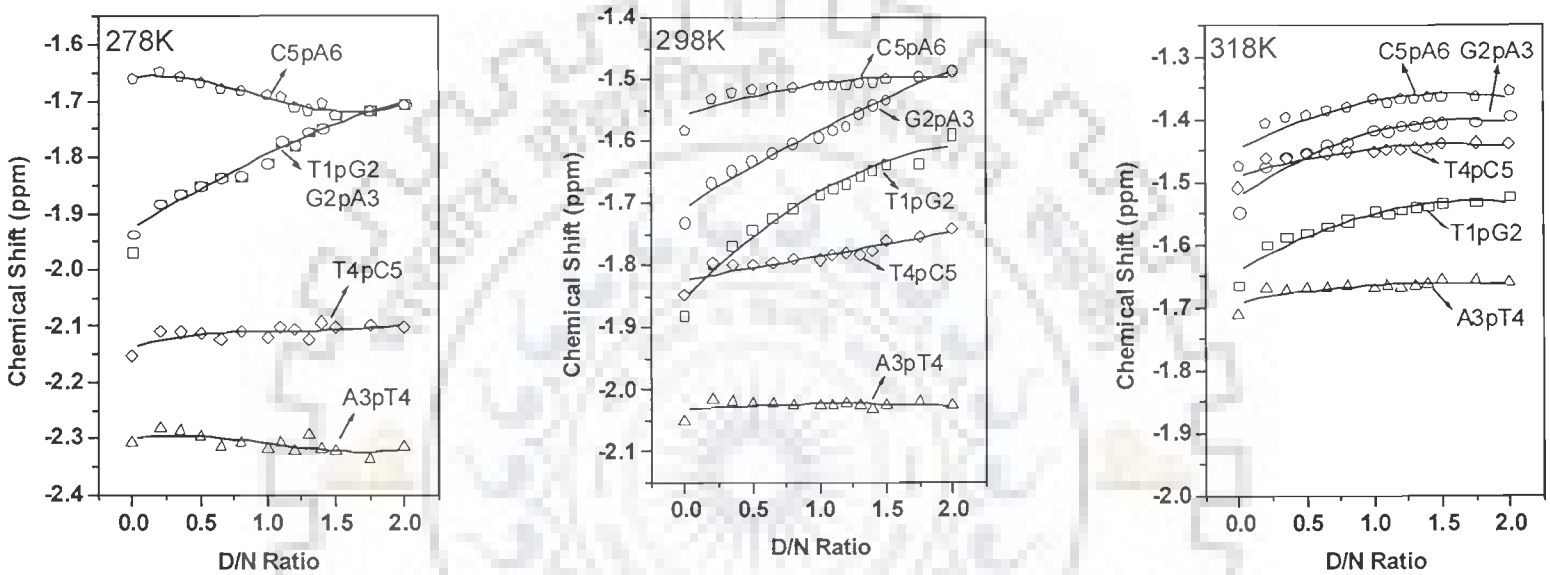

(a) (b) (c)

Figure 4.3 (a-c): ^{31}P Chemical shift variation of d–(TGATCA)$_2$ in complex with mitoxantrone, as a function D/N ratio (a) at 278K (b) at 298K (c) at 318K. (□ - T1pG2; ○ - G2pA3; Δ – A3pT4; ◇ - T4pC5; ⬡ - C5pA6)

Table 4.1: Chemical shift of ^{31}P resonances of the phosphate groups of DNA hexamer, in complex of mitoxantrone with d–$(TGATCA)_2$ at 278 K, 298 K, 318 K with different drug (D) to nucleic acid duplex (N) ratios (D / N). +ve $\Delta\delta$ indicates downfield shift whereas -ve $\Delta\delta$ indicates upfield shift. $\Delta\delta = (\delta_{D/N=2.0} - \delta_{D/N=0})$.

	278 K					298 K					318 K				
D/N	T1pG2	G2pA3	A3pT4	T4pC5	C5pA6	T1pG2	G2pA3	A3pT4	T4pC5	C5pA6	T1pG2	G2pA3	A3pT4	T4pC5	C5pA6
0.00	-1.969	-1.938	-2.308	-2.152	-1.662	-1.879	-1.731	-2.052	-1.847	-1.584	-1.665	-1.550	-1.710	-1.509	-1.475
0.20	-1.884	-1.884	-2.281	-2.108	-1.648	-1.797	-1.665	-2.015	-1.797	-1.530	-1.601	-1.477	-1.668	-1.463	-1.408
0.35	-1.866	-1.866	-2.286	-2.111	-1.656	-1.767	-1.645	-2.018	-1.800	-1.520	-1.589	-1.461	-1.672	-1.461	-1.396
0.50	-1.852	-1.852	-2.295	-2.114	-1.668	-1.742	-1.630	-2.021	-1.799	-1.515	-1.582	-1.456	-1.669	-1.456	-1.394
0.65	-1.837	-1.837	-2.313	-2.124	-1.678	-1.723	-1.616	-2.021	-1.795	-1.513	-1.572	-1.445	-1.668	-1.454	-1.386
0.80	-1.835	-1.835	-2.306	-2.109	-1.683	-1.705	-1.601	-2.027	-1.790	-1.513	-1.564	-1.437	-1.666	-1.452	-1.382
1.00	-1.812	-1.812	-2.317	-2.121	-1.691	-1.683	-1.592	-2.027	-1.791	-1.508	-1.550	-1.419	-1.671	-1.452	-1.369
1.10	-1.774	-1.774	-2.307	-2.101	-1.694	-1.673	-1.580	-2.027	-1.782	-1.507	-1.553	-1.422	-1.667	-1.449	-1.374
1.20	-1.780	-1.780	-2.320	-2.106	-1.712	-1.666	-1.574	-2.021	-1.780	-1.507	-1.545	-1.414	-1.668	-1.449	-1.369
1.30	-1.756	-1.756	-2.294	-2.124	-1.717	-1.655	-1.552	-2.025	-1.783	-1.506	-1.543	-1.413	-1.666	-1.447	-1.368
1.40	-1.750	-1.750	-2.318	-2.093	-1.704	-1.644	-1.541	-2.031	-1.778	-1.504	-1.539	-1.409	-1.664	-1.445	-1.366
1.50	-1.727	-1.727	-2.320	-2.103	-1.727	-1.635	-1.532	-2.025	-1.760	-1.500	-1.535	-1.408	-1.658	-1.440	-1.364
1.75	-1.718	-1.718	-2.315	-2.098	-1.718	-1.634	-1.495	-2.019	-1.755	-1.495	-1.534	-1.405	-1.658	-1.438	-1.365
2.00	-1.707	-1.707	-2.314	-2.102	-1.707	-1.588	-1.486	-2.025	-1.741	-1.486	-1.523	-1.397	-1.659	-1.440	-1.356
$\Delta\delta$	+0.262	+0.231	-0.006	+0.050	-0.045	+0.291	+0.245	+0.027	+0.106	+0.098	+0.142	+0.153	+0.051	+0.069	+0.119

Table 4.2: ^{31}P chemical shift of phosphate groups in the mitoxantrone with d–(TGATCA)$_2$ complex at drug (D) to nucleic acid duplex (N) ratio, D/N = 0, 1.0, 1.5 and 2.0 at 278K, 298K and 318K. The change in chemical shift, due to Drug-DNA complex formation is also indicated for the three complexes.

278K

Phosphate Group	Uncomplexed DNA $\delta_{D/N=0}$	Drug-DNA Complex					
		$\delta_{D/N=1}$	$\delta_{D/N=1}$- $\delta_{D/N=0}$	$\delta_{D/N=1.5}$	$\delta_{D/N=1.5}$- $\delta_{D/N=0}$	$\delta_{D/N=2}$	$\delta_{D/N=2}$- $\delta_{D/N=0}$
T1pG2	-1.969	-1.812	+0.157	-1.727	+0.242	-1.707	+0.262
G2pA3	-1.938	-1.812	+0.126	-1.727	+0.211	-1.707	+0.231
A3pT4	-2.308	-2.317	-0.009	-2.320	-0.012	-2.314	+0.006
T4pC5	-2.152	-2.121	+0.031	-2.103	+0.049	-2.102	+0.050
C5pA6	-1.662	-1.691	-0.029	-1.727	-0.065	-1.707	-0.045

298K

Phosphate Group	Uncomplexed DNA $\delta_{D/N=0}$	Drug-DNA Complex					
		$\delta_{D/N=1}$	$\delta_{D/N=1}$- $\delta_{D/N=0}$	$\delta_{D/N=1.5}$	$\delta_{D/N=1.5}$- $\delta_{D/N=0}$	$\delta_{D/N=2}$	$\delta_{D/N=2}$- $\delta_{D/N=0}$
T1pG2	-1.879	-1.683	+0.196	-1.635	+0.244	-1.588	+0.291
G2pA3	-1.731	-1.592	+0.139	-1.532	+0.199	-1.486	+0.245
A3pT4	-2.052	-2.027	+0.025	-2.025	+0.027	-2.025	+0.027
T4pC5	-1.847	-1.791	+0.056	-1.760	+0.087	-1.741	+0.106
C5pA6	-1.584	-1.508	+0.076	-1.500	+0.084	-1.486	+0.098

318K

Phosphate Group	Uncomplexed DNA $\delta_{D/N=0}$	Drug-DNA Complex					
		$\delta_{D/N=1}$	$\delta_{D/N=1}$- $\delta_{D/N=0}$	$\delta_{D/N=1.5}$	$\delta_{D/N=1.5}$- $\delta_{D/N=0}$	$\delta_{D/N=2}$	$\delta_{D/N=2}$- $\delta_{D/N=0}$
T1pG2	-1.665	-1.550	0.115	-1.535	+0.130	-1.523	+0.142
G2pA3	-1.550	-1.419	0.131	-1.408	+0.142	-1.396	+0.154
A3pT4	-1.710	-1.671	0.039	-1.658	+0.052	-1.659	+0.051
T4pC5	-1.509	-1.452	0.057	-1.440	+0.069	-1.440	+0.069
C5pA6	-1.475	-1.369	0.106	-1.364	+0.111	-1.356	+0.119

+ve $\Delta\delta$ indicates downfield shift

-ve $\Delta\delta$ indicates up field shift

Local conformational heterogeneity in the sugar-phosphate backbone has been noted in the form of sequence specific variations or as a result of drug or protein binding to local regions of polynucleotides (Calladine, 1982; Dickerson, 1983; Saenger, 1984; Anderson et al, 1987). While ^{1}H NMR can provide detailed information on the overall conformation of the sugar rings and bases of oligonucleotides, it generally is unable to provide information on the conformation of the phosphate ester backbone since no direct inter-proton distance constraints are available though NOESY spectra. ^{31}P chemical shifts vary in response to local, sequence specific and induced environmental distortions in the duplex geometry (Calladine, 1982; Dickerson, 1983; Ott and Eckstein, 1985; Schroeder et al, 1989). Theoretical studies have shown that variation in conformation of two of the six torsional angles (α: O3'-P-O5'-C5' and ζ: C3'-O3'-P-O5') can cause perturbations in ^{31}P shifts. A switching from energetically more favorable B_I conformation ($\zeta = g^-$, $\alpha = g^-$) to the more flexible B_{II} conformation ($\zeta = t$, $\alpha = g^-$) having energy 1 Kcal/mol higher than B_I, introduces a downfield shift of about 1.5 ppm (Gorenstein et al, 1977). The dispersion in ^{31}P chemical shifts of oligonucleotides has also been attributed to different populations of B_I and B_{II} states (Gorenstein, 1992). ^{31}P chemical shift has also been correlated with degree of unwinding of duplex DNA resulting from increase in the length of the sugar phosphate backbone to accommodate intercalation of drug chromophore. Besides, the ester O-P-O bond angle distortions in drug-duplex DNA complexes also affect the chemical shift. Widening of ester O-P-O angle is expected to produce an upfield shift (Gorenstein, 1984; Gorenstein, 1975) while narrowing of this bond angle causes a downfield shift. Purely electrostatic associations between drug and nucleic acid on the

other hand produce only small and generally upfield ^{31}P chemical shifts (Patel, 1979; Wilson et al., 1982).

The change in chemical shifts obtained for the ^{31}P resonances of mitoxantrone-d-$(TGATCA)_2$ complex can be compared with corresponding $\Delta\delta$ values reported in literature (Table 4.3a–b) for binding of mitoxantrone with d–$(CGCG)_2$ (Lown et al, 1985b), d–$(CGATCG)_2$ (Kotovych et al, 1986), 2-pyrido[1, 2–e]purine–4–yl)amino–ethanol with d–$(CGATCG)_2$ (Favier et al, 2001), berberine with d–$(AAGAATTCTT)_2$ (Mazzini et al, 2003), nogalamycin with d–$(GCATGC)_2$ (Searle et al, 1988), adriamycin and methoxy–morpholinodoxorubicin with d–$(CGATCG)_2$ and d–$(CGTACG)_2$ (Mazzini et al, 1998). In case of external binding drugs, pyridopurine (Favier et al, 2001) and berberine (Mazzini et al, 2003), downfield shift in the range 0–0.17 ppm have been reported. On the other hand adriamycin, morpholinyldoxorubicin, daunorubicin and nogalamycin (Mazzini et al, 1998; Ragg et al, 1988; Searle et al, 1988), which intercalate between two base pairs of DNA oligomer, lead to downfield shifts up to 1.57 ppm of phosphorus resonances at the intercalation site or at site adjacent to it. Earlier shifts ~2.6 ppm has been reported on intercalation of aromatic chromophores in DNA (Gorenstein et al, 1992; Patel et al, 1976; Patel et al, 1974; Patel et al, 1982). Studies on mitoxantrone show downfield field shift up to 0.15–0.34 ppm (Lown et al, 1985b; Kotovych et al, 1986).

^{31}P chemical shift variations in nucleotides reflect the conformation of the phosphodiester groups at the level of the P–O5' and O3'–P bonds i.e. the values of torsion angles α = O3'–P—O5'–C5'and ζ = C3'–O3'–P–O5'. For a nucleotide in a B–DNA type conformation, the phosphate groups are normally found in gauche$^-$, gauche$^-$ (g^-

, g^-) conformation with α and ζ angles of -60° and -90°, respectively whereas the gauche$^-$, trans (g^-, t) conformation (α = -60°, ζ = 180°) is generally associated with a deshielding of 1.5 ppm. Such transition from g^-, g^- to g^-, t on intercalation of drug chromophore by opening of adjacent base pairs at intercalation site from a distance of 3.4 to 6.8 Å have been reported in X–ray crystallographic structure of adriamycin and daunomycin to d–CGATCG, d–TGATCA, d–CGTACG sequences (Frederick et al, 1990) as well in similar NMR structures (Mazzini et al, 1998). The pyridopurine (Favier at al, 2001) and berberine (Mazzini et al, 2003), which does not show such large shifts in phosphorus resonances on binding to DNA, have been shown to bind externally in the restrained molecular dynamics structures obtained by using experimental intermolecular inter proton distances from NOESY spectra. Thus it may be inferred that binding of mitoxantrone to d–$(TGATCA)_2$ does not lead to opening of base pairs, which is generally associated with large down field shifts of ^{31}P resonance, of the order of 1.6–2.6 ppm (Gorenstein et al, 1992; Patel et al, 1976; Patel et al, 1974; Patel et al, 1982).

4.1.1.2. Temperature Dependence Studies

^1H decoupled ^{31}P NMR spectra of hexanucleotide were obtained over the temperature range from 2°C to 55°C. At ambient temperatures, the ^{31}P resonances resolve into five distinct signals corresponding to five phosphate groups in d–$(TGATCA)_2$ (Fig. 4.4a). Temperatures lower and higher than the ambient cause some of the signals to shift towards each other and to overlap. Also there is no evidence of considerable line broadening, the change in linewidth ($\Delta\omega_{1/2}$) with temperature observed for the five phosphate resonances are ~5Hz with maximum being A3pT4 (5.56Hz) and lowest T1pG2 (4.69Hz). These data are quite indicative of the fact that the hexanucleotide remains

intact over the temperature range between 2°C to 55°C, or new signals would have become apparent.

The variation of ^{31}P NMR spectra of d–$(TGATCA)_2$ and its complex with mitoxantrone at D/N ratios of 1.0, 1.5, and 2.0 in the temperature range 2°C to 55°C. was examined (Fig. 4.4 (b-d), Table 4.4a and 4.4b), it shows the variation of chemical shift as a function of temperature. The signals are found to be shifted with temperature, which may be due to shift in the following equilibrium:

$$\text{Duplex} \rightleftharpoons \text{Single strand}$$

$$\text{Duplex + mitoxantrone} \rightleftharpoons \text{mitoxantrone – duplex}$$

$$\text{2 mitoxantrone} \rightleftharpoons (\text{mitoxantrone})_2$$

These reactions correspond to single strand transition, drug–DNA complexation and self association of mitoxantrone to form dimer molecules (Davies et al, 2001b). It is observed that shift in ^{31}P resonances in uncomplexed d–$(TGATCA)_2$ in the range 2–55 °C are very gradual and not abrupt (Fig. 4.4a). This is consistent with the earlier observations (Patel, 1977) on change in chemical shift with temperature due to helix to coil transition. Table 4.4 a-b shows the shift in ^{31}P resonances with temperature in the bound complexes are gradual and the total change, $\Delta\delta = \delta_{328\ K} - \delta_{278\ K}$, is almost same in the complexes having different D/N ratios.

Table 4.3a: Chemical shift of free (δ^f bound (δ^b), and change in chemical shift due to binding, $\Delta\delta = \delta^b - \delta^f$ in phosphate groups of some of the drug–DNA complexes taken from literature.

Phosphate Group	Mazzini et al., 1998 d-(CGATCG)$_2$ + Adriamycin			Mazzini et al., 1998 d-(CGTACG)$_2$ + Adriamycin			Searle et al., 1988 d -(GCATGC)$_2$ + Nogalamycin		
	δ^f	δ^b	$\Delta\delta$	δ^f	δ^b	$\Delta\delta$	δ^f	δ^b*	$\Delta\delta$
C1pG2/ G1pC2	-0.91	-0.48	+0.43	-1.03	-0.58	+0.45	-3.30	-2.90	+0.20
G2pA3/ C2pA3	-0.86	0.67	+1.53	-1.40	-0.56	+0.84	-3.00	-2.50	+0.50
A3pT4/ T3pA4	-1.26	-1.28	≤-0.2	-1.12	-1.26	-0.14	-3.40	-3.20	+0.20
T4pC5/ T4pG6	-1.06	-1.12	-0.06	-1.20	-1.34	-0.14	-3.10	-1.60	+1.50
C5pG6/ G5pC6	-0.73	0.84	+1.57	-0.90	+0.63	+1.53	-3.00	-3.00	+0.00
	Mazzini et al., 1988 d-(CGATCG)$_2$+ Morpholinodoxorubicin			Mazzini et al., 1988 d-(CGTACG)$_2$+ Morpholinodoxorubicin			Ragg et al., 1988 d-(CGTACG)$_2$+ Daunorubicin		
	δ^f	δ^b	$\Delta\delta$	δ^f	δ^b	$\Delta\delta$	δ^f	δ^b	$\Delta\delta$
C1pG2	-0.91	-0.32	+0.59	-1.03	-0.56	+0.47	-1.02	-1.45	-0.43
G2pA3 / G2pT3	-0.86	0.19	+1.05	-1.40	-0.50	+0.90	-1.42	-1.95	-0.53
A3pT4/ T3pA4	-1.26	-1.36	-0.10	-1.12	-1.45	-0.33	-1.08	-1.28	-0.20
T4pC5/ A4pC5	-1.06	-1.11	-0.05	-1.20	-1.46	-0.26	-1.28	-1.48	-0.20
C5pG6	-0.73	0.52	+1.25	-0.90	+0.22	+1.12	-0.88	+0.44	+1.32

+ve $\Delta\delta$ indicates downfield shift.
-ve $\Delta\delta$ indicates upfield shift.
* Tentative assignment

Table 4.3b: Chemical shift of free (δ^f), bound (δ^b), and the change in chemical shift due to binding, $\Delta\delta = \delta^b - \delta^f$ in phosphate resonances of some of the drug–DNA complexes taken from literature.

Phosphate Group	Lown et al., 1985b d-(CGCG)$_2$ + mitoxantrone			Kotovych et al., 1986 d-(CGATCG)$_2$ + mitoxantrone				Favier et al., 2001 d-(CGATCG)$_2$ + pyridopurine				Mazinni et al., 2003 d-(AAGAATTCTT)$_2$ + berberine			
	δ^f	δ^b	$\Delta\delta$		δ^f	δ^b	$\Delta\delta$		δ^f	δ^b	$\Delta\delta$		δ^f	δ^b	$\Delta\delta$
C1pG2	-3.46	-3.31	+0.15	C1pG2	-1.71	-1.70	+ 0.01	C1pG2	1.2	1.1	-0.1	A1pA2	-1.31	-1.19	+0.12
G2pA3	-3.30	-3.40	-0.10	G2pA3	-1.71	-1.70	+ 0.01	G2pA3	1.1	1.1	0.0	A2pG3	-1.00	-0.98	+0.02
C3pG4	-3.46	-3.31	+0.15	A3pT4	-2.19	-2.21	-0.02	A3pT4	0.7	0.8	-0.1	G3pA4	-1.14	-1.12	+0.02
				T4pC5	-1.95	-1.97	-0.02	T4pC5	0.4	0.5	-0.1	A4pA5	-1.40	-1.23	+0.17
				C5pG6	-1.59	-1..25	+0.34	C5pG6	1.2	1.2	0.0	A5pT6	-1.37	-1.40	+0.03
Mazzini et al., 2004 Topotecan+d(CGTACG)$_2$				Mazzini et al., 2004 Camptothecin+d(CGTACG)$_2$				Mazzini et al., 2004 Camptothecin+d(CGTATACG)$_2$				T6pT7	-1.18	-1.10	+0.08
C1pG2	-1.00	-1.00	0.00	C1pG2	-0.88	-0.95	+0.07	C1pG2	-0.94	-0.96	+0.02	T7pC8	-1.11	-1.07	+0.04
G2pT3	-1.29	-1.35	-0.06	G2pT3	-1.32	-1.33	+0.01	G2pT3	-1.33	-1.33	+0.00	C8pT9	-1.14	-1.10	+0.04
T3pA4	-1.08	-1.10	-0.02	T3pA4	-1.14	-1.17	-0.03	T3pA4	-1.03	-1.03	+0.00	T9pT10	-1.04	-1.07	+0.03
A4pC5	-1.12	-1.20	-0.08	A4pC5	-1.14	-1.17	-0.03	A4pC5	-1.33	-1.33	+0.00				
C5pG6	-0.90	-1.00	-0.10	C5pG6	-0.78	-0.85	+0.07	T5pA6	-1.10	-1.13	-0.03				
								A6pC7	-1.09	-1.11	+0.02				
								C7pG8	-0.82	-0.84	-0.02				

+ve $\Delta\delta$ indicates downfield shift -ve $\Delta\delta$ indicates upfield shift

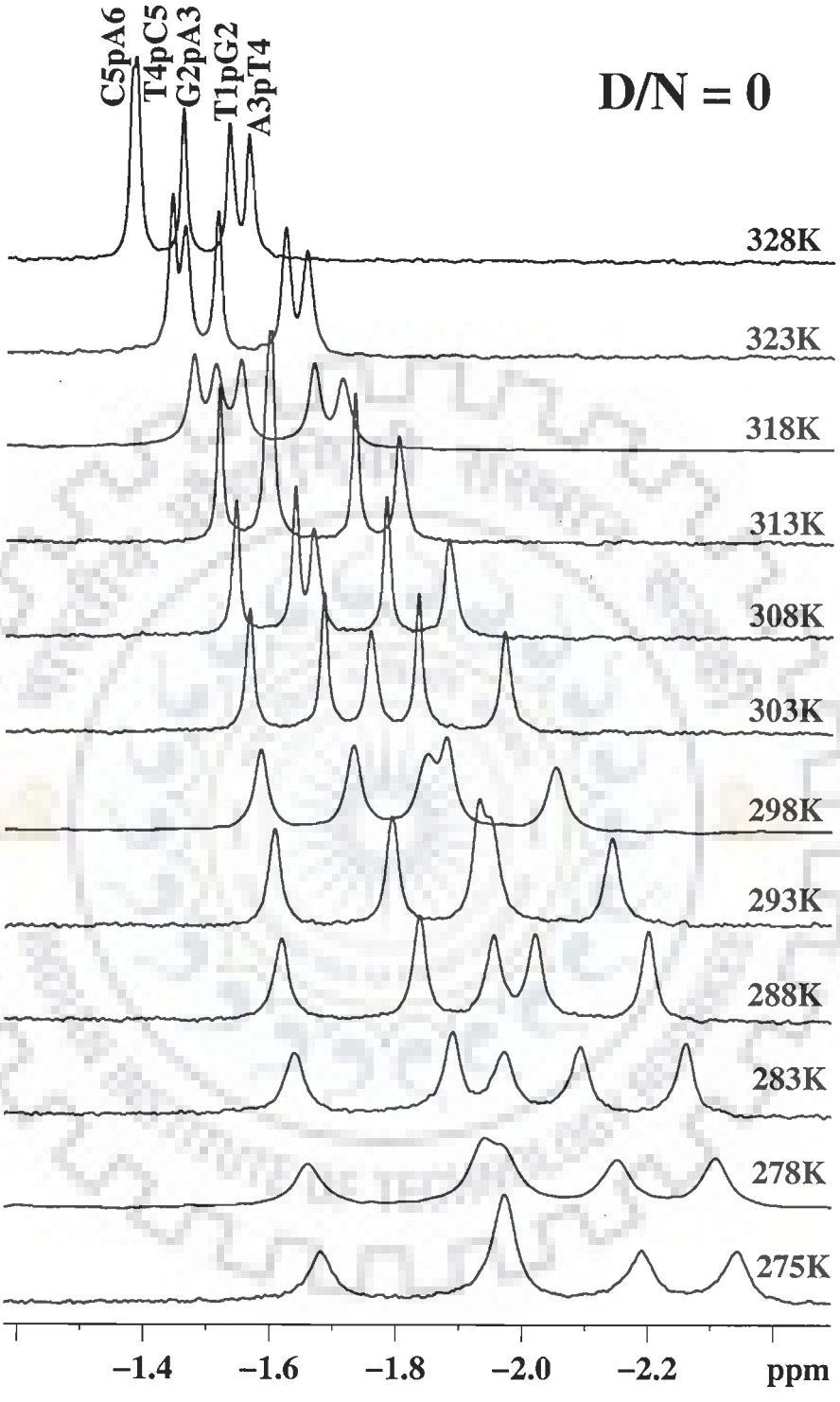

Figure 4.4a: Proton decoupled ^{31}P NMR spectra of d–$(TGATCA)_2$ as a function of temperature.

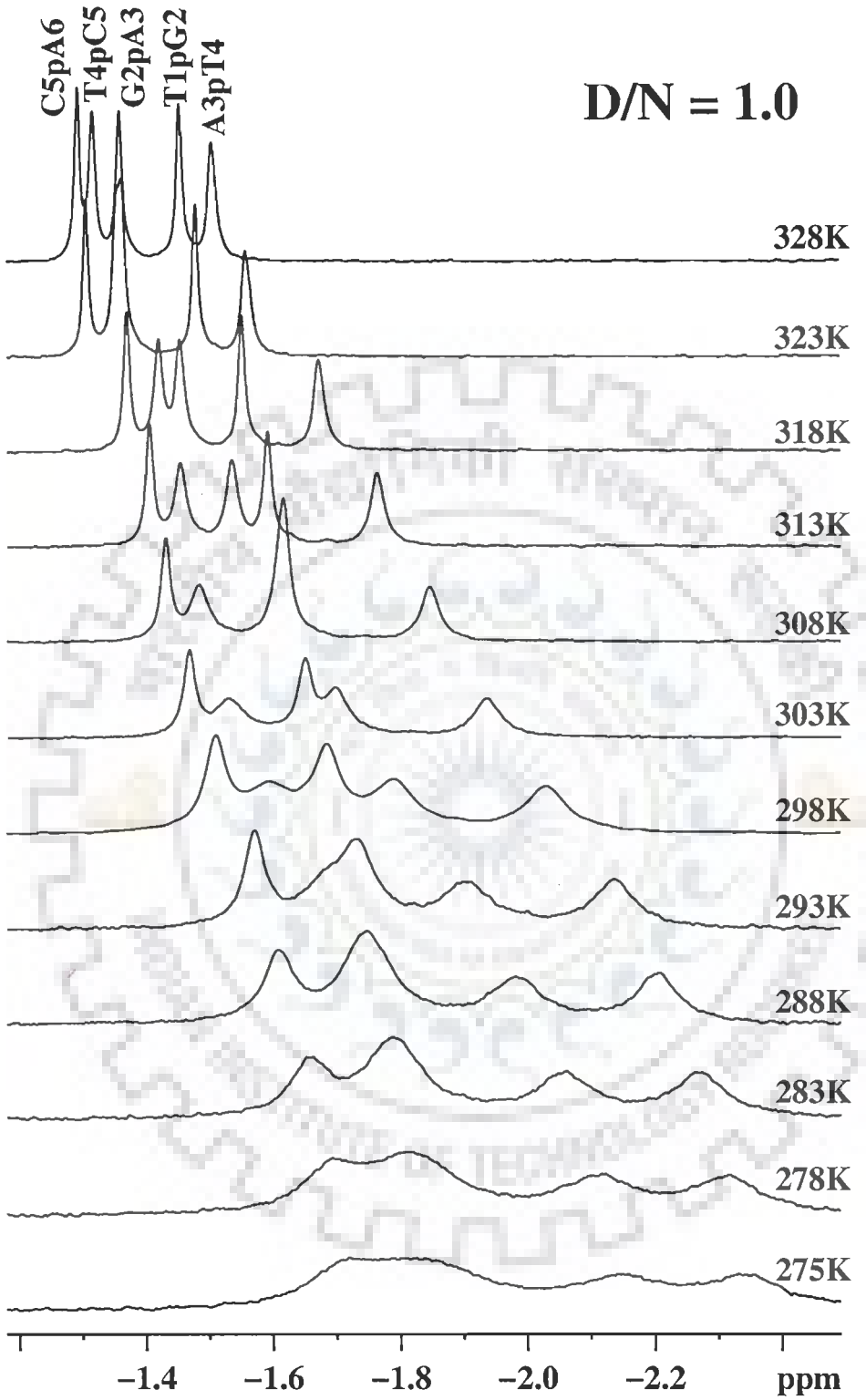

Figure 4.4b: Proton decoupled ^{31}P NMR spectra of d–$(TGATCA)_2$ complexed with mitoxantrone as a function of temperature at D/N ratio 1.0

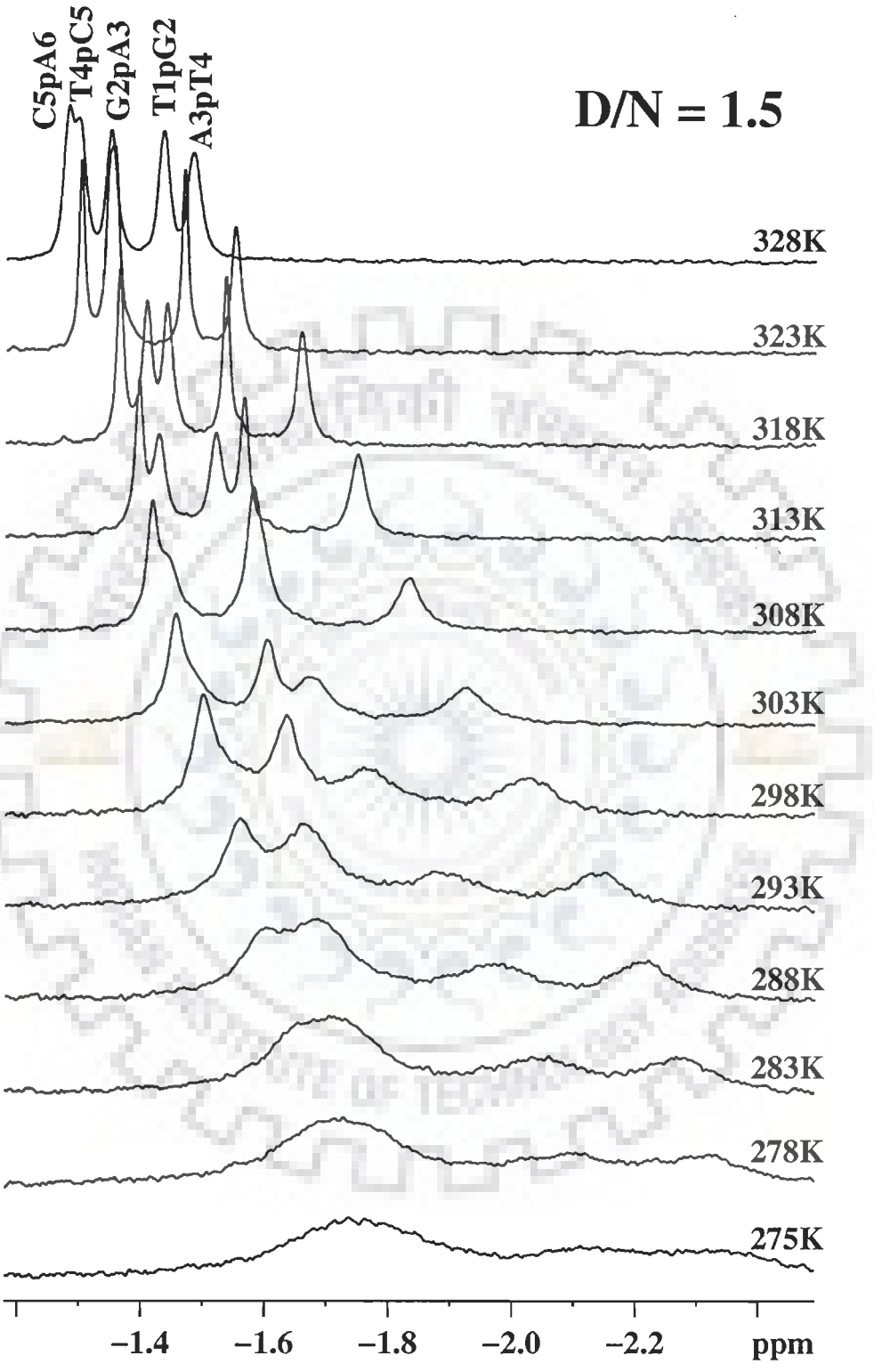

Figure 4.4c: Proton decoupled ^{31}P NMR spectra of d–$(TGATCA)_2$ complexed with mitoxantrone as a function of temperature at D/N ratio 1.5

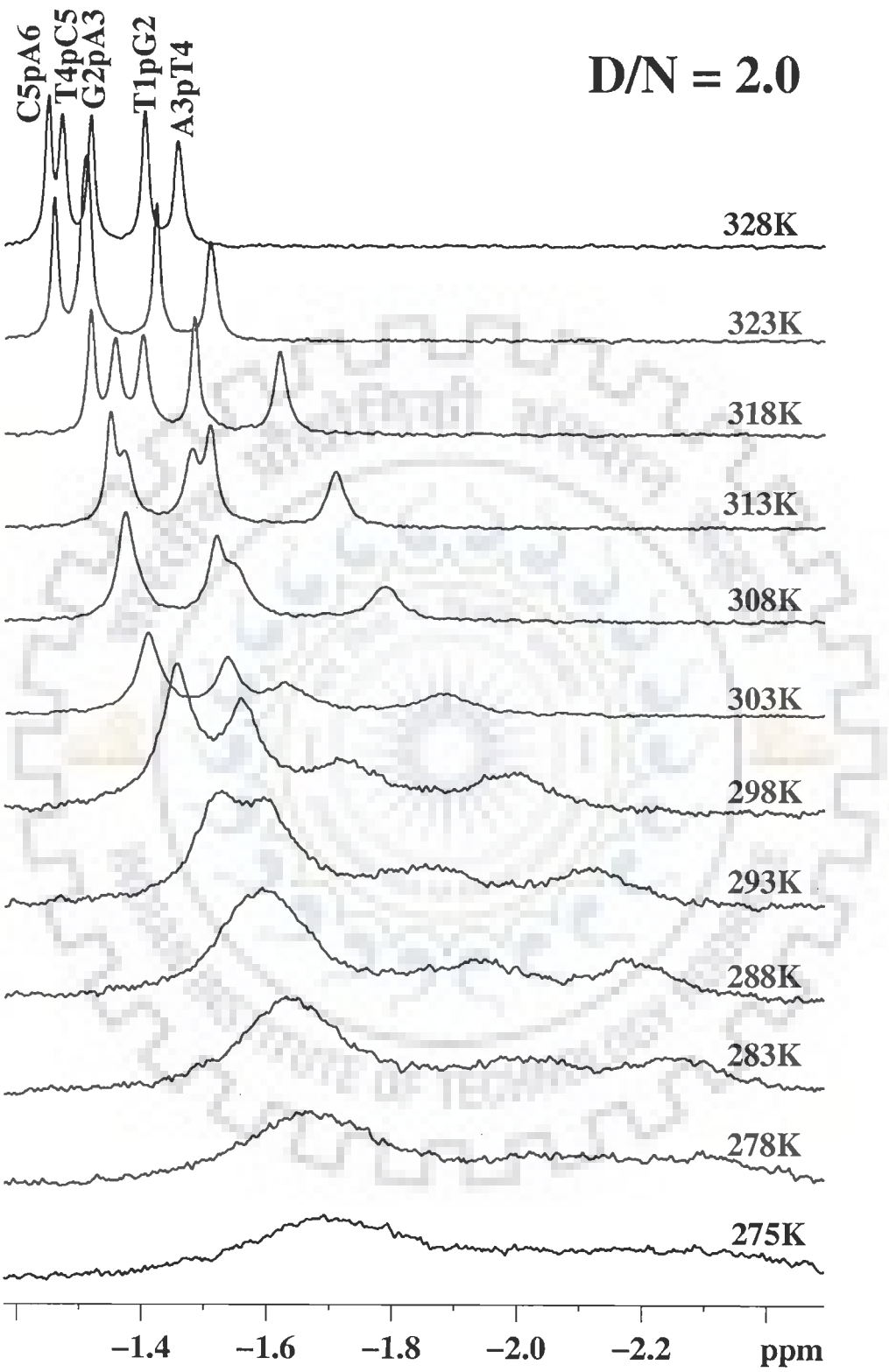

Figure 4.4d: Proton decoupled ^{31}P NMR spectra of d–$(TGATCA)_2$ complexed with mitoxantrone as a function of temperature at D/N ratio 2.0

Table 4.4a: ^{31}P chemical shift d-$(TGATCA)_2$ - mitoxantrone complex (D/N = 0, 1.0, 1.5, 2.0) as a function of temperature in the range 275-328 K where $\Delta\delta = \delta_{328K} - \delta_{275K}$.

	D/N = 0					D/N = 1.5				
Temp	T1pG2	G2pA3	A3pT4	T4pC5	C5pA6	T1pG2	G2pA3	A3pT4	T4pC5	C5pA6
275	-1.97	-1.97	-2.34	-2.19	-1.68	-1.74	-1.74	-2.32	-2.11	-1.74
278	-1.97	-1.94	-2.31	-2.15	-1.66	-1.73	-1.73	-2.32	-2.10	-1.73
283	-1.97	-1.89	-2.26	-2.09	-1.64	-1.71	-1.71	-2.27	-2.03	-1.71
288	-1.95	-1.84	-2.20	-2.02	-1.62	-1.68	-1.68	-2.22	-1.97	-1.61
293	-1.93	-1.79	-2.14	-1.95	-1.61	-1.66	-1.64	-2.15	-1.88	-1.56
298	-1.88	-1.73	-2.05	-1.85	-1.58	-1.64	-1.53	-2.03	-1.76	-1.50
303	-1.83	-1.68	-1.97	-1.76	-1.57	-1.60	-1.46	-1.92	-1.67	-1.46
308	-1.78	-1.64	-1.88	-1.67	-1.54	-1.58	-1.44	-1.83	-1.58	-1.42
313	-1.73	-1.60	-1.80	-1.60	-1.52	-1.56	-1.43	-1.75	-1.52	-1.40
318	-1.67	-1.55	-1.71	-1.51	-1.48	-1.54	-1.41	-1.66	-1.44	-1.36
323	-1.62	-1.51	-1.65	-1.46	-1.44	-1.47	-1.35	-1.55	-1.35	-1.30
328	-1.53	-1.46	-1.56	-1.38	-1.38	-1.43	-1.35	-1.48	-1.30	-1.28
δΔ	+0.44	+0.51	+0.78	+0.81	+0.31	+0.30	+0.39	+0.84	+0.82	+0.46
	D/N = 1.0					D/N = 2.0				
275	-1.82	-1.82	-2.33	-2.14	-1.72	-1.75	-1.75	-2.34	-2.13	-1.75
278	-1.81	-1.81	-2.32	-2.12	-1.69	-1.71	-1.71	-2.31	-2.10	-1.71
283	-1.79	-1.79	-2.26	-2.06	-1.66	-1.65	-1.65	-2.26	-2.07	-1.65
288	-1.75	-1.75	-2.21	-1.98	-1.61	-1.61	-1.60	-2.17	-1.93	-1.60
293	-1.73	-1.69	-2.14	-1.91	-1.57	-1.60	-1.54	-2.14	-1.87	-1.54
298	-1.68	-1.59	-2.03	-1.79	-1.51	-1.59	-1.49	-2.03	-1.74	-1.49
303	-1.65	-1.53	-1.94	-1.70	-1.47	-1.58	-1.45	-1.92	-1.67	-1.45
308	-1.62	-1.48	-1.85	-1.62	-1.43	-1.57	-1.42	-1.83	-1.59	-1.42
313	-1.59	-1.45	-1.76	-1.53	-1.41	-1.55	-1.41	-1.75	-1.52	-1.39
318	-1.55	-1.42	-1.67	-1.45	-1.37	-1.52	-1.40	-1.66	-1.44	-1.36
323	-1.48	-1.36	-1.56	-1.36	-1.31	-1.49	-1.37	-1.57	-1.37	-1.32
328	-1.45	-1.36	-1.50	-1.32	-1.29	-1.45	-1.36	-1.50	-1.31	-1.29
δΔ	+0.36	+0.46	+0.83	+0.83	+0.43	+0.31	+0.39	+0.85	+0.82	+0.46

Table 4.4b: The change in ^{31}P chemical shift, $\Delta\delta = \delta_{328K} - \delta_{275K}$, due to temperature in d-$(TGATCA)_2$ and in complex with mitoxantrone at drug (D) to nucleic acid duplex (N) ratio, D/N = 0, 1, 1.5, 1.75 and 2.0

Phosphate Group	D/N = 0	D/N = 1	D/N = 1.5	D/N = 1.75	D/N = 2.0
T1pG2	0.442	0.363	0.303	0.301	0.306
G2pA3	0.514	0.458	0.388	0.391	0.393
A3pT4	0.782	0.828	0.842	0.852	0.845
T4pC5	0.809	0.826	0.815	0.818	0.820
C5pA6	0.305	0.427	0.456	0.457	0.460

(+ve Δδ indicates downfield shift -ve Δδ indicates up field shift)

4.1.1.3. 2D ^{31}P - ^{31}P Exchange Spectra

Fig. 4.5 (a-b) show 2D ^{31}P NMR exchange spectrum of the complex of mitoxantrone with d–$(TGATCA)_2$ at drug to DNA (D/N) ratio of 1.0 and 2.0 at 275K. The one dimensional ^{31}P spectra are shown along both axes. In 2D ^{31}P NMR exchange spectrum, each of the 5 phosphorus signals seen in uncomplexed DNA is expected to give cross peak due to chemical exchange with its respective bound resonance. On binding of mitoxantrone to d–$(TGATCA)_2$, as the drug is progressively added to the hexanucleotide, only considerable broadening is observed with no additional cross peaks due to exchange between the bound and free phosphate resonances. Since only one set of resonances are observed for the complexes at different D/N ratios for free hexamer and hexamer bound to drug, it is expected that ^{31}P signals from the bound DNA are in fast exchange with the corresponding signals from free DNA to be followed individually at 275 K on NMR time scale.

The study on ^{31}P NMR of the drug-DNA complex provide an independent proof of the external binding of mitoxantrone to d-$(TGATCA)_2$ and the rate of exchange which is faster on NMR time scale. Although the ^{31}P NMR studies provide information on the conformation of the phosphate ester backbone, it is unable to provide detailed information on the overall conformation of the sugar rings and bases of oligonucleotides. Direct inter-proton distance (NOE) that is available through ^{1}H NMR studies are discussed further in this chapter and we have found the ^{31}P NMR results are consistent with proton NMR studies.

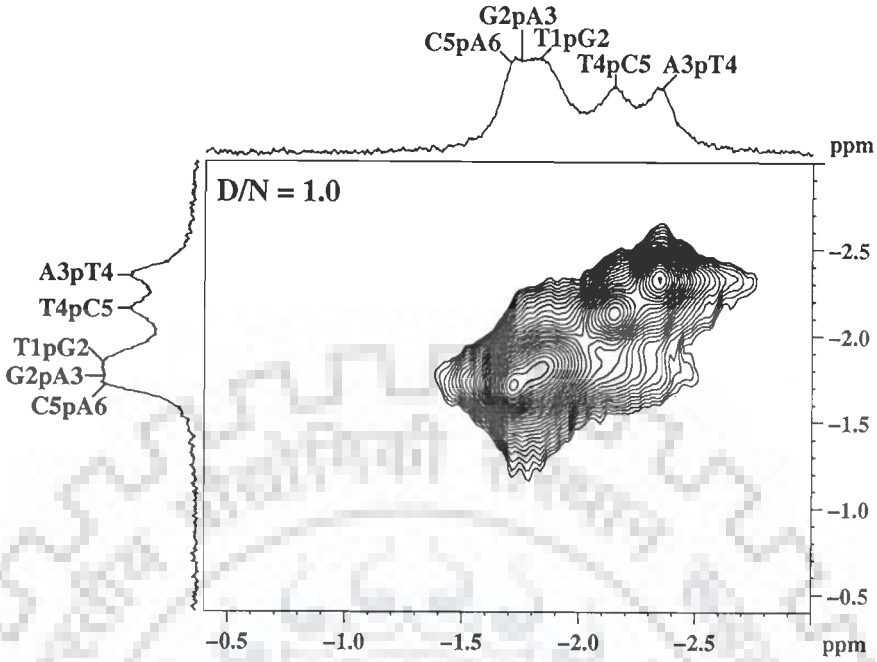

(Fig. 4.5a)

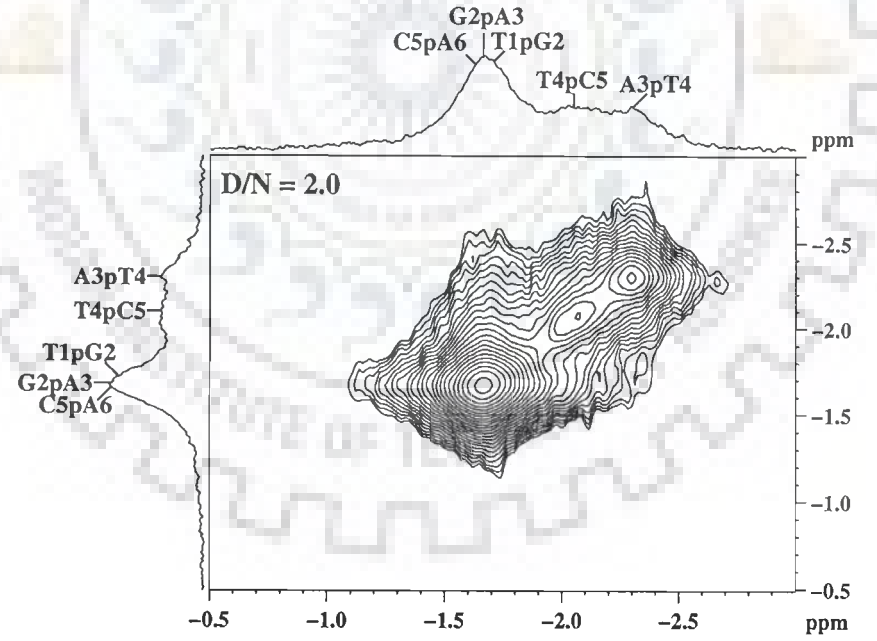

(Fig. 4.5b)

Figure 4.5(a-b): ^{31}P NMR exchange spectrum of the complex of mitoxantrone with d–$(TGATCA)_2$ at drug (D) to nucleic acid duplex (N) ratio, D/N of (a) 1.0 at 275K (b) 2.0 at 278K.

4.1.2. Proton NMR Studies of Mitoxantrone-d-$(TGATCA)_2$ Complex

Fig. 4.6(a–f) and 4.7 show the ^1H 1D NMR spectra of d–$(TGATCA)_2$ and change in chemical shift on successive addition of mitoxantrone to DNA at 278 K. Fig. 4.8 shows the change in mitoxantrone protons chemical shift as a function of D/N ratio. ^1H NMR spectra of the drug–DNA complex at D/N=1.0 and 2.0, as a function of temperature are shown in Fig. 4.9a–b. The 2D NMR experiments are carried out at 278 K as imino protons are sharpened and intensified at this temperature. Besides, DNA is expected to be present in duplex state at 278K. Fig. 4.10a–I show expansions of specific regions of 2D NOESY spectra of mitoxantrone complexed to d–$(TGATCA)_2$ in the stoichiometric ratio of D/N = 1.0. The assignment of spectral lines to specific protons of drug has been made by following the strategies used for assignment in NMR spectra of uncomplexed drug (Birlirakis et al, 1992; Davies et al, 2001b). The assignment of nucleotide protons has been carried out by following the strategies adopted for standard B–DNA structures that is, sequential NOEs (base $H8/H6)_n$–sugar $(H1')_{n-1}$, (base $H8/H6)_n$–sugar$(H2'')_{n-1}$, (base $H8/H6)_n$–sugar$(H2')_{n-1}$; expected NOEs due to several short intra nucleotide distances (Wuthrich, 1986) as well as our NMR data of uncomplexed d–$(TGATCA)_2$ (Barthwal et al, 2004). The T4NH imino proton was assigned based on the intense cross peak with A3H2 and NOEs with adenine amino protons of the corresponding base pair. G2NH shows connectivity with amino protons of the corresponding cytosine base pair. The low-field cytosine amino proton in turn shows an NOE contact with C5H5 and concluded to be the proton involved in the Watson-Crick hydrogen bond, as observed in literature (Boelens et al, 1985). The observation of the

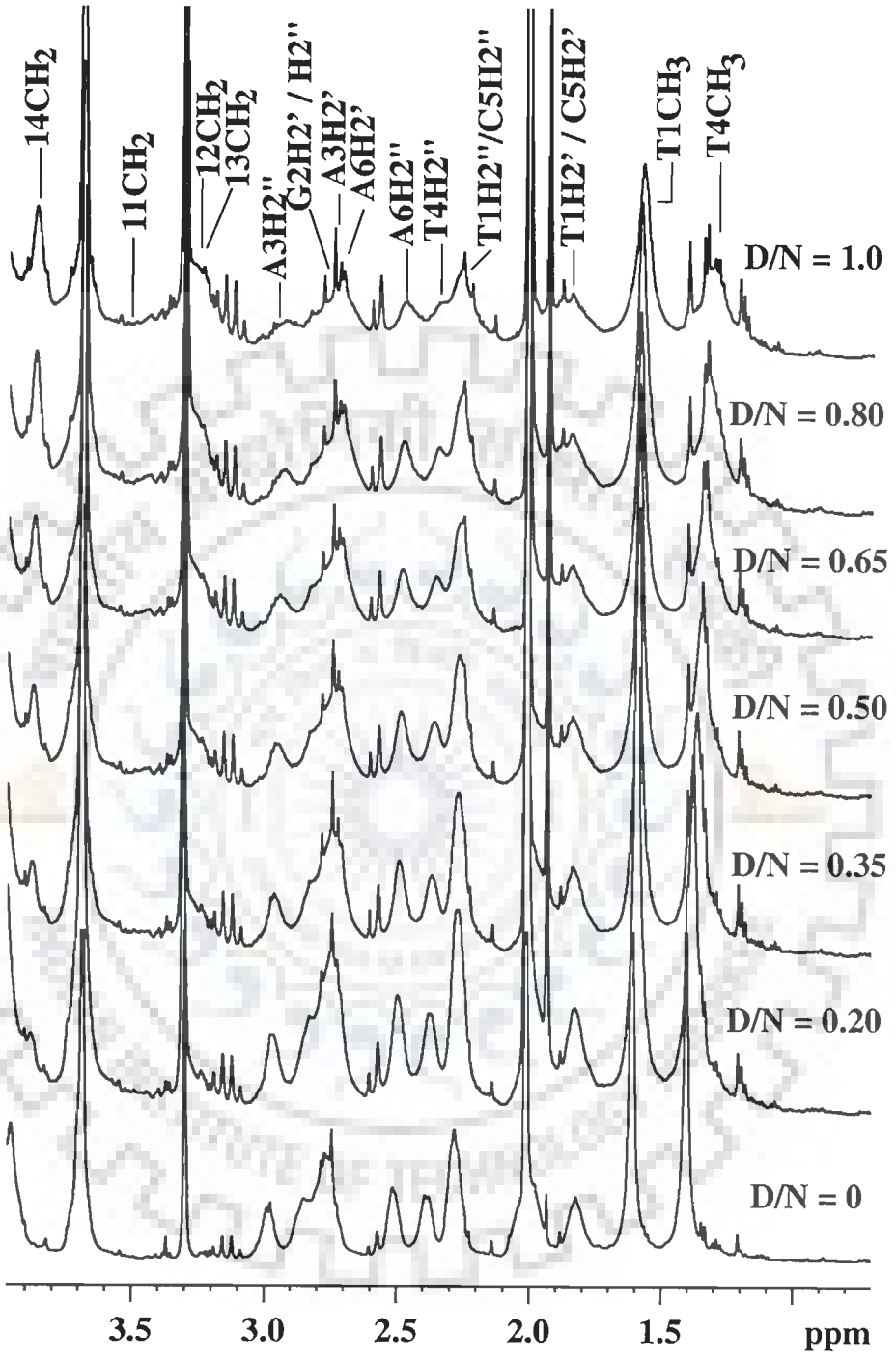

(Fig. 4.6a)

Figure 4.6 (a-f): Proton NMR spectra of complex of mitoxantrone with d–$(TGATCG)_2$ as a function of D/N ratio at 278 K

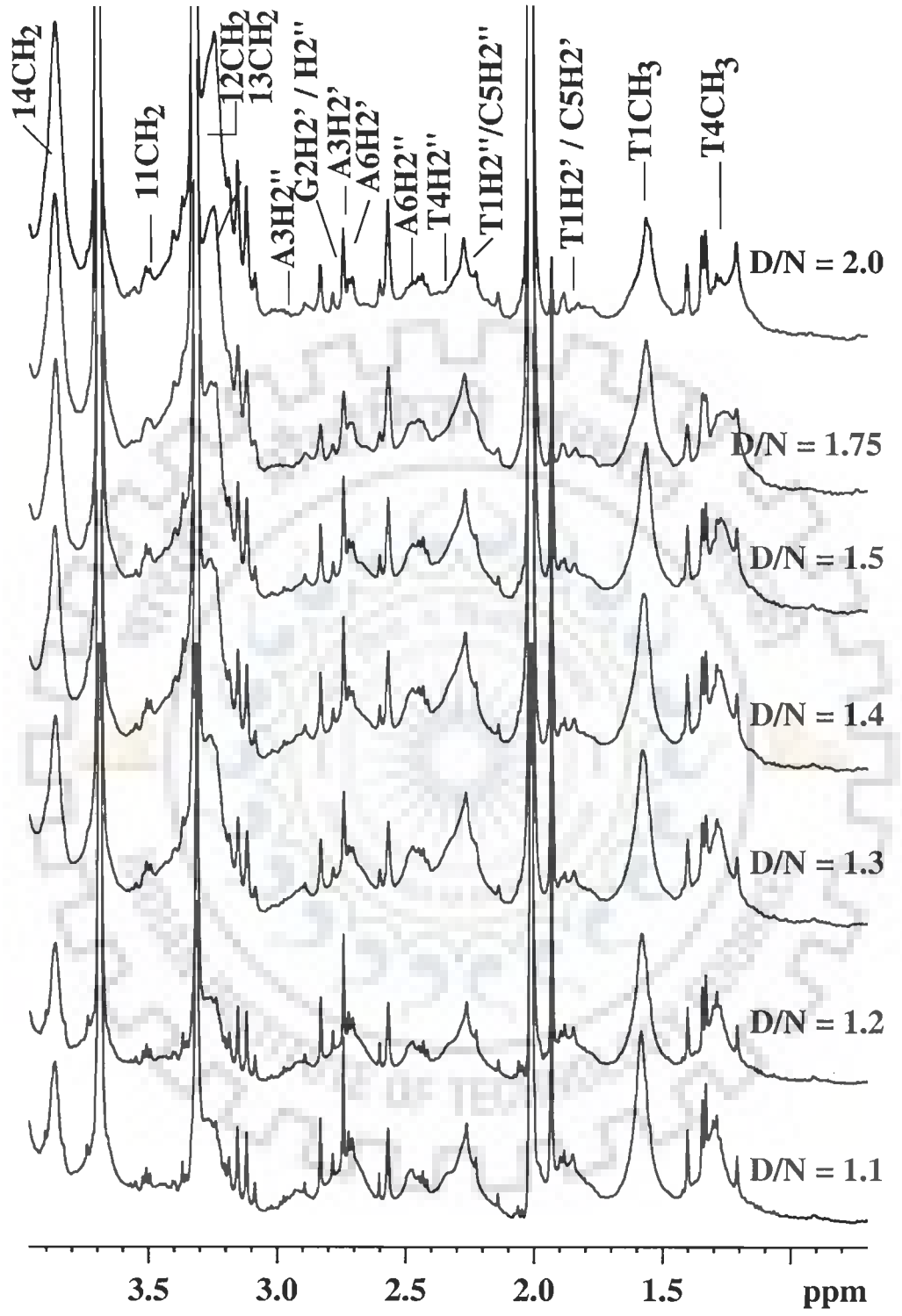
14CH2
11CH2
12CH2
13CH2
A3H2''
G2H2' / H2''
A3H2'
A6H2'
A6H2''
T4H2''
T1H2''/C5H2''
T1H2' / C5H2'
T1CH3
T4CH3
D/N = 2.0
D/N = 1.75
D/N = 1.5
D/N = 1.4
D/N = 1.3
D/N = 1.2
D/N = 1.1
3.5
3.0
2.5
2.0
1.5
ppm

(Fig. 4.6b)

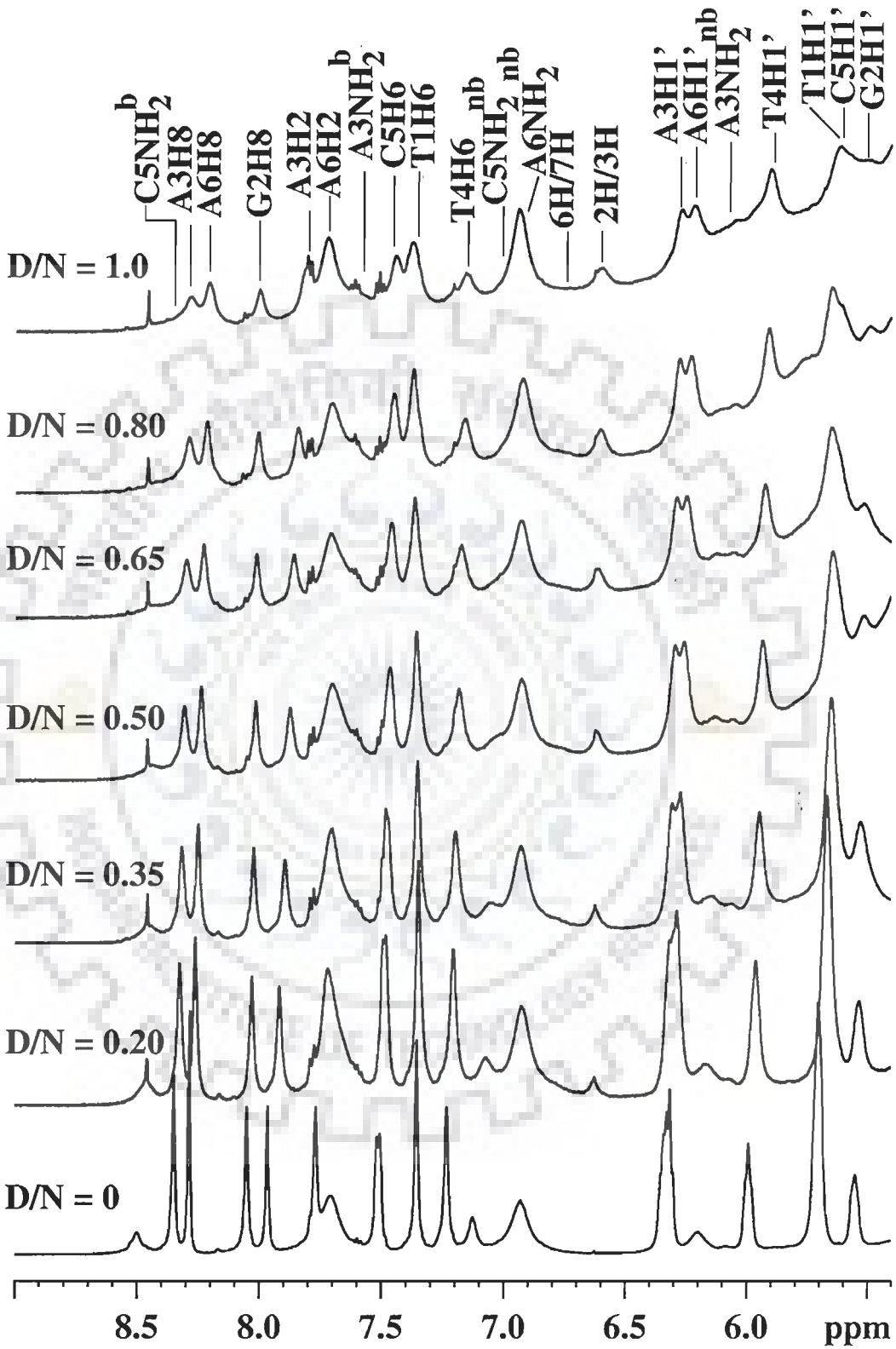
C5NH2 b
A3H8
A6H8
G2H8
A3H2
A6H2
A3NH2 b
C5H6
T1H6
T4H6
C5NH2 nb
A6NH2 nb
6H/7H
2H/3H
A3H1'
A6H1' nb
A3NH2
T4H1'
T1H1'
C5H1'
G2H1'
D/N = 1.0
D/N = 0.80
D/N = 0.65
D/N = 0.50
D/N = 0.35
D/N = 0.20
D/N = 0
8.5
8.0
7.5
7.0
6.5
6.0
ppm

(Fig. 4.6c)

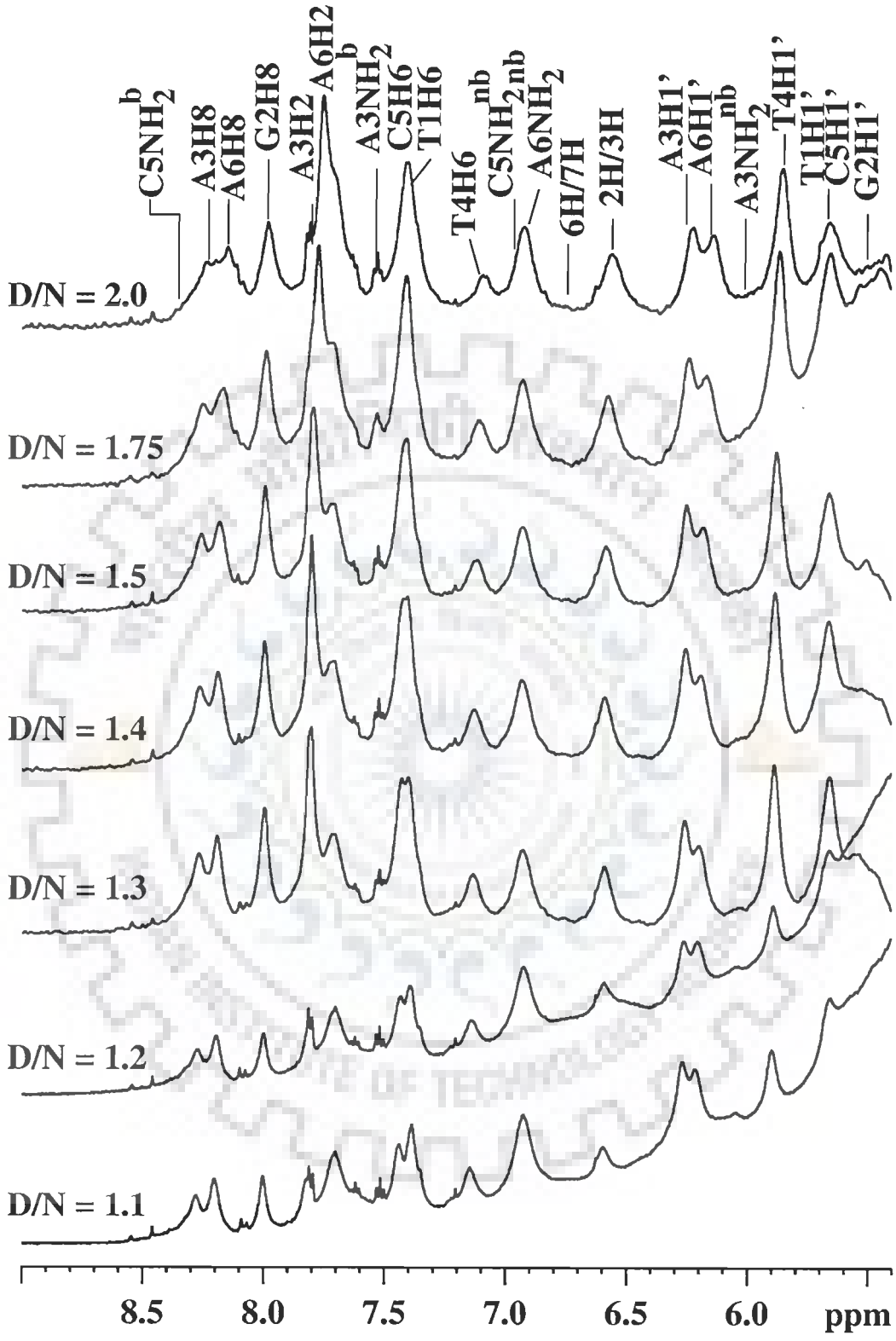
C5NH2b
A3H8
A6H8
G2H8
A3H2
A6H2b
A3NH2
C5H6
T1H6
T4H6
C5NH2nb
A6NH2
6H/7H
2H/3H
A3H1'
A6H1'
A3NH2nb
T4H1'
T1H1'
C5H1'
G2H1'
D/N = 2.0
D/N = 1.75
D/N = 1.5
D/N = 1.4
D/N = 1.3
D/N = 1.2
D/N = 1.1
8.5
8.0
7.5
7.0
6.5
6.0
ppm

(Fig. 4.6d)

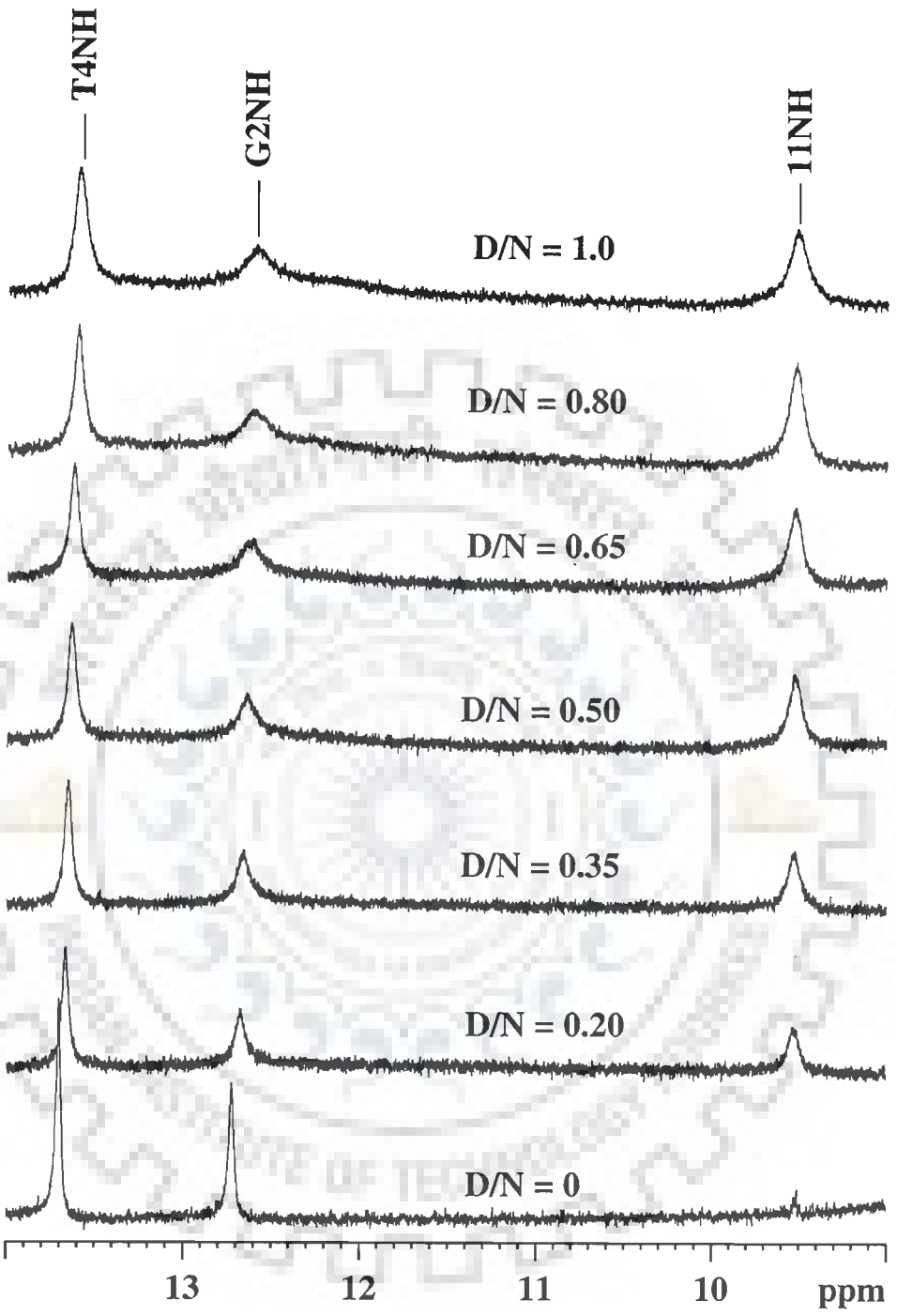
T4NH
G2NH
11NH
D/N = 1.0
D/N = 0.80
D/N = 0.65
D/N = 0.50
D/N = 0.35
D/N = 0.20
D/N = 0
13
12
11
10
ppm

(Fig. 4.6e)

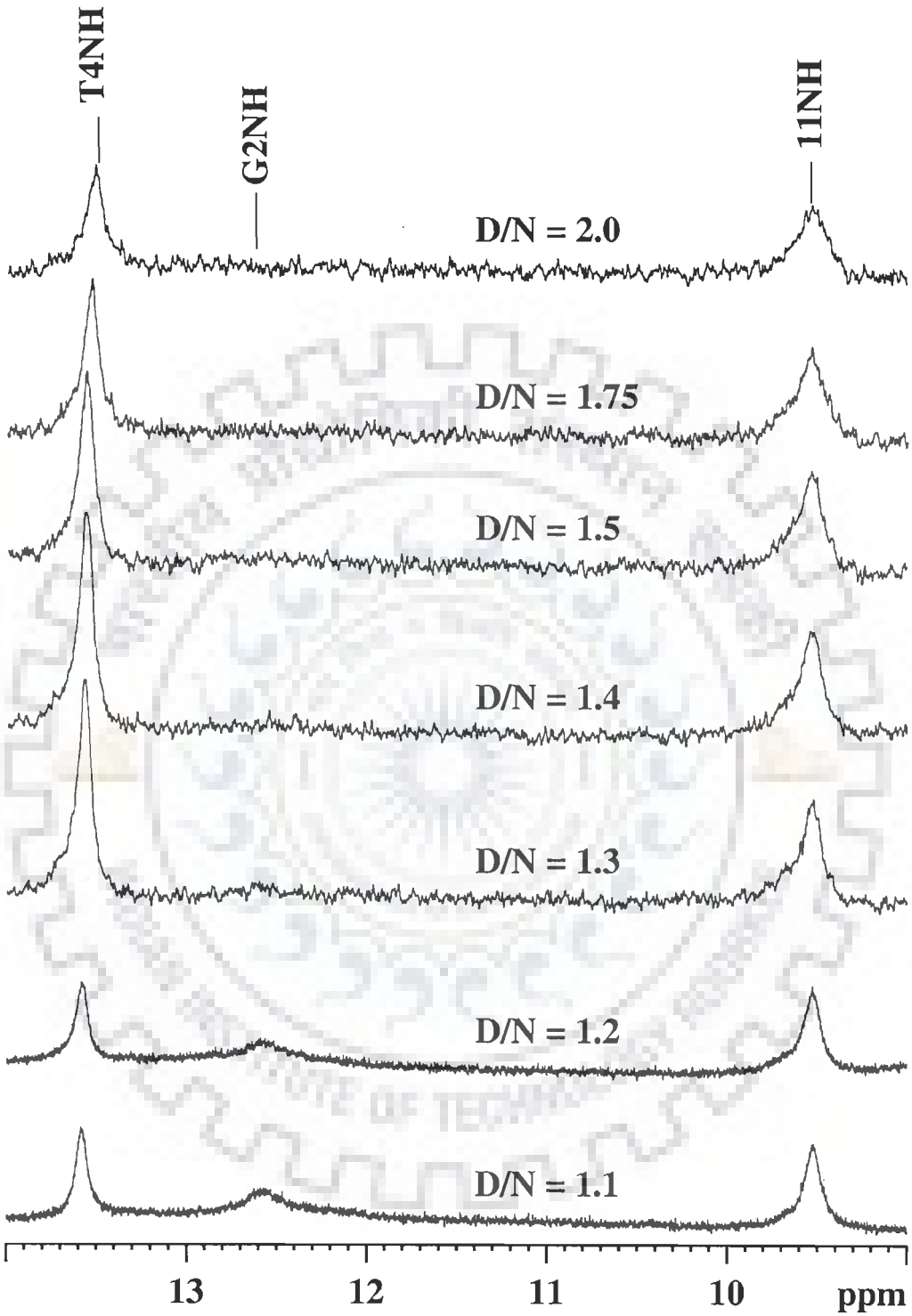
T4NH
G2NH
11NH
D/N = 2.0
D/N = 1.75
D/N = 1.5
D/N = 1.4
D/N = 1.3
D/N = 1.2
D/N = 1.1
13
12
11
10
ppm

(Fig. 4.6f)

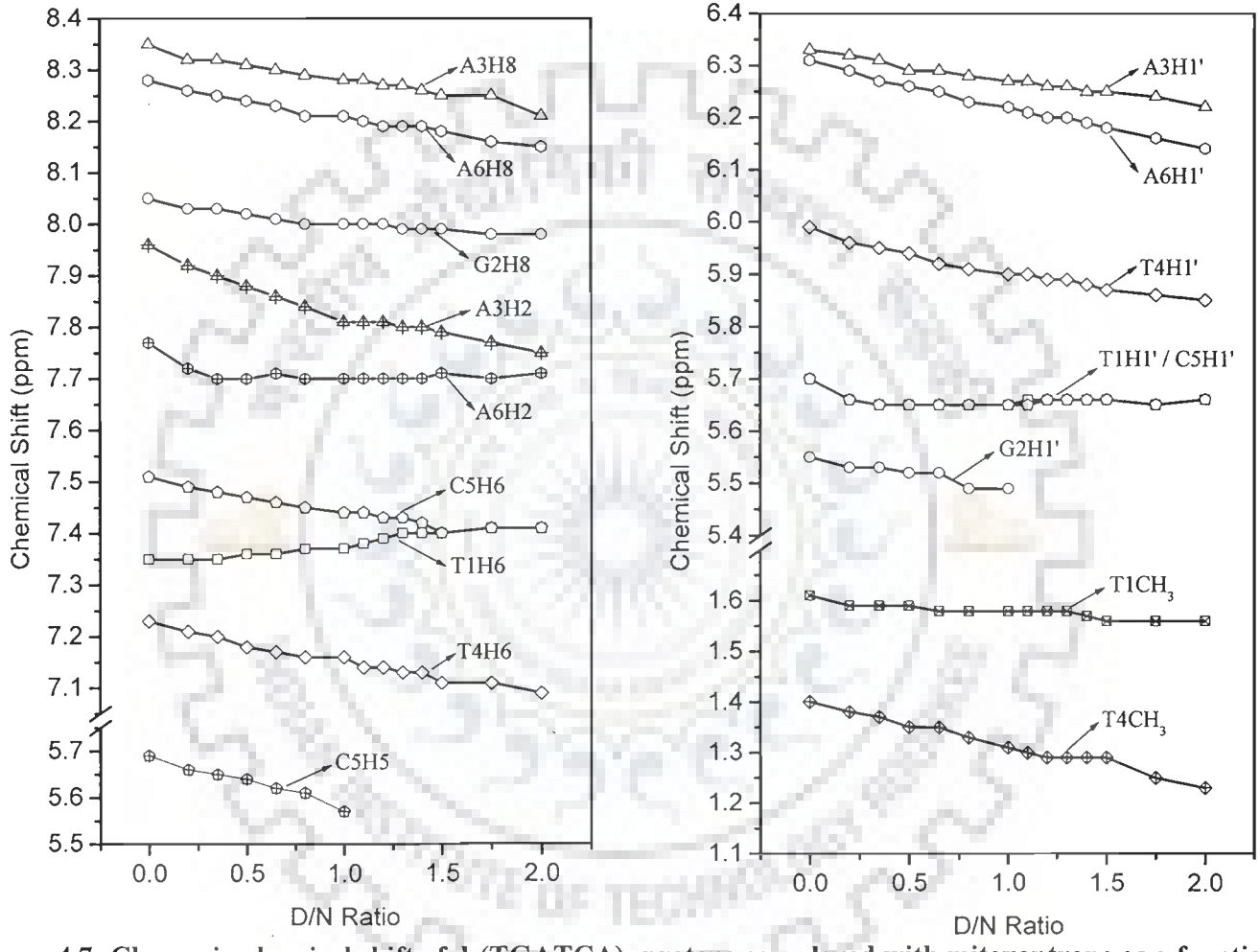

Figure 4.7: Change in chemical shift of d-$(TGATCA)_2$ protons complexed with mitoxantrone as a function of drug to DNA (D/N) ratio, 278 K

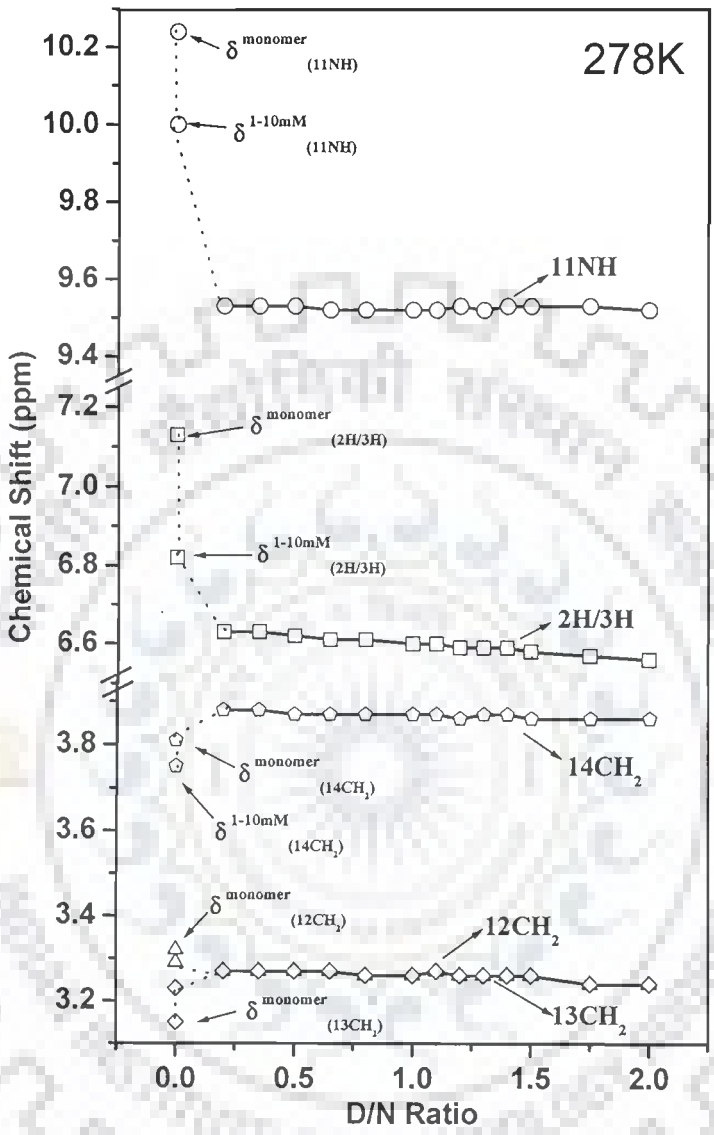

Figure 4.8: change in ^{1}H Chemical shift of mitoxantrone protons complexed with d-(TGATCA)$_2$ at various D/N ratio, 278 K.

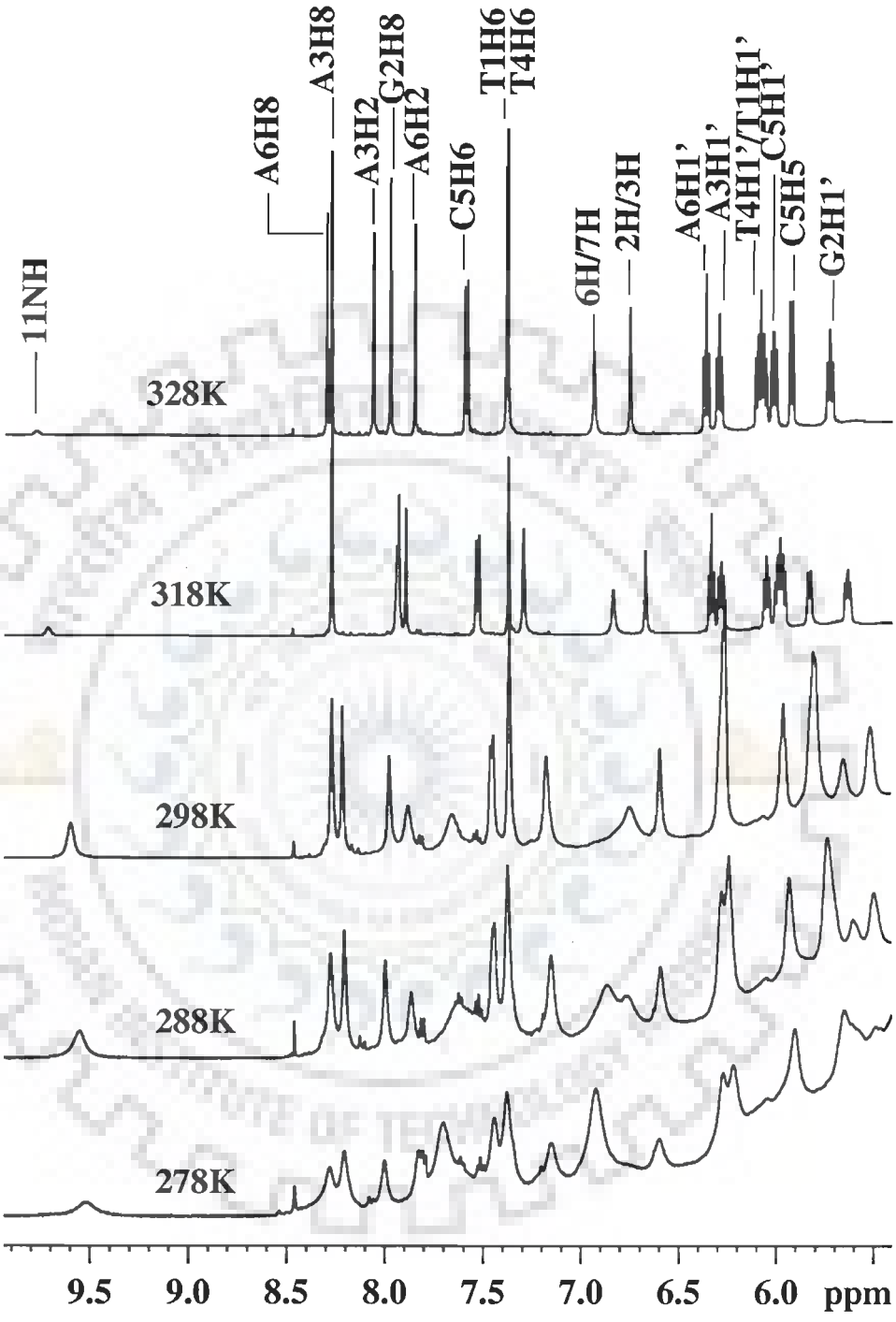

(Fig. 4.9a)

Figure 4.9: Proton NMR spectra of complex of mitoxantrone with d–$(TGATCG)_2$ as a function of temperature (a) D/N = 1.0 (b) D/N = 2.0

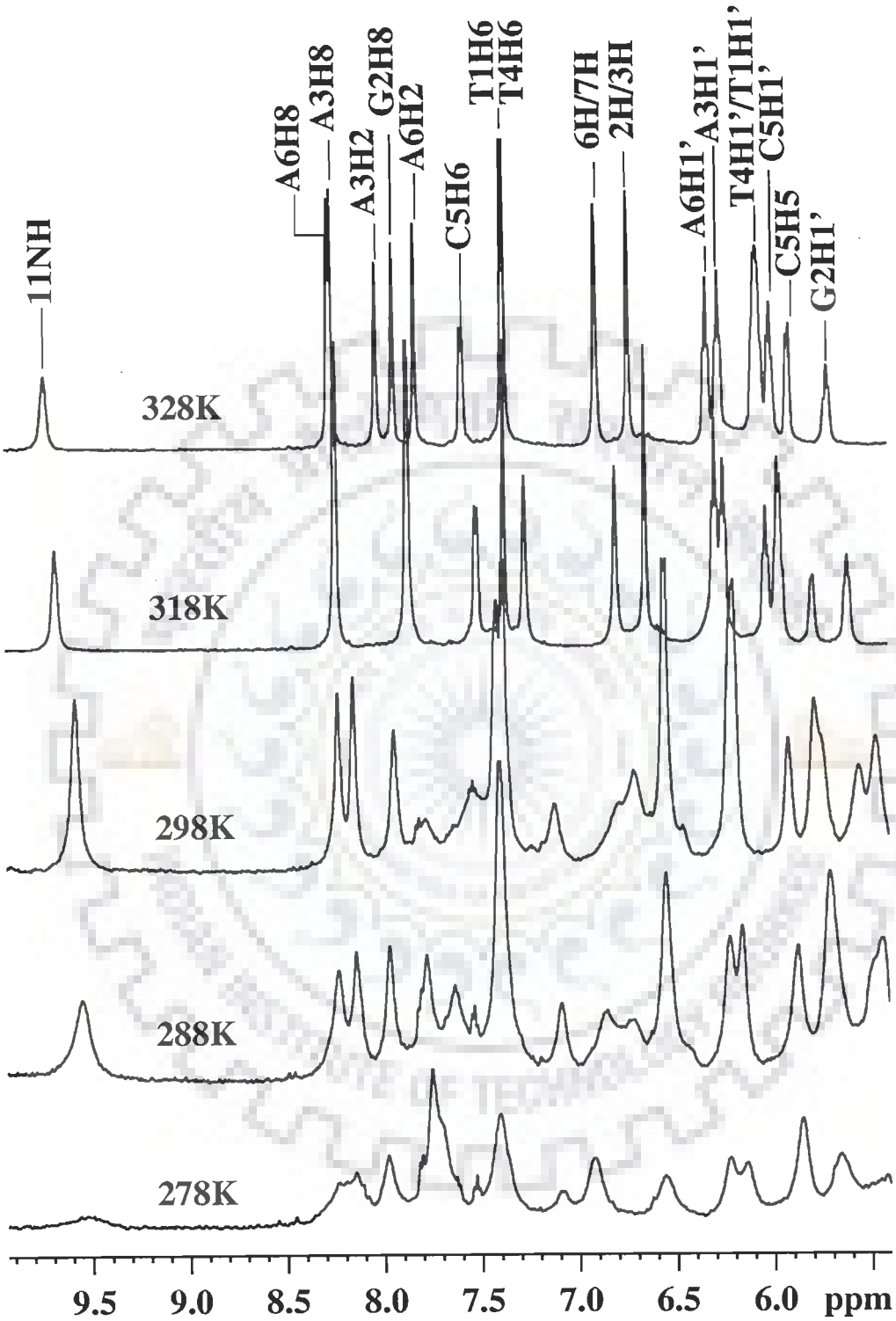
11NH
A6H8
A3H8
A3H2
G2H8
A6H2
C5H6
T1H6
T4H6
6H/7H
2H/3H
A6H1'
A3H1'
T4H1'/T1H1'
C5H1'
C5H5
G2H1'
328K
318K
298K
288K
278K
9.5
9.0
8.5
8.0
7.5
7.0
6.5
6.0
ppm

(Fig. 4.9b)

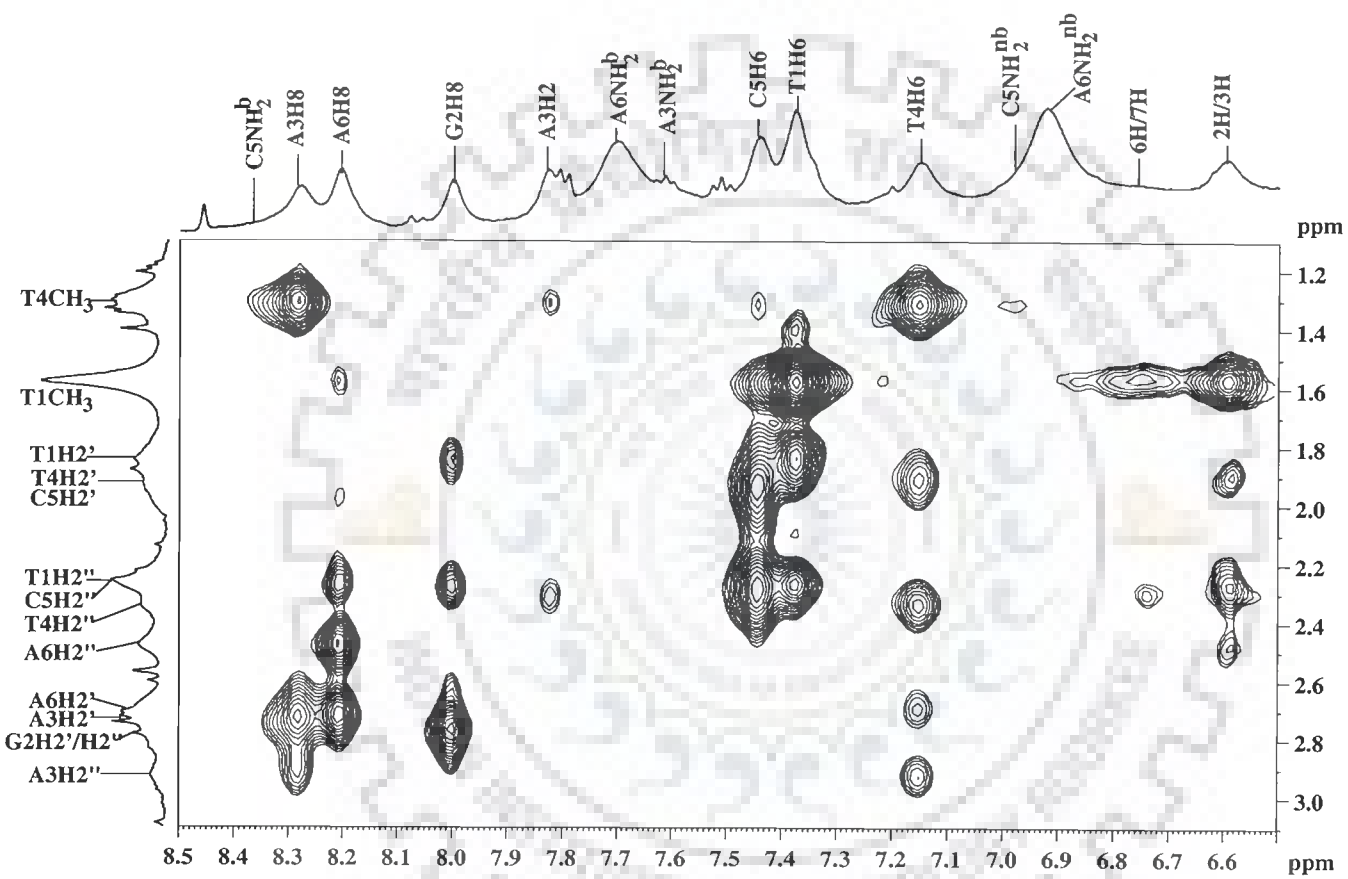

(Fig. 4.10a)

Figure 4.10a–i: Expansions of the specific regions of NOESY spectra of mitoxantrone complexed with d–$(TGATCA)_2$ to highlight specific connectivities.

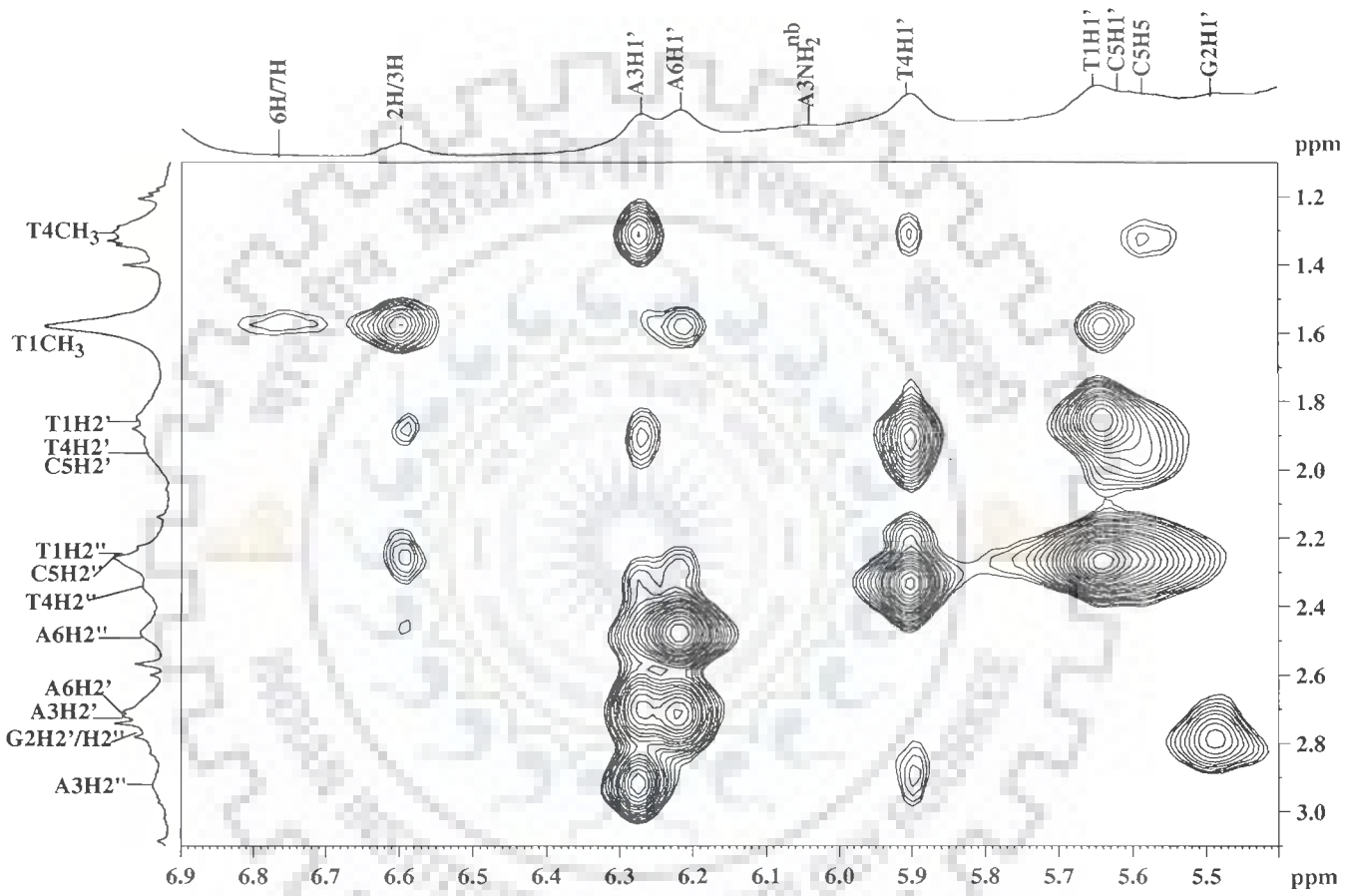
6H/7H
2H/3H
A3H1'
A6H1'
A3NH2nb
T4H1'
T1H1'
C5H1'
C5H5
G2H1'
ppm
1.2
1.4
1.6
1.8
2.0
2.2
2.4
2.6
2.8
3.0
T4CH3
T1CH3
T1H2'
T4H2'
C5H2'
T1H2''
C5H2''
T4H2''
A6H2''
A6H2'
A3H2'
G2H2'/H2''
A3H2''
6.9
6.8
6.7
6.6
6.5
6.4
6.3
6.2
6.1
6.0
5.9
5.8
5.7
5.6
5.5
ppm

(Fig. 4.10b)

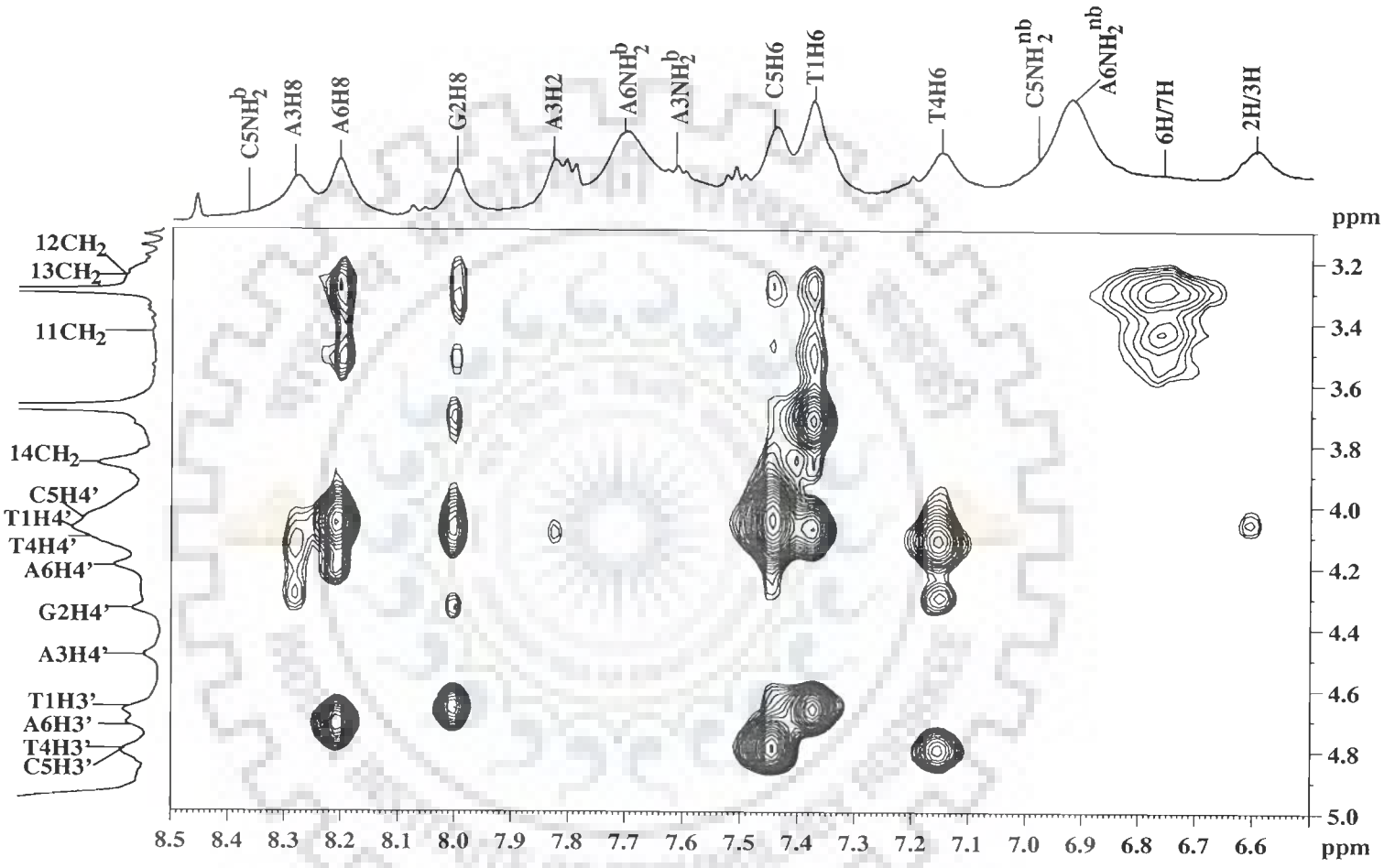
C5NH2b
A3H8
A6H8
G2H8
A3H2
A6NH2b
A3NH2b
C5H6
T1H6
T4H6
C5NH2nb
A6NH2nb
6H/7H
2H/3H
ppm
12CH2
13CH2
11CH2
14CH2
C5H4'
T1H4'
T4H4'
A6H4'
G2H4'
A3H4'
T1H3'
A6H3'
T4H3'
C5H3'
3.2
3.4
3.6
3.8
4.0
4.2
4.4
4.6
4.8
5.0
8.5 8.4 8.3 8.2 8.1 8.0 7.9 7.8 7.7 7.6 7.5 7.4 7.3 7.2 7.1 7.0 6.9 6.8 6.7 6.6
ppm

(Fig. 4.10c)

A6NH2nb
6H/7H
2H/3H
A3H1'
A6H1'
A3NH2nb
T4H1'
T1H1'
C5H1'
C5H5
G2H1'
ppm
12CH2
13CH2
11CH2
14CH2
C5H4'
T1H4'
T4H4'
A6H4'
G2H4'
A3H4'
T1H3'
A6H3'
T4H3'
C5H3'
3.2
3.4
3.6
3.8
4.0
4.2
4.4
4.6
4.8
5.0
7.0 6.9 6.8 6.7 6.6 6.5 6.4 6.3 6.2 6.1 6.0 5.9 5.8 5.7 5.6 5.5
ppm

(Fig. 4.10d)

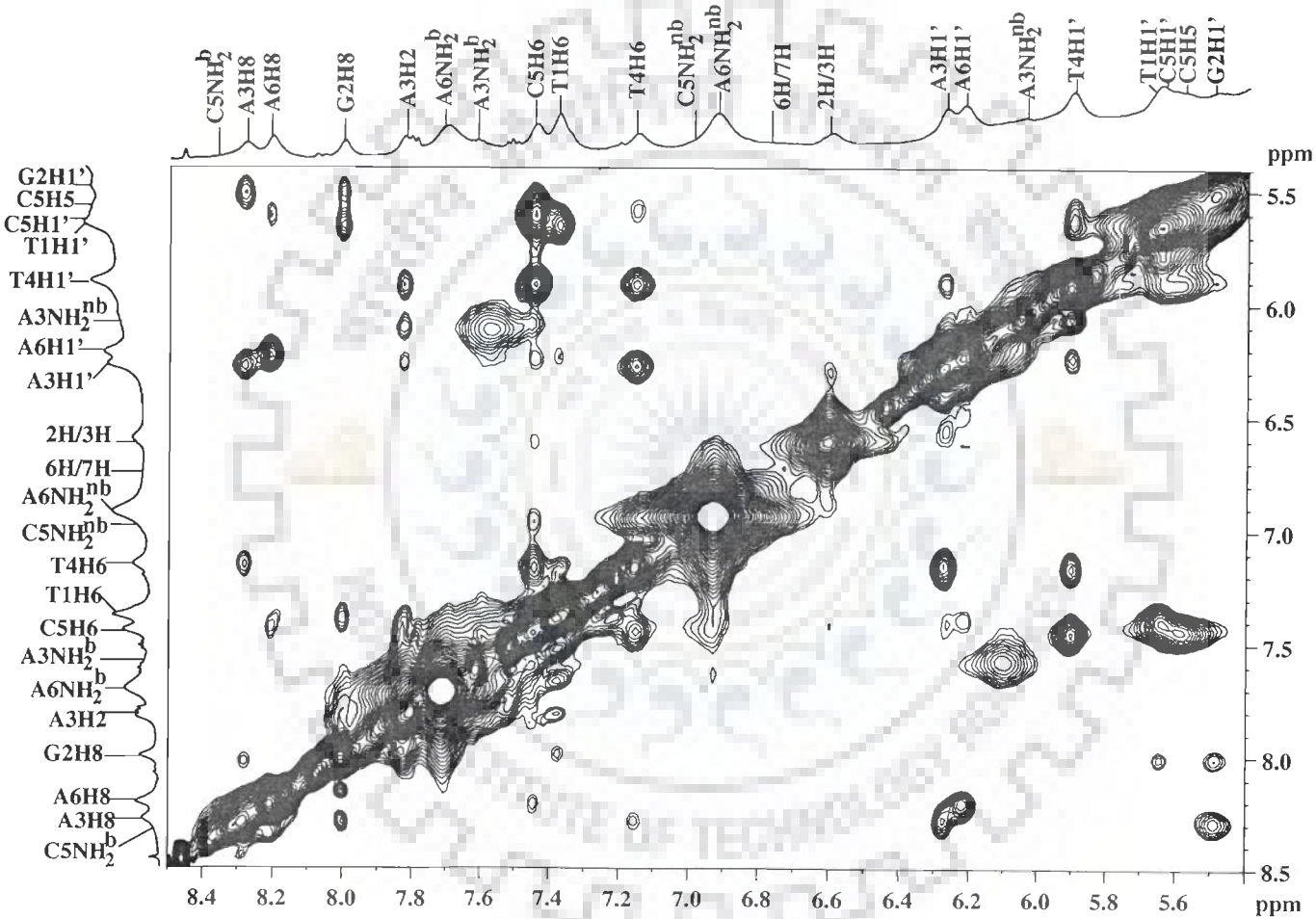
C5NH2b
A3H8
A6H8
G2H8
A3H2
A6NH2b
A3NH2b
C5H6
T1H6
T4H6
C5NH2nb
A6NH2nb
6H/7H
2H/3H
A3H1'
A6H1'
A3NH2nb
T4H1'
T1H1'
C5H1'
C5H5
G2H1'
ppm
5.5
6.0
6.5
7.0
7.5
8.0
8.5
8.4
8.2
8.0
7.8
7.6
7.4
7.2
7.0
6.8
6.6
6.4
6.2
6.0
5.8
5.6
ppm

(Fig. 4.10e)

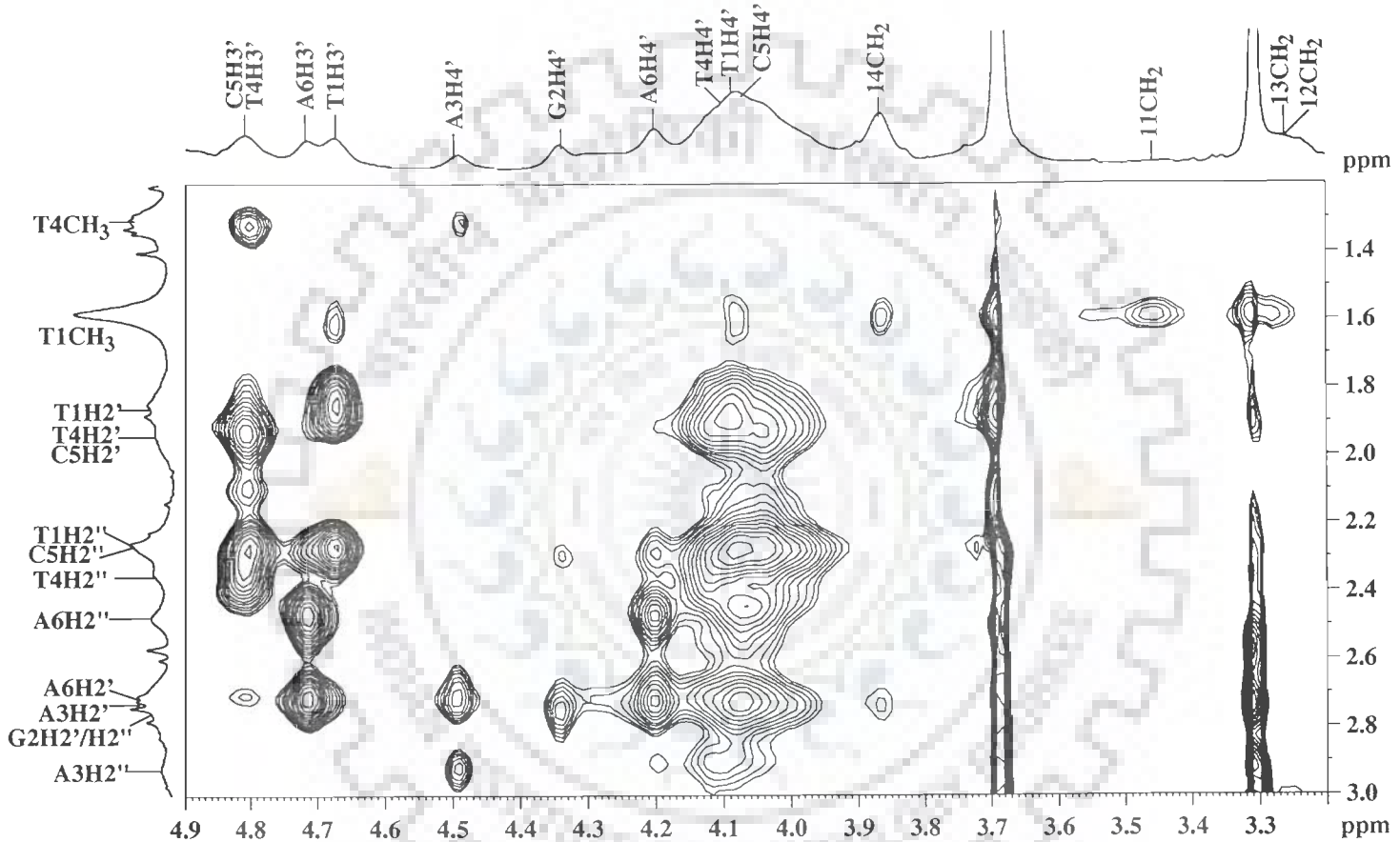
C5H3'
T4H3'
A6H3'
T1H3'
A3H4'
G2H4'
A6H4'
T4H4'
T1H4'
C5H4'
14CH2
11CH2
13CH2
12CH2
ppm
T4CH3
T1CH3
T1H2'
T4H2'
C5H2'
T1H2''
C5H2''
T4H2''
A6H2''
A6H2'
A3H2'
G2H2'/H2''
A3H2''
1.4
1.6
1.8
2.0
2.2
2.4
2.6
2.8
3.0
4.9 4.8 4.7 4.6 4.5 4.4 4.3 4.2 4.1 4.0 3.9 3.8 3.7 3.6 3.5 3.4 3.3
ppm

(Fig. 4.10f)

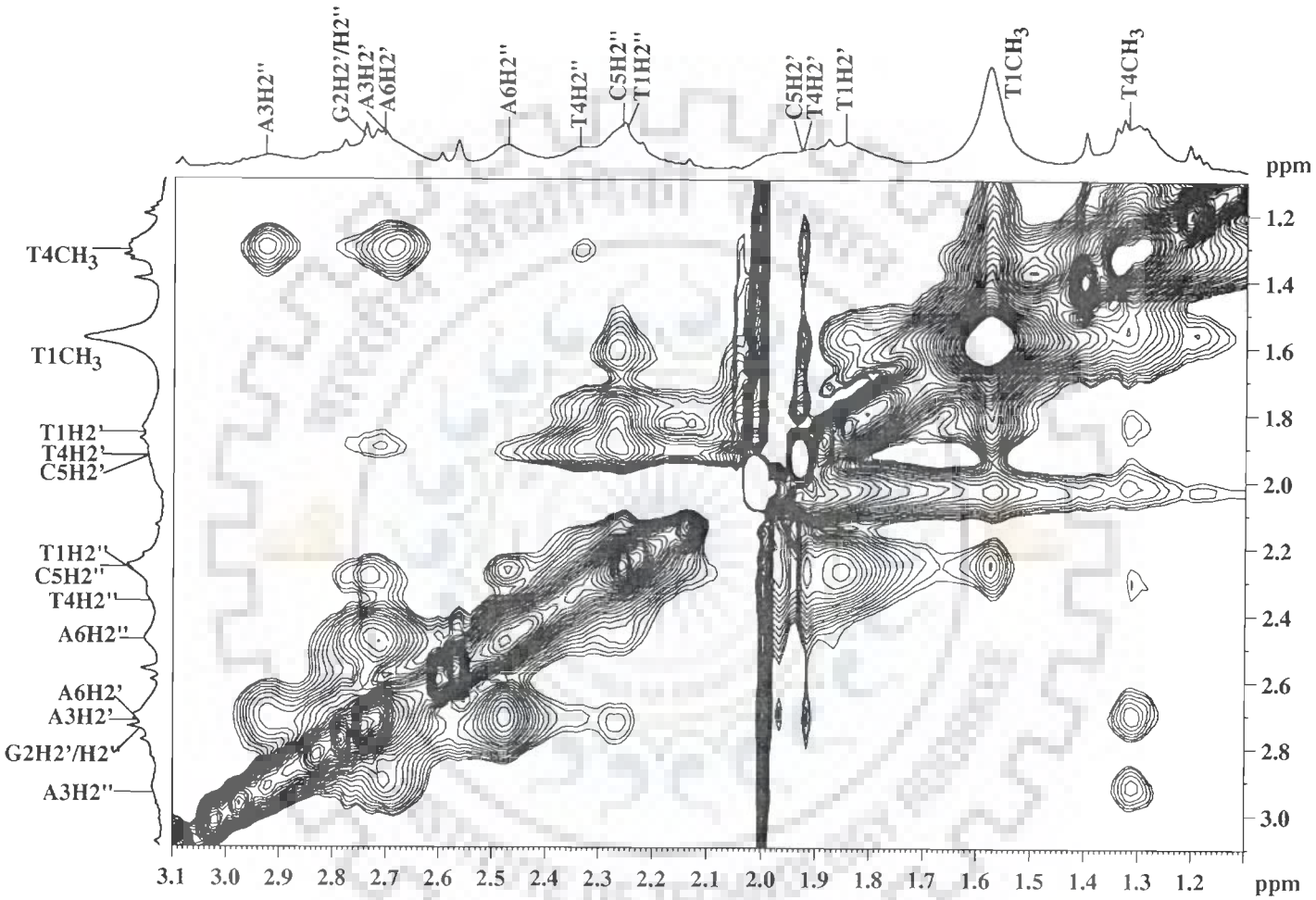
A3H2''
G2H2'/H2''
A3H2'
A6H2'
A6H2''
T4H2''
C5H2''
T1H2''
C5H2'
T4H2'
T1H2'
T1CH3
T4CH3
ppm
1.2
1.4
1.6
1.8
2.0
2.2
2.4
2.6
2.8
3.0
T4CH3
T1CH3
T1H2'
T4H2'
C5H2'
T1H2''
C5H2''
T4H2''
A6H2''
A6H2'
A3H2'
G2H2'/H2''
A3H2''
3.1 3.0 2.9 2.8 2.7 2.6 2.5 2.4 2.3 2.2 2.1 2.0 1.9 1.8 1.7 1.6 1.5 1.4 1.3 1.2
ppm

(Fig. 4.10g)

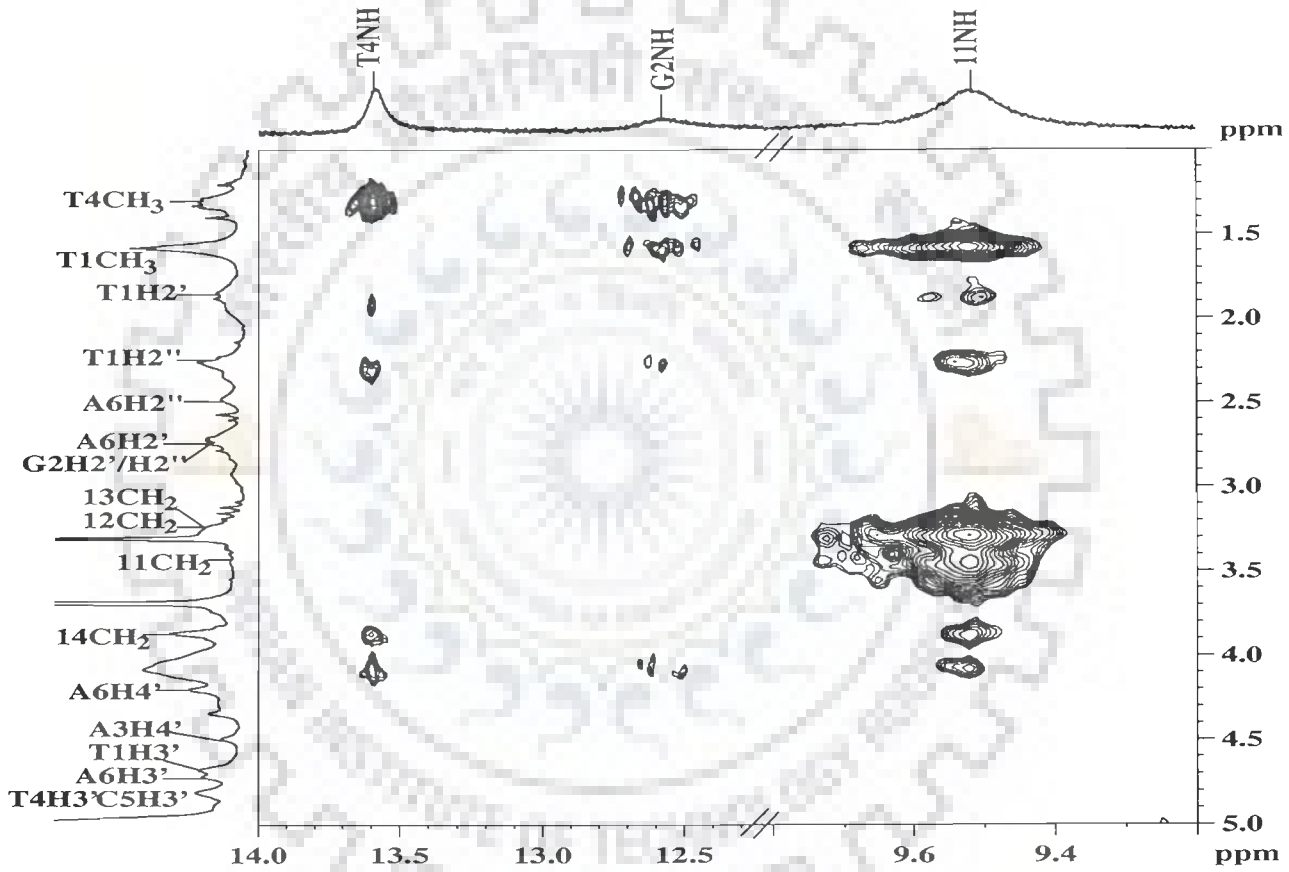
T4NH
G2NH
11NH
ppm
T4CH3
T1CH3
T1H2'
T1H2''
A6H2''
A6H2'
G2H2'/H2''
13CH2
12CH2
11CH2
14CH2
A6H4'
A3H4'
T1H3'
A6H3'
T4H3'/C5H3'
1.5
2.0
2.5
3.0
3.5
4.0
4.5
5.0
14.0
13.5
13.0
12.5
9.6
9.4
ppm

(Fig. 4.10h)

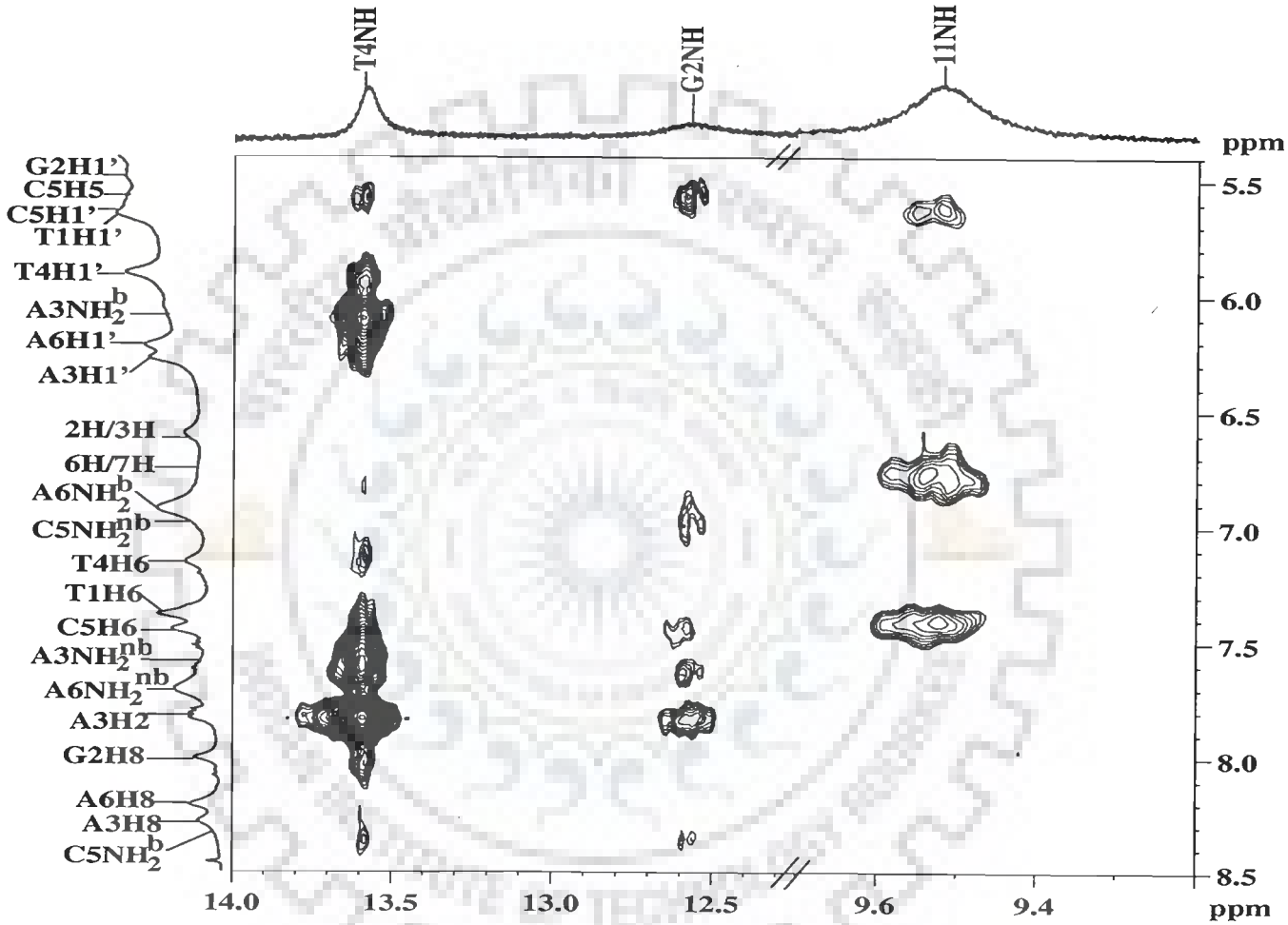
T4NH
G2NH
11NH
ppm
5.5
6.0
6.5
7.0
7.5
8.0
8.5
G2H1'
C5H5
C5H1'
T1H1'
T4H1'
A3NH2b
A6H1'
A3H1'
2H/3H
6H/7H
A6NH2b
C5NH2nb
T4H6
T1H6
C5H6
A3NH2nb
A6NH2nb
A3H2
G2H8
A6H8
A3H8
C5NH2b
14.0
13.5
13.0
12.5
9.6
9.4
ppm

(Fig. 4.10i)

Table 4.5: Chemical shift (ppm) of nucleic acid, d-$(TGATCA)_2$, protons in uncomplexed state (δ_f) and that bound to drug (δ_b) at drug (D) to nucleic acid duplex (N) ratio D/N=1.0 at 278 K. Also shown here is the change in chemical shift on binding, $\Delta\delta = \delta_{b(D/N=1.0)} - \delta_f$

Proton	T1			G2			A3			T4			C5			A6		
	δ_b	δ_f	$\Delta\delta$	δ_b	δ_f	$\Delta\delta$	δ_b	δ_f	$\Delta\delta$	δ_b	δ_f	$\Delta\delta$	δ_b	δ_f	$\Delta\delta$	δ_b	δ_f	$\Delta\delta$
H8/H6	7.38	7.35	+0.03	8.00	8.05	-0.05	8.28	8.35	-0.07	7.15	7.23	-0.08	7.44	7.51	-0.07	8.21	8.28	-0.07
H1'	5.65	5.70	-0.05	5.49	5.55	-0.06	6.27	6.33	-0.06	5.90	5.99	-0.09	5.65	5.70	-0.05	6.22	6.31	-0.09
H2'	1.84	1.82	+0.02	2.76	2.83	-0.07	2.71	2.74	-0.03	1.91	1.97	-0.06	1.93	2.03	-0.10	2.72	2.77	-0.05
H2"	2.27	2.27	+0.00	2.76	2.83	-0.06	2.92	2.98	-0.06	2.34	2.38	-0.04	2.28	2.29	-0.01	2.47	2.51	-0.04
H3'	4.67	4.67	+0.00	4.99	4.99	+0.00	4.99	5.04	-0.05	4.81	4.85	-0.04	4.80	4.81	-0.01	4.71	4.75	-0.04
H4'	4.08	4.07	+0.01	4.34	4.37	-0.03	4.49	4.53	-0.04	4.09	4.17	-0.08	4.04	3.99	+0.05	4.20	4.22	-0.02
H5'	3.72	3.68	+0.04	4.08	4.06	0.02	4.29	4.27	+0.02	4.29	3.95			3.95		4.06	4.08	-0.02
H5"							4.12	4.16	-0.04									
H5/H2/CH_3	1.58	1.61	-0.03				7.81	7.96	-0.15	1.31	1.40	-0.09	5.57	5.70	-0.13	7.70	7.77	-0.07
$NH_2{}^b$							7.58	7.70	-0.12				8.35	8.50	-0.15	7.70	7.70	+0.00
$NH_2{}^{nb}$							6.10	6.20	+0.10				6.98	7.12	-0.14	6.92	6.93	-0.01
NH				12.60	12.72	-0.12				13.59	13.70	-0.11						

-ve $\Delta\delta$ indicates upfield shift
+ve $\Delta\delta$ indicates downfield shift

Table 4.6: Chemical shift (ppm), δ^b, of drug protons bound to nucleic acid duplex at drug (D) to nucleic acid (N) ratio D/N = 1; that in free state, δ^f (concentration 10 mM); and that in monomeric form, $\delta^{monomer}$ (concentration 10μM) at 278 K. Change in chemical shift, due to binding, that is, $\Delta\delta = \delta^b - \delta^f$ with respect to free drug as well as $\Delta\delta' = \delta^b - \delta^{monomer}$ with respect to the drug in monomeric state (Manpreet, 2006) are also shown.

Protons	$\delta^b_{(D/N=1)}$	δ^f	$\Delta\delta = \delta^b_{(D/N=1)} - \delta^f$	$\delta^{monomer}$	$\Delta\delta' = \delta^b_{(D/N=1)} - \delta^{monomer}$
6H/7H	6.76	6.93	-0.17	7.39	-0.63
2H/3H	6.60	6.97	-0.37	7.13	-0.53
$11CH_2$	3.46	3.60	-0.14	3.75	-0.29
$12CH_2$	3.26	3.32	-0.06	3.29	-0.03
$13CH_2$	3.26	3.23	+0.03	3.15	+0.11
$14CH_2$	3.87	3.81	+0.06	3.75	+0.12
11NH	9.52	10.00	-0.48	10.24	-0.72

-ve Δδ indicates upfield shift on binding

+ve Δδ indicates downfield shift on binding

Table 4.7a: Chemical shift (ppm) of nucleotide, d-(TGATCA)$_2$, protons as a function of drug (D) to nucleic acid duplex (N) ratio, D/N, at 278 K. Also shown here is the change in chemical shift on binding, $\Delta\delta = \delta_{D/N=2.0} - \delta_{D/N=0.0}$.

D/N Ratio	T1H1'	G2H1'	A3H1'	T4H1'	C5H1'	A6H1'	T1H6	G2H8	A3H8	T4H6
0.00	5.70	5.55	6.33	5.99	5.70	6.31	7.35	8.05	8.35	7.23
0.20	5.66	5.53	6.32	5.96	5.66	6.29	7.35	8.03	8.32	7.21
0.35	5.65	5.53	6.31	5.95	5.65	6.27	7.35	8.03	8.32	7.20
0.50	5.65	5.52	6.29	5.94	5.65	6.26	7.36	8.02	8.31	7.18
0.65	5.65	5.52	6.29	5.92	5.65	6.25	7.36	8.01	8.30	7.17
0.80	5.65	5.49	6.28	5.91	5.65	6.23	7.37	8.00	8.29	7.16
1.00	5.65	5.49	6.27	5.90	5.65	6.22	7.37	8.00	8.28	7.16
1.10	5.66	-	6.27	5.90	5.65	6.21	7.38	8.00	8.28	7.14
1.20	5.66	-	6.26	5.89	5.66	6.20	7.39	8.00	8.27	7.14
1.30	5.66	-	6.26	5.89	5.66	6.20	7.40	7.99	8.27	7.13
1.40	5.66	-	6.25	5.88	5.66	6.19	7.40	7.99	8.26	7.13
1.50	5.66	-	6.25	5.87	5.66	6.18	7.40	7.99	8.25	7.11
1.75	5.65	-	6.24	5.86	5.65	6.16	7.41	7.98	8.25	7.11
2.00	5.66	-	6.22	5.85	5.66	6.14	7.41	7.98	8.21	7.09
$\Delta\delta$	- 0.04	-	- 0.11	- 0.14	- 0.04	- 0.17	0.06	- 0.07	- 0.14	- 0.14

D/N Ratio	C5H6	A6H8	C5H5	T1CH_3	T4CH_3	A3H2	A6H2	G2NH	T4NH
0.00	7.51	8.28	5.69	1.61	1.40	7.96	7.77	12.72	13.70
0.20	7.49	8.26	5.66	1.59	1.38	7.92	7.72	12.68	13.66
0.35	7.48	8.25	5.65	1.59	1.37	7.90	7.70	12.65	13.65
0.50	7.47	8.24	5.64	1.59	1.35	7.88	7.70	12.64	13.63
0.65	7.46	8.23	5.62	1.58	1.35	7.86	7.71	12.62	13.62
0.80	7.45	8.21	5.61	1.58	1.33	7.84	7.70	12.61	13.60
1.00	7.44	8.21	5.57	1.58	1.31	7.81	7.70	12.60	13.59
1.10	7.44	8.20	-	1.58	1.30	7.81	7.70	12.59	13.59
1.20	7.43	8.19	-	1.58	1.29	7.81	7.70	12.57	13.57
1.30	7.43	8.19	-	1.58	1.29	7.80	7.70	12.61	13.56
1.40	7.42	8.19	-	1.57	1.29	7.80	7.70	12.54	13.56
1.50	7.40	8.18	-	1.56	1.29	7.79	7.71	12.54	13.55
1.75	7.41	8.16	-	1.56	1.25	7.77	7.70	-	13.53
2.00	7.41	8.15	-	1.56	1.23	7.75	7.71	-	13.51
$\Delta\delta$	- 0.10	- 0.13	-	- 0.05	- 0.17	- 0.21	- 0.06	-	- 0.19

-ve $\Delta\delta$ indicates upfield shift
+ve $\Delta\delta$ indicates downfield shift.

Table 4.7b: Chemical shift (ppm) of drug (mitoxantrone) protons as a function of drug (D) to nucleic acid duplex (N) ratio, D / N, at 278 K. Also shown here is the maximum change in chemical shift due to binding, with respect to drug in free self associated form, δ_{free},(1–10 mM, 278 K) as well as the drug in monomeric form, $\delta^{monomer}$. $\Delta\delta = (\delta_{D/N=2.0} - \delta^{monomer})$; $\Delta\delta' = (\delta_{D/N=2.0} - \delta^{free})$.

D/N Ratio	2H/3H	6H/7H	11NH	$11CH_2$	$12CH_2$	$13CH_2$	$14CH_2$
$\delta_{monomer}$	7.13	7.39	10.24	3.75	3.29	3.15	3.75
δfree	6.97	6.93	10.00	3.60	3.32	3.23	3.81
0.20	6.63	-	9.53	-	3.27	3.27	3.88
0.35	6.63	-	9.53	-	3.27	3.27	3.88
0.50	6.62	-	9.53	-	3.27	3.27	3.87
0.65	6.61	-	9.52	-	3.27	3.27	3.87
0.80	6.61	-	9.52	-	3.26	3.26	3.87
1.00	6.60	-	9.52	-	3.26	3.26	3.87
1.10	6.60	-	9.52	-	3.27	3.27	3.87
1.20	6.59	-	9.53	-	3.26	3.26	3.86
1.30	6.59	-	9.52	-	3.26	3.26	3.87
1.40	6.59	-	9.53	-	3.26	3.26	3.87
1.50	6.58	-	9.53	-	3.26	3.26	3.86
1.75	6.57	-	9.53	-	3.24	3.24	3.86
2.00	6.56	-	9.52	-	3.24	3.24	3.86
Δδ	-0.57	-	-0.72	-	-0.05	0.09	0.11
Δδ'	-0.41	-	-0.48	-	-0.08	0.01	0.05

-ve Δδ indicates upfield shift
+ve Δδ indicates downfield shift.

Table 4.8a: Interproton distance (Å) obtained from Sequential NOE connectivities (ds) of nucleotide protons in the drug-DNA complex at D/N = 1.0 at 278 K, estimated from NOESY spectra using C5H6-C5H5 = 2.40Å as a standard reference. Overlap of peaks is indicated as o.

Connectivity	Distance	Connectivity	Distance	Connectivity	Distance
G2H8-T1H1'	3.49	T4H6-A3H2'	3.84	C5H5-T4H6	3.76
G2H8-T1H2'	3.61	T4H6-A3H2"	2.21	C5H6-T4H6	3.67
G2H8-T1H2"	3.08	T4H2'-A3H2"	3.57	A6H8-C5H1'	3.46
G2H8-T1H3'	4.32	T4H6-A3H8	3.87	A6H8-C5H2'	3.62
G2H8-T1H6	4.90	$T4CH_3$ -A3H8	3.49	A6H8-C5H2"	3.0
A3H8-G2H1'	3.43	$T4CH_3$ -A3H2"	2.68	A6H8-C5H6	3.12
A3H8-G2H2'	o	C5H6-T4H1'	3.51		
A3H8-G2H2"	o	C5H6-T4H2'	o		
A3H8-G2H8	4.52	C5H6-T4H2"	2.46		
T4H6-A3H1'	3.02	C5H5-T4H1'	4.06		

Table 4.8b: Interproton distance (Å) obtained from intra nucleotide NOE connectivities (di) of sugar protons in nucleic acid of the drug-DNA complex at D/N = 1.0 at 278 K, estimated from NOESY spectra using C5H6-C5H5 = 2.40Å as a standard reference. Overlap of peaks is indicated as o.

Cross peak	T1	G2	A3	T4	C5	A6
H1'- H2'	2.73	2.64	2.60	2.67	o	2.70
H1'- H2"	o	2.34	2.52	2.49	o	2.33
H1'- H3'	3.68	-	-	3.42	3.86	3.54
H1'- H4'	o	3.64	3.84	2.88	o	2.98
H2' - H2"	2.04	o	2.06	o	o	2.14
H2'- H3'	2.35	-	-	2.26	2.25	2.46
H2'- H4'	o	2.73	3.51	o	o	2.50
H2"- H3'	2.64	-	-	2.52	2.70	2.69
H2"- H4'	o	3.73	3.94	o	o	3.66
H3'- H4'	2.54	-	-	2.47	o	2.56

Table 4.8c: Interproton distance (Å) obtained from intra nucleotide NOE connectivities (di) of base to sugar protons of nucleic acid in the drug-DNA complex at D/N = 1.0 at 278 K, estimated from NOESY spectra using C5H6-C5H5 = 2.40Å as a standard reference. Overlap of peaks is indicated as o.

Cross peak	T1	G2	A3	T4	C5	A6
H8/H6-H1'	3.62	3.89	3.98	3.54	o	3.74
H8/H6-H2'	2.25	2.28	2.42	2.38	2.35	2.22
H8/H6-H2"	3.28	2.80	3.51	3.38	3.28	3.45
H8/H6-H3'	3.62	-	-	4.27	3.74	4.12
H8/H6-H4'	4.04	3.94	4.17	3.83	3.65	4.29

Table 4.8d: NOE connnectivities observed in NOESY spectra of the drug – DNA complex at Drug/DNA ratio (D/N) = 1.0 at 278 K. The very strong (ss), strong (s), medium (ws), weak (w), very weakly (ww) intense cross peaks correspond to distances in the range ss 1.8 – 2.5 Å, s 2.5 – 3.0 Å, ws 3.0 – 3.5 Å, w 3.5 – 4.0 Å, ww 4.0 – 5.0 Å, respectively in the NOESY spectra. Overlap of cross peaks is indicated as o.

Cross peak	NOE Intensity	Cross peak	NOE Intensity	Cross peak	NOE Intensity
Intranucleotide (di)		Internucleotide & Interstrand within Base pair (dpi)		Internucleotide Interstrand & Sequential (dps)	
G2NH – $G2NH_2^b$	vw	G2NH – $C5NH_2^b$	vw	T4NH – G2NH	vw
A3H2 – $A3NH_2^b$	o	A3H2 – T4NH	ss	A3H2 – G2NH	vw
A3H2 – $A3NH_2^{nb}$	m	$A3NH_2^b$ – T4NH	s	$A3NH_2^b$ – G2NH	vw
$A3NH_2^b$– $A3NH_2^{nb}$	ss	$A3NH_2^{nb}$ – T4NH	s		
T4NH – $T4CH_3$	w				
$C5NH_2^b$– C5H5	w	Internucleotide Intrastrand & Sequential (dps)			
$C5NH_2^{nb}$– C5H5	w	G2NH – A3H2	vw		
$C5NH_2^b$– C5H6	vw	G2NH – $A3NH_2^b$	vw		
$C5NH_2^{nb}$– C5H6	o	A3H2 – T4NH	ss		
A6H2 – $A6NH_2^b$	w	$A3NH_2^b$ – T4NH	s		
$C5NH_2^b$– $C5NH_2^{nb}$	m	T4NH – $C5NH_2^b$	vw		

Table 4.9: Interproton distance (Å) obtained from NOE cross peaks within the drug protons in the drug-DNA complex at D/N = 1.0 at 278 K, estimated from NOESY spectra using $13CH_2$-$14CH_2$ as a standard reference. Overlap of peaks is indicated as o.

Connectivity	Distance	Uncomplexed drug
$11CH_2$ – 6H/7H	2.81	2.15
$11CH_2$ – 11NH	3.03	2.69
$11CH_2$ –$12CH_2$/$13CH_2$	o	2.83/3.08
$12CH_2$/$13CH_2$ – 6H/7H	2.72	2.55 ($12CH_2$)
$12CH_2$/$13CH_2$ – 11NH	2.91	3.32 ($12CH_2$)
$12CH_2$/$13CH_2$ – $14CH_2$	2.38	2.40 ($13CH_2$)
$14CH_2$ – 6H/7H	-	-
$14CH_2$ – 11NH	4.22	-
11NH – 6H/7H	3.82	3.60-4.70

Table 4.10: Interproton distance (Å) obtained from intermolecular NOE connectivities between d-(TGATCA)$_2$, and the mitoxantrone in the drug-DNA complex at D/N = 1.0 at 278 K, estimated from NOESY spectra using C5H6-C5H5 = 2.40Å as a standard reference.

Cross peak	NOE Distance	rMD Distance	Cross peak	NOE Distance	rMD Model	Cross peak	NOE Distance	rMD Distance
2H/3H – T1CH_3	2.98	3.85	12CH_2/13CH_2 – T1CH_3	2.62	2.69	11CH_2 – A6H8	4.54	3.94
2H/3H – T1H2"	3.71	4.89	12CH_2/13CH_2 – T1H6	3.43	4.39	11NH – T1CH_3	3.25	3.63
2H/3H – A6H2"	4.39	3.81	12CH_2/13CH_2 – A6H8	4.32	4.71	11NH – T1H1'	4.22	3.40
2H/3H – T1H6	3.96	3.54	12CH_2/13CH_2 – T1H1'	3.46	2.51	11NH – T1H2'	4.66	5.41
2H/3H – T1H4'	3.97	4.00	12CH_2/13CH_2 – T1H2"	3.11	4.24	11NH – T1H4'	4.53	6.59
2H/3H – A6H8	4.23	4.15	12CH_2/13CH_2 – T1H3'	3.59	4.54	11NH – A6H1'	5.15	5.45
2H/3H – A6H1'	3.18	3.45	11CH_2 – T1CH_3	2.61	3.22	11NH – T1H6	3.98	5.04
6H/7H – T1CH_3	3.53	4.60	11CH_2 – T1H1'	3.61	3.64	11NH – T1H2"	4.17	4.37
6H/7H – T1H6	3.97	3.50	11CH_2 – T1H6	3.38	4.13	14CH_2 – T1CH_3	3.43	4.82

shifts as function of temperature further helped to resolve the overlapping resonance peaks. The position of each and every resonance was thus ascertained and unambiguous assignment was done. The chemical shift positions of uncomplexed drug and DNA, drug–DNA complex (D/N =1.0) and the change in chemical shift due to binding are given in Tables 4.5, 4.6 and 4.7a-b. The observed intra molecular and intermolecular NOE contacts are listed in Tables 4.8-4.10.

4.1.2.1. Effects of Titrimetric Addition of Mitoxantrone

On addition of drug to DNA, new resonance peaks pertaining to drug protons start appearing, with increase in intensity as D/N ratio increases. The spectral lines start broadening uniformly at higher ratios indicating binding of drug to DNA. The change in chemical shift ($\Delta\delta$) of base and H1' protons with increasing D/N ratio are gradual and small in magnitude (Fig. 4.7). The $\Delta\delta$ increases with D/N ratio as more and more DNA oligomer binds to the drug and a 0.09 ppm upfield shift was observed for T4H1' and A6H1' protons at D/N =1.0. On further increasing the stoichiometry upto D/N = 2.0, A6H1' showed the maximum upfield shift of 0.17 ppm. 0.14 ppm upfield shift was observed for T4H1', A3H8, T4H6 and A6H8. $T4CH_3$ and A3H2 showed considerable upfield shift of 0.17 and 0.21 ppm respectively at 278K (Table 4.7a). In uncomplexed d–$(TGATCA)_2$, T4NH and G2NH resonances appear at 13.70 and 12.72 ppm, respectively. While the T1NH resonance is not observed presumably due to exchange with water solvent. Both T4NH and G2NH broaden considerably with increasing ratio of mitoxantrone, the broadening in the case of G2NH is more significant with the resonance being completely merged with the base line at D/N ratio of 1.30. Both imino protons show considerable shift of ~0.2 ppm on increasing the D/N upto 2.0. The same trend was almost observed for change in chemical shift when the titration was followed through at 298K. In the base and H1' protons A6H1',

T4H1', A3H1', T4H6 and A6H8 showed maximum upfield shift than other protons. $T4CH_3$ and A3H2 showed considerable upfield shift of 0.17 and 0.24 ppm respectively. A6H2 which was not showing any considerable shift at 278K, observed an upfield shift of 0.32 ppm at 298K.

The shift in drug protons on binding are expected to be maximum at low D/N ratio when maximum amount of drug is present in the bound state The ring protons, 6H/7H, 2H/3H and 11NH, shift upfield 0.63, 0.53 and 0.72 ppm, substantially with respect to the chemical shift position of drug monomer, $\delta^{monomer}$ in 1:1 drug to DNA complex at 278 K (Fig. 4.8 and Table 4.7b). The chemical shift data of 10 μM mitoxantrone is considered to be that due to drug in monomeric state (Manpreet, 2006). The shift in the side chain protons $11CH_2$, $12CH_2$, $13CH_2$ and $14CH_2$ are comparatively less, except for $11CH_2$ with reasonable upfield shift of 0.29 ppm. No further significant variation of chemical shift was observed with increasing D/N ratio (Fig. 4.8). Large upfield shifts on binding for 11NH and protons attached to the aromatic ring (6H/7H and 2H/3H) suggests that aromatic chromophore of mitoxantrone may be stacked with base pairs of DNA. The change in chemical shift ($\Delta\delta$) observed at 298K were almost the same, with ring protons, 6H/7H, 2H/3H and 11NH having maximum upfield shift and reasonable shift in the case of $11CH_2$. Other side chain protons observe no significant change in chemical shift at 298 K.

The concentration of drug molecules is in mM range at D/N >1 and is expected to be in free state (δ^f) at D/N >1, hence in self–associated form (Davies et al, 2001b). Throughout the titration followed at 278K, 298K and 318K only one resonance line is observed for both DNA and drug protons, with gradual shift upfield as the concentration of drug is increased. It is suggested that the signals could be in fast exchange regime, where the chemical shift difference for a proton in the free and

bound states is much smaller than the inverse lifetime of either state. The observed resonance is considered to be an average of free and bound proton in the conditions of the study.

All the spectral lines are somewhat uniformly broadened on binding, as the internal motions are affected and the protons are getting immobilized. The imino protons of DNA, T4NH and G2NH broaden considerably with temperature at 293 K but 11NH of drug is a distinct sharp peak even at temperature of 328 K (Fig. 4.9b). This may be due to hydrogen bonding of 11NH with carbonyl of anthraquinone ring and lack of exchange with solvent. The substantial upfield shift in 11NH, 6H/7H, 2H/3H and $11CH_2$ respectively on binding is indicative of stacking of mitoxantrone aromatic chromophore with base pair of DNA, perhaps T1.A6 base pair. This stacking may result in insignificant shift of $12CH_2$, $13CH_2$ and $14CH_2$ protons, as observed. The shift observed in resonances of DNA protons is not significant. In fact the change in chemical shift is not a sufficient indicator of the interaction, instead the observed intermolecular short contacts are a direct proof of the structure of a specific drug–DNA complex.

4.1.2.2. Structure of the Complex

The 2D NOESY spectra of drug–DNA complex at D/N=1.0 have been investigated extensively at mixing time (τ_m) of 300, 200, 150 and 100ms. The intensities of cross peaks have been estimated qualitatively as strong intense (ss), strong (s) medium (ws) and weakly (w) and very weakly (ww) intense for distances of about 1.8 – 2.5, 2.5 – 3.0, 3.0 – 3.5, 3.5 – 4.0, and 4.0 – 5.0 Å, respectively from the spectra recorded at τ_m = 200 ms. The observed NOEs for (a) sequential connectivities, (b) intranucleotide connectivities within sugar (c) intranucleotide base to sugar connectivities and (d) connectivities involving amino and imino protons of base pairs

are given in Table 4.8a–d. The base sequence d–$(TGATCA)_2$ being self–complementary is responsible for a high symmetry in the NMR spectra. The observation of NOE between the imino proton G2NH, 12.60 ppm and the amino proton of the hydrogen bonded partner namely $C5NH_2^b$, 8.35 ppm in NOESY spectra, establish Watson–Crick base pairing at G2.C5 base pairs in the duplex. Similarly the observation of NOEs between imino proton of thymine, T4NH and A3H2 and amino protons of adenine residues (that is, pairs T4NH 13.59 ppm, A3H2 7.81 ppm; T4NH 13.59 ppm, $A3NH_2^b$ 7.58 ppm) establish Watson and Crick pairing in A3.T4 base pairs.

The sequential connectivities base $(H6/H8)_n$ to $(H1')_{n-1}$, $(H2')_{n-1}$, $(H2'')_{n-1}$, base $(H6/H8)_{n-1}$ connectivities are observed at all base pair steps (Table 4.8a). Some of the sequential connectivities among adjacent base pairs, expected for a typical B–DNA structure, are also observed (Table 4.8d). This clearly demonstrates that DNA duplex is intact and predominantly adopts a B–DNA structure, apparently with no opening between base pairs to accommodate drug chromophore as expected on binding by a typical intercalator.

The base H6/H8–H1' connectivity (Table 4.8c) suggests the residues to be more close to anti conformation. The base to H1' connectivity for the C5 residue is strongly in overlap with the base to H5 connectivity. The deoxyribose conformation may be estimated from intrasugar distances of a nucleotide residue (Wuthrich et al, 1986). Strong intense cross peaks are observed for H1'–H2", H1'–H2', H1'–H3'. The presence of more intense intraresidue H6/H8–H2' than interresidue H6/H8–H2' shows the predominance of S–conformation for the deoxyribose ring. The observed intense cross peaks corresponding to H2"–H3' and H3'–H4' distances show that N–conformer may be present. The presence of moderately intense intranucleotide base

H6/H8–H3' connectivities also confirm the presence of minor N–conformer (Barthwal et al, 2004) in deoxyribose of T1, T4, C5 and A6 residues. The NOE connectivity corresponding to H1'–H4' for G2 and A3 residue is weakly intense as compared to that for T4 and A6 (Table 4.8b).

Table 4.9 shows the intramolecular NOE connectivities observed within the drug molecule in the drug–DNA complex at D/N= 1.0. It is observed that 11NH is close to $11CH_2$, $12CH_2/13CH_2$ (overlap) protons as compared to 6H/7H protons. Also the ring protons 6H/7H are close to $11CH_2$, $12CH_2/13CH_2$ protons, as expected. However, the inter–molecular peaks expected for mitoxantrone dimer due to self-aggregation i.e., 2H/3H with $11CH_2$, $12CH_2$, $13CH_2$, $14CH_2$, 6H/7H protons are clearly missing (Davies et al, 2001b). This shows the drug molecule is bound as monomer molecule to the DNA in the complex.

There are many intermolecular cross peaks between drug and the terminal base pair of DNA is observed like 2H/3H – $T1CH_3$, 2H/3H – T1H6, $11CH_2$ – T1H1', 11NH – A6H1', $11CH_2$ – A6H8 (Table 4.10) which proves that the drug is present at the terminal base pairs of DNA duplex. Also d-$(TGATCA)_2$ does not open to accommodate aromatic chromophore of the mitoxantrone between base pairs, as evidenced by presence of all sequential inter proton connectivities in the two dimensional nuclear Overhauser enhancement spectra (Figs. 4.10a-i). To confirm further the binding of drug to DNA, DOSY studies are done.

4.1.2.3. Diffusion Measurements

The NMR diffusion measurements for mitoxantrone (10mM) and d-$(TGATCA)_2$-Mitoxantrone complex of D/N ratio 2.0, were done at 303 K in D_2O using Stimulated echo sequence incorporating bipolar gradients. The diffusion time

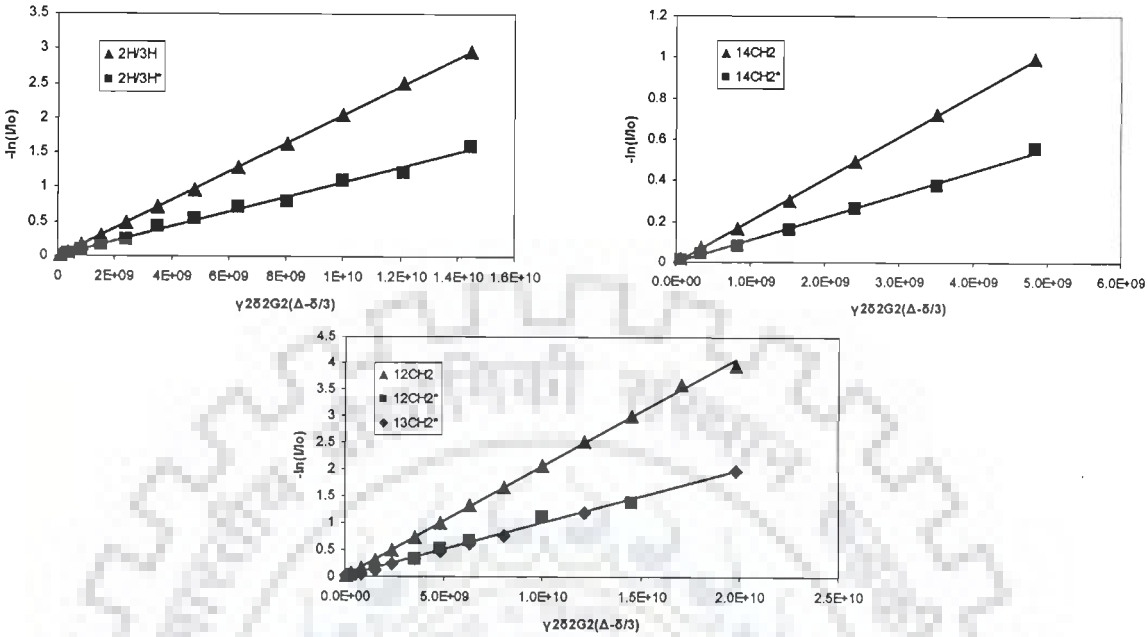

* Drug proton in Drug-DNA complex

Figure 4.11: NMR diffusion measurements at 30°C for mitoxantrone protons alone (▲) and in d-(TGATCA)$_2$ (■). The diffusion coefficient is the slope of the plot –ln(I/Io) versus $\gamma_H^2\delta^2G_z^2(\Delta-\delta/3)$. Samples were prepared in D2O, 100 mM Nacl, 20 mM Phosphate buffer, pH 7.0

Table 4.11: Diffusion coefficients (10^{-10} m^2/s) of mitoxantrone protons alone and in complex with DNA at 30°C

Proton	MTX 10mM 303K	TGMTX (D/N =2.0) 303K
6H/7H	2.081	0.777
2H/3H	2.049	1.077
11CH2	2.059	0.626
12CH2	2.074	1.015
13CH2	2.283	0.967
14CH2	2.064	1.105

(Δ) and the length of diffusion gradient (δ) used were 100ms and 6ms, respectively. The data were processed by fitting the diffusion decays using the SimFit algorithm provided with Bruker processing software- Topspin (version 1.3) and also verified by plotting $-\ln(I/Io)$ versus $\gamma_H^2\delta^2G_z^2(\Delta-\delta/3)$. The slope of the line provides the Diffusion coefficient (D), according to the equation.

$$I / Io = -\exp[D\gamma_H^2\delta^2G_z^2(\Delta-\delta/3)]$$

γ, gyromagnetic ratio (hydrogen); δ, duration of gradient pulse; Gz, gradient amplitude; Δ, delay during which molecule diffuses; I, peak volume; Io, initial peak volume.

We found that mitoxantrone alone has a diffusion coefficient (D) of ~2.0 x 10^{-10} m^2/s. However, in the presence of hexamer, mitoxantrone diffused with D = ~1.0 x 10^{-10} m^2/s, indicating a strong interaction with DNA (Table 4.11). Figure 4.11 shows the plot of $-\ln(I/Io)$ versus $\gamma_H^2\delta^2G_z^2(\Delta-\delta/3)$ for 2H/3H, $14CH_2$ and $12CH_2$ protons alone and in complex with hexamer. The exceptions were 6H/7H and $11CH_2$ protons of complex; accurate measurement of the diffusion was not possible as 6H/7H and $11CH_2$ signals were considerably broadened on drug binding with DNA. The diffusion measurements indicate that the majority of the ligand is associated with the DNA, even when present in 2-fold molar excess as in our NOESY experiments.

4.1.3. Restrained Molecular Dynamics Studies

Restrained molecular dynamics permits the system to undergo conformational and momentum changes so that different parts of the phase space accessible to the molecule can be explored and stable conformations are identified by energy minimization. Based on the observed intermolecular and intramolecular NOE data an initial model with mitoxantrone stacked between two molecules of d-$(TGATCA)_2$ was considered. The schematic representation of the initial model used in rMD, is shown

in Fig. 4.12. DNA1 and DNA2 refer to the two hexamer duplex above and below the mitoxantrone chromophore. Distance restraints between atoms involved in the Watson–Crick hydrogen bonding pairs are imposed in the structure calculations based on experimental evidence from NOESY spectra. The final structure obtained after restrained Molecular Dynamics is shown in Fig. 4.13. Table 4.12a indicates an assessment of refined structures after equilibration (at the end of 25 ps) in terms of energetics including restraint violations energies and root mean square derivative of energy with respect to atomic coordinates. The total potential energy of the final structure is 263 kcal mol^{-1}, which is significantly lower than the corresponding energy of initial model structure (1891 kcal mol^{-1}). The forcing potential, which indicates contribution to potential energy due to violations of both experimental distances data, exhibits a decrease from 429 to 176 kcal mol^{-1} after restrained energy minimization and restrained molecular dynamics. A summary of experimental restraints and statistical analysis of family of structures generated by restrained molecular dynamics (rMD) is shown in Table 4.12b. All helical parameters, backbone torsional angles, and sugar conformations of the resulting rMD structures were thoroughly analyzed with the program CURVES, version 5.1 (Lavery et al, 1996; Lavery et al, 1989). Plot of the helicoidal parameters as a function of residue position in the duplex is shown in Figure 4.14 a-b , along with that for structures of A-DNA and BDNA. The overlap geometry at different base pair steps along the sequence in mitoxantrone - d-$(TGATCA)_2$ is shown in Figure 4.15a-b. Base sequence dependent variations in helicoidal parameters are evident. Among the base pairs-axis parameters, the X-displacement (dx) are ~ 1.5Å for all residues which is close to a value of -0.7Å as seen in canonical B-DNA structure. The y-axis displacement (dy) varies from +0.2 to -0.3Å with no significant variation with base sequence. The base pairs are inclined (η)

at an angle of 0° to +4° terminal T1 and A6 residues inclined upto -5°. The tip angle (θ) being larger at the 3' end (±4°). Among the intra-base parameters, the shear and buckle fluctuates along the base sequence.

Stagger and stretch is fairly large for the TA base pairs at both ends. The variations in the propeller twist are significantly large. For the three base pairs in the middle, negative values in the range -12 to -8 are observed. Large negative values of propeller twist in AT and TA base pairs have been reported in literature (Dronberger et al, 1998; Mujeeb et al, 1993) and may possibly occur to avoid steric clashes between the CH_3 group of thymine and 5' neighboring sugar in AX/XT base pairs step (Hunter, 1993). The magnitude of base pair opening lies close to standard BDNA for all base pairs except for terminal base pairs.

Table 4.12a: Energy terms (Kcal mol^{-1}) for starting structure and final rMD structure

Structure	Total	Bond	Angle	Dihedral
Initial	1891	208	307	282
Final	263	125	104	98
	Vdw	Electrostatic	Restraint	
Initial	798	-181	429	
Final	34	-152	176	

Table 4.12a: Summary of Experimental restraints and statistical analysis of final structure generated by restrained molecular dynamics (rMD)

Parameter	
	No. of Distance Restraints
Intra residue	256
Inter residue	92
Inter molecular	27
Average pairwise RMSD	Initial = 0 Final = 0.88
Average residuewise RMSD	T1=0.99, G2=0.85, A3=1.02 T4=0.89, C5=0.88, A6=0.94 Mitoxantrone=1.18

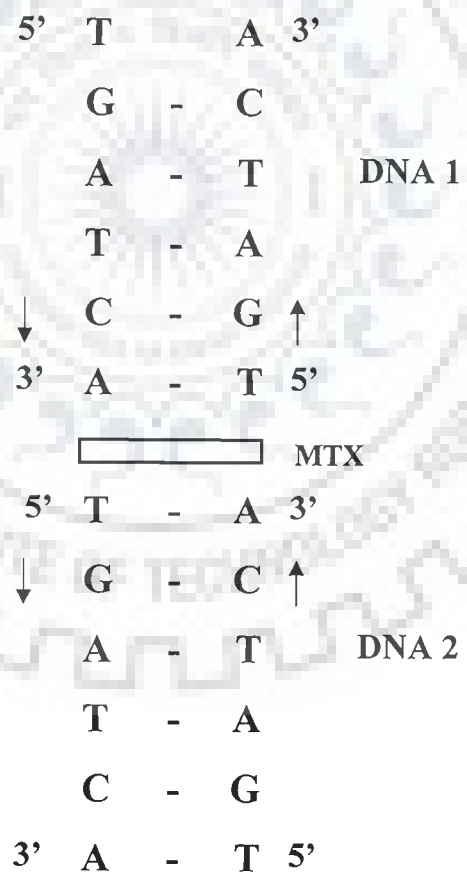

Figure 4.12: Schematic Representation of Mitoxantrone (MTX) - d-$(TGATCA)_2$ Complex

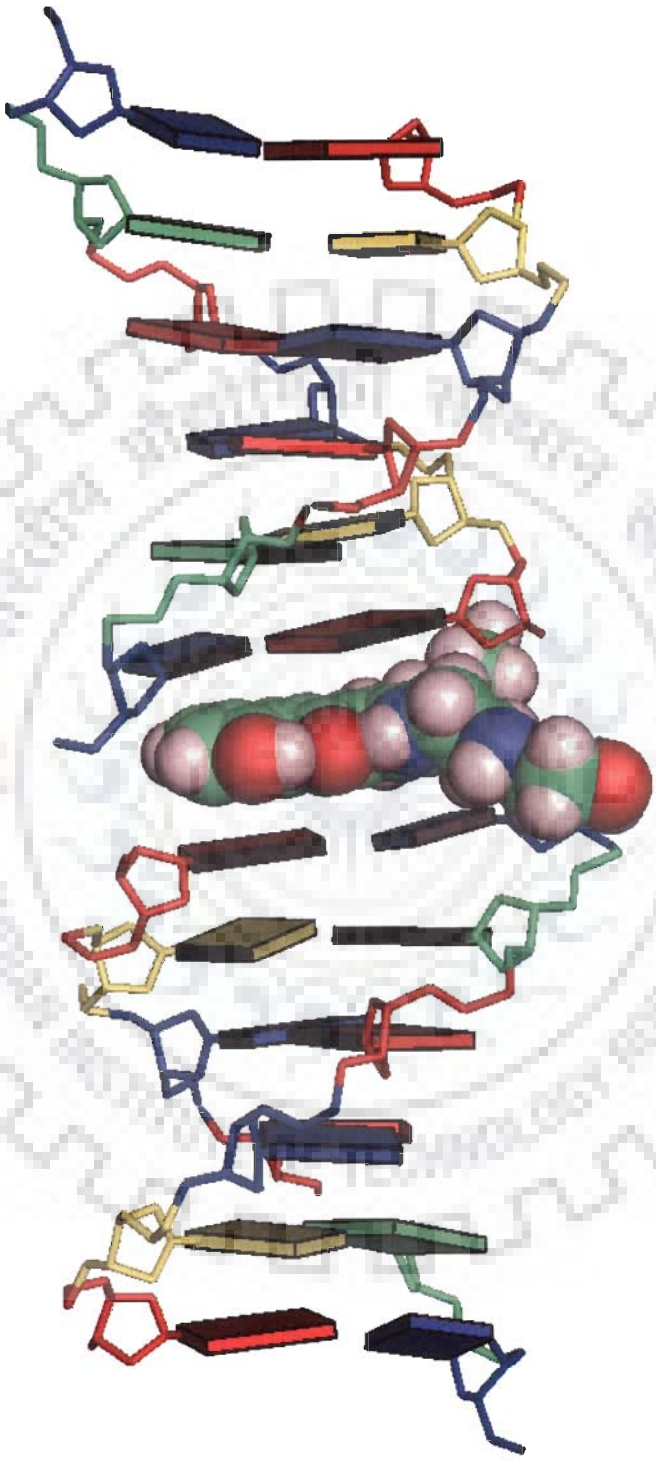

Figure 4.13: Block Representation of final rMD structure of Mitoxantrone d-(TGATCA)$_2$ Complex

Table 4.13: Backbone torsional angles, pseudoratation phase angle and glycosidic bond rotation of the final structure.

DNA1		α		β		γ		δ	
Strand I	Strand II	Strand I	Strand II	Strand I	Strand II	Strand I	Strand II	Strand I	Strand II
T1	A12	.....	61.55	.....	134.14	51.98	-42.05	75.67	160.67
G2	C11	83.96	-67.06	-176.01	169.67	-166.77	58.19	142.03	148.19
A3	T10	64.81	-70.16	-178.04	-179.74	-87.15	58.46	160	147.29
T4	A9	-73.15	-73.22	175.22	-171.97	58.46	53.42	148.01	140.75
C5	G8	-73.32	65.9	140.74	147.15	45.66	167.4	149.81	149.78
A6	T7	32.14	.....	95.92	.....	-42.65	52.99	160.01	69.01
DNA2									
T1	A12	64.72	-66.58	.....	-171.56	52.8	54.59	70.03	141.39
G2	C11	57.92	-71.82	-171.41	135.49	-74.91	52.35	155.57	114.15
A3	T10	-69.21	-76.18	154.9	139.56	-60.86	44.01	162.38	137.31
T4	A9	-69.72	-76.22	-175.03	178.65	57.36	56.73	145.93	151.41
C5	G8	58.58	84.13	174.21	-179.46	60.01	-165.96	148.55	140.78
A6	T7		.....	136.49	.....	-39.44	52.59	160.81	75.22
B-DNA		-63		136		54.0		123	

DNA1		ε		ζ		χ		P	
Strand I	Strand II	Strand I	Strand II	Strand I	Strand II	Strand I	Strand II	Strand I	Strand II
T1	A12	21.26	.....	-86.61	.....	-103.96	-89.25	77.98	211.01
G2	C11	-154.25	-169.84	-124.21	-124.52	-119.67	-116.3	153.24	169.88
A3	T10	-171.43	-162.09	-96.36	-129.88	-102.55	-96.9	199.44	169.64
T4	A9	-102.39	-169.15	-128.99	-108.08	-102.57	-104.83	155.32	169.98
C5	G8	-79.89	-166.53	124.74	-101.94	-100.52	-116.25	152.62	176.21
A6	T7	.....	43	.....	-90.74	-82.05	-125.47	199.6	79.71
DNA2									
T1	A12	162.73	.....	-88.18	.....	-139.75	-118.13	75.95	161.83
G2	C11	-158.4	-178.68	-126.09	-99.32	-124.19	-123.75	177.98	124.65
A3	T10	-179.48	-97.71	-99.01	-113.01	-96.47	-105.45	207.46	141.01
T4	A9	-166.28	-91.51	-119.92	-126.62	-95.76	-105.64	173.12	160.56
C5	G8	-172.35	-159.33	-128.66	-106.54	-109.61	-119.3	171.75	156.58
A6	T7	.....	22.24	.....	-87.09	-95.93	-104.16	209.37	77.18
B-DNA		-169		-108		-105		162	

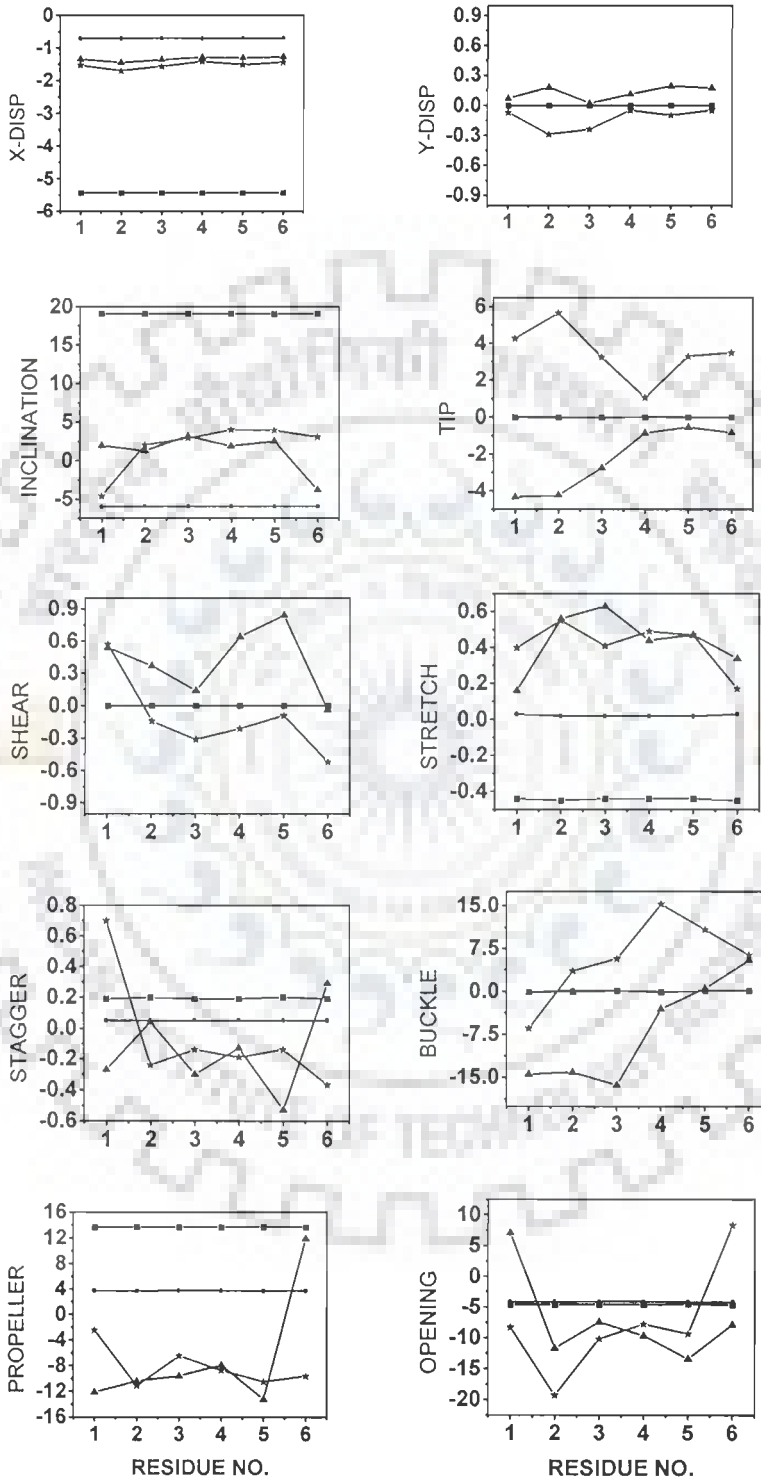
X-DISP
Y-DISP
INCLINATION
TIP
SHEAR
STRETCH
STAGGER
BUCKLE
PROPELLER
OPENING
RESIDUE NO.
RESIDUE NO.

(Fig. 4.14a)

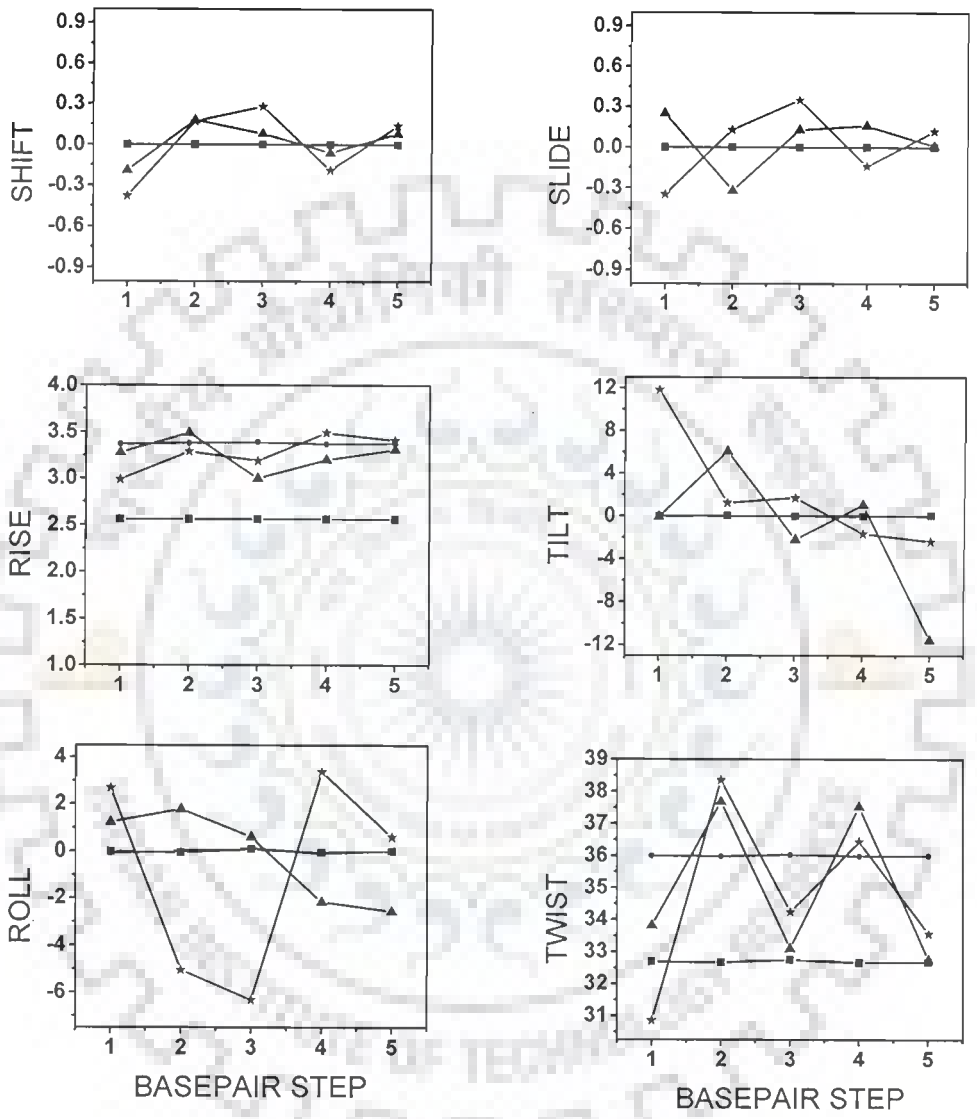

(Fig. 4.14b)

Figure 4.14: (a) and (b) Helical parameters for d-TGATCA complexed with mitoxantrone calculated for structure obtained by restrained molecular dynamics simulation (DNA1 - ▲; DNA2 - ★) and that for canonical A-DNA (■) and B-DNA (●)

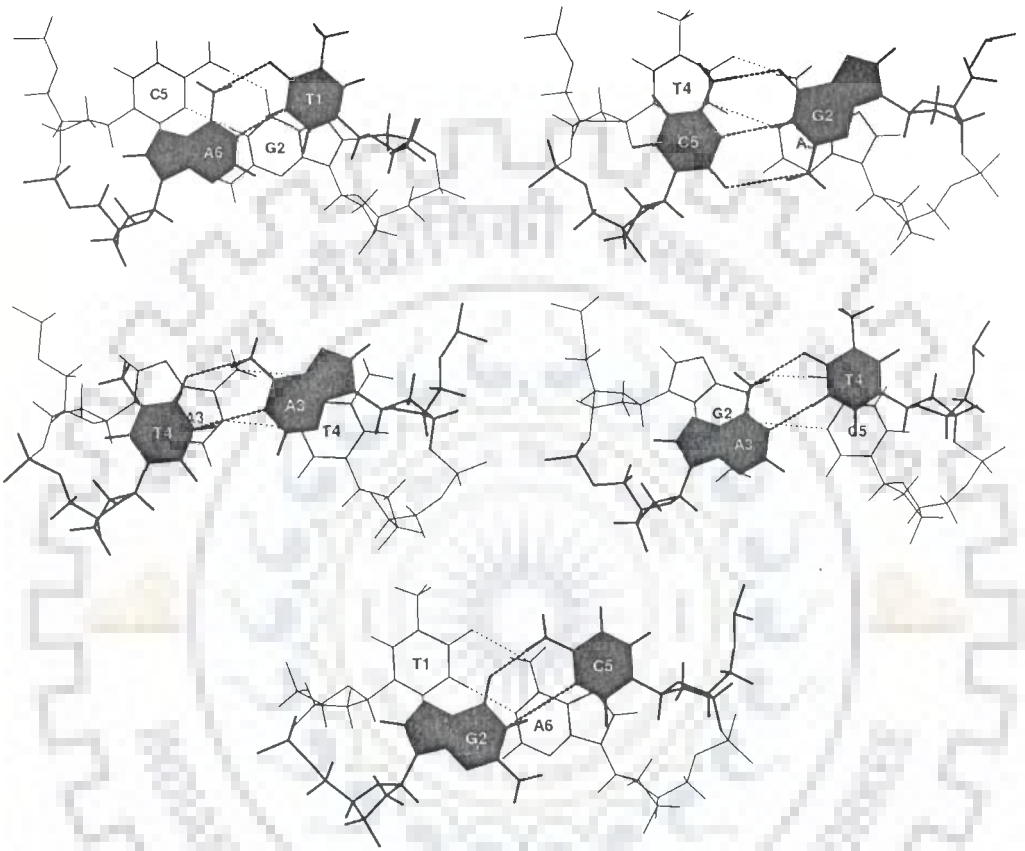

(Fig. 4.15a)

Figure 4.15: Overlap geometry of base pairs at different steps along the sequence (a) DNA1 (b) DNA2

(Fig. 4.15b)

In regular A-DNA and B-DNA geometries, global values of the inter-base pair parameters shift (Dx), slide (Dy), roll (ρ), and tilt (τ) are essentially zero. For the final rMD structure, the shift does not show significant variations with the base sequence. The slide is between ± 0.3Å for all base pair steps. The rise per residue (Dz) is about 3.0 to 3.5Å for all base pair steps. The shift, slide and rise observed are agreement with standard BDNA. The tilt angle fluctuates for terminal residues and appears to be in line with BDNA geometry for all other residues. The roll angle (ρ) varies within -6 to +3°. Positive roll opens the angle between the base pairs towards the minor groove; as a result a wider minor groove and bending towards major groove causing a curvature in the helix occurs. The absence of large positive roll also indicates that base stacking preserved. The twist (Ω) fluctuates fairly along the base pair steps. At the terminal sites T1pG2 and C5pA6, the twist angle is 31-34°. The groove widths of the double helix are defined using the coordinates of the phosphate atoms (Bhattacharya and Bansal, 1992; Mujeeb et al, 1993). In the hexanucleotide only one major and one minor groove exists in the middle of the helix. The width and depth of major groove is found to be 14.9 and 1.7Å while the corresponding values for minor groove are 5.3 and 5.2Å, respectively.

The values of torsional angles obtained for the final rMD structure using CURVES, along with the values for canonical B-DNA are given in Table 4.13. There is difference in absolute values of torsional angles of the two duplex DNA molecules, but the general features and trends with base sequence are identical. The backbone torsional angles are not defined by the restraints obtained from NOESY spectra. We have used a low force constant to permit a smooth search, which is conformationally compatible with other structural features. The torsional angle β, adopts a *trans* conformation similar to that of BDNA for all residues except for the A6 residue of

DNA1. The torsional angle α fluctuates between *gauche*- and *gauche*+ conformations among the residues of both DNA1 and DNA2. Torsional angle γ and δ mostly adopts gauche+ and *trans* conformation respectively for various residues. Notable exception for γ is the G2/G8 residues of both DNA molecules adopting *trans* conformation and for δ, T1/T7 residues of both DNA molecules adopts *gauche*+ conformation. *trans* conformation is mostly observed for ε. ζ of T1/T7 adopts gauche- conformation. No significant change is observed for glycosyl bond rotation chi (χ) in both the DNA molecules. It can thus be seen that the DNA backbone uses a symmetrical mechanism to form complex with mitoxantrone.

4.2. Conclusions

The shift in ^{31}P resonances with temperature in the bound complexes are gradual and the total change, $\Delta\delta = \delta_{328\ K} - \delta_{278\ K}$, is almost same in the complexes having different D/N ratios. The variation of chemical shift with D/N ratio is small and does not show any saturation behavior as would be expected if chromophore of mitoxantrone is to intercalate between base pairs. Further even at higher mitoxantrone concentration, there is absence of a large downfield shift ~1.5 ppm in ^{31}P chemical shifts, as observed with intercalators. These observations preclude intercalation and point towards external binding mode of mitoxantrone with d–$(TGATCA)_2$. ^{31}P-^{31}P exchange spectrum of the d–$(TGATCA)_2$ - mitoxantrone complex at various D/N ratios shows the same. Intermolecular contacts observed between mitoxantrone and d–$(TGATCA)_2$ show that mitoxantrone is close to T1.A6 base pair. T1CH_3 is in close proximity to 2H/3H, 6H/7H, 11CH_2, 12CH_2/13CH_2 and 11NH drug protons. T1CH_3 is close to 2H/3H and 6H/7H, which are situated at opposite ends of the aromatic chromophore of drug molecule. 2H/3H proton is simultaneously close to protons which are located on opposite sides of T1.A6 base pair, as indicated by connectivity

with T1H2" and T1H6 as well as with A6H2", A6H8 and A6H1' protons. Similarly, 11CH_2 shows contact with T1H6 and A6H8; 11NH with A6H1' and T1H1'. Such NOE connectivities are possible only if mitoxantrone aromatic chromophore binds externally to the terminal base pairs of DNA, preferably stacked between two molecules of DNA. Presence of all internucleotide sequential connectivities suggests that the DNA does not open up to accommodate the drug chromophore as observed with intercalators. The ^{1}H NMR studies also support the external mode of binding. Also, throughout the titration only one resonance signal is observed for both DNA and drug protons, with gradual change in chemical shift as the concentration of drug increased. It is suggested the signals are in fast exchange regime and the observed resonance is considered to be an average of free and bound proton. Mitoxantrone is shown to have faster dissociation rates for Poly dA–dT than for Poly dG–dC of an order of magnitude (Krishnamoorthy et al, 1986). Conformational analysis shows DNA hexamer in complexed state adopts a conformation close to that of canonical B–DNA structure. All the duplex pair peaks, sequential intra and inter–strand peaks exist. Consecutive base pairs do not open and therefore we conclude that mitoxantrone binds externally to the DNA duplex, in close proximity to T1.A6 base pair.

Chapter 5

Studies on Complex of Mitoxantrone with d-(CGTACG)$_2$ by Phosphorous-31, Proton Nuclear Magnetic Resonance Spectroscopy and Restrained Molecular Dynamics Approach

This chapter contains the following studies of the complex of mitoxantrone-d-(CGTACG)$_2$ by one- and two-dimensional ^{31}P and ^{1}H NMR followed by restrained molecular dynamics simulations.

- The two dimensional ^{1}H - ^{31}P Heteronuclear Multiple Bond Correlation (HMBC) of 2.76 mM d-(CGTACG)$_2$ at 278 K for the assignment of ^{31}P resonances.
- Titrations by recording ^{31}P and ^{1}H 1D NMR versus drug (D)/DNA duplex (N) ratio, 0.1, 0.2, 0.3, 0.4, 0.5, 0.6, 0.7, 0.8, 0.9, 1.0, 1.2, 1.35, 1.5, 1.65, 1.80 and 2.0 at 275 K and 298 K.
- 2D ^{31}P - ^{31}P exchange spectra of mitoxantrone in complex with d-(CGTACG)$_2$ by a phase-sensitive NOESY with mixing time of 150 ms at 275 K for D/N = 0.2, 0.5 and 1.0
- 2D ^{1}H - ^{1}H NOESY at D/N = 0.5, 1.0, 1.5, 2.0 using mixing time τ_m =100, 200, 300 ms at 275 K in 90% H_2O and 10% D_2O.
- Restrained molecular dynamics studies on the solution structure for the complex of mitoxantrone with d-(CGTACG)$_2$ using inter-proton distances obtained from 2D ^{1}H NOESY as restraints.
- Analysis of the converged structure in terms of time average for the various conformational and helical parameters.

5.1 RESULTS AND DISCUSSION

5.1.1 Phosphorous-31 NMR Studies of Mitoxantrone-d-$(CGTACG)_2$ Complex

5.1.1.1 d-$(CGTACG)_2$

The assignments of ^{31}P nuclei in d-$(CGTACG)_2$ were performed by using the 2D ^{1}H - ^{31}P HMBC (Fig. 5.1). The positions of the bases in the hexamer are designated as follows: d–(C1pG2pT3pA4pC5pG6)$_2$. The three-bond scalar couplings between $(^{31}P)_n$ nuclei in the phosphate backbone and the $(H3')_n$ and four-bond coupling with $(H4')_{n+1}$ protons are observed (Fig. 5.1). The identification of the cross peaks were done on the basis of proton assignments, which have been done by using 2D NOESY spectra. Scalar couplings involving H3' and H4' are considered for the assignment purpose as H5'/5" are overlapped highly. All five three bond scalar coupling of $(^{31}P)_n$ with $(H3')_n$ of the sugar residue i.e., C1pG2 – C1H3', G2pT3 – G2H3', T3pA4 – T3H3', A4pC5 – A4H3' and C5pG6 – C5H3' are observed (Fig. 5.1) . In addition ^{4}J couplings of the phosphorous to the $(H4')_{n+1}$ protons of the sugar residues i.e., C1pG2 – G2H4', G2pT3 – T3H4', T3pA4 – A4H4', A4pC5 – C5H4' and C5pG6 – G6H4' are also clearly evident. Two of the H4' signals (A4 and G2) are separated from the H5' overlapped regions and their connectivities through the four-bond couplings with T3pA4 and C1pG2 phosphates, confirm their assignments (Table 5.1). Accordingly the phosphate resonances at -1.68, -1.45, -1.32, -1.28 and -1.12 were assigned as G2pT3^{f}, A4pC5^{f}, T3pA4^{f}, C1pG2^{f}, and C5pG6^{f} respectively in uncomplexed d-$(CGTACG)_2$ at 275K (Fig 5.2 and Table 5.1). The assigned resonances are in accordance with earlier ^{31}P NMR studies on d-$(CGTACG)_2$ by Ragg et al, 1988 and Mazzini et al, 1998.

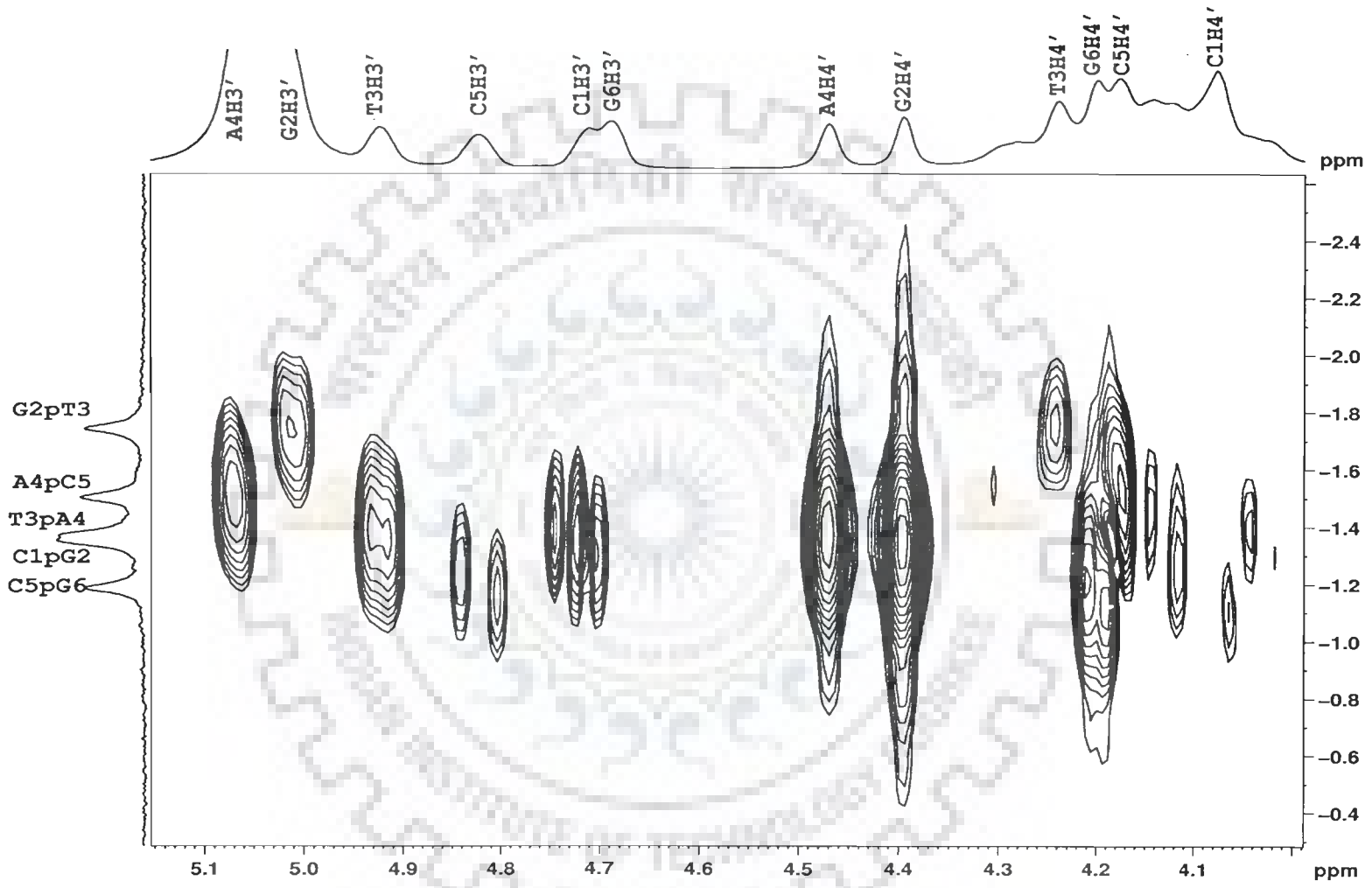

Figure.5.1: Two dimensional ^{31}P - ^{1}H Heteronuclear Multiple Bond Correlation (HMBC) Spectra 2.76 mM d-$(CGTACG)_2$ at 278K

Table 5.1: Chemical shift of ^{31}P resonances of the phosphate groups of d–(CGTACG)$_2$ in complex with mitoxantrone at 275 K and 298 K with increasing drug (D) to nucleic acid duplex (N) ratio (D / N). +ve Δδ indicates downfield shift whereas -ve Δδ indicates upfield shift. $\Delta\delta = (\delta_{D/N=2.0} - \delta_{D/N=0})$.

	275 K					298 K				
D/N	C1pG2[f]	G2pT3[f]	T3pA4[f]	A4pC5[f]	C5pG6[f]	C1pG2[f]	G2pT3[f]	T3pA4[f]	A4pC5[f]	C5pG6[f]
0.00	-1.28	-1.68	-1.32	-1.45	-1.12	-1.06	-1.43	-1.14	-1.21	-0.94
0.10	-1.29	-1.69	-1.32	-1.46	-1.13	-1.06	-1.43	-1.15	-1.21	-0.95
0.20	-1.29	-1.71	-1.33	-1.47	-1.15	-1.07	-1.45	-1.17	-1.22	-0.97
0.30	-1.30	-1.73	-1.35	-1.49	-1.17	-1.08	-1.47	-1.19	-1.24	-0.99
0.40	-1.30	-1.73	-1.35	-1.50	-1.18	-1.08	-1.48	-1.20	-1.24	-1.00
0.50	-1.30	-1.74	-1.36	-1.50	-1.18	-1.08	-1.49	-1.21	-1.24	-1.00
0.60	-1.30	-1.75	-1.36	-1.51	-1.19	-1.08	-1.50	-1.21	-1.25	-1.01
0.70	-1.30	-1.76	-1.36	-1.52	-1.20	-1.08	-1.50	-1.22	-1.25	-1.01
0.80	-1.30	-1.76	-1.36	-1.52	-1.21	-1.08	-1.50	-1.22	-1.25	-1.02
0.90	-1.30	-1.76	-1.36	-1.52	-1.21	-1.08	-1.50	-1.23	-1.25	-1.02
1.00	-1.30	-1.77	-1.37	-1.53	-1.22	-1.08	-1.50	-1.23	-1.25	-1.02
1.20	-1.30	-1.78	-1.37	-1.53	-1.22	-1.08	-1.50	-1.24	-1.25	-1.03
1.35	-1.30	-1.79	-1.37	-1.54	-1.22	-1.08	-1.52	-1.24	-1.25	-1.03
1.50	-1.30	-1.79	-1.37	-1.54	-1.22	-1.08	-1.52	-1.25	-1.25	-1.03
1.65	-1.30	-1.79	-1.37	-1.54	-1.22	-1.08	-1.53	-1.26	-1.25	-1.03
1.8	-1.30	-1.79	-1.37	-1.54	-1.22	-1.08	-1.53	-1.27	-1.25	-1.03
2.0	-1.30	-1.79	-1.37	-1.54	-1.22	-1.08	-1.53	-1.27	-1.25	-1.03
Δδ	-0.02	-0.11	-0.05	-0.09	-0.10	-0.02	-0.10	-0.13	-0.04	-0.09

Table 5.2: ^{31}P chemical shift of free (δ^f) and bound (δ^b) phosphate groups in the mitoxantrone– d–(CGTACG)$_2$ complex obtained from ^{31}P exchange spectrum at drug (D) to nucleic acid duplex (N) ratios, D / N = 0.2, 0.5 and 1.0. The change in chemical shift, $\Delta\delta = \delta^b - \delta^f$, due to binding is also indicated. +ve Δδ indicates downfield shift.

At 275 K	D/N 0.2:1			D/N 0.5:1			D/N 1:1		
Phosphate group	δ_b	δ_f	Δδ	δ_b	δ_f	Δδ	δ_b	δ_f	Δδ
C1pG2	-0.86	-1.29	+0.43	-0.89	-1.30	+0.41	-0.90	-1.30	+0.40
G2pT3	-1.43	-1.71	+0.28	-1.43	-1.74	+0.31	-1.45	-1.77	+0.32
T3pA4	-	-1.33	-	-	-1.36	-	-	-1.37	-
A4pC5	-1.19	-1.47	+0.28	-1.20	-1.50	+0.30	-1.22	-1.53	+0.31
C5pG6	-0.88	-1.15	+0.27	-0.89	-1.18	+0.29	-	-1.22	-

5.1.1.2 Mitoxantrone-d-(CGTACG)$_2$ Complex

The complex of d-(CGTACG)$_2$ with mitoxantrone was made by addition of 3.5 - 5 µl of mitoxantrone from the stock solution (36 mM) to the d-(CGATCG)$_2$ solution till D/N ratio 2.0. The sample was prepared in 90% water and 10% D_2O. The spectra were recorded at 275 K (Fig. 5.2a-b) and 298 K (Fig. 5.2c-d) to look at the rate of exchange of the drug-DNA complex. The addition of mitoxantrone to a solution of the oligomer d-(CGTACG)$_2$ induces a moderate upfield shift as compared to the resonances from free hexamer (Fig. 5.3), but broaden severely with increase in D/N ratio. Only five resonances corresponding to the free hexamer are observed on the formation of the DNA-drug complex. At higher concentration of drug a broad hump is observed low field in the ^{31}P NMR spectrum, as shown in Fig. 5.2b. But on drug binding, each of the five phosphorus signals is expected to give cross peak due to chemical exchange with its respective bound resonance in the 2D ^{31}P NMR exchange spectrum.

(a) 2D ^{31}P - ^{31}P Exchange Spectra

The assignments of bound phosphorus resonance signals are done by ^{31}P - ^{31}P 2D NOESY spectra (Figs. 5.4a-c) at various D/N ratios 0.2, 0.5 and 1.0 at 275 K. The one dimensional ^{31}P spectra at 275 K are shown along both the axes. The five free phosphate resonances are already assigned (Table 5.1) through the ^{1}H - ^{31}P correlation experiment. It is observed in Figs. 5.4a-c that four signals belonging to the phosphate group of free specie is correlated to another phosphate resonance shifted downfield, with respect to it due to exchange correlation. The corresponding downfield shifted signal is accordingly assigned as the ^{31}P signal of bound DNA in the drug-DNA complex. The bound phosphate resonances are assigned as C1pG2^b, G2pT3^b, A4pC5^b and C5pG6^b in the

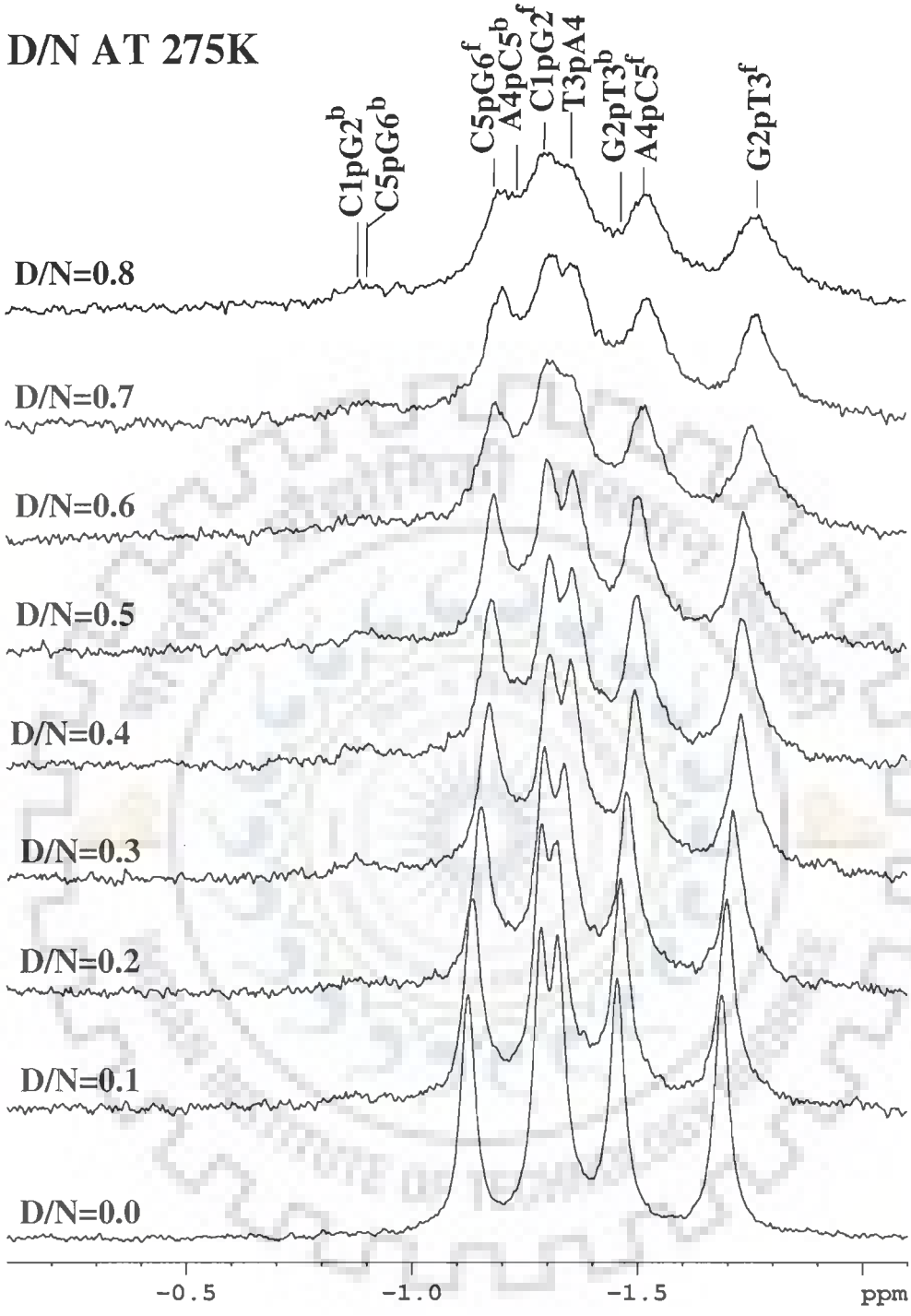

(Fig. 5.2a)

Figure 5.2(a-b): Proton decoupled ^{31}P NMR spectra of 2.76 mM d–$(CGTACG)_2$ in uncomplexed state and complexed with mitoxantrone with increasing drug (D) to nucleic acid duplex (N) ratios, D/N, at 275 K.

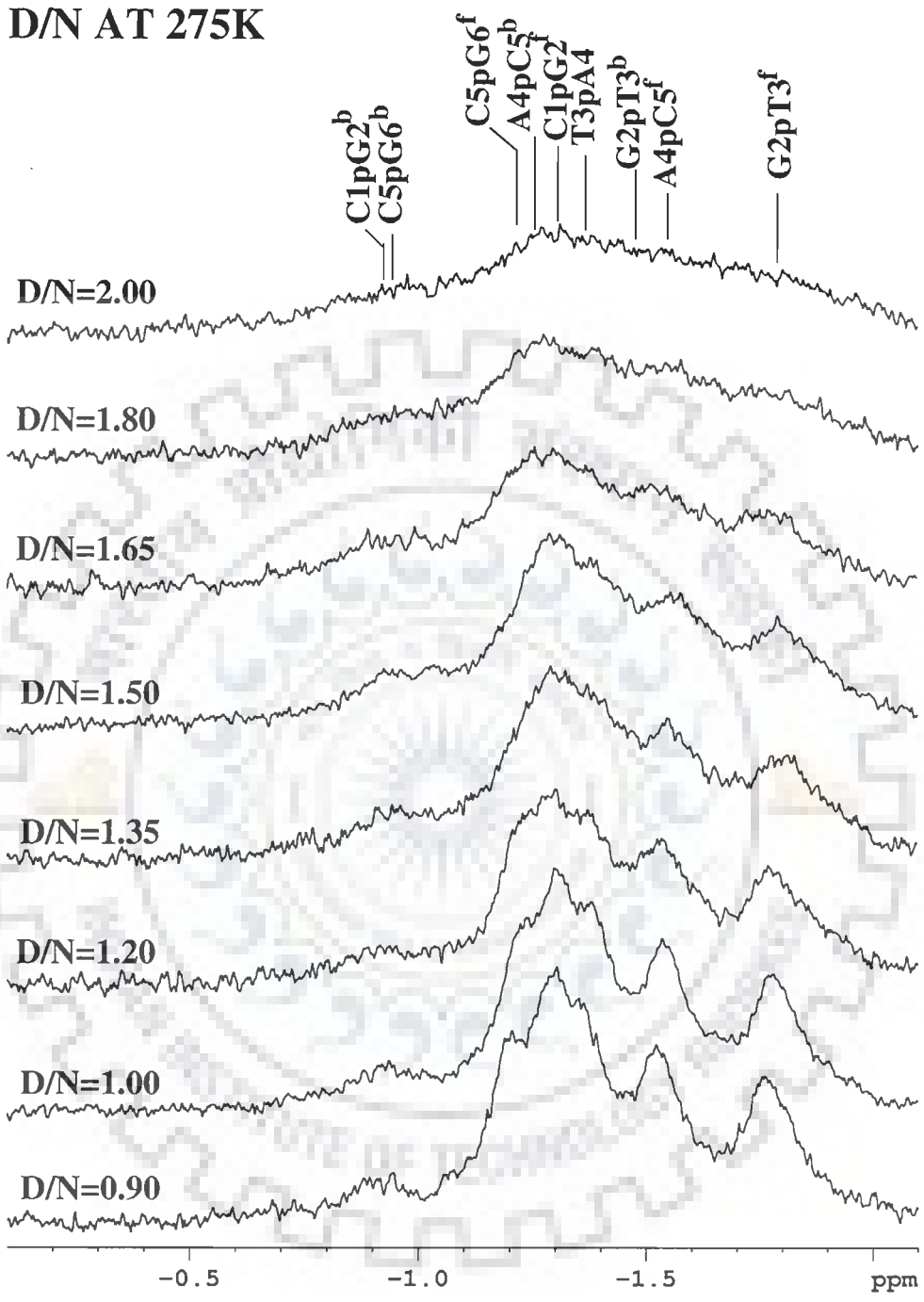
D/N AT 275K
C1pG2b
C5pG6b
C5pG6f
A4pC5b
A4pC5f
C1pG2f
T3pA4
G2pT3b
A4pC5f
G2pT3f
D/N=2.00
D/N=1.80
D/N=1.65
D/N=1.50
D/N=1.35
D/N=1.20
D/N=1.00
D/N=0.90
-0.5
-1.0
-1.5
ppm

(Fig. 5.2b)

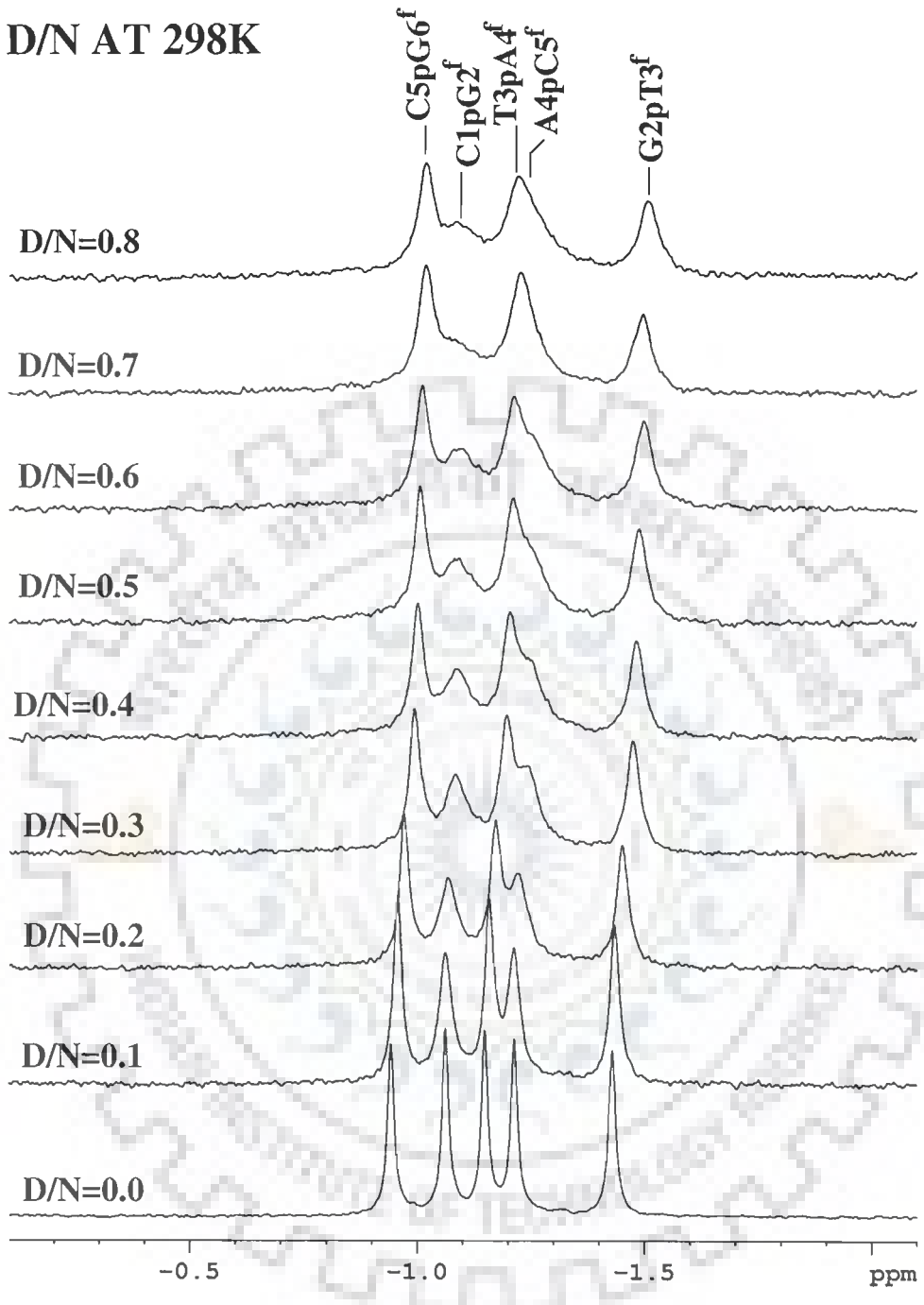

(Fig. 5.2c)

Figure 5.2(c-d): Proton decoupled ^{31}P NMR spectra of 2.76 mM d–$(CGTACG)_2$ in uncomplexed state and complexed with mitoxantrone with increasing drug (D) to nucleic acid duplex (N) ratios, D/N, at 298 K.

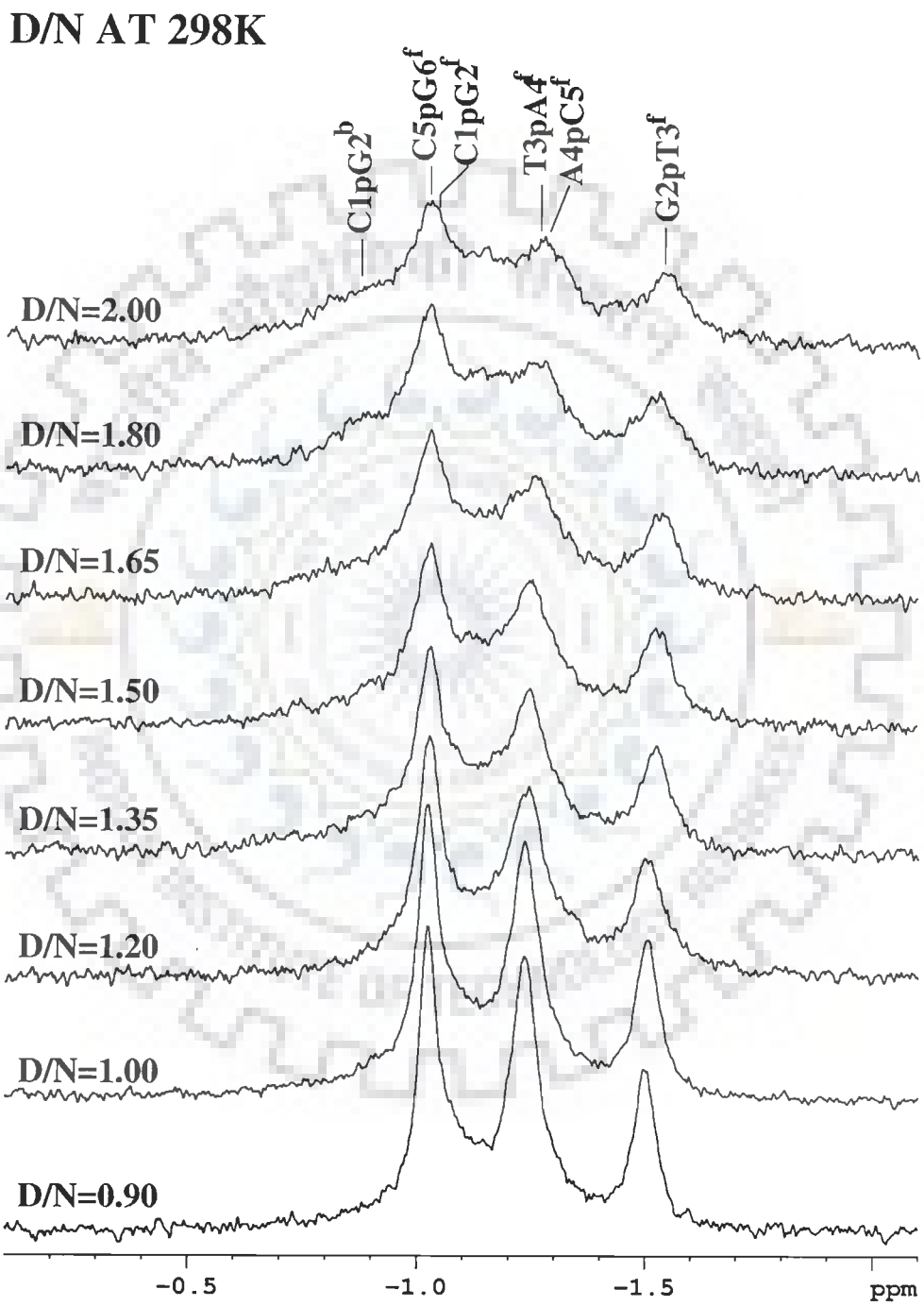
D/N AT 298K
C1pG2b
C5pG6f
C1pG2f
T3pA4f
A4pC5f
G2pT3f
D/N=2.00
D/N=1.80
D/N=1.65
D/N=1.50
D/N=1.35
D/N=1.20
D/N=1.00
D/N=0.90
-0.5
-1.0
-1.5
ppm

(Fig. 5.2d)

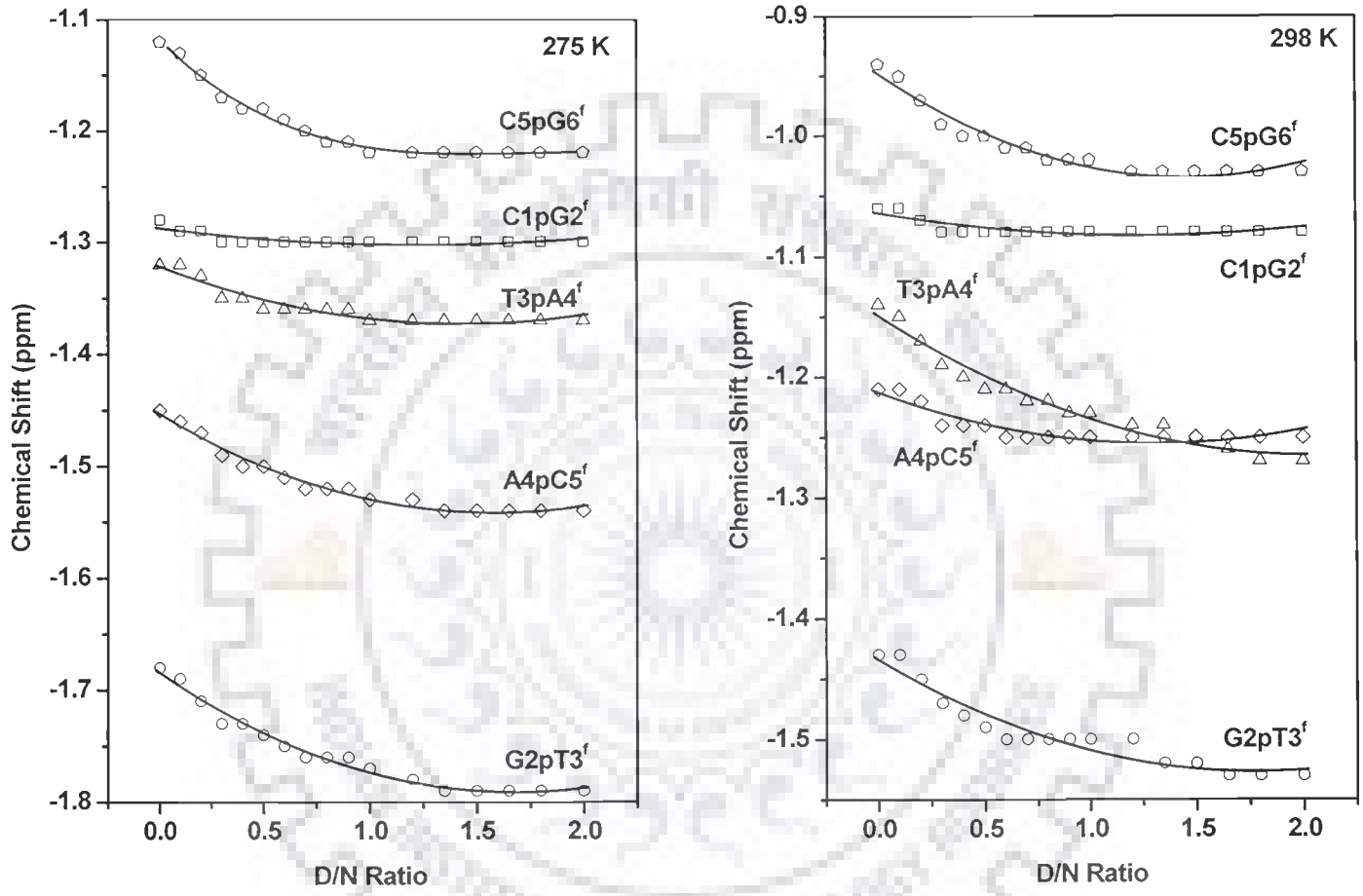

Figure 5.3: ^{31}**P Chemical shift variation of d–(CGTACG)$_2$ in complex with mitoxantrone, as a function D/N ratio (a) at 278K (b) at 298K (□ - T1pG2; ○ - G2pA3; Δ – T3pT4; ◇ - A4pC5; ⬠ - C5pG6).**

complex (Fig. 5.4 and Table 5.2). ^{31}P-^{31}P NOESY exchange clearly proves the fact that there are bound and free species in slow exchange on NMR time scale and yielded $\Delta\delta$ of the drug-DNA

(b) Chemical Shift

It is observed that the C1pG2^f, G2pT3^f, T3pA4^f, A4pC5^f and C5pG6^f resonances shift ($\Delta\delta = \delta^b - \delta^f$) upfield by 0.02, 0.11, 0.05, 0.09 and 0.10 ppm, respectively for the complex of D/N 2.0 at 275K (Table 5.1). The chemical shift of free signals does not change significantly with D/N ratios at 275 K except for the G2pT3^f and C5pG6^f. This also correlates with the upfield shift observed for G2pT3^f and C5pG6^f at 298K. The chemical shift values for the bound resonances of d-$(CGTACG)_2$ obtained from ^{31}P exchange spectrum are listed in Table 5.2, along with the change in chemical shift, $\Delta\delta = \delta^b - \delta^f$ with respect to the corresponding resonance from uncomplexed DNA at D/N = 0.2, 0.5 and 1.0. The significant downfield shift in C1pG2^b (0.40 ppm) resonance and the strong exchange correlation of the bound and free specie (Fig. 5.4) indicates that interaction occurs at this step. The sites adjacent to the interaction site are affected and show downfield shifts G2pT3^b (0.32 ppm), A4pC5^b (0.31 ppm) and C5pG6^b (0.29 ppm).

As discussed in chapter 4, ^{31}P chemical shift variations in nucleotides reflect the conformation of the phosphodiester groups at the level of the P–O5' and O3'–P bonds i.e. the values of torsion angles α = O3'–P—O5'–C5'and ζ = C3'–O3'–P–O5'. For a nucleotide in a B–DNA type conformation, the phosphate groups are normally found in gauche$^-$, gauche$^-$ (g^-, g^-) conformation (B_I) with α and ζ angles of -60° and -90°, respectively whereas the gauche$^-$, trans (g^-, t) B_{II} conformation (α = -60°, ζ = 180°) is

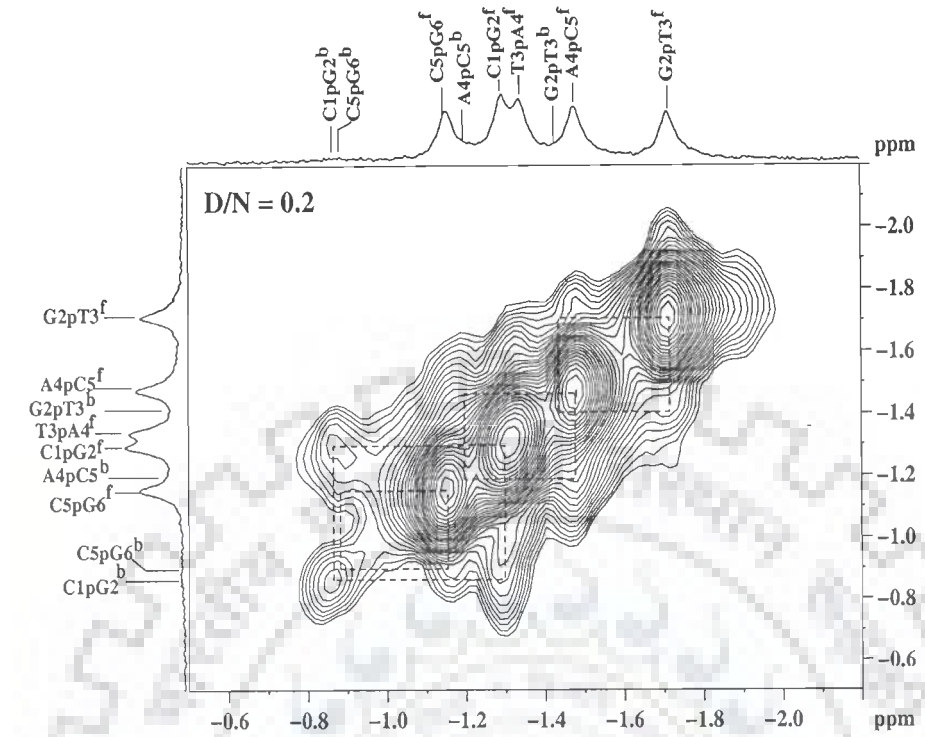

(Fig. 5.4a)

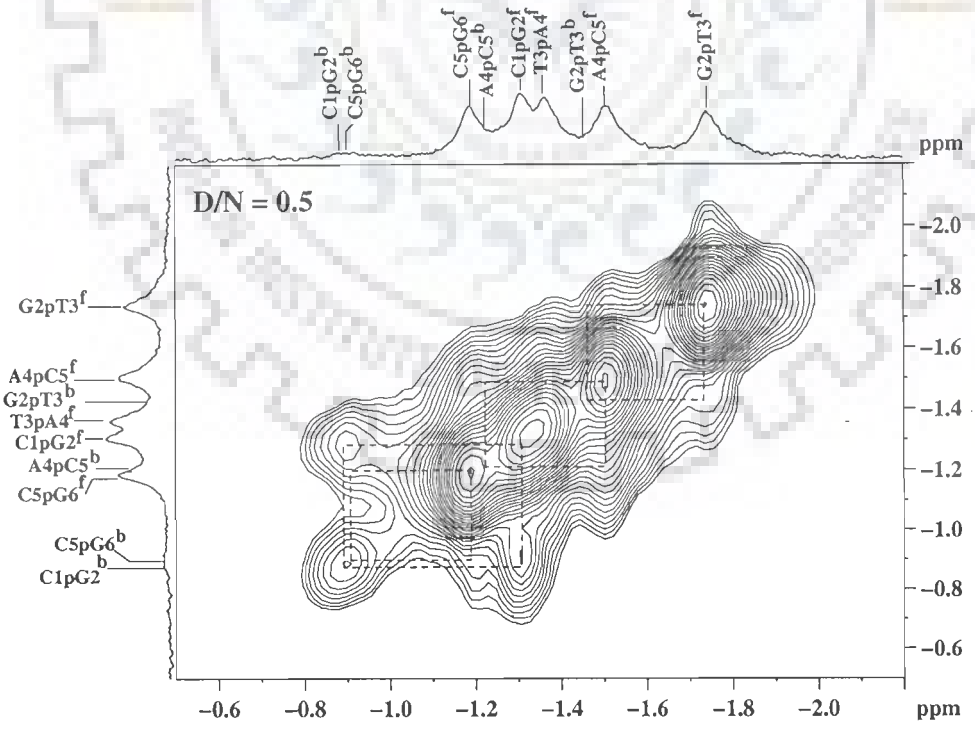

(Fig. 5.4b)

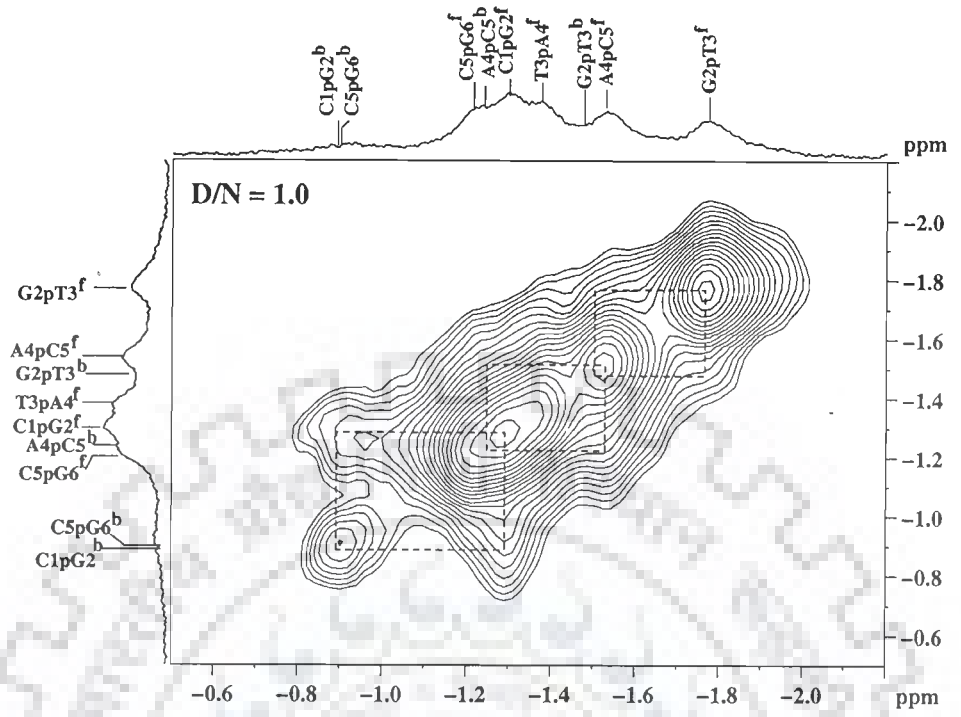

(Fig. 5.4c)

Figure 5.4: ^{31}P - ^{31}P NOESY exchange spectrum at 150 ms of the complex of mitoxantrone with d-$(CGTACG)_2$ at drug (D) to nucleic acid duplex (N) ratios, D/N of (a) 0.2, (b) 0.5, and (c) 1.0 at 275K.

generally associated with a deshielding of 1.5 ppm. Downfield shifts induced by drug are associated with the change in ζ torsional angle from g- to trans conformation and the ester O-P-O bond angle distortion. Thus we may infer that mitoxantrone induces an increase in the g, t conformation for C1pG2 step to accommodate the stacking of the drug aromatic chromophore externally. The downfield shift of other sites G2pT3^b (0.32 ppm), A4pC5^b (0.31 ppm) and C5pG6^b (0.29 ppm) seems to indicate distortions in O-P-O bond angle at the level of these phosphate bonds. It may also be noted that such large downfield shifts observed for interaclation are absent in earlier studies on mitoxantrone (Kotovych et al,

1986; Lown et al, 1985b). Also, for pyridopurine (Favier et al, 2001) and berberine (Mazzini et al, 2003), which show shifts less than 0.20 ppm in phosphorus resonances on binding to DNA (chapter 4, Table 4.3b), have been shown to bind externally. Although the ^{31}P NMR studies provide independent information on the conformation of the phosphate ester backbone, it is unable to provide detailed information on the overall conformation of the complex of mitoxantrone with d-$(CGTACG)_2$. ^{1}H NMR results discussed further in this chapter provide detailed conformational details of interaction.

5.1.2 Proton NMR Studies of Mitoxantrone-d-$(CGTACG)_2$ Complex

The proton NMR spectra of the complex of mitoxantrone-d-$(CGTACG)_2$ at various drug (D) / DNA (N) ratio, D/N at 275 K are shown in Fig. 5.5 (a-f). At 275 K, the imino protons signals are sharpened and intensified. Besides, hexamer DNA is expected to be present completely in duplex state at 275 K. Titration studies at 298 K were also done, to know that if the drug stabilizes the drug-DNA complex at 298 K. The assignment of spectral lines to specific protons of drug has been made by following the strategies used for assignment in NMR spectra of uncomplexed drug (Birlirakis et al, 1992; Davies et al, 2001) and as discussed in chapter 3. The assignment of nucleotide protons has been carried out by following the strategies adopted for standard B–DNA structures that is, sequential NOEs (base $H8/H6)_n$–sugar $(H1')_{n-1}$, (base $H8/H6)_n$–sugar$(H2'')_{n-1}$, (base $H8/H6)_n$–sugar$(H2')_{n-1}$; expected NOEs due to several short intra nucleotide distances (Wüthrich, 1986). The T3NH imino proton was assigned based on the intense cross peak with A4H2 and NOEs with adenine amino protons of the corresponding base pair. G2NH shows strong connectivity with amino protons of the corresponding cytosine base pair. The low-field cytosine amino proton in turn shows an NOE contact with corresponding

CH5 and concluded to be the proton involved in the Watson-Crick hydrogen bond (Boelens et al, 1985). The position of each and every resonance was thus ascertained and unambiguous assignment was done. The chemical shift positions of DNA and drug in the drug–DNA complex at D/N =1.0 and the change in chemical shift due to binding are given in Tables 5.3 and 5.4. It may be noted in Table 5.4 that the chemical shift of a very low concentration of mitoxantrone (10 μM) has been taken to be that due to monomer ($\delta^{monomer}$) (Manpreet, 2006), as the drug is self–associated at millimolar concentrations (δ^{f}) (Davies et al, 2001).

5.1.2.1 Effects of Ttitrimetric Addition of Mitoxantrone

On successive addition of drug to DNA, no significant shift in the DNA and drug proton resonances were observed at 275 and 298 K (Fig. 5.6, 5.7 and Table 5.5a-b, 5.6a-b) while new resonance peaks spectra pertaining to drug protons start appearing (Fig. 5.5 a-f) which increase in intensity as D / N ratio increases, particularly 11NH, $14CH_2$ and 1OH/4OH resonances are clearly evident. Sharp resonance peaks are observed up to D / N ~ 1.0. The spectral lines start broadening uniformly at higher ratios, indicative of binding of DNA to drug. In uncomplexed d-$(CGTACG)_2$, T3NH, G6NH and G2NH peaks appear at 13.66, 13.12 and 12.89 ppm respectively in the imino region of the spectrum. The presence of the T3NH, G6NH and G2NH imino resonances at 275 K confirm the duplex state of the hexamer with the Watson and Crick base pairs intact in the sequence. The intensity of G6NH resonance is comparatively less and broadened to other two imino resonances. This may be attributed to increase fraying at the end of DNA which leads to a significant exchange of NH proton with that of water solvent. On

Table 5.3: Chemical shift (ppm) of d-$(CGTACG)_2$ protons in uncomplexed state (δ_f) and that bound to drug (δ_b) at drug (D) to nucleic acid duplex (N) ratio D/N=1.0 at 275 K. Also shown here is the change in chemical shift on binding, $\Delta\delta = \delta_{b(D/N=1.0)} - \delta_f$.

Proton	C1			G2			T3			A4			C5			G6		
	δ_b	δ_f	$\Delta\delta$	δ_b	δ_f	$\Delta\delta$	δ_b	δ_f	$\Delta\delta$	δ_b	δ_f	$\Delta\delta$	δ_b	δ_f	$\Delta\delta$	δ_b	δ_f	$\Delta\delta$
H8/H6	7.61	7.67	-0.06	8.02	8.04	-0.02	7.34	7.35	-0.01	8.36	8.38	-0.02	7.31	7.32	-0.01	7.86	7.92	-0.06
H1'	5.60	5.70	-0.10	5.97	6.00	-0.03	5.63	5.66	-0.03	6.23	6.26	-0.03	5.60	5.62	-0.02	6.05	6.14	-0.09
H2'	2.05	2.07	-0.02	2.73	2.73	+0.00	2.21	2.18	+0.03	2.73	2.73	0.00	1.88	1.90	-0.02	2.59	2.62	-0.03
H2"	2.42	2.44	-0.02	2.79	2.81	-0.02	2.46	2.46	+0.00	2.89	2.90	-0.01	2.26	2.30	-0.04	2.27	2.37	-0.10
H3'	4.66	4.71	-0.05	5.00	5.01	-0.01	4.92	4.94	-0.02	5.03	5.04	-0.01	4.80	4.82	-0.02	4.66	4.69	-0.03
H4'	4.05	4.08	-0.03	4.38	4.39	-0.01	4.22	4.24	-0.02	4.45	4.47	0.02	4.16	4.17	-0.01	4.18	4.19	-0.01
H5/H2	5.78	5.83	-0.05	-	-	-	-	-	-	7.54	7.59	-0.05	5.35	5.39	-0.04	-	-	-
NH_2^b	8.18	8.18	0.00	-	7.35	-	-	-	-	7.85	7.92	-0.07	8.30	8.37	-0.07	-	-	-
NH_2^{nb}	6.96	7.03	-0.07	-	6.72	-	-	-	-	6.27	6.31	-0.04	6.87	6.85	+0.02	-	-	-
#NH				11.99	12.86	-0.87	13.41	13.68	-0.27							12.39	13.09	-0.70
#CH_3							1.33	1.54	-0.23									

observed as bound and free species at D/N = 1.0
-ve $\Delta\delta$ indicates upfield shift
+ve $\Delta\delta$ indicates downfield shift

Table 5.4: Chemical shift (ppm), δ^b, of drug protons bound to nucleic acid duplex at drug (D) to nucleic acid (N) ratio D/N = 1.0; that in free state, δ^f (concentration 10 mM); and that in monomeric form, $\delta^{monomer}$ (concentration 10μM) at 278 K. Change in chemical shift, due to binding, that is, $\Delta\delta = \delta^b - \delta^f$ with respect to free drug as well as $\Delta\delta' = \delta^b - \delta^{monomer}$ with respect to the drug in monomeric state are also shown.

Protons	$\delta^b_{(D/N=1)}$	δ^f	$\Delta\delta = \delta^b_{(D/N=1)} - \delta^f$	$\delta^{monomer}$	$\Delta\delta' = \delta^b_{(D/N=1)} - \delta^{monomer}$
6H/7H	7.09	6.93	+0.16	7.39	-0.30
2H/3H	6.45	6.97	-0.52	7.13	-0.68
$11CH_2$	3.44	3.60	-0.16	3.75	-0.31
$12CH_2$	3.23	3.32	-0.09	3.29	-0.06
$13CH_2$	3.23	3.23	0.00	3.15	+0.08
$14CH_2$	3.83	3.81	+0.02	3.75	+0.08
# 11NH	9.29	9.42	-0.13	10.24	-0.95

observed as bound and free species at D/N = 1.0

-ve Δδ indicates upfield shift on binding

+ve Δδ indicates downfield shift on binding

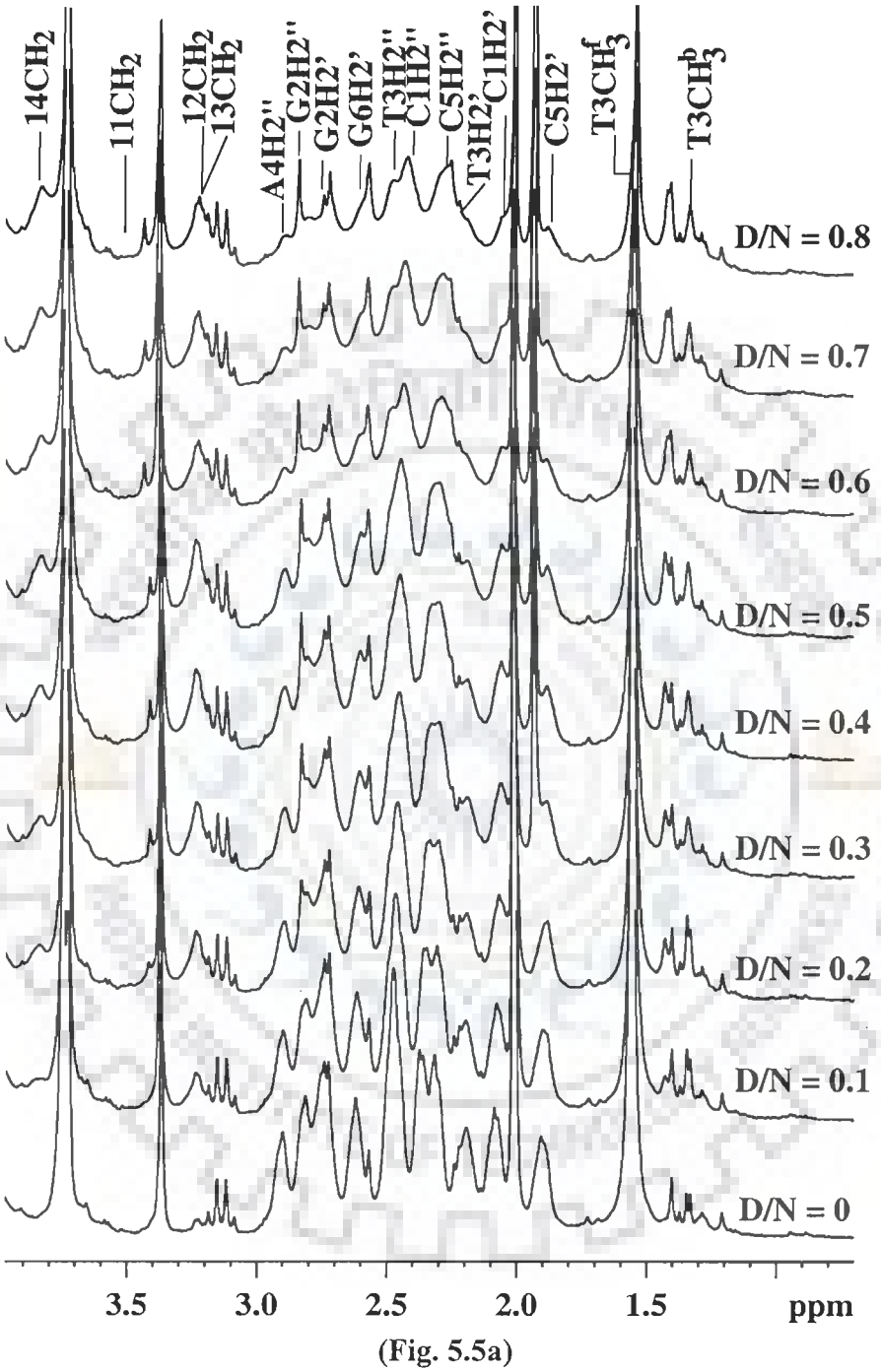

(Fig. 5.5a)

Figure 5.5 (a-f): Proton NMR spectra of 2.76 mM d–$(CGTACG)_2$ in uncomplexed state and complexed with mitoxantrone with increasing drug (D) to nucleic acid duplex (N) ratios, D/N, at 275 K.

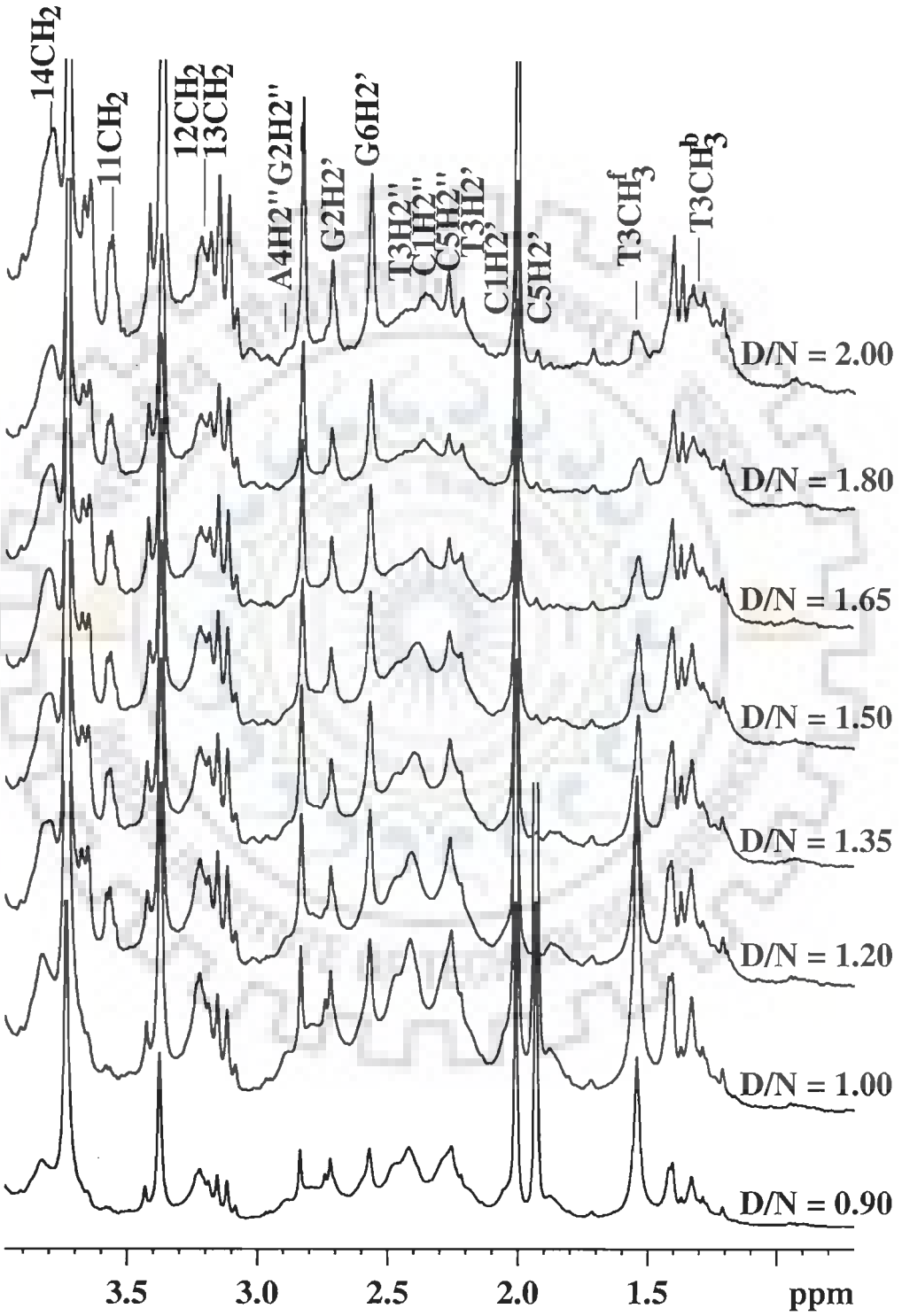
14CH2
11CH2
12CH2
13CH2
A4H2''G2H2''
G2H2'
G6H2'
T3H2''
C1H2''
C5H2''
T3H2'
C1H2'
C5H2'
T3CH3f
T3CH3b
D/N = 2.00
D/N = 1.80
D/N = 1.65
D/N = 1.50
D/N = 1.35
D/N = 1.20
D/N = 1.00
D/N = 0.90
3.5
3.0
2.5
2.0
1.5
ppm

(Fig. 5.5b)

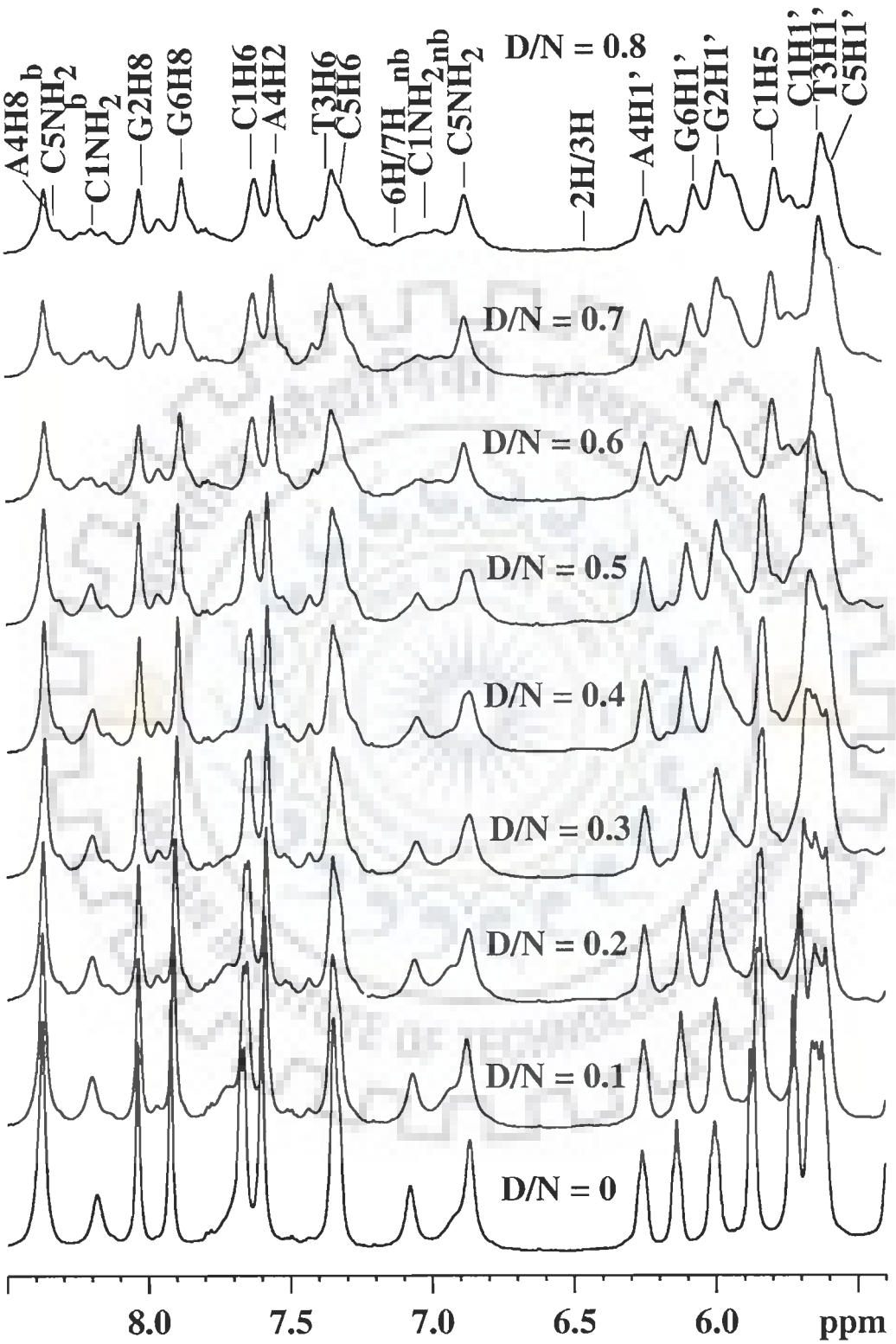
A4H8 b
C5NH2 b
C1NH2
G2H8
G6H8
C1H6
A4H2
T3H6
C5H6
6H/7H nb
C1NH2 nb
C5NH2
D/N = 0.8
2H/3H
A4H1'
G6H1'
G2H1'
C1H5
C1H1'
T3H1'
C5H1'
D/N = 0.7
D/N = 0.6
D/N = 0.5
D/N = 0.4
D/N = 0.3
D/N = 0.2
D/N = 0.1
D/N = 0
8.0
7.5
7.0
6.5
6.0
ppm

(Fig. 5.5c)

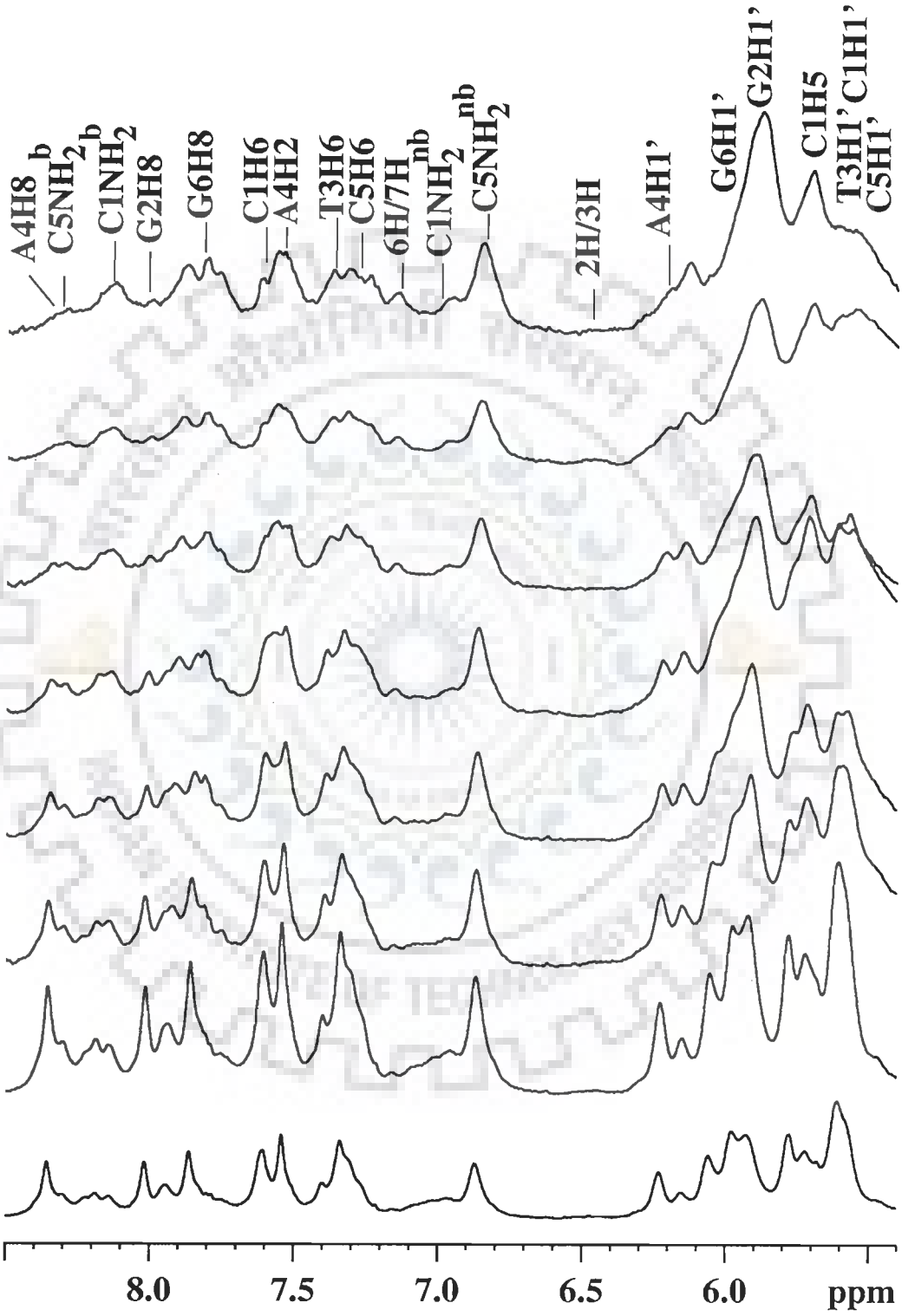
A4H8 b
C5NH2 b
C1NH2 b
G2H8
G6H8
C1H6
A4H2
T3H6
C5H6
6H/7H nb
C1NH2 nb
C5NH2 nb
2H/3H
A4H1'
G6H1'
G2H1'
C1H5
T3H1'C1H1'
C5H1'
8.0
7.5
7.0
6.5
6.0
ppm

(Fig. 5.5d)

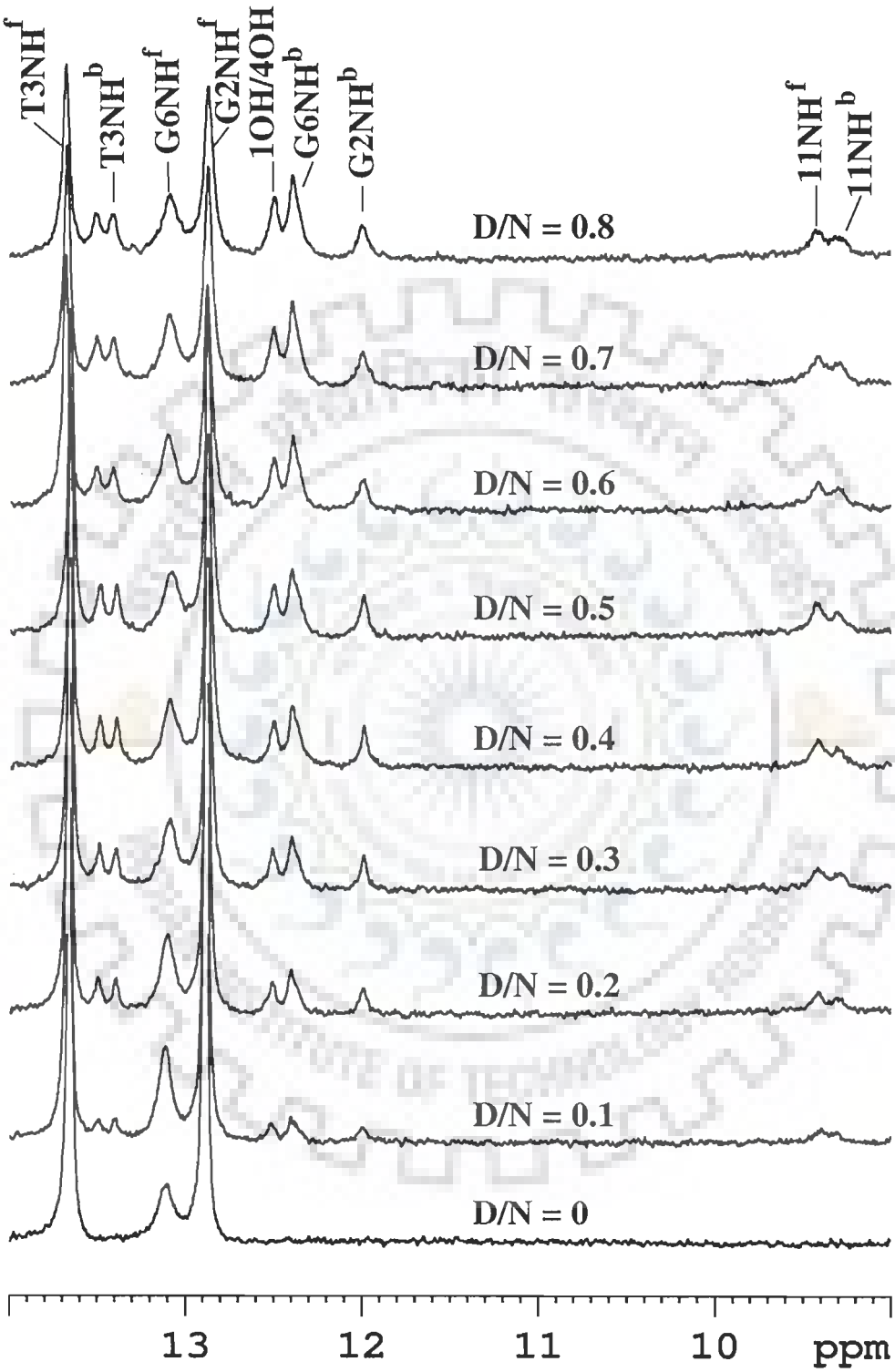
T3NH^f
T3NH^b
G6NH^f
G2NH^f
1OH/4OH
G6NH^b
G2NH^b
11NH^f
11NH^b
D/N = 0.8
D/N = 0.7
D/N = 0.6
D/N = 0.5
D/N = 0.4
D/N = 0.3
D/N = 0.2
D/N = 0.1
D/N = 0
13
12
11
10
ppm

(Fig. 5.5e)

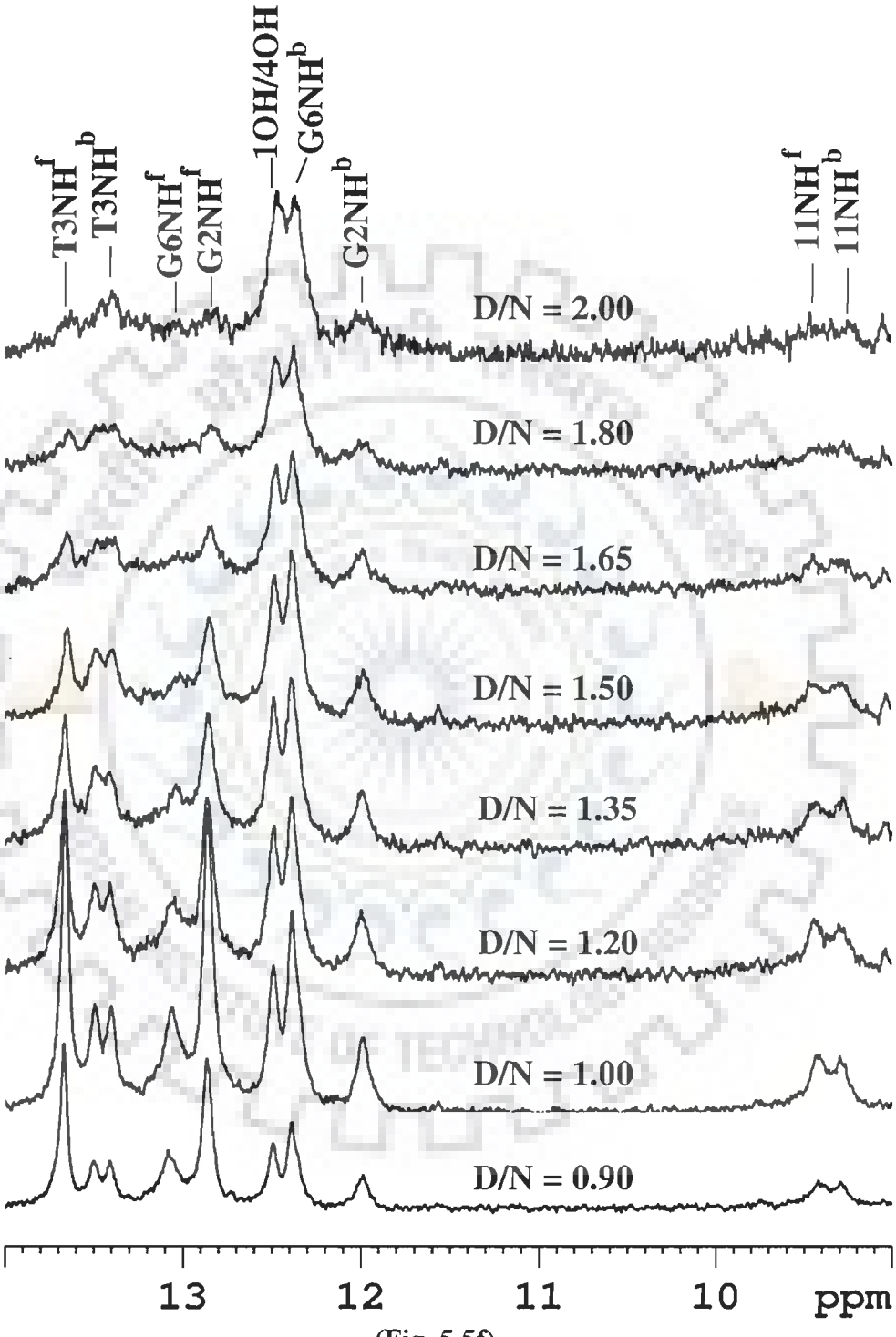
T3NH^f
T3NH^b
G6NH^f
G2NH^f
1OH/4OH
G6NH^b
G2NH^b
11NH^f
11NH^b
D/N = 2.00
D/N = 1.80
D/N = 1.65
D/N = 1.50
D/N = 1.35
D/N = 1.20
D/N = 1.00
D/N = 0.90
13
12
11
10
ppm

(Fig. 5.5f)

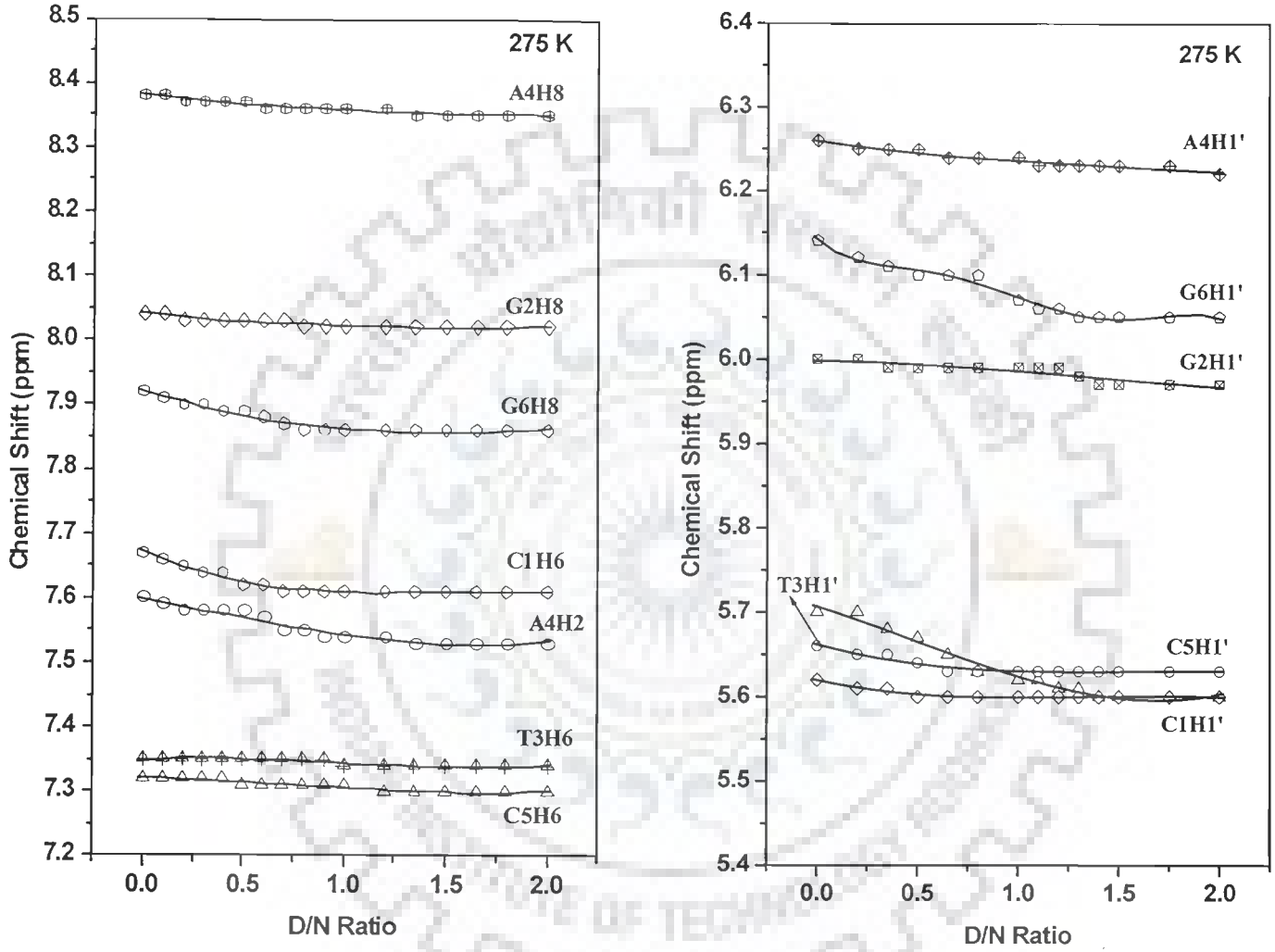

Figure 5.6: Chemical shift of base and H1' protons of d-$(CGTACG)_2$ complexed with mitoxantrone as a function of drug to DNA (D/N) ratio, 275 K.

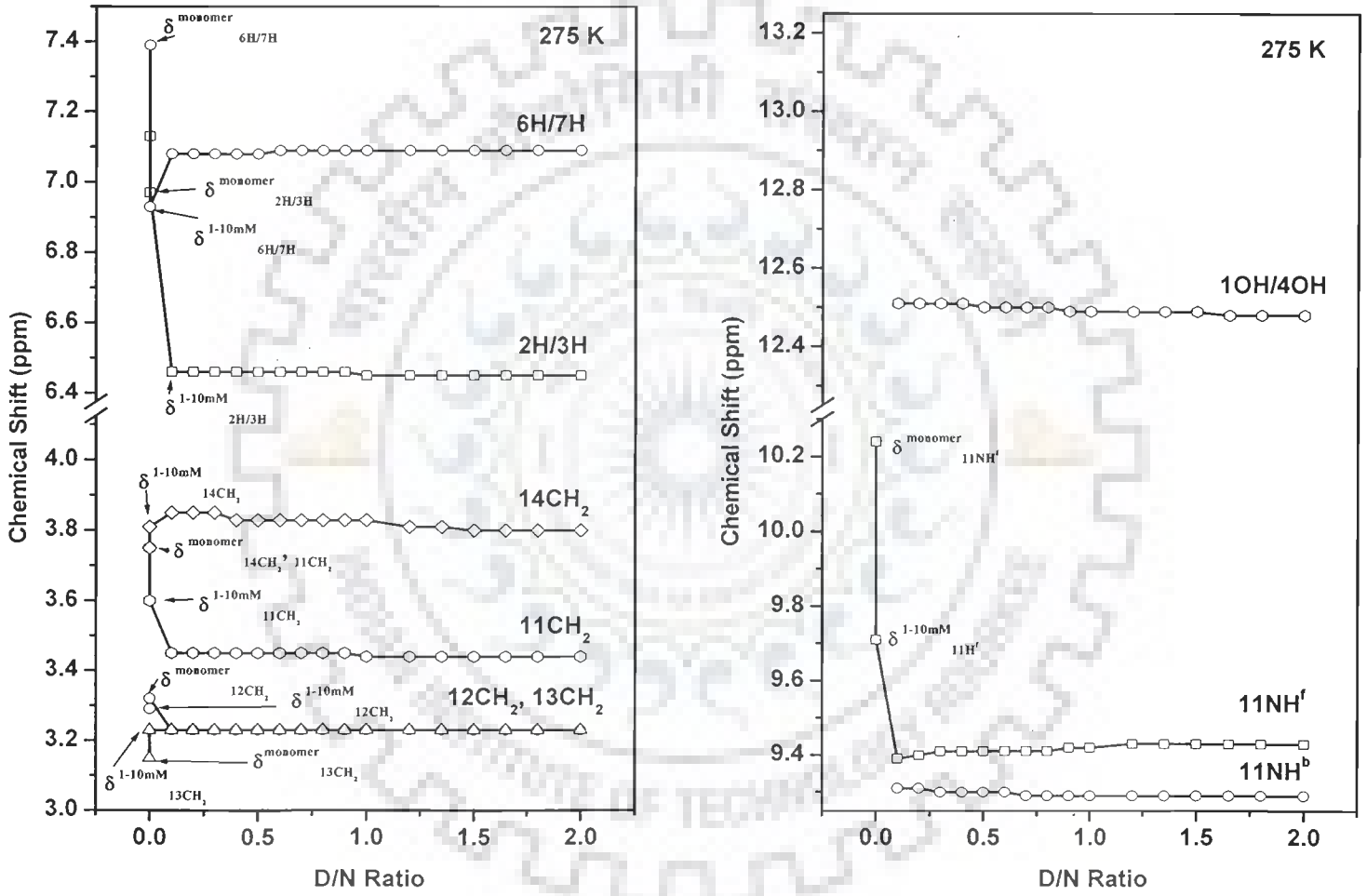

Figure 5.7: ^{1}H Chemical shift of mitoxantrone protons complexed with d-(TGATCA)$_2$ at various D/N ratio, 275 K.

Table 5.5a: Chemical shift (ppm) of nucleotide, d-$(CGTACG)_2$, protons as a function of drug (D) to nucleic acid duplex (N) ratio, D/N, at 275 K. Also shown here is the change in chemical shift on binding, $\Delta\delta = \delta_{D/N=2.0} - \delta_{D/N=0.0}$.

D/N Ratio	C1H1'	G2H1'	T3H1'	A4H1'	C5H1'	G6H1'	C1H6	G2H8	T3H6	A4H8	C5H6
0.00	5.70	6.00	5.66	6.26	5.62	6.14	7.67	8.04	7.35	8.38	7.32
0.10	5.70	6.00	5.65	6.25	5.61	6.12	7.66	8.04	7.35	8.38	7.32
0.20	5.68	5.99	5.65	6.25	5.61	6.11	7.65	8.03	7.35	8.37	7.32
0.30	5.67	5.99	5.64	6.25	5.60	6.10	7.64	8.03	7.35	8.37	7.32
0.40	5.65	5.99	5.63	6.24	5.60	6.10	7.64	8.03	7.35	8.37	7.32
0.50	5.63	5.99	5.63	6.24	5.60	6.10	7.62	8.03	7.35	8.37	7.31
0.60	5.62	5.99	5.63	6.24	5.60	6.07	7.62	8.03	7.35	8.36	7.31
0.70	5.62	5.99	5.63	6.23	5.60	6.06	7.61	8.03	7.35	8.36	7.31
0.80	5.61	5.99	5.63	6.23	5.60	6.06	7.61	8.02	7.35	8.36	7.31
0.90	5.61	5.98	5.63	6.23	5.60	6.05	7.61	8.02	7.35	8.36	7.31
1.00	5.60	5.97	5.63	6.23	5.60	6.05	7.61	8.02	7.34	8.36	7.31
1.20	5.60	5.97	5.63	6.23	5.60	6.05	7.61	8.02	7.34	8.36	7.30
1.35	5.60	5.97	5.63	6.23	5.60	6.05	7.61	8.02	7.34	8.35	7.30
1.50	5.60	5.97	5.63	6.22	5.60	6.05	7.61	8.02	7.34	8.35	7.30
1.65	5.60	5.97	5.63	6.22	5.60	6.05	7.61	8.02	7.34	8.35	7.30
1.80	5.60	5.97	5.63	6.22	5.60	6.05	7.61	8.02	7.34	8.35	7.30
2.00	5.60	5.97	5.63	6.22	5.60	6.05	7.61	8.02	7.34	8.35	7.30
Δδ	+0.10	-0.03	-0.03	-0.04	-0.02	-0.09	-0.06	-0.02	-0.01	-0.03	-0.02

D/N Ratio	G6H8	G2NH^f	G2NH^b	T3NH^f	T3NH^b	G6NH^f	G6NH^b	T3CH3^f	T3CH3^b	A4H2
0.00	7.92	12.89	-	13.66	-	13.12	-	1.56	-	7.60
0.10	7.91	12.89	11.99	13.67	13.40	13.12	12.40	1.55	1.33	7.59
0.20	7.90	12.88	11.99	13.67	13.40	13.10	12.40	1.55	1.33	7.58
0.30	7.90	12.88	11.99	13.67	13.40	13.09	12.40	1.55	1.33	7.58
0.40	7.89	12.88	11.99	13.67	13.40	13.09	12.40	1.55	1.33	7.58
0.50	7.89	12.88	11.99	13.67	13.40	13.09	12.39	1.55	1.33	7.58
0.60	7.88	12.88	11.99	13.67	13.41	13.09	12.39	1.54	1.33	7.57
0.70	7.87	12.88	11.99	13.68	13.41	13.09	12.39	1.54	1.33	7.55
0.80	7.86	12.88	11.99	13.68	13.41	13.09	12.39	1.54	1.33	7.55
0.90	7.86	12.86	11.99	13.68	13.41	13.09	12.39	1.54	1.33	7.54
1.00	7.86	12.86	11.99	13.68	13.41	13.09	12.39	1.54	1.33	7.54
1.20	7.86	12.86	11.99	13.68	13.41	13.07	12.39	1.54	1.33	7.54
1.35	7.86	12.86	11.99	13.68	13.41	13.07	12.39	1.54	1.33	7.53
1.50	7.86	12.86	11.99	13.68	13.41	13.07	12.39	1.54	1.33	7.53
1.65	7.86	12.86	11.99	13.68	13.41	13.07	12.39	1.54	1.33	7.53
1.80	7.86	12.86	11.99	13.68	13.41	13.07	12.39	1.54	1.33	7.53
2.00	7.86	12.86	11.99	13.68	13.41	13.07	12.39	1.54	1.33	7.53
Δδ	-0.06	-0.03	-	+0.02	+0.01	-0.05	-	-0.02	-	-0.07

-ve Δδ indicates upfield shift
+ve Δδ indicates downfield shift.

Table 5.5b: Chemical shift (ppm) of drug (mitoxantrone) protons as a function of drug (D) to nucleic acid duplex (N) ratio, D / N, at 275 K. Also shown here is the maximum change in chemical shift due to binding, with respect to drug in free self associated form, δ^{free} (10 mM, 275 K) as well as the drug in monomeric form, $\delta^{monomer}$. $\Delta\delta = (\delta_{D/N=2.0} - \delta^{monomer})$; $\Delta\delta' = (\delta_{D/N=2.0} - \delta^{free})$.

D/N Ratio	2H/3H	6H/7H	11NH^{f}	11NH^{b}	11CH_2	12CH_2	13CH_2	14CH_2	1OH/4OH
$\delta^{monomer}$	7.13	7.39	10.24	-	3.75	3.29	3.15	3.75	-
δ^{free}	6.97	6.93	9.71	-	3.60	3.32	3.23	3.81	13.19
0.10	6.46	7.08	9.39	9.31	3.45	3.23	3.23	3.85	12.51
0.20	6.46	7.08	9.40	9.31	3.45	3.23	3.23	3.85	12.51
0.30	6.46	7.08	9.41	9.30	3.45	3.23	3.23	3.85	12.51
0.40	6.46	7.08	9.41	9.30	3.45	3.23	3.23	3.83	12.51
0.50	6.46	7.08	9.41	9.30	3.45	3.23	3.23	3.83	12.50
0.60	6.46	7.09	9.41	9.30	3.45	3.23	3.23	3.83	12.50
0.70	6.46	7.09	9.41	9.29	3.45	3.23	3.23	3.83	12.50
0.80	6.46	7.09	9.41	9.29	3.45	3.23	3.23	3.83	12.50
0.90	6.46	7.09	9.42	9.29	3.45	3.23	3.23	3.83	12.49
1.00	6.45	7.09	9.42	9.29	3.44	3.23	3.23	3.83	12.49
1.20	6.45	7.09	9.43	9.29	3.44	3.23	3.23	3.81	12.49
1.35	6.45	7.09	9.43	9.29	3.44	3.23	3.23	3.81	12.49
1.50	6.45	7.09	9.43	9.29	3.44	3.23	3.23	3.80	12.49
1.65	6.45	7.09	9.43	9.29	3.44	3.23	3.23	3.80	12.48
1.80	6.45	7.09	9.43	9.29	3.44	3.23	3.23	3.80	12.48
2.00	6.45	7.09	9.43	9.29	3.44	3.23	3.23	3.80	12.48
$\Delta\delta$	-0.68	-0.30	-0.81	-	-0.31	-0.06	+0.08	+0.05	-
$\Delta\delta'$	-0.52	-0.16	-0.28	-	-0.16	-0.09	0.00	-0.01	-0.71

-ve $\Delta\delta$ indicates upfield shift
+ve $\Delta\delta$ indicates downfield shift.

Table 5.6a: Chemical shift (ppm) of nucleotide, d-(CGTACG)2, protons as a function of drug (D) to nucleic acid duplex (N) ratio, D/N, at 298 K. Also shown here is the change Chemical shift on binding, $\Delta\delta = \delta_{D/N=2.0} - \delta_{D/N=0.0}$.

D/N Ratio	C1H1'	G2H1'	T3H1'	A4H1'	C5H1'	G6H1'	C1H6	G2H8	T3H6
0.00	5.80	6.00	5.71	6.25	5.71	6.14	7.66	8.02	7.32
0.10	5.80	6.00	5.71	6.25	5.71	6.14	7.66	8.01	7.32
0.20	5.79	6.00	5.70	6.25	5.70	6.13	7.65	8.01	7.31
0.30	5.79	6.00	5.70	6.24	5.70	6.12	7.64	8.01	7.31
0.40	5.78	5.99	5.70	6.24	5.70	6.11	7.64	8.01	7.30
0.50	5.76	5.98	5.70	6.24	5.70	6.10	7.64	8.01	7.30
0.60	5.76	5.98	5.69	6.24	5.69	6.10	7.63	8.01	7.30
0.70	5.76	5.98	5.69	6.23	5.69	6.10	7.63	8.01	7.30
0.80	5.76	5.97	5.69	6.23	5.69	6.09	7.63	8.01	7.30
0.90	5.76	5.97	5.69	6.22	5.69	6.08	7.63	8.01	7.30
1.00	5.76	5.96	5.69	6.22	5.69	6.07	7.62	8.01	7.29
1.20	5.76	5.96	5.69	6.20	5.69	6.07	7.62	8.01	7.29
1.35	5.76	5.95	5.69	6.19	5.69	6.07	7.62	8.01	7.28
1.50	5.76	5.94	5.69	6.18	5.69	6.07	7.62	8.01	7.28
1.65	5.76	5.93	5.69	6.18	5.69	6.07	7.61	8.01	7.26
1.80	5.76	5.92	5.69	6.18	5.69	6.07	7.61	8.01	7.26
2.00	5.76	5.91	5.69	6.16	5.69	6.07	7.60	8.01	7.25
Δδ	-0.04	-0.08	-0.03	-0.09	-0.02	-0.07	-0.06	-0.01	-0.07

D/N Ratio	A4H8	C5H6	G6H8	A4H2	T3CH3[f]	G2NH[f]	T3NH[f]
0.00	8.35	8.35	7.91	7.65	1.57	12.83	13.51
0.10	8.35	8.35	7.91	7.65	1.57	12.83	13.51
0.20	8.34	8.34	7.90	7.65	1.56	12.83	13.51
0.30	8.34	8.34	7.90	7.64	1.56	12.83	13.51
0.40	8.33	8.33	7.90	7.64	1.56	12.83	13.51
0.50	8.33	8.33	7.90	7.64	1.56	12.83	13.51
0.60	8.33	8.33	7.89	7.63	1.56	12.83	13.47
0.70	8.31	8.31	7.89	7.63	1.56	12.83	13.47
0.80	8.31	8.31	7.89	7.63	1.56	12.83	13.47
0.90	8.31	8.31	7.89	7.63	1.56	12.82	13.47
1.00	8.30	8.30	7.88	7.62	1.56	12.82	13.40
1.20	8.30	8.30	7.88	7.62	1.56	12.82	13.40
1.35	8.30	8.30	7.88	7.62	1.56	12.82	13.40
1.50	8.30	8.30	7.87	7.62	1.56	12.82	13.34
1.65	8.30	8.30	7.87	7.61	1.56	12.82	13.31
1.80	8.30	8.30	7.87	7.61	1.56	12.82	13.31
2.00	8.30	8.30	7.86	7.60	1.56	12.82	13.31
Δδ	-0.05	-0.05	-0.04	-0.05	-0.01	-0.01	-0.20

-ve Δδ indicates upfield shift

Table 5.6b: Chemical shift (ppm) of drug (mitoxantrone) protons as a function of drug (D) to nucleic acid duplex (N) ratio, D / N, at 298 K. Also shown here is the maximum change in chemical shift due to binding, with respect to drug in free self associated form, δ^{free} (10 mM, 298 K). $\Delta\delta = (\delta_{D/N=2.0} - \delta^{free})$.

D/N Ratio	2H/3H	6H/7H	11NH[f]	$11CH_2$	$12CH_2$	$13CH_2$	$14CH_2$	1OH/4OH
δ^{free}	6.83	6.95	9.79	3.69	3.39	3.33	3.93	-
0.10	6.89	7.06	9.42	3.45	3.26	3.26	3.87	12.51
0.20	6.89	7.06	9.42	3.45	3.26	3.26	3.87	12.51
0.30	6.89	7.06	9.42	3.45	3.26	3.26	3.86	12.51
0.40	6.89	7.06	9.42	3.45	3.26	3.26	3.86	12.51
0.50	6.89	7.06	9.42	3.45	3.26	3.26	3.86	12.51
0.60	6.89	7.06	9.42	3.44	3.25	3.25	3.86	12.51
0.70	6.89	7.06	9.42	3.44	3.25	3.25	3.86	12.51
0.80	6.89	7.06	9.42	3.44	3.25	3.25	3.85	12.51
0.90	6.89	7.06	9.42	3.44	3.25	3.25	3.85	12.51
1.00	6.88	7.04	9.42	3.44	3.25	3.25	3.85	12.50
1.20	6.88	7.04	9.42	3.43	3.25	3.25	3.85	12.50
1.35	6.88	7.04	9.42	3.42	3.24	3.24	3.85	12.50
1.50	6.88	7.04	9.42	3.42	3.24	3.24	3.84	12.47
1.65	6.85	7.04	9.42	3.42	3.21	3.21	3.84	12.47
1.80	6.85	7.01	9.40	3.42	3.21	3.21	3.83	12.47
2.00	6.85	7.01	9.40	3.42	3.21	3.21	3.83	12.47
$\Delta\delta$	+0.02	+0.06	-0.39	-0.27	-0.18	-0.12	-0.10	-

-ve $\Delta\delta$ indicates upfield shift
+ve $\Delta\delta$ indicates downfield shift.

addition of mitoxantrone to DNA, additional resonance peaks are observed in this region at 13.41, 12.49, 12.39 and 11.99 ppm at D / N = 1.0, besides the 11 NH peaks at about 9.42 and 9.29 ppm. Since T3NH, G6NH and G2NH appear at 13.66, 13.12 and 12.89 ppm in uncomplexed d–$(CGTACG)_2$, accordingly the resonances at 13.68, 13.09 and 12.86 are designated as $T4NH^f$, $G6NH^f$ and $G2NH^f$, in the d–$(CGTACG)_2$ complexed to mitoxantrone at D / N = 1.0. The 2D NOESY spectra (Fig. 5.8g) showed that pairs of protons resonating at 13.68, 13.41; 13.09, 12.39; and 12.86, 11.99 shows cross peaks with each other due to exchange phenomenon expected between free and DNA bound to drug in the solution. Subsequently the resonances at 13.41, 12.39 and 11.99 ppm get assigned to $T4NH^b$, $G6NH^b$ and $G2NH^b$ in the d–$(CGTACG)_2$ complexed to drug at D / N = 1.0.

The intensity of $G6NH^f$ peak is significantly lesser than that of $G2NH^f$ and $T4NH^f$. Also the NOE cross peaks of $G6NH^f$ and $G6NH^b$ resonance is considerably weaker in intensity than the NOE cross peak of T4NH and G2NH. This indicates that G6NH proton which completely exchanges with water in uncomplexed d– $(CGTACG)_2$ and the line width of G6NH is also greater than that of G2NH and T4NH. On increasing the concentration of mitoxantrone, the G6NH proton is immobilized in the drug–DNA complex. This is evidenced from the intensity increase of the $G6NH^b$ signal with increasing drug concentration (Fig. 5.5e and 5.5f). with increasing D/N ratio the $T4NH^f$ and $G2NH^f$ signals gradually decrease in their intensity by contributing to the growing signals of $T4NH^b$ and $G2NH^b$. At D / N =2.0, they eventually die out to show that almost the entire hexamer is bound with the excess of drug present in solution.

The sharp $T3CH_3$ peak appearing at 1.56 ppm in uncomplexed d–$(CGATCG)_2$ decreases in intensity as D / N ratio increase and a new, relatively broad, peak appearing

at 1.33 ppm (Fig. 5.5a and 5.5b) gets assigned to $T4CH_3$ of DNA bound to the drug molecule (designated hereafter as $T3CH_3^b$). It is noted that $T3CH_3^b$ shows all expected interproton NOE connectivities with T3H6, G2H8, G2H1', A4H1', $T3NH^b$, $G2NH^b$ (Fig. 5.8h) and A4H2', A4H2" (Fig. 5.8c), but are weaker in intensity than the corresponding NOEs of $T4CH_3^f$ protons resonating at 1.54 ppm at D / N = 1.0.

The 11NH resonance of mitoxantrone at 9.29 ppm increases in intensity with D / N ratio. However in addition, another peak starts appearing at 9.42 ppm (Fig. 5.6e-f). These two resonances show chemical exchange in 2D NOESY spectra (Fig. 5.8g) and resonances shows NOE cross peak with 6H/7H, $11CH_2$, $12CH_2$ and $13CH_2$ protons (Table 5.8). The upfield resonance peak at 9.29 ppm is assigned to 11NH proton in the bound species, designated as $11NH^b$, while that at 9.42 ppm is the corresponding proton in free state, that is $11NH^f$ as D / N increases more and more drug exist in free state and the intensity of 9.42 ppm peak increases. This is further corroborated by the fact that the $11NH^b$ resonance at 9.29 ppm show intermolecular NOE crosspeaks with specific nucleic acid protons C1H6 and G6H1' (Table 5.9, Fig. 5.8e) whereas $11NH^f$ at 9.42 ppm does not give any such intermolecular connectivity with hexamer protons.

The existence of a set of resonances for T3NH, G2NH, G6NH, $T3CH_3$ and 11NH (drug) clearly demonstrates that the drug thus indeed binds to the DNA hexamer and there is a slow exchange of free and bound DNA on NMR time scale at 275 K.

The palindromic symmetry of the system implies that two binding sites are available for the drug. The change in chemical shift ($\Delta\delta$) of base and H1' protons with D / N ratio at 275 K (Table 5.5a and Fig. 5.6) and 298 K (Table 5.6a) are gradual and small in magnitude. The $\Delta\delta$ increases with D / N ratio as more and more DNA oligomer binds

to the drug a maximum of 0.10 to 0.09 ppm upfield shift is observed for C1H1' and G6H1' protons at 275 K (Fig. 5.6). All the bound imino protons on the DNA oligomer are upfield shifted with respect to the corresponding imino protons in free state (Table 5.3); the shift being 0.87, 0.27 and 0.70 ppm for G2NH; T3NH and G6NH, respectively. The $T3CH_3$ resonance shifts upfield by 0.23 ppm on complexation. Such changes may be attributed to structural changes due to complexation.

The shift in drug protons on binding is expected to be maximum at low D / N ratio, when maximum amount of drug is present in the bound state. We do not observe any significant variation of δ with increasing D / N ratio (Fig. 5.7). The ring protons, 6H /7H and 2H / 3H, shift upfield substantially by 0.30 and 0.68 ppm at D / N = 1.0, with respect to the chemical shift position of drug in monomer state at 10 μM or lower concentration (Manpreet, 2006) (Table 5.4). The 11NH proton shifts upfield by 0.95 ppm. The shift in the side chain protons $12CH_2$, $13CH_2$ and $14CH_2$ are comparatively less (< 0.1 ppm) except for $11CH_2$ with upfield shift of 0.31 ppm. No further significant variation of chemical shift was observed with increasing D/N ratio, Table 5.5b. Large upfield shifts on binding for 11NH, $11CH_2$ and protons attached to the aromatic ring, 6H/7H and 2H/3H suggests that aromatic chromophore of mitoxantrone is well stacked with base pairs of DNA and involved in the interaction. Some of the drug is in free state at D / N = 1, the concentration of which is likely to be in mM range and hence expected to be in self–associated form (Davies et al, 2001b). Difference in chemical shift, $\Delta\delta = \delta^b - \delta^f$, is 0.13 ppm (upfield) for free and bound species of 11NH proton (Table 5.4). It is noteworthy that 1OH/4OH proton which exchanges with water, appears at 12.49 ppm in

the spectra of drug–DNA complex at 275 K. Apparently 1OH/4OH is expected to participate in the binding and gets immobilized.

5.1.2.2 Structure of the Complex

The 2D NOESY spectra of drug–DNA complex at stoichiometric D / N ratio of 1.0 (Fig. 5.8a-h) have been investigated extensively at mixing time (τ_m) of 100, 200 and 300 ms. The intensities of cross peak have been estimated qualitatively as very strong (ss), strong (s), medium (ws), weak (w), very weakly (ww) intense cross peaks for distances in the range ss 1.8 – 2.5 Å, s 2.5 – 3.0 Å, ws 3.0 – 3.5 Å, w 3.5 – 4.0 Å, ww 4.0 – 5.0 Å, respectively from the spectra recorded at τ_m = 200 ms. The observed NOE for (a) sequential connectivities, (b) intranucleotide connectivities within sugar (c) intranucleotide base to sugar connectivities, and (d) connectivities involving amino and imino protons of base pairs are given in Table 5.7a-d. The connectivities within the drug molecules are given in Table 5.8. The intermolecular connectivities of drug protons to nucleic acid protons in the complex are given in Table 5.9, respectively. The sequential base (H6 / H8)n to (H1')n-1, (H2')n-1, (H2")n-1, (H3')n-1, base (H6 / H8)n-1 connectivities are observed at all base pair steps (Table 5.7a). The observation of NOEs between the imino protons of guanine bases and the amino protons of the hydrogen bonded partner cytosine bases in NOESY spectra i.e., $C1NH_2^{nb}$, $G6NH^b$; $C5NH_2^b$, $G2NH^b$ (Fig. 5.8d and 5.8e) establish Watson–Crick base pairing at all dG–dC base pair in the duplex. Similarly the observation of NOEs between imino proton of thymine and H2 and amino protons of adenine residues i.e., pairs $T3NH^b$, A4H2; $T3NH^b$, $A4NH_2$ (Fig. 5.8d) establish Watson and Crick pairing at all dA–dT base pairs. All sequential connectivities among adjacent base pairs, expected for a typical B–DNA structure, are

observed (Table 5.7a). This clearly demonstrates that DNA duplex is intact, apparently with no opening of base pairs to accommodate drug chromophore as expected on binding of typical intercalator to the DNA molecule. The base sequence d–$(CGTACG)_2$ being self–complementary is responsible for a high symmetry in the NMR spectra, which remains unbroken in the presence of drug.

Table 5.8 shows some of the intramolecular NOE connectivities observed within the drug molecule in the drug–DNA complex at D / N = 1.0. It is observed that $11NH^b$ is close to $11CH_2$, $12CH_2$ / $13CH_2$ (overlap) and $14CH_2$ protons. Also the ring protons 6H / 7H are close to $12CH_2$ / $13CH_2$ and $14CH_2$ protons. However, the inter–molecular peaks observed in mitoxantrone dimer (Davies et al, 2001b) i.e., 2H / 3H with $11CH_2$, $12CH_2$, $13CH_2$, $14CH_2$, 6H / 7H protons are clearly missing. This shows the drug molecule though present in millimolar concentration at D / N = 1.0 in solution, does not exist as a dimer and is bound as monomer molecule to the DNA.

Table 5.9 gives a list of short intermolecular contacts observed between mitoxantrone and d-$(CGTACG)_2$. Several intermolecular contacts are close to C1.G6 base pair. Since $12CH_2$ and $13CH_2$ overlaps with each other, their proximity to other protons cannot be ascertained unambiguously. $11NH^b$ gives close contacts with G6H1', C1H6 and C1H5. $14CH_2$ is close to both G6H8 and C1H6. 1OH/4OH is in proximity to C1H1', C1H4' and G6H1'. Similarly, $12CH_2$ / $13CH_2$ protons show close intermolecular contacts with C1, C5 and G6 residues (Table 5.9). We observe mitoxantrone protons ($11NH^b$, 1OH/4OH, $12CH_2$ / $13CH_2$ and $14CH_2$) simultaneously close to C1 and G6 residue protons of DNA which are located on opposite sides of C1.G6 base pair. This is not possible if mitoxantrone aromatic chromophore intercalates between

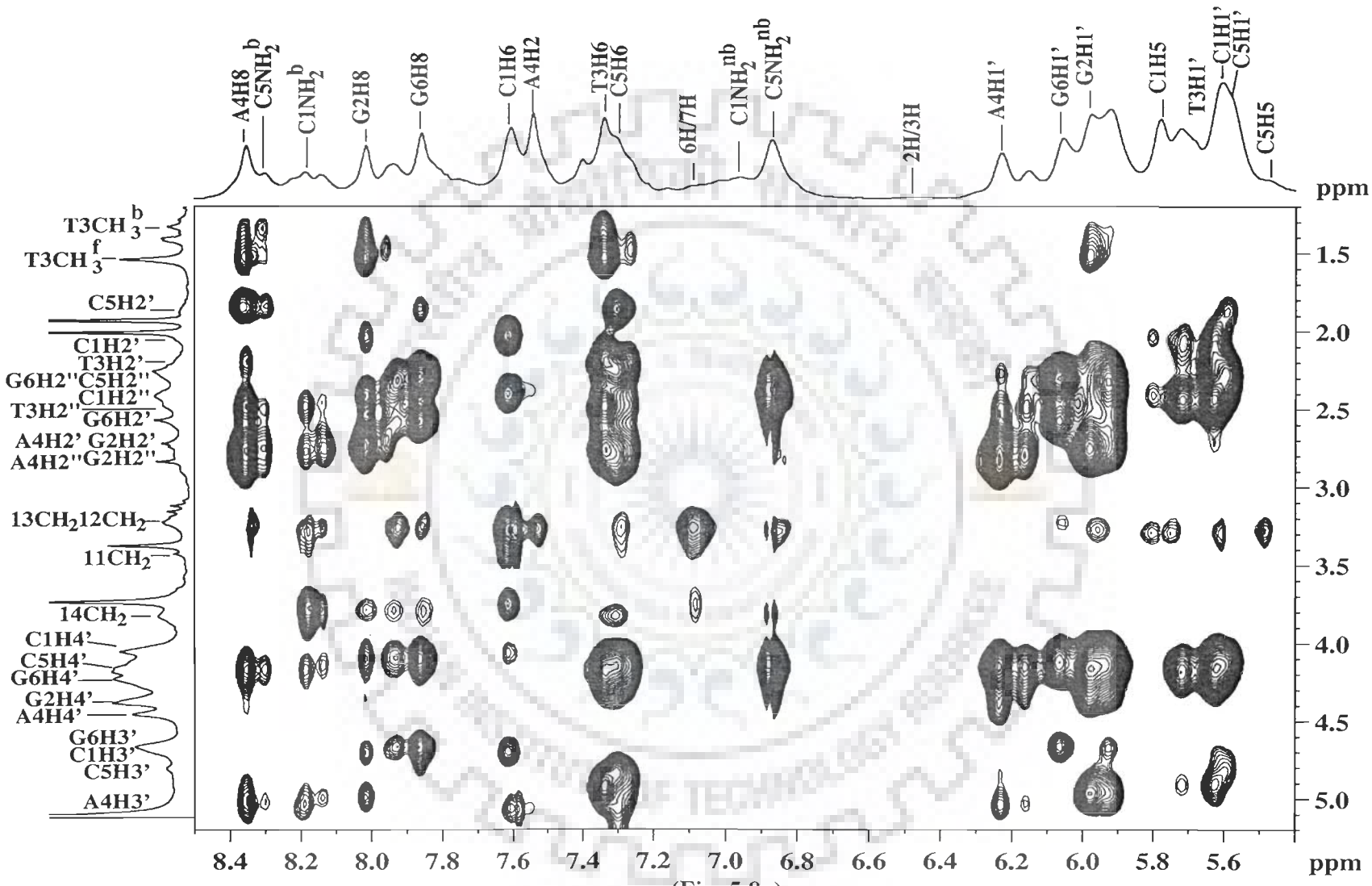

(Fig. 5.8a)

Figure 5.8(a-h): Expansions of various regions of 2D NOESY spectrum of mitoxantrone-d-$(CGTACG)_2$ complex in H_2O at 275 K.

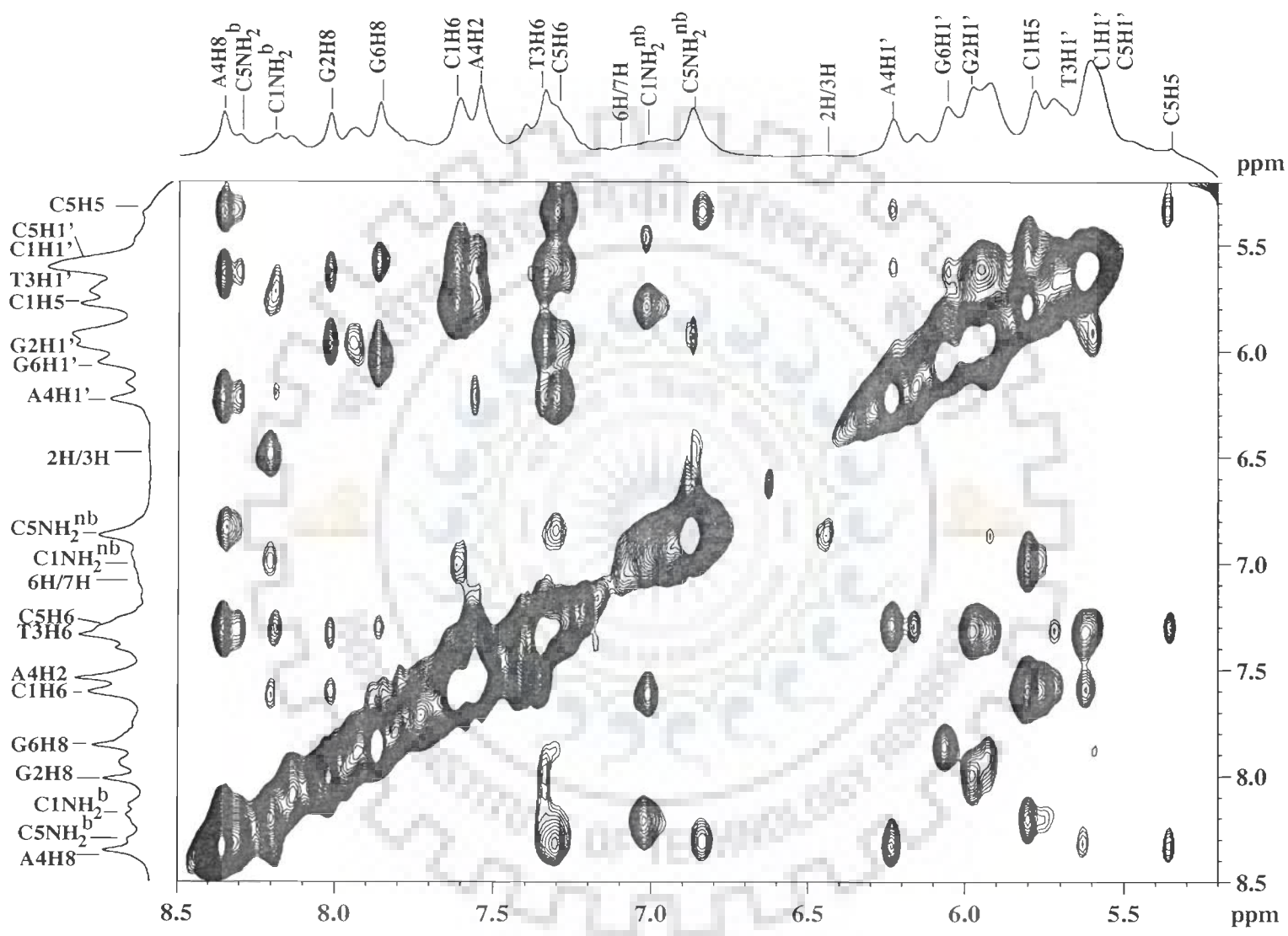
A4H8
C5NH2b
C1NH2b
G2H8
G6H8
C1H6
A4H2
T3H6
C5H6
6H/7H
C1NH2nb
C5NH2nb
2H/3H
A4H1'
G6H1'
G2H1'
C1H5
T3H1'
C1H1'
C5H1'
C5H5
ppm
8.5
8.0
7.5
7.0
6.5
6.0
5.5
ppm

(Fig. 5.8b)

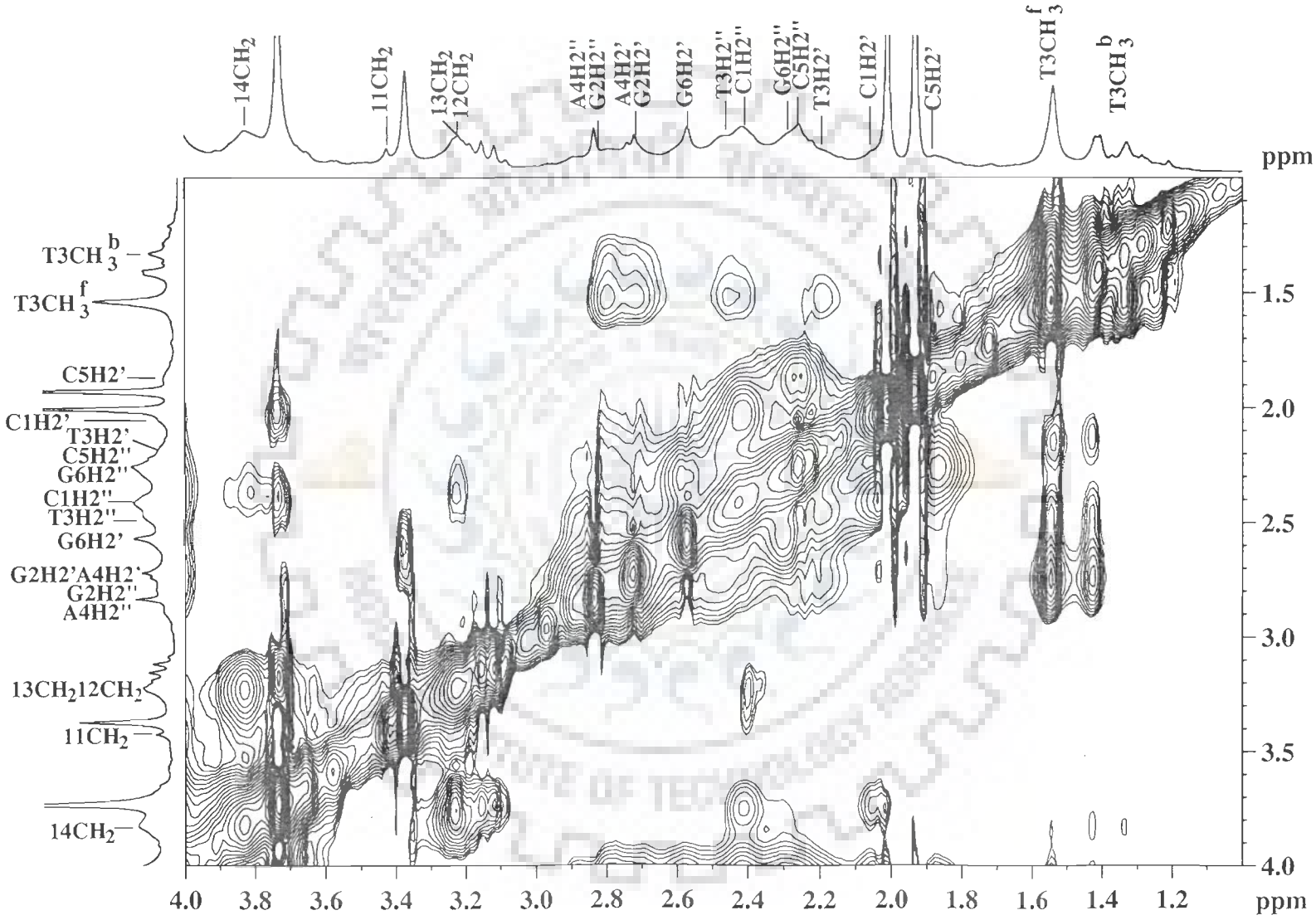
14CH2
11CH2
13CH2
12CH2
A4H2''
G2H2''
A4H2'
G2H2'
G6H2'
T3H2''
C1H2''
G6H2''
C5H2''
T3H2'
C1H2'
C5H2'
T3CH3 f
T3CH3 b
ppm
T3CH3 b
T3CH3 f
C5H2'
C1H2'
T3H2'
C5H2''
G6H2''
C1H2''
T3H2''
G6H2'
G2H2'A4H2'
G2H2''
A4H2''
13CH212CH2
11CH2
14CH2
1.5
2.0
2.5
3.0
3.5
4.0
4.0 3.8 3.6 3.4 3.2 3.0 2.8 2.6 2.4 2.2 2.0 1.8 1.6 1.4 1.2
ppm

(Fig. 5.8c)

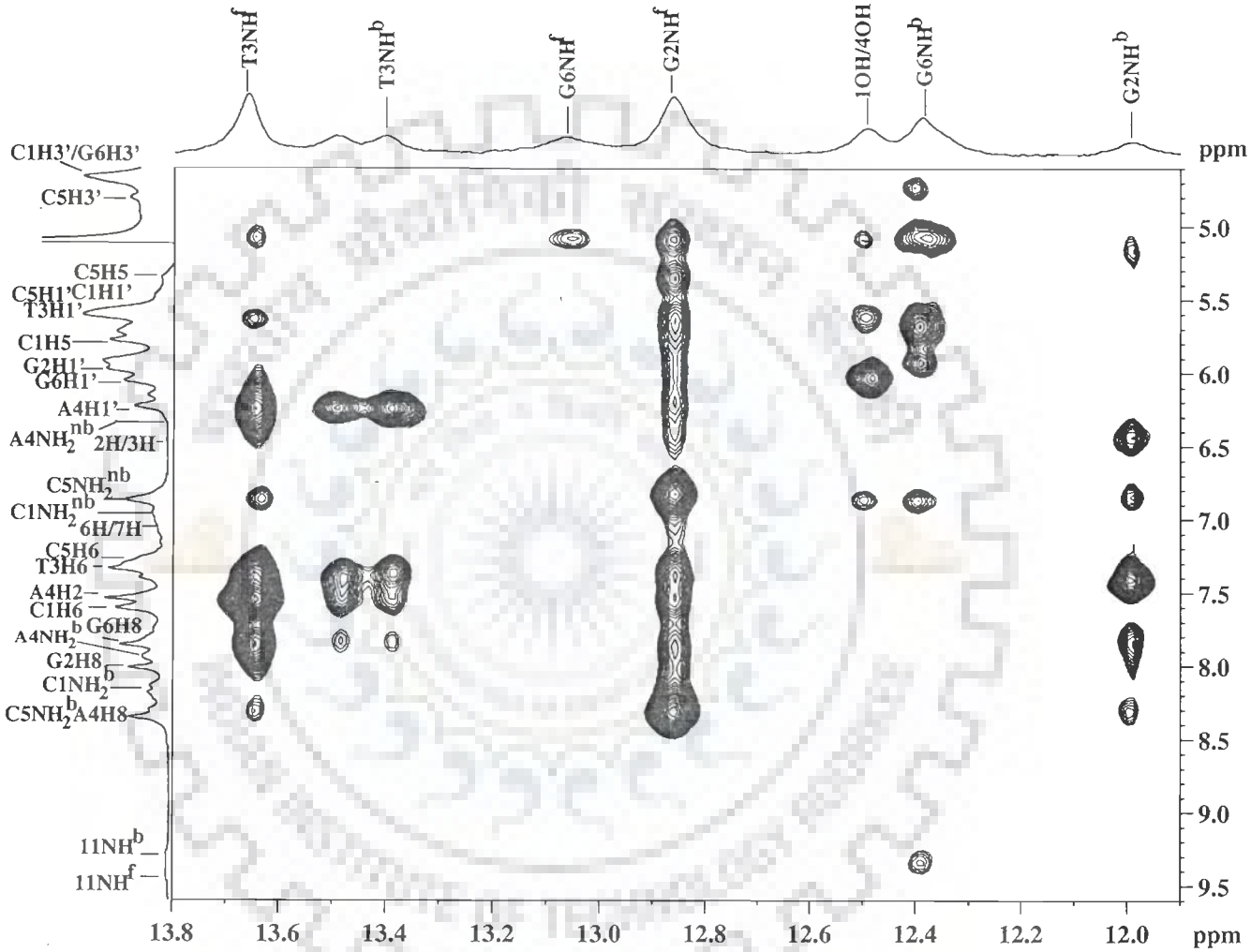
T3NH^f
T3NH^b
G6NH^f
G2NH^f
1OH/4OH
G6NH^b
G2NH^b
ppm
C1H3'/G6H3'
C5H3'
C5H5
C5H1'C1H1'
T3H1'
C1H5
G2H1'
G6H1'
A4H1'
A4NH2^nb 2H/3H
C5NH2^nb
C1NH2^nb 6H/7H
C5H6
T3H6
A4H2
C1H6
A4NH2^b G6H8
G2H8
C1NH2^b
C5NH2^b A4H8
11NH^b
11NH^f
5.0
5.5
6.0
6.5
7.0
7.5
8.0
8.5
9.0
9.5
13.8
13.6
13.4
13.2
13.0
12.8
12.6
12.4
12.2
12.0
ppm

(Fig. 5.8d)

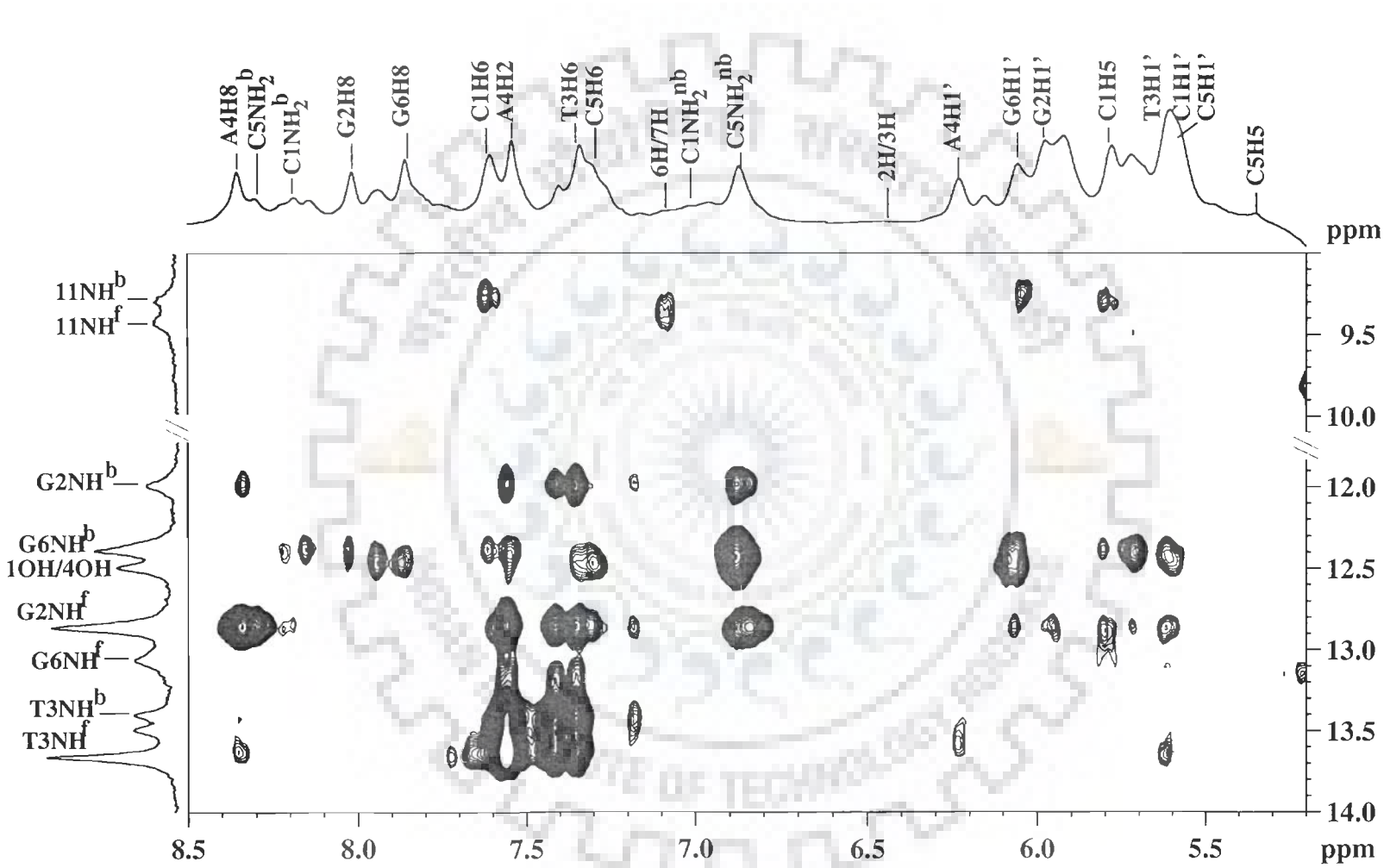
A4H8
C5NH2b
C1NH2b
G2H8
G6H8
C1H6
A4H2
T3H6
C5H6
6H/7H
C1NH2nb
C5NH2nb
2H/3H
A4H1'
G6H1'
G2H1'
C1H5
T3H1'
C1H1'
C5H1'
C5H5
ppm
11NHb
11NHf
G2NHb
G6NHb
1OH/4OH
G2NHf
G6NHf
T3NHb
T3NHf
9.5
10.0
12.0
12.5
13.0
13.5
14.0
8.5
8.0
7.5
7.0
6.5
6.0
5.5
ppm

(Fig. 5.8e)

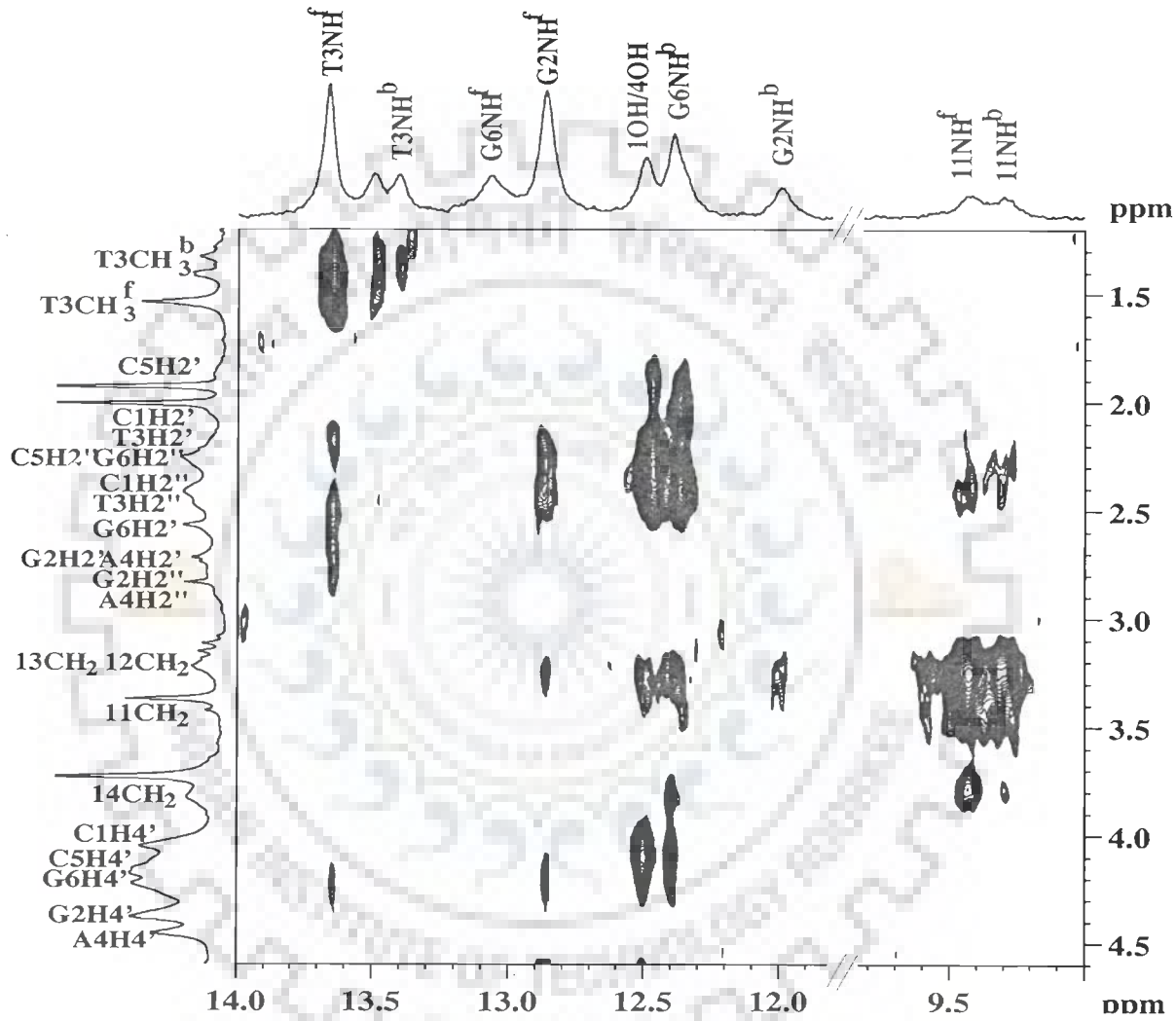
T3NH^f
T3NH^b
G6NH^f
G2NH^f
1OH/4OH
G6NH^b
G2NH^b
11NH^f
11NH^b
ppm
T3CH3^b
T3CH3^f
C5H2'
C1H2'
T3H2'
C5H2'G6H2''
C1H2''
T3H2''
G6H2'
G2H2'A4H2'
G2H2''
A4H2''
13CH2 12CH2
11CH2
14CH2
C1H4'
C5H4'
G6H4'
G2H4'
A4H4'
1.5
2.0
2.5
3.0
3.5
4.0
4.5
14.0
13.5
13.0
12.5
12.0
9.5
ppm

(Fig. 5.8f)

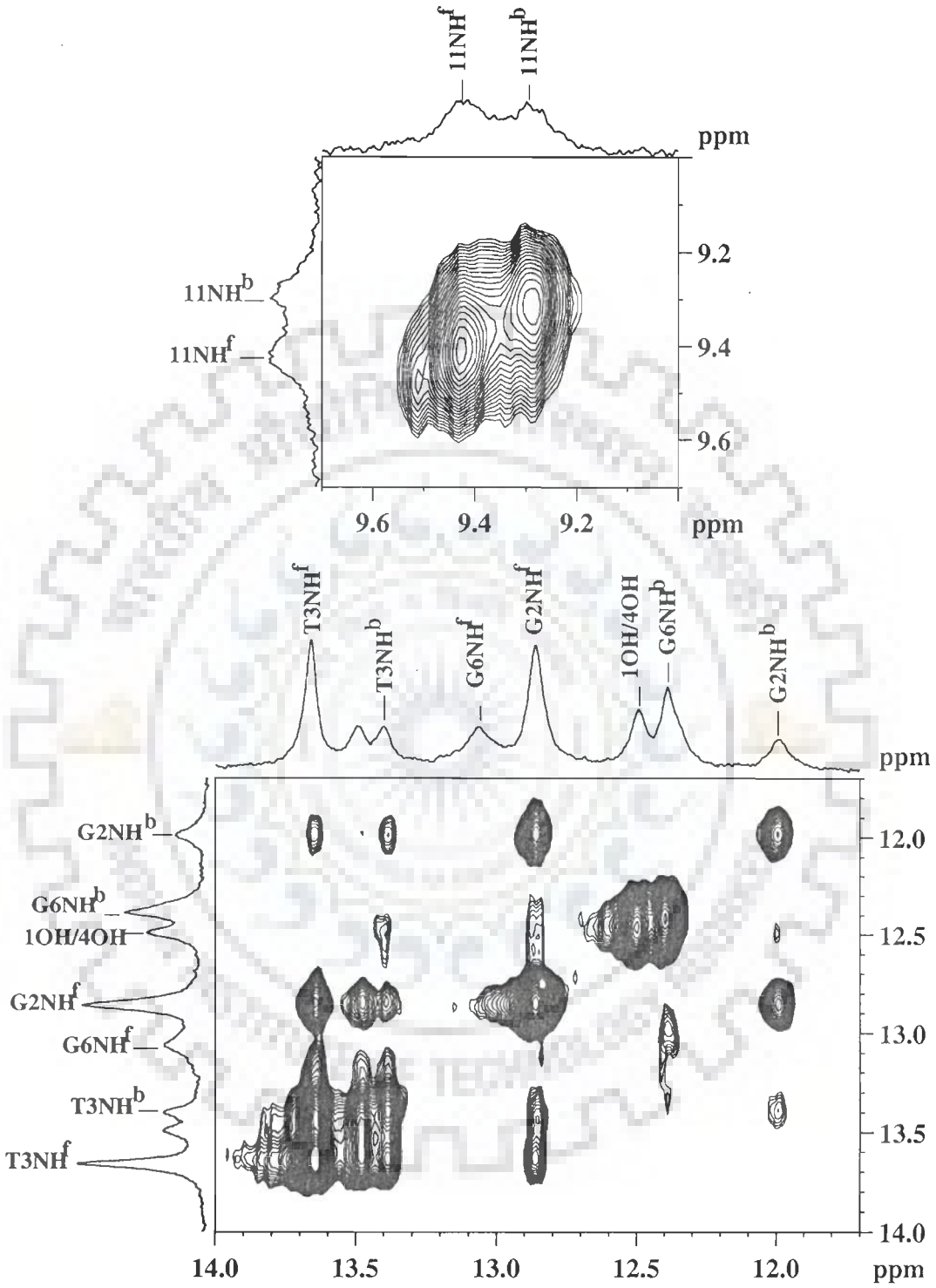
11NH^f
11NH^b
ppm
11NH^b
11NH^f
9.2
9.4
9.6
9.6
9.4
9.2
ppm
T3NH^f
T3NH^b
G6NH^f
G2NH^f
1OH/4OH
G6NH^b
G2NH^b
ppm
G2NH^b
G6NH^b
1OH/4OH
G2NH^f
G6NH^f
T3NH^b
T3NH^f
12.0
12.5
13.0
13.5
14.0
14.0
13.5
13.0
12.5
12.0
ppm

(Fig. 5.8g)

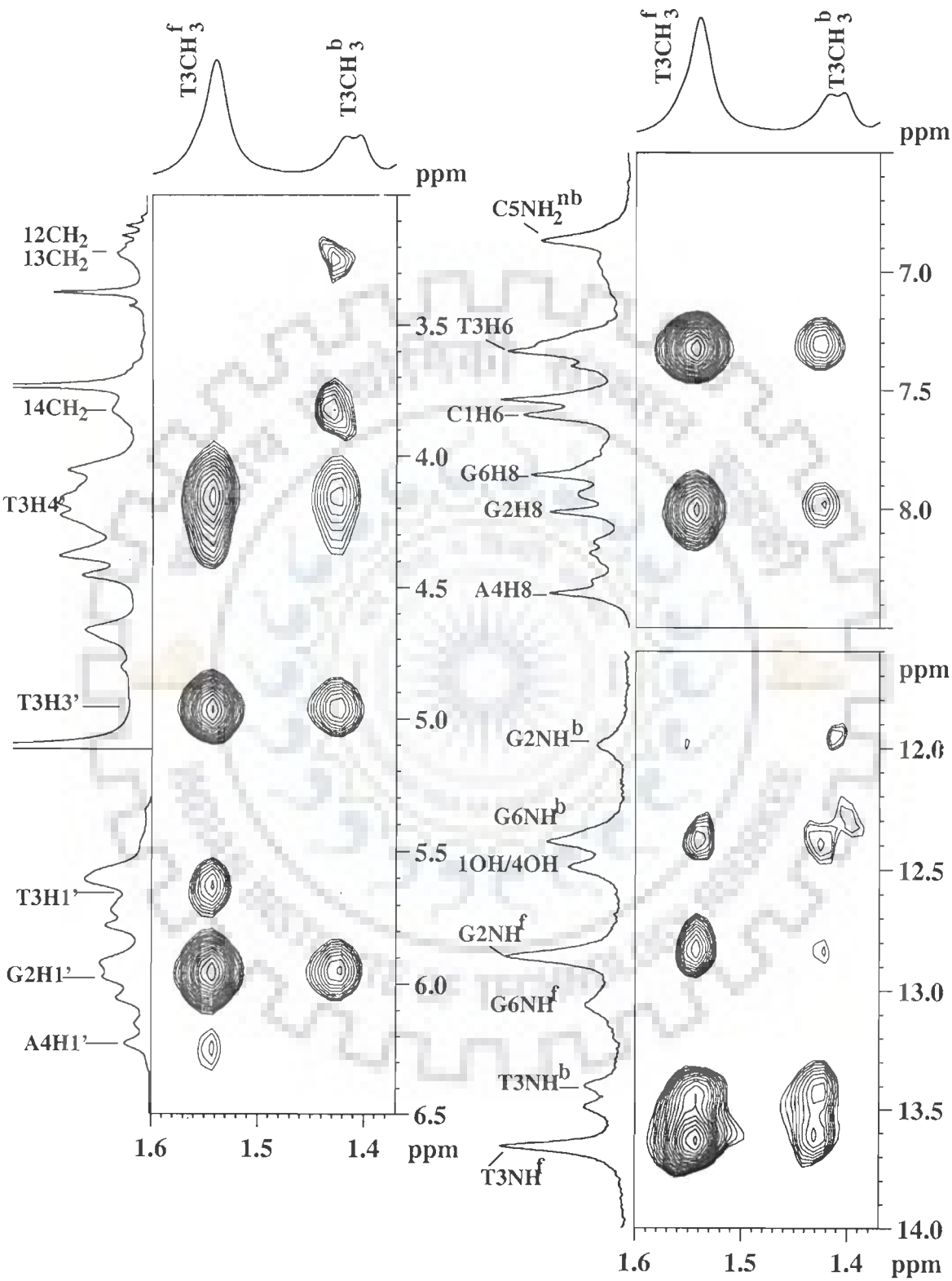
T3CH3f
T3CH3b
ppm
12CH2
13CH2
14CH2
T3H4'
T3H3'
T3H1'
G2H1'
A4H1'
3.5 T3H6
C1H6
4.0
G6H8
G2H8
4.5
A4H8
5.0
G2NHb
G6NHb
5.5
1OH/4OH
G2NHf
6.0
G6NHf
T3NHb
6.5
T3NHf
1.6
1.5
1.4
ppm
C5NH2nb
7.0
7.5
8.0
12.0
12.5
13.0
13.5
14.0

(Fig. 5.8h)

Table 5.7a: Inter residue sequential NOE cross peaks (ds) of nucleotide protons in the drug-DNA complex observed from the NOESY spectra at D/N = 1.0 at 275 K. The very strong (ss), strong (s), medium (ws), weak (w), very weakly (ww) intense cross peaks correspond to distances in the range ss 1.8 – 2.5 Å, s 2.5 – 3.0 Å, ws 3.0 – 3.5 Å, w 3.5 – 4.0 Å, ww 4.0 – 5.0 Å, respectively. Overlap of cross peaks is indicated as o.

Connectivity	Intensity	Connectivity	Intensity
C1pG2 step		A4pC5 step	
C1H1'- G2H8	ws	A4H1'- C5H6	s
C1H2'- G2H8	ws	A4H2'- C5H6	o
C1H2"- G2H8	s	A4H2"- C5H6	o
C1H3'- G2H8	w	A4H3'- C5H6	o
C1H4'- G2H8	ws	A4H1' - C5H5	ww
C1H6 - G2H8	ww	A4H8 - C5H5	s
G2pT3 step		A4H8 - C5H6	s
G2H1' - T3H6	s	C5pG6 step	
G2H2' - T3H6	s	C5H1'– G6H8	ws
G2H2"- T3H6	ss	C5H2'– G6H8	ws
G2H3' - T3H6	o	C5H2" – G6H8	ss
G2H8 - T3H6	w	C5H3'– G6H8	o
T3pA4 step		C5H6– G6H8	ww
T3H1'- A4H8	ws		
T3H2'- A4H8	w		
T3H2"- A4H8	s		
T3H3'- A4H8	o		
T3H6 - A4H3'	w		
T3H6 - A4H8	s		

Table 5.7b: Intra nucleotide NOE connectivities (di) of sugar protons of nucleic acid in the drug-DNA complex observed from the NOESY spectra at D/N = 1.0 at 275 K. The very strong (ss), strong (s), medium (ws), weak (w), very weakly (ww) intense cross peaks correspond to distances in the range ss 1.8 – 2.5 Å, s 2.5 – 3.0 Å, ws 3.0 – 3.5 Å, w 3.5 – 4.0 Å, ww 4.0 – 5.0 Å, respectively. Overlap of cross peaks is indicated as o.

Cross peak	C1	G2	T3	A4	C5	G6
H1'- H2'	o	o	ws	ws	ws	s
H1'- H2"	ss	ss	ss	ss	o	ss
H1'- H3'	o	s	w	ws	ws	ws
H1'- H4'	ss	o	s	s	o	s
H2' - H2"	ss	o	o	o	ss	ss
H2'- H3'	ss	ss	o	o	s	ss
H2'- H4'	m	o	o	o	s	o
H2"- H3'	s	o	ss	s	ss	o
H2"- H4'	o	o	o	m	o	o
H3'- H4'	ss	ss	s	s	s	o

Table 5.7c: Intra nucleotide NOE connectivities (di) of base to sugar protons of nucleic acid in the drug-DNA complex observed from the NOESY spectra at D/N = 1.0 at 275 K. The very strong (ss), strong (s), medium (ws), weak (w), very weakly (ww) intense cross peaks correspond to distances in the range ss 1.8 – 2.5 Å, s 2.5 – 3.0 Å, ws 3.0 – 3.5 Å, w 3.5 – 4.0 Å, ww 4.0 – 5.0 Å, respectively. Overlap of cross peaks is indicated as o.

Cross peak	C1	G2	T3	A4	C5	G6
H8/H6-H1'	o	ws	s	ws	o	ws
H8/H6-H2'	ss	ss	ss	o	s	ss
H8/H6-H2"	s	ss	s	o	o	o
H8/H6-H3'	ws	w	o	ws	o	ws
H8/H6-H4'	ww	ww	o	ww	o	ws

Table 5.7d: NOE connnectivities in the drug – DNA complex at D/N = 1.0 at 275 K. The very strong (ss), strong (s), medium (m), weak (w), very weakly (vw) intense cross peaks correspond to distances in the range ss 1.8 – 2.5 Å, s 2.5 – 3.0 Å, ws 3.0 – 3.5 Å, w 3.5 – 4.0 Å, ww 4.0 – 5.0 Å, respectively in the NOESY spectra. Overlap of cross peaks is indicated as o.

dps - Internucleotide, Intrastrand and sequential	D/N = 1.0	di - Intranucleotide	D/N = 1.0
G2NH^{f} – C1H1'	ws	C1NH$_2$^{b}- C1NH$_2$^{nb}	ws
G2NH^{f}–T3CH$_3$^{f}	ws	C5NH$_2$^{b} - C5NH$_2$^{nb}	ws
C1H1'- G2NH^{f}	ws	C1NH$_2$^{nb}-C1H5	ws
C1H1'- G2NH^{b}	ws	C1NH$_2$^{b}- C1H5	s
G2NH^{b} - T3NH^{b}	w	C1NH$_2$^{b} - 1H6	ww
G2NH^{f} - T3NH^{f}	w	C1NH$_2$^{nb}- C1H6	ws
T3NH^{b} - A4NH$_2$^{b}	ww	G2NH - G2NH$_2$^{b}	s
T3NH^{b} - A4NH$_2$^{nb}	s	G2NH^{b} - G2NH$_2$^{b}	ws
T3NH^{f} - A4NH$_2$^{nb}	ss	G2NH^{b} - G2NH$_2$^{nb}	ws
T3NH^{f} - A4NH$_2$^{b}	ss	G2NH^{f} - G2NH$_2$^{b}	ws
T3NH^{b}- A4H2	ss	G2NH^{f} - G2NH$_2$^{nb}	ws
T3NH^{f} - A4H2	ws	T3NH^{f} - T3CH$_3$^{f}	s
C5H1' - G6NH2^{b}	ws	T3NH^{b} - T3CH$_3$^{b}	ws
T3CH$_3$^{f}- G2H2'	o	T3NH^{f} - T3CH$_3$^{b}	w
T3CH$_3$^{f}- G2H2"	o	T3NH^{f} - T3CH$_3$^{f}	ws
T3CH$_3$^{f}- G2H1'	s	C5NH$_2$^{b} - C5H5	w
T3CH$_3$^{b}- G2H1'	ws	C5NH$_2$^{nb} - C5H5	ws
T3CH$_3$^{f}- G2H8	s	C5NH$_2$^{b} - C5H6	w
T3CH$_3$^{b}- G2H8	w	C5NH$_2$^{nb} - C5H6	w
T3CH$_3$^{f}- A4H8	ws		
T3CH$_3$^{b}- A4H8	w		
dps - Internucleotide, Interstrand and sequential		dpi- Internucleotide and within base pair	
C5NH$_2$^{b} - T3CH$_3$^{b}	ww	G2NH^{f} - C5NH$_2$^{b}	s
G2NH^{b} – G6NH^{b}	ww	G2NH^{f} - C5NH$_2$	s
		G2NH^{b} - C5NH$_2$^{b}	s
		G2NH^{b} - C5NH$_2$^{nb}	s
		G2NH^{f} - C5H5	ws

Table 5.8: Intensities of NOE cross peaks (di) within the drug molecule in the drug-DNA complex at D/N = 1.0 at 275 K. The very strong (ss), strong (s), medium (ws), weak (w) and very weakly (ww) intense cross peaks refer to distances in the range ss 1.8 – 2.5 Å, s 2.5 – 3.0 Å, ws 3.0 – 3.5 Å, w 3.5 – 4.0 Å, ww 4 – 5 Å, respectively from the NOESY spectra, Fig. 6a-m. Overlap of peaks is indicated as o.

Cross peak	Intensity	Uncomplexed drug (Å)
$11NH^f$-$11CH_2$	o	2.69
$11NH^b$ - $11CH_2$	o	-
$11NH^f$-$12CH_2/13CH_2$	s	3.32 ($12CH_2$)
$11NH^b$ - $12CH_2/13CH_2$	s	-
$11NH^f$ - $14CH_2$	w	-
$11NH^b$ - $14CH_2$	ww	-
$11NH^f$ - 6H/7H	w	3.60 - 4.70
6H/7H - $11CH_2$	o	2.15
6H/7H - $12CH_2/13CH_2$	s	2.55 ($12CH_2$)
6H/7H - $14CH_2$	ws	-
$14CH_2$ - $13CH_2$	ss	2.40

Table 5.9: Intermolecular NOE connectivities between d-$(CGTACG)_2$ and mitoxantrone in the drug-DNA complex at D/N =1.0 from NOESY spectra at 275 K. The very strong (ss), strong (s), medium (ws), weakly (w) and very weekly (ww) intense cross peaks correspond to distance of ss 1.8 – 2.5 Å, s 2.5 – 3.0 Å, ws 3.0 – 3.5 Å, w 3.5 – 4.0 Å, ww 4 – 5 Å. Overlap of peaks is indicated as o.

Cross peak	Intensity	Distance rMD Model (Å)
$11NH^b$ - G6H1'	ww	4.67
$11NH^b$ - C1H6	ww	4.86
$11NH^b$ - C1H5	ww	4.92
$11NH^b$ - C1H2"	w	3.96
$11NH^b$ - $G6NH^b$	w	4.85
$14CH_2$ – G2H8	w	4.10
$14CH_2$ – G6H8	w	4.15
$14CH_2$ –C1H6	s	2.90
$14CH_2$ – C5H6	ws	3.68
12/13 CH_2 – $G6NH^b$	w	4.02
12/13 CH_2 – $G2NH^b$	ww	5.99
12/13 CH_2 – $C5NH_2{}^b$	ww	5.02
12/13 CH_2 – $C5NH_2{}^{nb}$	ww	3.98
12/13 CH_2 – $C1NH_2{}^b$	w	3.90
12/13 CH_2 – C1H2"	ws	3.81
12/13 CH_2 – C1H1'	ww	4.14
12/13 CH_2 – G6H8	ww	5.01
12/13 CH_2 – C1H6	ws	3.76
12/13 CH_2 – C1H5	w	4.78
12/13 CH_2 – C5H6	w	4.28
12/13 CH_2 – C5H5	ww	5.15
$14CH_2$ – $G6NH^b$	ww	5.72
$14CH_2$ – $C5NH_2{}^{nb}$	ww	4.72
$14CH_2$ – C1H2"	ws	3.14
$11CH_2$ – C1H6	ws	3.85
1OH/4OH – C1H2"	s	2.86
1OH/4OH – C1H4'	ws	3.98
1OH/4OH – C1H1'	w	3.13
1OH/4OH – G6H1'	s	3.07

two base pairs of DNA like other intercalators (Chen et al, 1979) having conjugated aromatic rings. Apparently drug is binding externally to the hexamer sequence in a specific orientation which gives rise to the observed NOEs.

The addition of mitoxantrone in increasing amounts to DNA hexamer does not cause the ^{1}H as well as ^{31}P resonances to drift continuously, except for C5H1' and G6H1'. The T3NH, G2NH, G6NH and $T3CH_3$ resonance lines, instead gives rise to new set of broad signals upfield at the expense of the intensities of the original ones, as evidenced by Fig. 5.5e and 5.5f. The direct proof of mitoxantrone binding to C1.G6 base pair comes from 2D ^{31}P NMR exchange spectra showing strong exchange correlation between bound and free C1pG2 resonance at stoichometric ratio of 0.2, 0.5 as well as 1.0 (Fig. 5.4).The same is also clear in the NH region of ^{1}H NOESY spectra (Fig. 5.8g) showing exchange of free and bound T3NH, G2NH and G6NH. There has been considerable evidence in literature that mitoxantrone binds preferentially to CG sites (Panousis et al, 1994). It has slower dissociation rates for Poly dG–dC than for Poly dA–dT by an order of magnitude (Krishnamoorthy et al, 1986). The existence of intermolecular NOEs involving $11CH_2$, $12CH_2$, $13CH_2$ and 14 CH_2 with C1H6, C1H5, C3H6, G4H8 protons in 1:1 complex of mitoxantrone with d–$(CGCG)_2$ duplex has been demonstrated (Lown et al, 1985b). Also 6H / 7H proton is close to C3H4' and G4H4' proton and G2H8 and C3H5 protons are significantly broadened in that complex (Lown et al, 1985b). Our detailed NMR analysis shows that all internucleotide sequential connectivities (Table 5.7a) exist. Further, the DNA hexamer in complexed state is expected to adopt a conformation close to that of canonical B–DNA structure. All the duplex pair peaks, including sequential intra and inter–strand peaks, exist. Thus it may be

concluded that mitoxantrone binds externally to the DNA duplex, being in close proximity to C1.G6 base pair. All the spectral lines are somewhat uniformly broadened on binding as the internal motions are affected and the protons are getting immobilized. Notable among these are the G6NH which being easily accessible to solvent water, exchange freely in uncomplexed d–$(CGTACG)_2$ and are broadened as compared to G2NH and T3NH, but are observable in both free and bound state in the 1:1 mitoxantrone d–$(CGTACG)_2$ complex.

The 11NH proton of mitoxantrone shows substantial upfield shift 0.95 ppm on binding while 6H/7H and 2H/3H shift by 0.30 ppm and 0.66 ppm, respectively (Table 5.4). This is indicative of stacking of mitoxantrone chromophore with base pair of DNA, perhaps with the C1.G6 base pair. This may result in insignificant shift of $12CH_2$, $13CH_2$ and $14CH_2$ protons as observed (Table 5.4). The shift in resonance peaks of DNA protons is not significant. In fact the change in chemical shift is not alone a sufficient indicator of the interaction, instead the observed intermolecular short contacts (Table 5.9) are direct proof of the structure of a specific drug–DNA complex.

5.1.3 Restrained Molecular Dynamics Studies

A model of the complex based on intermolecular (Table 5.9), intramolecular (within drug and within DNA hexamer) NOEs (Tables 5.7 a-d) was considered. The schematic representation of the initial model of mitoxantrone with d-$(CGTACG)_2$ is shown in Fig. 5.9. Distance restraints between atoms involved in the Watson–Crick hydrogen bonding pairs are imposed in the structure calculations based on experimental evidence by NOESY spectra. The front and side view of the final structure obtained after

Restrained Molecular Dynamics is shown in Fig. 5.10. The stacking interaction of mitoxantrone with respect to C1.G6 base pair is shown in Fig. 5.11

Table 5.10 indicates an assessment of refined structures after equilibration (at the end of 25 ps) in terms of energetics including restraint violations energies. The total potential energy of the final structure is 462 kcal mol^{-1}, which is significantly lower than the corresponding energy of initial model B-DNA structure (3479 kcal mol^{-1}). The forcing potential, which indicates contribution to potential energy due to violations of both experimental distances data, exhibits a decrease from 2153 to 336 kcal mol^{-1} after restrained energy minimization and restrained molecular dynamics. Summary of experimental restraints and statistical analysis of family of structures generated by restrained molecular dynamics (rMD) is shown in Table 5.11

All helical parameters, backbone torsional angles, and sugar conformations of the resulting rMD structures were thoroughly analyzed with the program CURVES, version 5.1 (Lavery et al, 1996; Lavery et al, 1989). Plot of the helicoidal parameters as a function of residue position in the duplex is shown in Figure 5.12 a-b, along with classical structures of A-DNA and BDNA. The overlap geometry at different base pair steps along the sequence in mitoxantrone - d-$(CGTACG)_2$ is shown in Figure 5.13. In the base pair-axis parameters, the average value of x-displacement is 0.81 Å. The average y-axis displacement (dy) is 0.0 Å. The rMD structure display inclination values of terminal C.G base pair deviating maximum from the average value of 7.74°. Among intra base parameters, the stagger (Sz) and stretch (Sy) values vary much from their ideal values for terminal residues. The shear (Sx) values lie within ±1.0 Å of the average. Base pair opening lies in the range 6 to 15 for all base pairs in all rMD structure. In regular A-DNA

and B-DNA geometries, global values of the inter base pair parameters - shift (Dx), slide (Dy), roll (rho) and tilt (tau) are essentially zero. For rMD structures, the observed shift and slide values are small and do not show any significant variation with the base pair step. The rise per residue (Dz) approximately lies with in the range 3.2 - 3.7 Å that is standard for B-DNA. The variation of tilt value is ± 6° deviated from the ideal B-DNA value. The twist angle varies between 31° -43°. The backbone torsional angles and glycosidic bond rotation values (Table 5.12) show that the conformation of the structure obtained from rMD is close to that of the B-DNA. Thus d-$(CGTACG)_2$ on binding to mitoxantrone has the global helical parameters near to standard B-DNA values, indicating that the drug is binding externally to DNA.

Table 5.10: Energy terms (Kcal mol^{-1}) for starting and final rMD structure.

Structure	Total	Bond	Angle	Dihedral
Initial	3479	483	496	321
Final	462	43	147	122
	Vdw	Electrostatic	Restraint	
Initial	355	-168	2153	
Final	143	-224	336	

Table 5.11: Summary of Experimental restraints and statistical analysis of final structure generated by restrained Molecular Dynamics (rMD)

Parameter	
	No. of Distance Restraints
Intra residue	146
Inter residue	34
Inter molecular	23
Average pairwise RMSD	Initial = 0 Final = 0.69
Average residuewise RMSD	C1=0.61, G2=0.82., T3=1.32 A4=0.89, C5=1.14, G6=1.09 Mitoxantrone=0.72

Table 5.12: Backbone torsional angles, pseudoratation phase angle and glycosidic bond rotation of the final structure in degrees analyzed using CURVES program.

		α		β		γ		δ	
Strand I	Strand II	Strand I	Strand II	Strand I	Strand II	Strand I	Strand II	Strand I	Strand II
C1	G12	.....	....	.....	....	50.68	52.64	142.95	140.93
G2	C11	-57.32	-65.13	-177.81	160.35	52.60	5.036	149.58	136.63
T3	A10	-78.82	-64.83	-146.65	-172.68	54.58	51.28	143.58	143.79
A4	T9	-65.78	-79.07	-173.96	-141.01	52.27	54.28	142.79	141.91
C5	G8	-59.54	-56.34	160.65	-170.23	47.44	51.86	138.13	149.29
G6	C7	.....	.....	.....	.....	52.81	47.50	140.17	138.72
B-DNA		-63		136		54.0		123	

		ε		ζ		χ		P	
Strand I	Strand II	Strand I	Strand II	Strand I	Strand II	Strand I	Strand II	Strand I	Strand II
C1	G12	....	...	.....	.....	-127.95	-119.40	155.33	167.71
G2	C11	171.41	-141.34	-99.19	-137.50	-96.89	-118.24	188.33	138.86
T3	A10	175.59	178.70	-112.54	-94.39	-109.76	-112.42	153.55	168.32
A4	T9	-179.95	170.96	-94.70	-107.22	-112.97	-109.30	165.03	153.31
C5	G8	-151.03	168.44	-132.06	-97.58	-110.65	-95.19	143.58	188.92
G6	C7	....	...	.....	.....	-116.17	-121.50	167.84	153.68
B-DNA		-169		-108		-105		162	

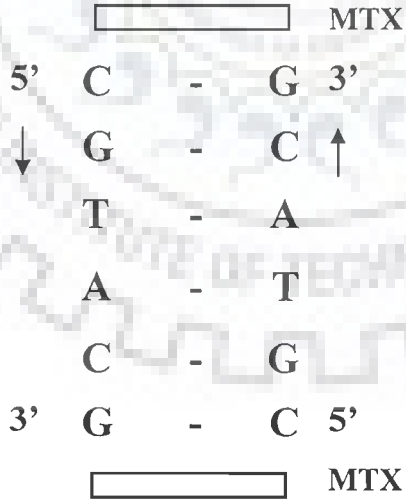

Figure 5.9: Schematic Representation of mitoxantrone (MTX) in complex with d-$(CGTACG)_2$

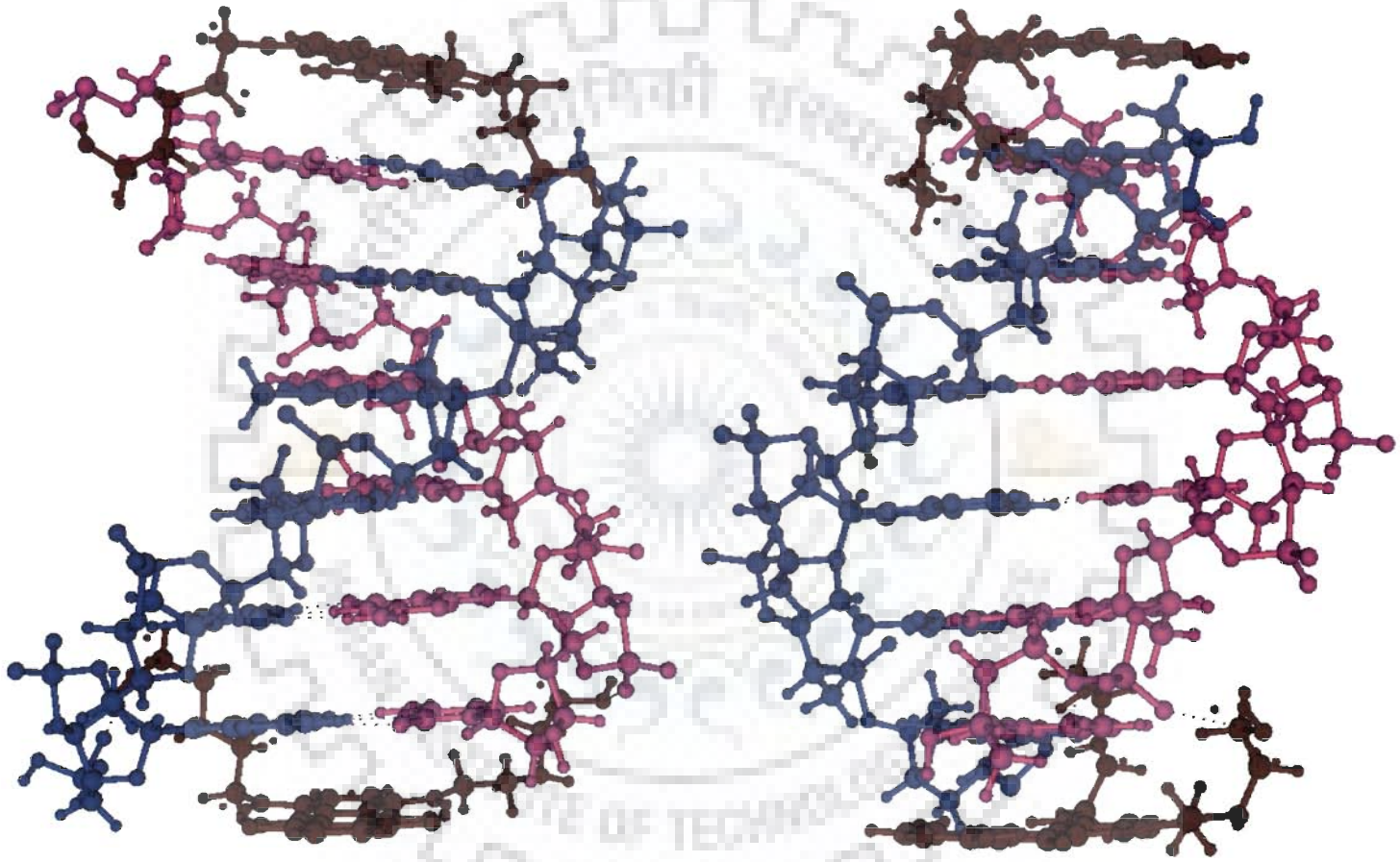

Figure 5.10: The final rMD structure of d-(CGTACG)$_2$-mitoxantrone derived from the NOE data, showing mitoxantrone stacked to the terminal C1.G6 base pair (a) front view (b) side view.

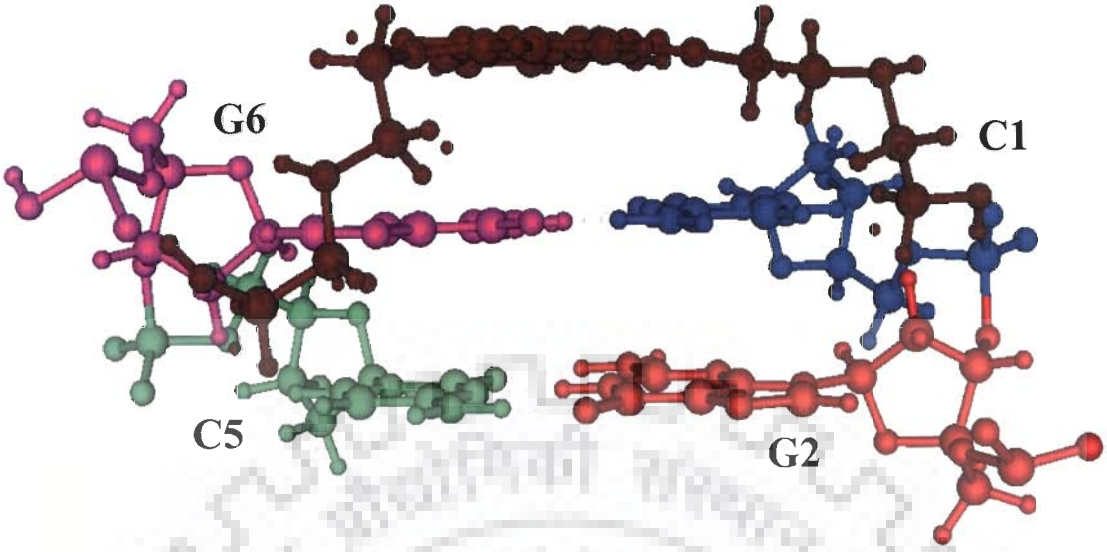

(Fig. 5.11a)

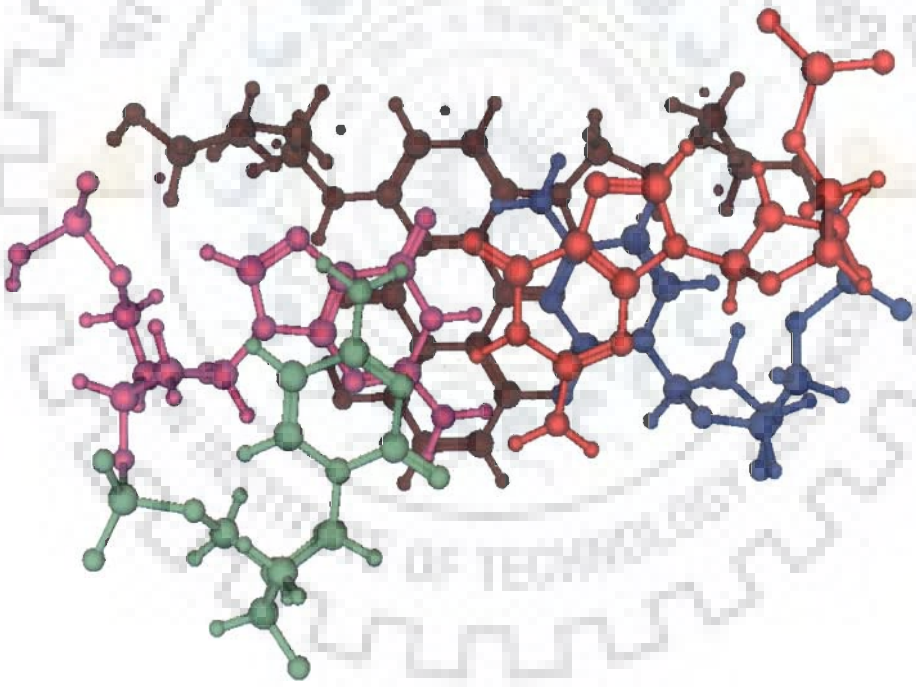

(Fig. 5.11b)

Figure 5.11: Stacking interaction of mitoxantrone with respect to terminal base pairs of d-$(CGTACG)_2$ (a) front view (b) top view.

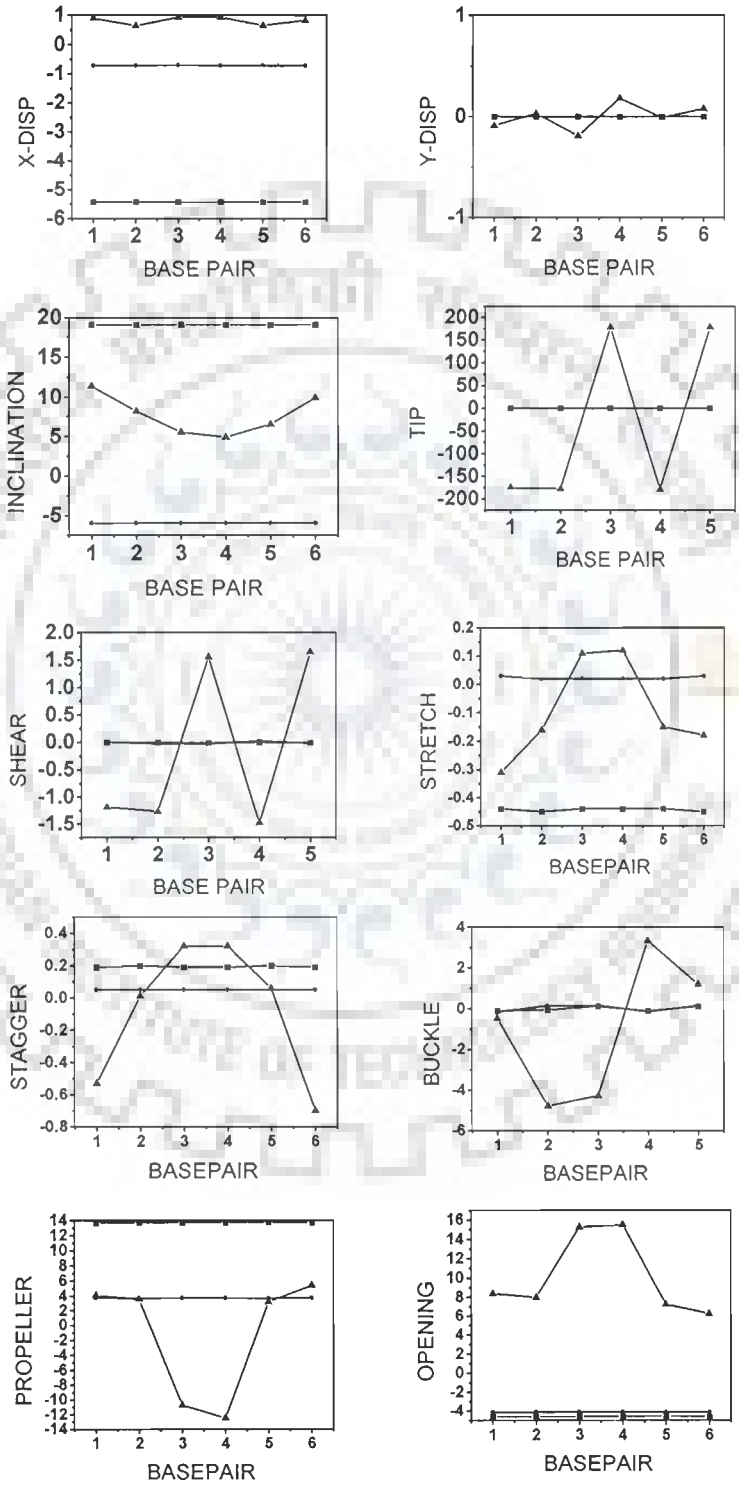
X-DISP
BASE PAIR
Y-DISP
BASE PAIR
INCLINATION
BASE PAIR
TIP
BASE PAIR
SHEAR
BASE PAIR
STRETCH
BASEPAIR
STAGGER
BASEPAIR
BUCKLE
BASEPAIR
PROPELLER
BASEPAIR
OPENING
BASEPAIR

(Fig. 5.12a)

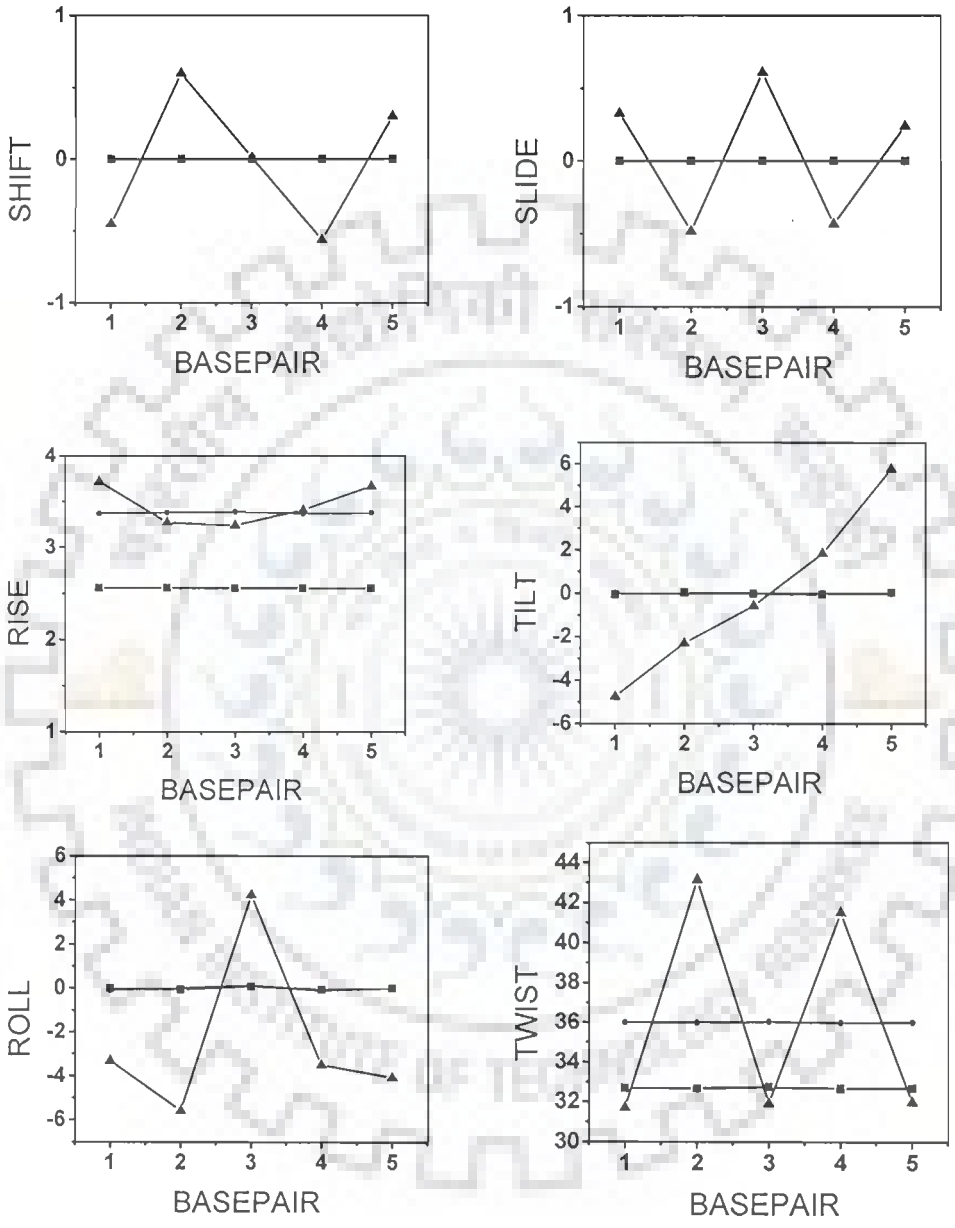

(Fig. 5.12b)

Figure 5.12: Helical parameters for d-(CGTACG)$_2$ complexed with mitoxantrone calculated for structure obtained by restrained molecular dynamics simulation, canonical A-DNA (■) and B-DNA(●) (a) Global Base pair – axis and base – base parameters (b) Global inter-base pair parameters.

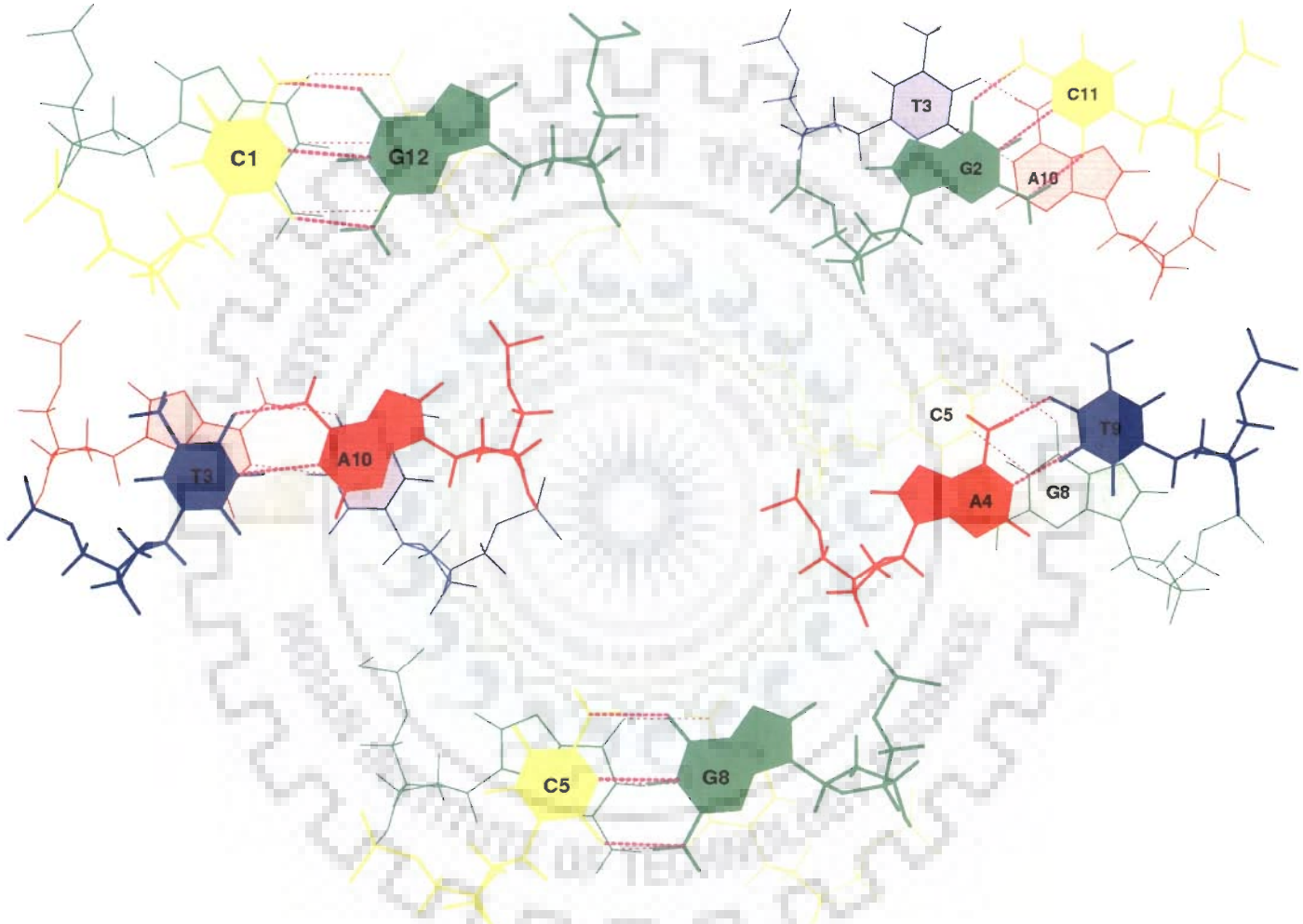

Figure 5.13: Overlap of base pairs at different base pair steps in d-$(CGTACG)_2$-mitoxantrone complex showing stacking interactions.

5.2 CONCLUSIONS

The ^{31}P resonance assignment was performed using $^{1}H - ^{31}P$ HMBC. Titration studies show that addition of mitoxantrone to DNA hexamer does not cause the ^{1}H as well as ^{31}P resonances to drift continuously, except for C5H1' and G6H1'. The T3NH, G2NH, G6NH and $T3CH_3$ resonance lines, instead gives rise to new set of broad signals upfield at the expense of the intensities of the free resonances. 2D ^{31}P NMR exchange spectrum shows strong exchange correlation between bound and free C1pG2 resonance at stoichometric ratio of 0.2, 0.5 and 1.0. The bound C1pG2 resonance is 0.40 ppm downfield shifted with respect to its free resonance. Absence of large downfield shift in ^{31}P NMR spectra suggest that there is no characteristic unwinding of the DNA helix and stretching of base pair separation due to change in backbone torsional angle ζ , C3'–O3'–P–O5' from gauche$^-$ to trans as observed with intercalators. There is a slow exchange on NMR time scale between free and bound species as exhibited by separate bound and free resonance for DNA protons – T3NH, G6NH, G2NH, $T3CH_3$ and 11NH of mitoxantrone. This is supported by the observed exchange of free and bound T3NH, G2NH and G6NH in the imino region of the ^{1}H NOESY spectra. Several intermolecular contacts are close to C1.G6 base pair. $11NH^b$ gives close contacts with G6H1', C1H6 and C1H5. $14CH_2$ is close to both G6H8 and C1H6. 1OH/4OH is in proximity to C1H1', C1H4' and G6H1'. Mitoxantrone protons ($11NH^b$, 1OH/4OH, $12CH_2/13CH_2$ and $14CH_2$) are simultaneously close to C1 and G6 residue protons of DNA which are located on opposite sides of C1.G6 base pair. This is not possible if mitoxantrone aromatic chromophore intercalates between base pairs of DNA. The presence of intra base pair, sequential inter base pair and all sequential intramolecular NOE connectivities, show that all base pairs in d-$(CGTACG)_2$

are intact on binding with mitoxantrone. The drug exists in monomeric form in the bound complex as NOE connectivities, characteristic for self associated mitoxantrone are absent. Mitoxantrone binds externally to d-$(CGTACG)_2$ and the aromatic chromophore stacking with C1.G6 base pairs leading to large upfield shifts in 6H / 7H, 2H / 3H and particularly 11NH protons ($\Delta\delta \sim 0.95$ ppm upfield) and specific drug protons in close proximity of DNA protons. It is evident from the ^{1}H and ^{31}P NMR results that the base pairs do not open up to accommodate the aromatic anthraquinone chromophore like a typical intercalators, such as ethidium bromide, daunomycin, adrimycin, actinomycin. Apparently drug is binding externally to the hexamer, which gives rise to the observed NOEs. Stacking at ends has been observed in X-ray crystallographic study of ametantrone, a closely related analogue of mitoxantrone with d-$(CGTACG)_2$ (Yang et al, 2000). The observed results are in contrast with transcriptional assay studies which show that mitoxantrone chromophore intercalates at 5' (A/T) CA and 5' (A/T) CG sites of DNA (Panousis et al, 1994).

Chapter 6

Studies on Complex of Mitoxantrone with d-(TGTACA)$_2$ by Phosphorous-31, Proton Nuclear Magnetic Resonance Spectroscopy and Restrained Molecular Dynamics Approach

This chapter contains the following studies of the complex of mitoxantrone-d-(TGTACA)$_2$ by one- and two-dimensional ^{31}P and ^{1}H NMR followed by restrained molecular dynamics simulations:

- The two dimensional ^{1}H - ^{31}P Heteronuclear Multiple Bond Correlation (HMBC) of 4.0 mM d-(TGTACA)$_2$ at 278 K for the assignment of ^{31}P resonances.
- Titrations by recording ^{31}P and ^{1}H 1D NMR versus drug (D)/DNA duplex (N) ratio, 0.1, 0.2, 0.3, 0.4, 0.5, 0.6, 0.7, 0.8, 0.9, 1.0, 1.2, 1.35, 1.5, 1.65, 1.80 and 2.0 at 275 K and 298 K.
- 2D ^{31}P - ^{31}P exchange spectra of mitoxantrone complexed with d-(TGTACA)$_2$ by a phase-sensitive NOESY with mixing time of 200 ms at 275 K for D/N = 0.2, 0.5 and 1.0.
- 2D ^{1}H - ^{1}H NOESY at D/N = 0.5, 1.0, 1.5, 2.0 using mixing time τ_m =100, 200, 300 ms at 275 K in 90% H_2O and 10% D_2O.
- Restrained molecular dynamics studies on the solution structure for the complex of mitoxantrone with d-(TGTACA)$_2$ using inter-proton distances obtained from 2D ^{1}H NOESY as restraints.
- Analysis of the converged structure in terms of time average for the various conformational and helical parameters.

6.1 RESULTS AND DISCUSSION

6.1.1 Phosphorus-31 NMR Studies of Mitoxantrone-d-$(CGTACG)_2$ Complex

6.1.1.1 d-$(TGTACA)_2$

^{31}P NMR is a useful probe for the geometric arrangement about the phosphate group since it provides direct information about DNA backbone. The assignments of ^{31}P nuclei in d-$(TGTACA)_2$ were performed by using the 2D ^{1}H - ^{31}P HMBC (Fig. 6.1). For the purpose of this discussion, the positions of the bases in the hexamer are designated as follows: d–(T1pG2pT3pA4pC5pA6)$_2$. The ^{31}P resonances resolve into five distinct signals corresponding to the five phosphate groups at the ambient temperature. The three-bond scalar couplings between $(^{31}P)_n$ nuclei in the phosphate backbone and the $(H3')_n$ and four-bond coupling with $(H4')_{n+1}$ protons are observed (Fig. 6.1). The identification of the H3' and H4' cross peaks were done on the basis of proton assignments, which have been done by using 2D NOESY spectra. Scalar couplings involving H3' and H4' are considered for the assignment purpose as H5'/5" are overlapped highly. All five three bond scalar coupling of $(^{31}P)_n$ with $(H3')_n$ of the sugar residue i.e., T1pG2 – T1H3', G2pT3 – G2H3', T3pA4 – T3H3', A4pC5 – A4H3' and C5pA6 – C5H3' are observed (Fig. 6.1). In addition ^{4}J couplings of the phosphorous to the $(H4')_{n+1}$ protons of the sugar residues i.e., T1pG2 – G2H4', G2pT3 – T3H4', T3pA4 – A4H4', A4pC5 – C5H4' and C5pA6 – A6H4' are also clearly evident. H4' signal of A4 residue is separated from the H5' overlapped region and its connectivity through the four-bond coupling with T3pA4 phosphate, confirm assignment. Accordingly the phosphate resonances at -2.14, -1.79, -1.70, -1.66 and -1.42 were assigned as G2pT3^{f}, A4pC5^{f}, T1pG2^{f}, T3pA4^{f} and C5pA6^{f} respectively in uncomplexed d-$(TGTACA)_2$ at 275K (Table 6.1).

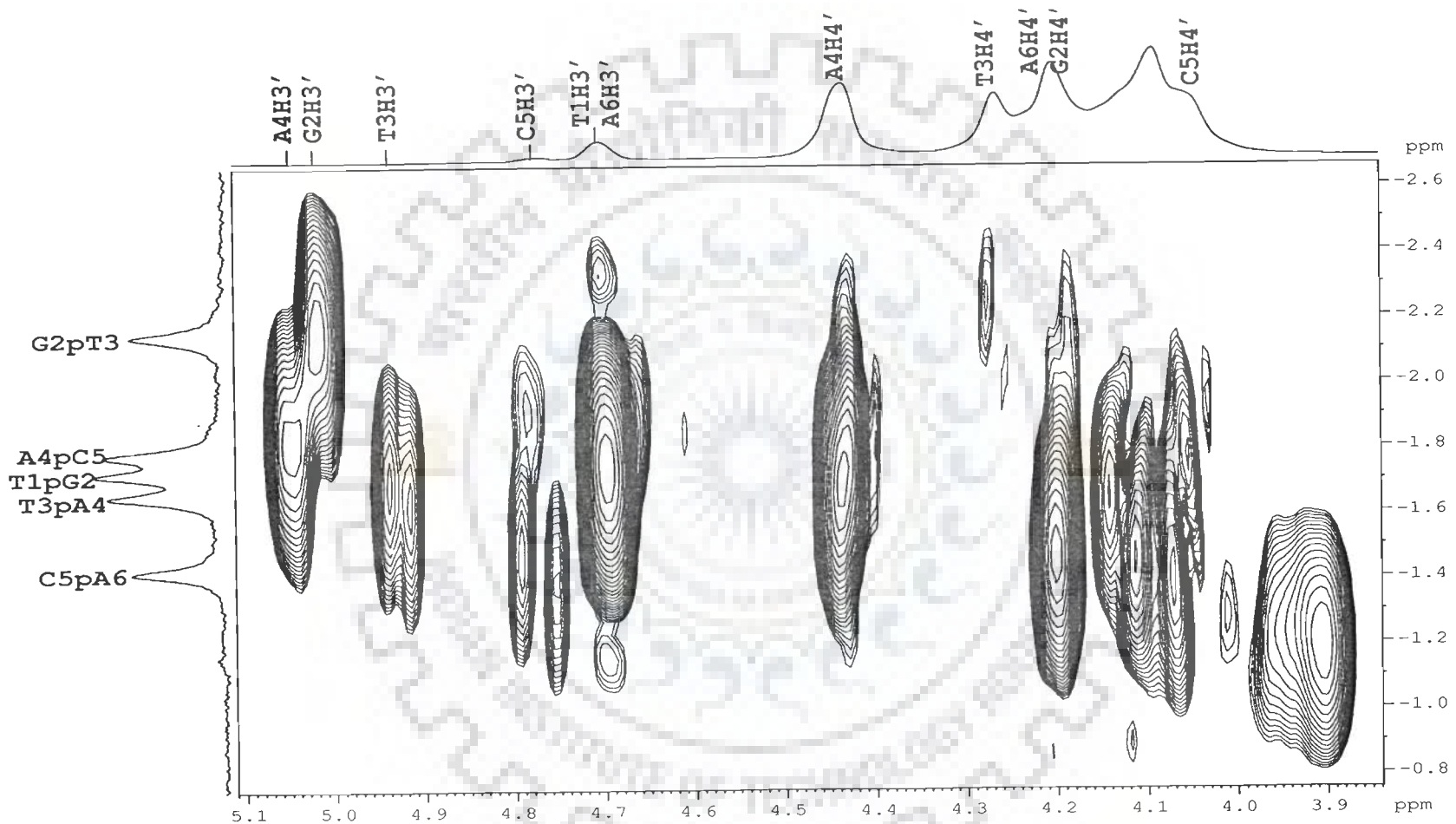

Figure 6.1: Two dimensional ^{31}P - ^{1}H Heteronuclear Multiple Bond Correlation (HMBC) Spectra 4.0 mM d-$(TGTACA)_2$ at 278K.

Table 6.1: Chemical shift of ^{31}P resonances of the phosphate groups of DNA hexamer, in complex of mitoxantrone with d–(TGTACA)$_2$ at 275 K and 298 K with different drug (D) to nucleic acid duplex (N) ratio (D/N). +ve Δδ indicates downfield shift. $\Delta\delta = (\delta_{D/N=2.0} - \delta_{D/N=0})$.

	275 K					298 K				
D/N	T1pG2^f	G2pT3^f	T3pA4^f	A4pC5^f	C5pA6^f	T1pG2^f	G2pT3^f	T3pA4^f	A4pC5^f	C5pA6^f
0.00	-1.70	-2.14	-1.66	-1.79	-1.42	-1.51	-1.83	-1.50	-1.51	-1.30
0.10	-1.66	-2.12	-1.66	-1.78	-1.41	-1.50	-1.82	-1.50	-1.51	-1.30
0.20	-1.65	-2.11	-1.65	-1.77	-1.41	-1.48	-1.81	-1.48	-1.51	-1.29
0.30	-1.64	-2.09	-1.64	-1.75	-1.41	-1.47	-1.80	-1.47	-1.51	-1.29
0.40	-1.64	-2.09	-1.64	-1.75	-1.41	-1.46	-1.79	-1.46	-1.51	-1.28
0.50	-1.60	-2.07	-1.60	-1.73	-1.40	-1.45	-1.79	-1.45	-1.51	-1.28
0.60	-1.60	-2.06	-1.60	-1.73	-1.38	-1.43	-1.78	-1.43	-1.50	-1.27
0.70	-1.60	-2.05	-1.60	-1.73	-1.38	-1.41	-1.73	-1.41	-1.51	-1.26
0.80	-1.60	-2.05	-1.60	-1.73	-1.38	-1.40	-1.76	-1.40	-1.51	-1.26
0.90	-1.60	-2.04	-1.60	-1.72	-1.38	-1.39	-1.72	-1.39	-1.50	-1.26
1.00	-1.60	-2.03	-1.60	-1.72	-1.38	-1.37	-1.73	-1.37	-1.50	-1.24
1.20	-1.60	-2.03	-1.60	-1.72	-1.38	-1.36	-1.70	-1.36	-1.50	-1.23
1.35	-1.60	-2.03	-1.60	-1.72	-1.38	-1.33	-1.66	-1.33	-1.49	-1.21
1.50	-1.60	-2.03	-1.60	-1.72	-1.38	-1.31	-1.66	-1.31	-1.49	-1.20
1.65	-1.60	-2.03	-1.60	-1.72	-1.38	-1.30	-1.64	-1.30	-1.49	-1.19
1.8	-1.60	-2.03	-1.60	-1.72	-1.38	-1.30	-1.64	-1.30	-1.49	-1.18
2.0	-1.60	-2.03	-1.60	-1.72	-1.38	-1.30	-1.64	-1.30	-1.49	-1.18
Δδ	+0.10	+0.11	+0.06	+0.07	+0.04	+0.21	+0.19	+0.20	+0.02	+0.12

Table 6.2: ^{31}P chemical shift assignments of free (δ^f) and bound (δ^b) phosphate groups obtained from ^{31}P exchange spectrum of the mitoxantrone– d–(TGTACA)$_2$ complex at drug (D) to nucleic acid duplex (N) ratios, D / N = 0.2, 0.5 and 1.0 at 275 K. The change in chemical shift, $\Delta\delta = \delta^b - \delta^f$, due to binding is also indicated for the three complexes. +ve Δδ indicates downfield shift.

At 275 K	D/N 0.2:1			D/N 0.5:1			D/N 1:1		
Phosphate group	δ_b	δ_f	Δδ	δ_b	δ_f	Δδ	δ_b	δ_f	Δδ
T1pG2	-0.57	-1.65	+1.08	-0.47	-1.60	+1.13	-0.45	-1.60	+1.15
G2pT3	-1.78	-2.11	+0.33	-1.74	-2.07	+0.33	-1.68	-2.03	+0.35
T3pA4	-1.15	-1.65	+0.50	-1.10	-1.60	+0.50	-1.08	-1.60	+0.52
A4pC5	-	-1.77	-	-	-1.73	-	-	-1.72	-
C5pA6	-0.98	-1.41	+0.43	-0.95	-1.40	+0.45	-0.92	-1.38	+0.46

6.1.1.2 Mitoxantrone-d-(TGTACA)$_2$ Complex

The complex of d-(TGTACA)$_2$ with mitoxantrone was made by addition of mitoxantrone from the stock solution (36 mM) to the d-(TGTACA)$_2$ solution till it reaches 2:1 ratio. The sample was prepared in 90% water and 10% D_2O. The addition of mitoxantrone to a solution of the oligomer d-(TGTACA)$_2$ induces a moderate downfield shift as compared to the resonances from free hexamer, but broaden severely with increase in D/N ratio. The spectra were recorded at 275 K (Fig. 6.2a-b) and 298 K (Fig. 6.2c-d) to look at the slow and fast exchange. The line broadening is quite evident after D/N = 1.0 at 275 K (Fig. 6.2b) and at higher ratios the peaks are too broad to resolve. In ^{31}P 1D NMR studies only five resonances corresponding to the free hexamer are observed on the formation of the DNA-drug complex. But on drug binding, each of the five phosphorus signals is expected to give cross peak due to chemical exchange with its respective bound resonance in the 2D ^{31}P NMR exchange spectrum.

(a) 2D ^{31}P - ^{31}P Exchange Spectra

The assignment of bound phosphorus resonance signals in mitoxantrone - d-(TGTACA)$_2$ complex are done by ^{31}P - ^{31}P 2D NOESY spectra (Figs. 6.3a-b) at various D/N ratios 0.5, 1.0 at 275 K. The one dimensional ^{31}P spectra are shown along the both axes. The five free phosphate resonances were already assigned at 275 K (Table 6.1) using the ^{1}H - ^{31}P correlation experiment. It is observed that each of the signals belonging to the phosphate group of free specie is correlated to another phosphate resonance shifted downfield, with respect to it due to exchange correlation. The corresponding downfield shifted signal is accordingly assigned as the ^{31}P signal in bound DNA. Accordingly, the bound phosphate resonances were assigned as T1pG2^b, G2pT3^b, T3pA4^b and C5pA6^b in

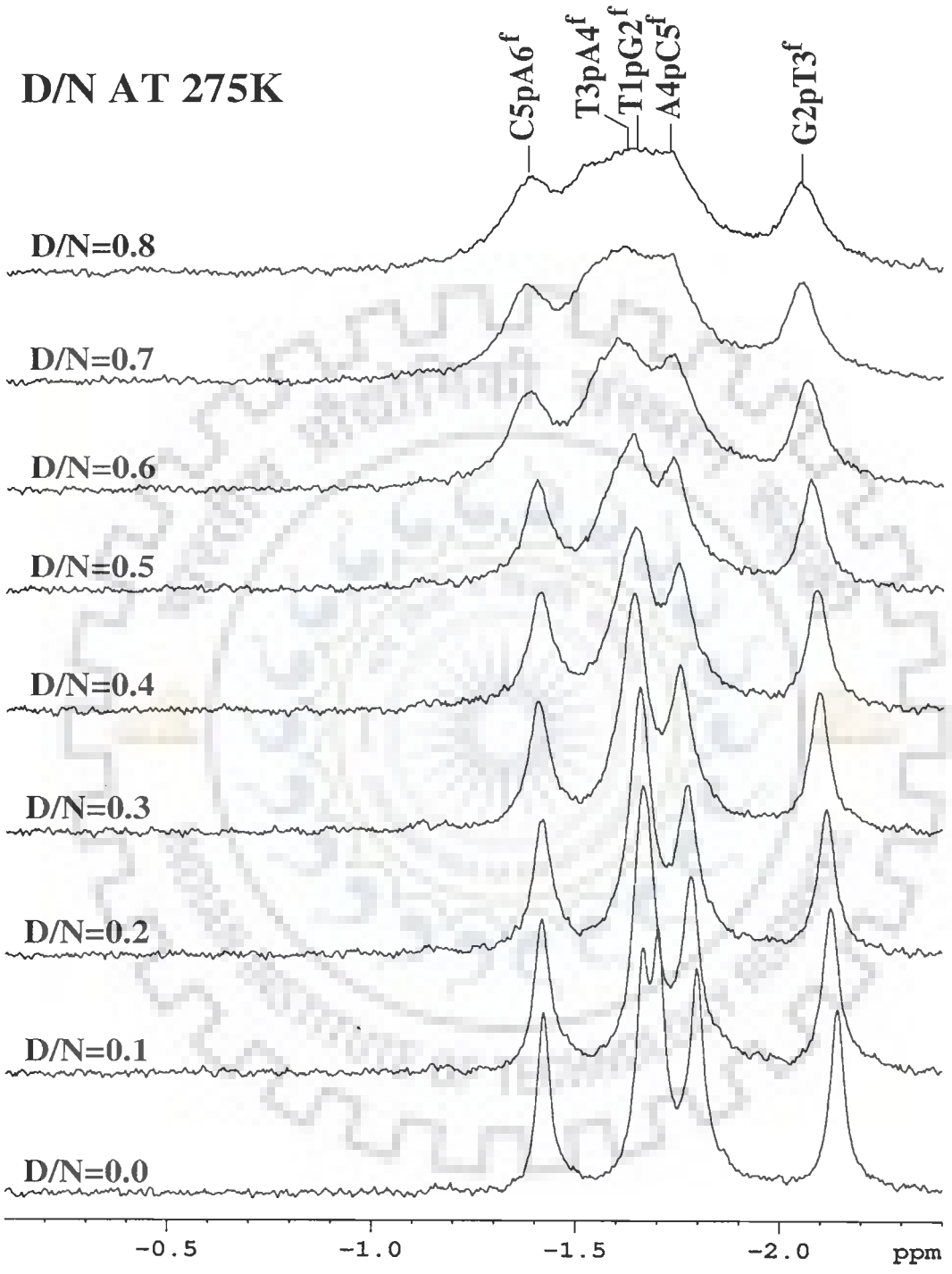

(a)

Figure 6.2(a-b): Proton decoupled ^{31}P NMR spectra of 4.0 mM d–$(TGTACA)_2$ in uncomplexed state and complexed with mitoxantrone with increasing drug (D) to nucleic acid duplex (N) ratio, D/N, at 275 K.

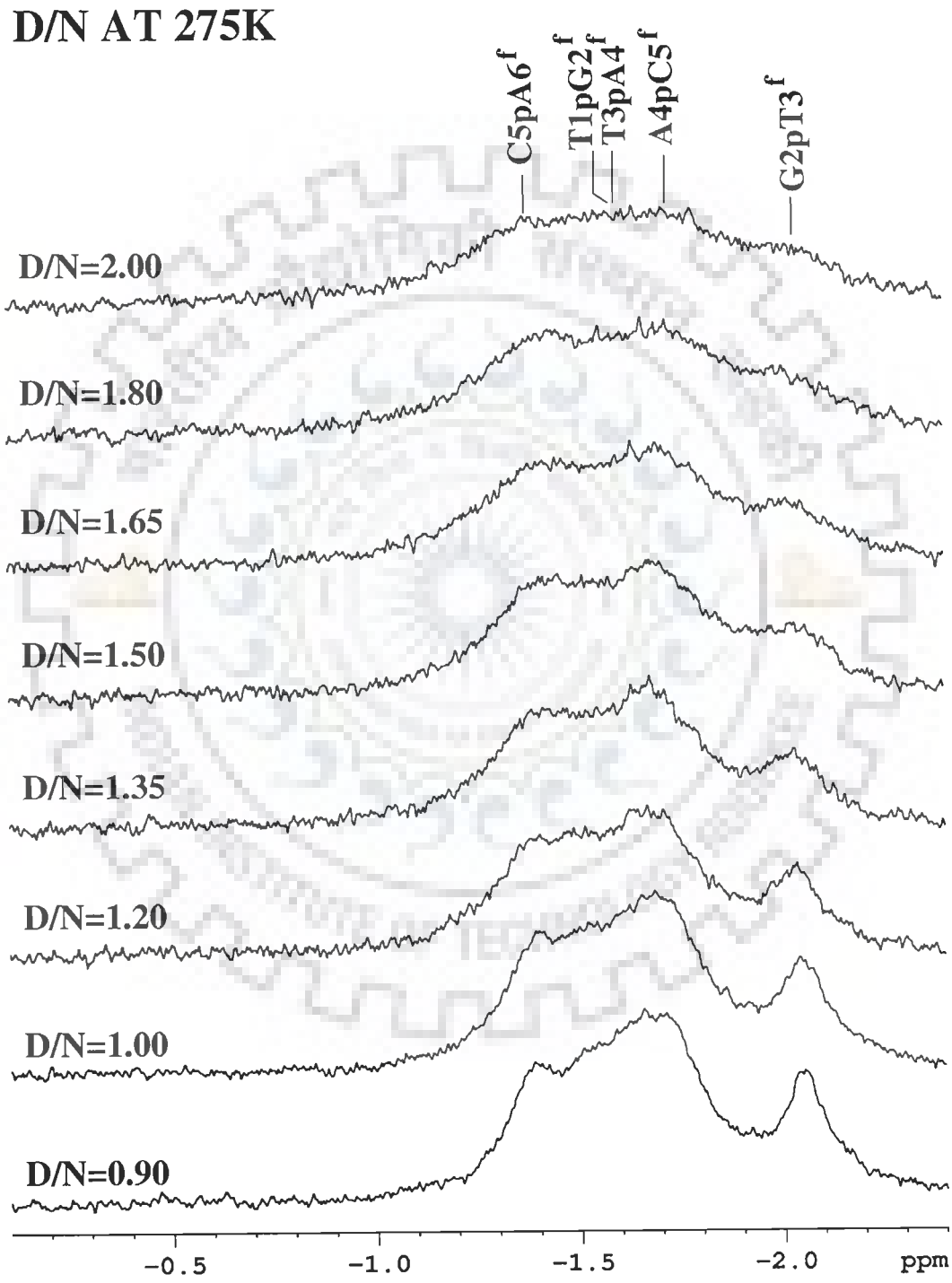
D/N AT 275K
C5pA6f
T1pG2f
T3pA4f
A4pC5f
G2pT3f
D/N=2.00
D/N=1.80
D/N=1.65
D/N=1.50
D/N=1.35
D/N=1.20
D/N=1.00
D/N=0.90
-0.5
-1.0
-1.5
-2.0
ppm

(Fig. 6.2b)

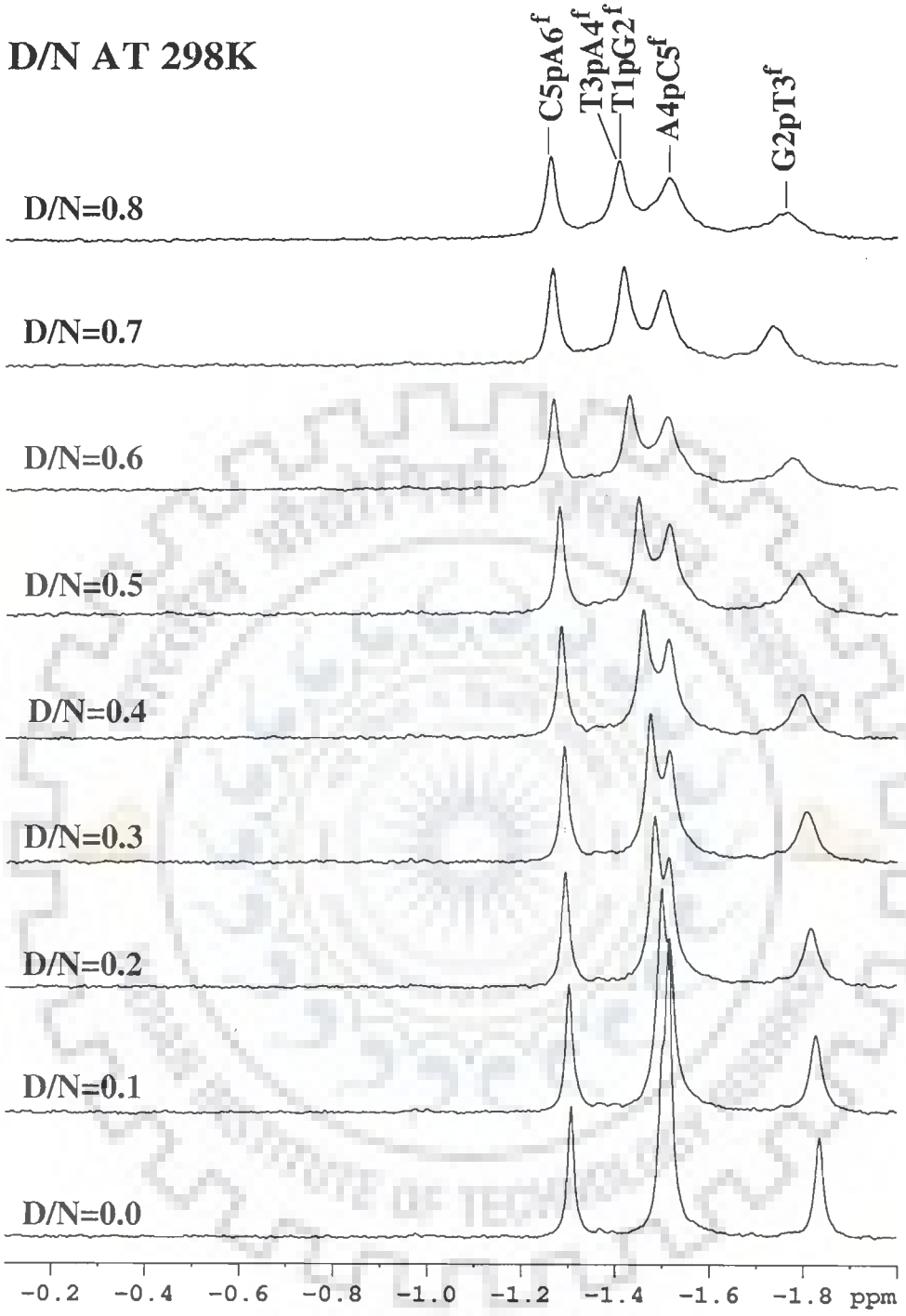

(c)

Figure 6.2(c-d): Proton decoupled ^{31}P NMR spectra of 4.0 mM d–$(TGTACA)_2$ in uncomplexed state and complexed with mitoxantrone with increasing drug (D) to nucleic acid duplex (N) ratio, D/N, at 275 K

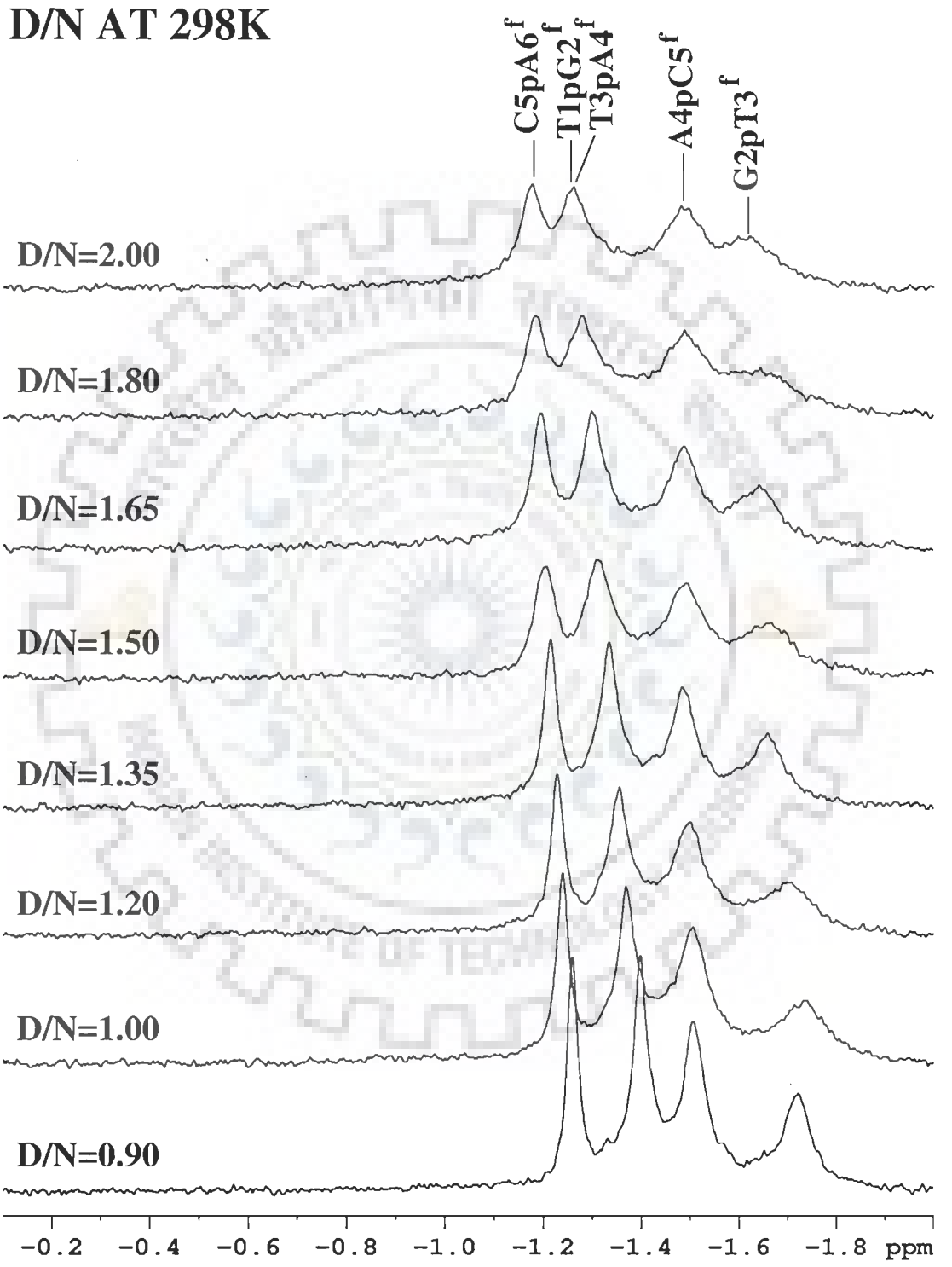
D/N AT 298K
C5pA6f
T1pG2f
T3pA4f
A4pC5f
G2pT3f
D/N=2.00
D/N=1.80
D/N=1.65
D/N=1.50
D/N=1.35
D/N=1.20
D/N=1.00
D/N=0.90
-0.2 -0.4 -0.6 -0.8 -1.0 -1.2 -1.4 -1.6 -1.8 ppm

(Fig. 6.2d)

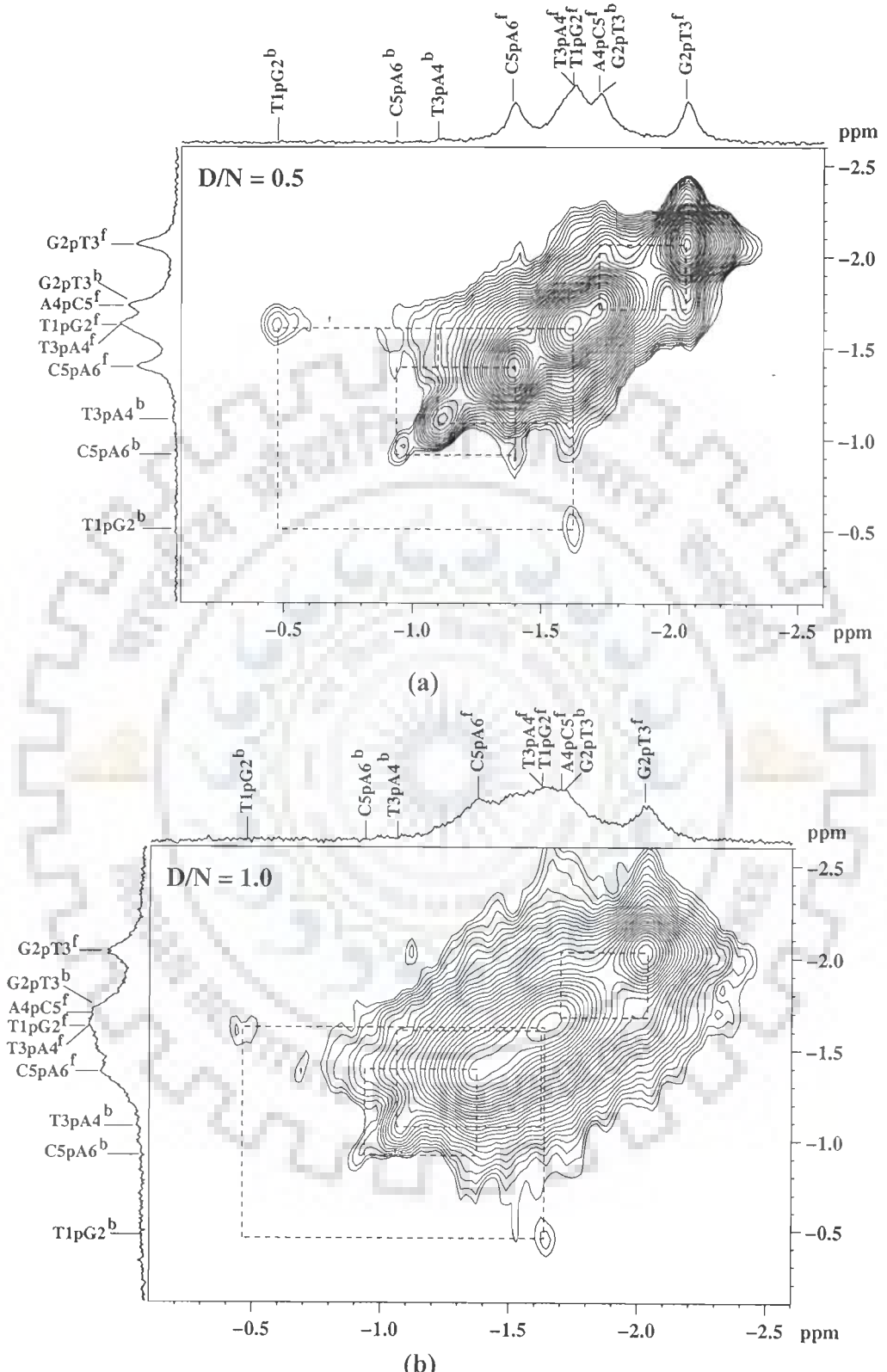

Figure 6.3: ^{31}P - ^{31}P NOESY exchange spectrum at 200 ms of the complex of mitoxantrone with d-$(TGTACA)_2$ at drug (D) to nucleic acid duplex (N) ratio, D/N of (a) 0.5 and (b) 1.0 at 275K.

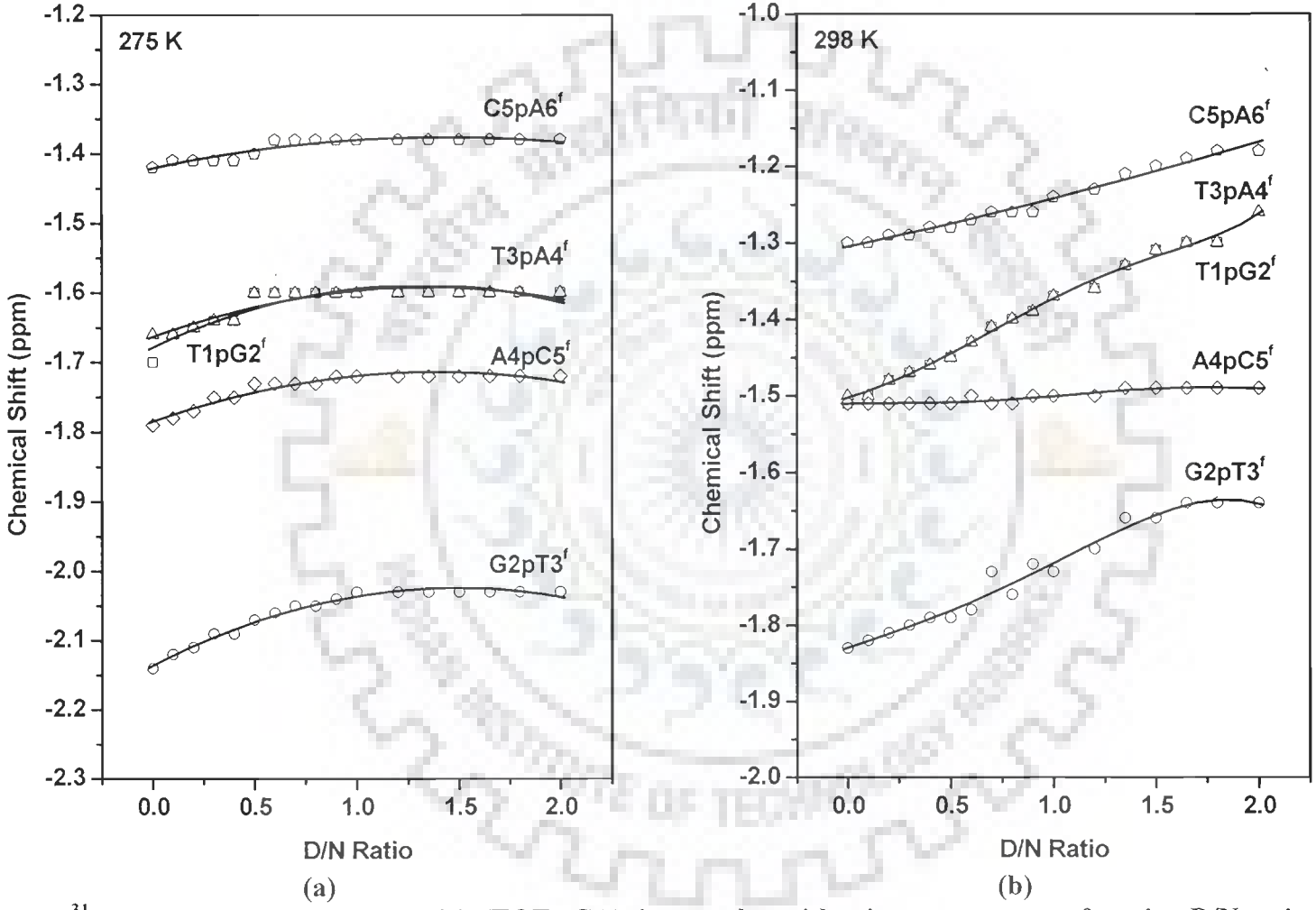

Figure 6.4: ^{31}**P Chemical shift variation of d–(TGTACA)$_2$ in complex with mitoxantrone, as a function D/N ratio (a) at 278K (b) at 298K (□ - T1pG2; ○ - G2pA3; Δ – T3pT4; ◇ - A4pC5; ⬠ - C5pA6)**

the drug-DNA complex (Fig.6.3). ^{31}P-^{31}P NOESY exchange clearly proves the fact that there are bound and free species in slow exchange on NMR time scale and yielded $\Delta\delta$ of the drug-DNA complex.

(b) Sequence Specificity of Mitoxantrone

It is observed that the T1pG2^f, G2pT3^f, T3pA4^f, A4pC5^f and C5pA6^f resonances shift ($\Delta\delta = \delta^b - \delta^f$) downfield by 0.10, 0.11, 0.06, 0.07 and 0.04 ppm, respectively for the complex of D/N 2.0 at 275K (Table 6.1). All five phosphate resonances show almost similar downfield shift in the titration experiments performed at 298 K (Table 6.1 and Fig. 6.4b). The chemical shift of free signals does not change significantly with D/N ratios at 275 K except for the T1pG2^f and G2pT3^f (Fig. 6.4a). Significant downfield shift of 1.15 ppm observed between bound and free resonances of T1pG2 (Table 6.2 and Fig. 6.3) resonance indicate that interaction with mitoxantrone occurs with this step. The interaction also affects other sites, which show downfield shift G2pT3 (0.35 ppm), T3pA4 (0.52 ppm) and C5pA6 (0.46 ppm). As discussed in chapter 4, ^{31}P chemical shift variations in nucleotides reflect the conformation of the phosphodiester groups at the level of the P–O5' and O3'–P bonds i.e. the values of torsion angles α = O3'–P—O5'–C5'and ζ = C3'–O3'–P–O5'. For a nucleotide in a B–DNA type conformation, the phosphate groups are normally found in gauche$^-$, gauche$^-$ (g^-, g^-) conformation (B_I) with α and ζ angles of -60° and -90°, respectively whereas the gauche$^-$, trans (g^-, t) B_{II} conformation (α = -60°, ζ = 180°) is generally associated with a deshielding of 1.5 ppm. Such transition from g^-, g^- to g^-, t on intercalation of drug chromophore by opening of adjacent base pairs at intercalation site from a distance of 3.4 to 6.8 Å have been reported in X–ray crystallographic structure of adriamycin and daunomycin to d–CGATCG, d–

TGATCA, d–CGTACG sequences (Frederick et al, 1990) as well in similar NMR structures (Mazzini et al, 1998), chapter 4, Table 6.3a. The pyridopurine (Favier at al, 2001) and berberine (Mazzini et al, 2003), which does not show such large shifts in phosphorus resonances on binding to DNA (chapter 4, Table 6.3b), have been shown to bind externally. T1pG2 signal in d–$(TGTACA)_2$ complex is downfield shifted by 1.15 ppm and it may be inferred that binding of mitoxantrone to d–$(TGTACA)_2$ does lead to local drug–induced distortions leading to change in phosphate backbone conformation from gauche, gauche (α = -60°, ζ = -90°) to gauche, trans (α = -60°, ζ = -180°). ^{31}P NMR studies show that there is no opening of base pairs to accommodate drug chromophore, which is generally associated with large down field shifts of ^{31}P resonance, of the order of 1.6–2.6 ppm (Gorenstein et al, 1992; Patel et al, 1976; Patel et al, 1974; Patel et al, 1982). Downfield shifts induced by drug are associated with the change in ζ torsional angle from g- to trans conformation and the ester O-P-O bond angle distortion. The downfield shift of other sites G2pT3 (0.35 ppm), T3pA4 (0.52 ppm) and C5pA6 (0.46 ppm) seems to indicate distortions in O-P-O bond angle at the level of these phosphate bonds. It may also be noted that such large downfield shifts are absent in earlier studies on mitoxantrone (Kotovych et al., 1986; Lown et al., 1985b). Also other ^{31}P signals in d–$(TGATCA)_2$ and d–$(CGTACG)_2$ complexes discussed in chapter 4 and chapter 5 respectively, shift downfield to a much lesser extent, by about 0.2-0.4 ppm. Thus we see that mitoxantrone is sequence specific as the affinity of mitoxantrone for TpG having pyrimidine site adjacent to it (d-$(TGTACA)_2$) is showing greater binding than the TpG having purine site adjacent to it (d-$(TGATCA)_2$). This study is further supported by proton NMR.

6.1.2 Proton NMR Studies of Mitoxantrone-d-$(CGTACG)_2$ Complex

6.1.2.1 Effects of Titrimetric Addition of Mitoxantrone

Fig. 6.5a-f shows the proton NMR spectra of mitoxantrone-d-$(CGTACG)_2$ Complex at 275 K on successive addition of drug to DNA. Most of the NMR experiments are carried out at 275 K as imino protons are sharpened and intensified at this temperature. Besides, DNA is expected to be present completely in duplex state at 275 K. The unambiguous assignments of nucleotide and drug protons at D/N 1.0 are shown in Table 6.3 and 6.4 respectively. The assignment of spectral lines to specific protons of drug has been made by following the strategies used for assignment in NMR spectra of uncomplexed drug (Birlirakis et al, 1992; Davies et al, 2001) and as discussed in chapter 3. Hexamer assignments has been carried out by following strategies adopted for standard B–DNA structures that is, sequential NOEs (base H8/H6)$_n$–sugar (H1')$_{n-1}$, (base H8/H6)$_n$–sugar(H2")$_{n-1}$, (base H8/H6)$_n$–sugar(H2')$_{n-1}$; expected NOEs due to several short intranucleotide distances (Wüthrich, 1986) as well as our NMR data of uncomplexed d–$(TGATCA)_2$ published earlier (Barthwal et al, 2004). The change in chemical shift ($\Delta\delta$) of base and H1' protons at D / N ratio are obtained at 275 K (Table 6.5a and Fig. 6.6) and 298 K (Table 6.6a). The same for drug protons are given in Table 6.5b, 6.6b and Fig. 6.7. Using the 2D NOESY experiments, carried out at 275 K for 1:1 complex, it was possible to ascertain the position of each and every proton resonance of drug as well as the hexamer. The chemical shift positions of drug in 1:1 drug–DNA complex and the change in chemical shift due to binding, with respect to uncomplexed drug monomer are given in Table 6.4. It may be noted that the data of 10 μM mitoxantrone has been taken to

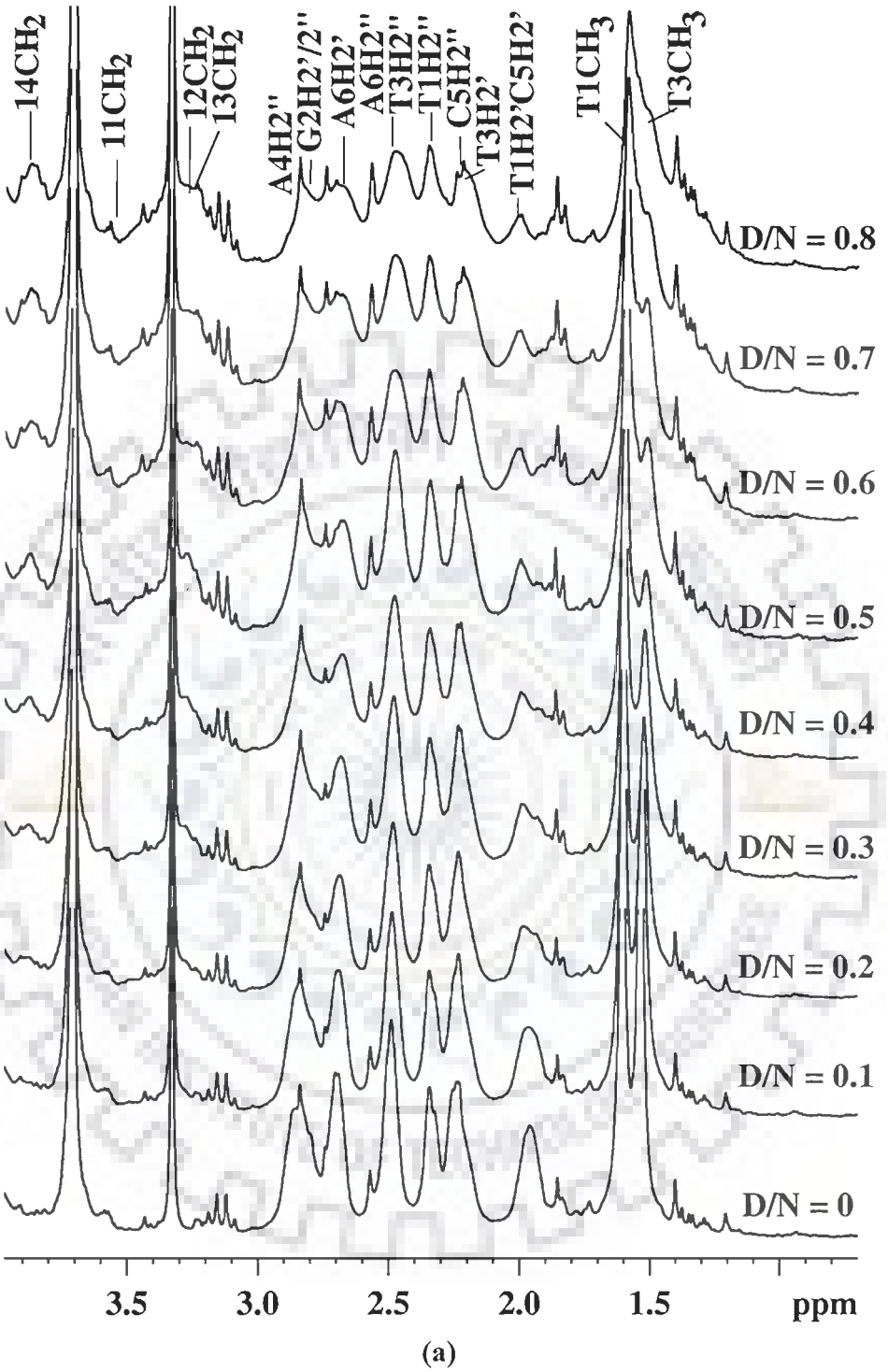

(a)

Figure 6.5(a-f): Proton NMR spectra of 4.0 mM d–$(TGTACA)_2$ in uncomplexed state and complexed with mitoxantrone with increasing drug (D) to nucleic acid duplex (N) ratio, D/N, at 275 K

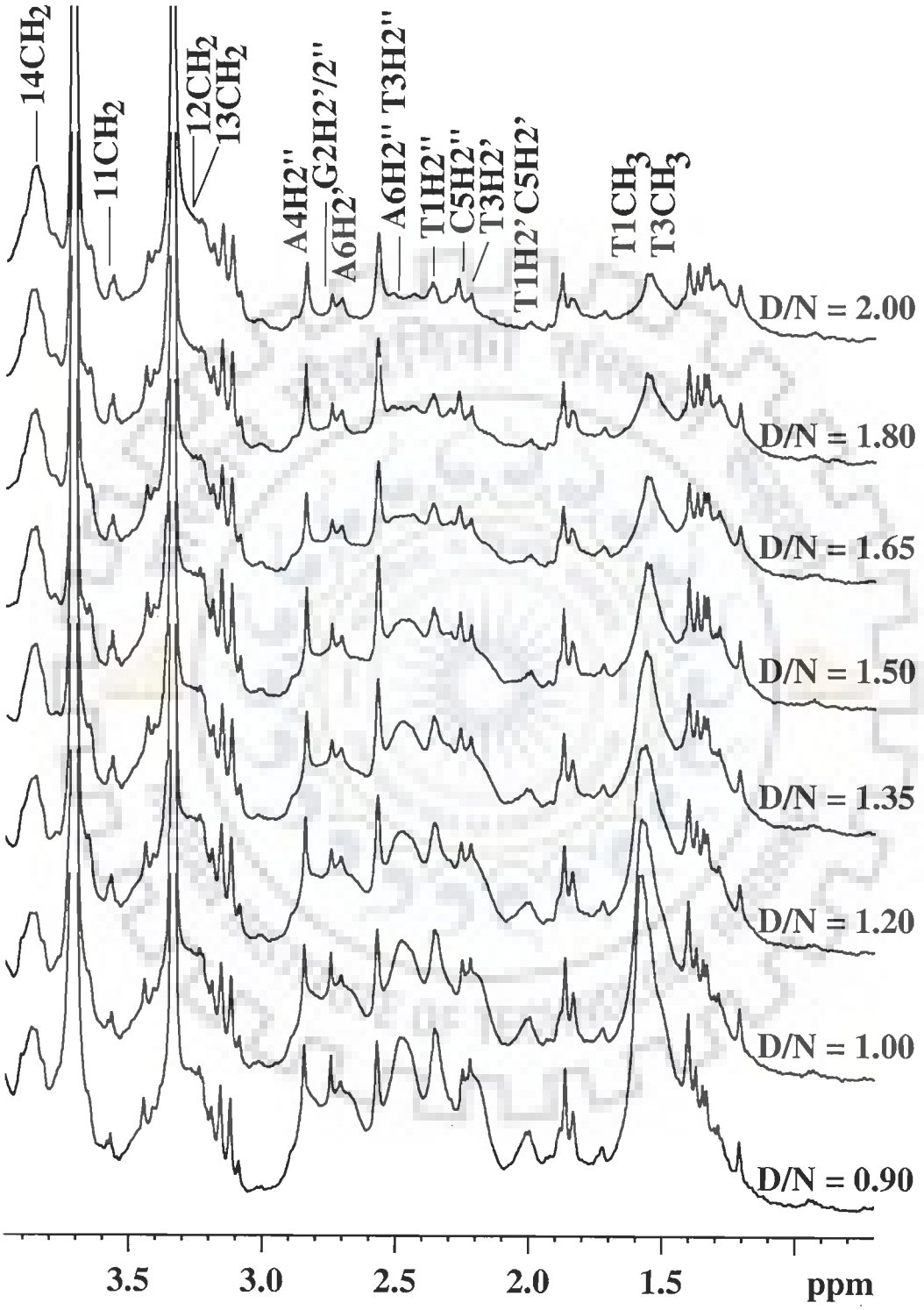
14CH2
11CH2
12CH2
13CH2
A4H2''
A6H2
G2H2'/2''
A6H2''
T3H2''
T1H2''
C5H2''
T3H2'
T1H2'
C5H2'
T1CH3
T3CH3
D/N = 2.00
D/N = 1.80
D/N = 1.65
D/N = 1.50
D/N = 1.35
D/N = 1.20
D/N = 1.00
D/N = 0.90
3.5
3.0
2.5
2.0
1.5
ppm

(Fig. 6.5b)

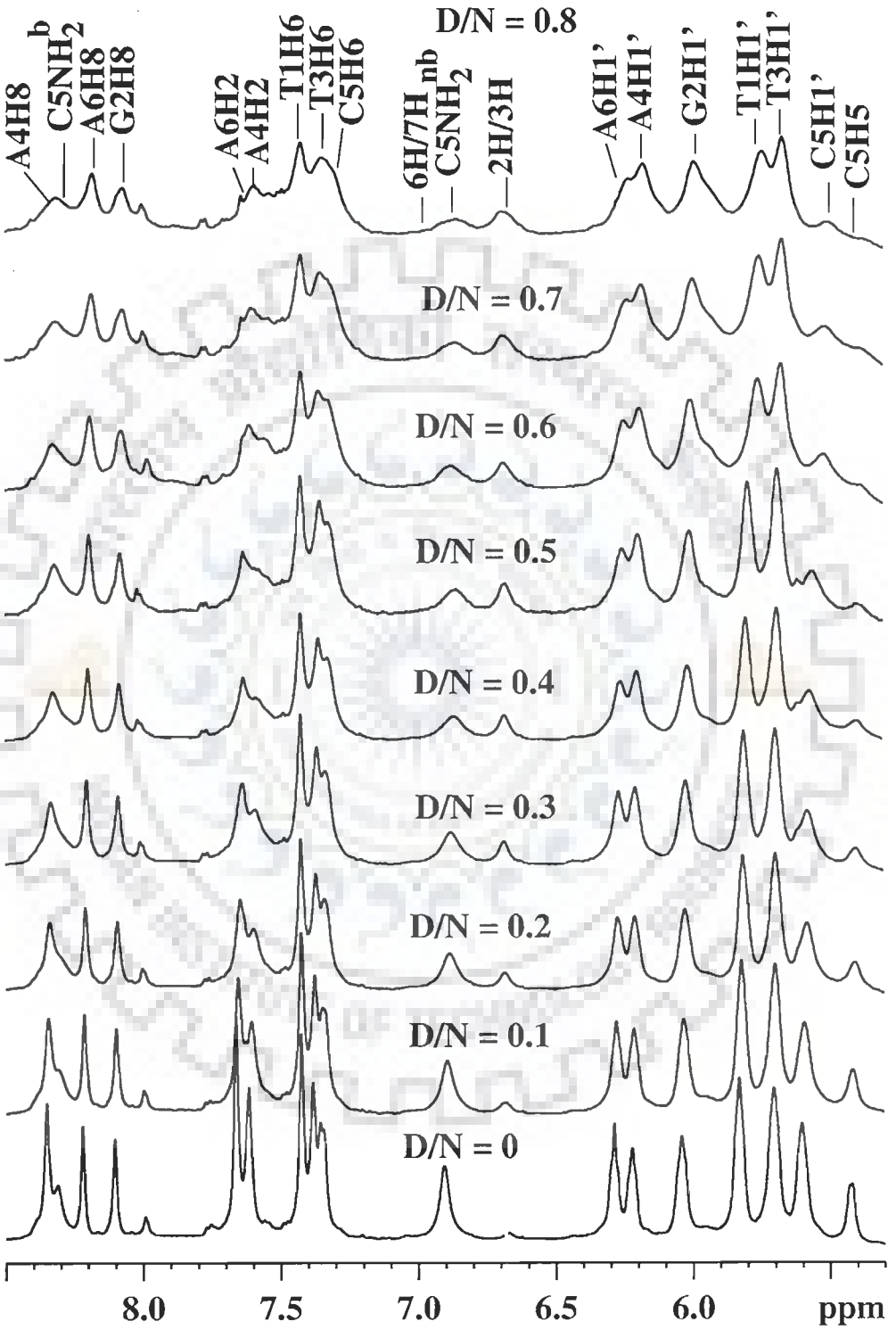
A4H8
C5NH2b
A6H8
G2H8
A6H2
A4H2
T1H6
T3H6
C5H6
6H/7Hnb
C5NH2
2H/3H
A6H1'
A4H1'
G2H1'
T1H1'
T3H1'
C5H1'
C5H5
D/N = 0.8
D/N = 0.7
D/N = 0.6
D/N = 0.5
D/N = 0.4
D/N = 0.3
D/N = 0.2
D/N = 0.1
D/N = 0
8.0
7.5
7.0
6.5
6.0
ppm

(Fig. 6.5c)

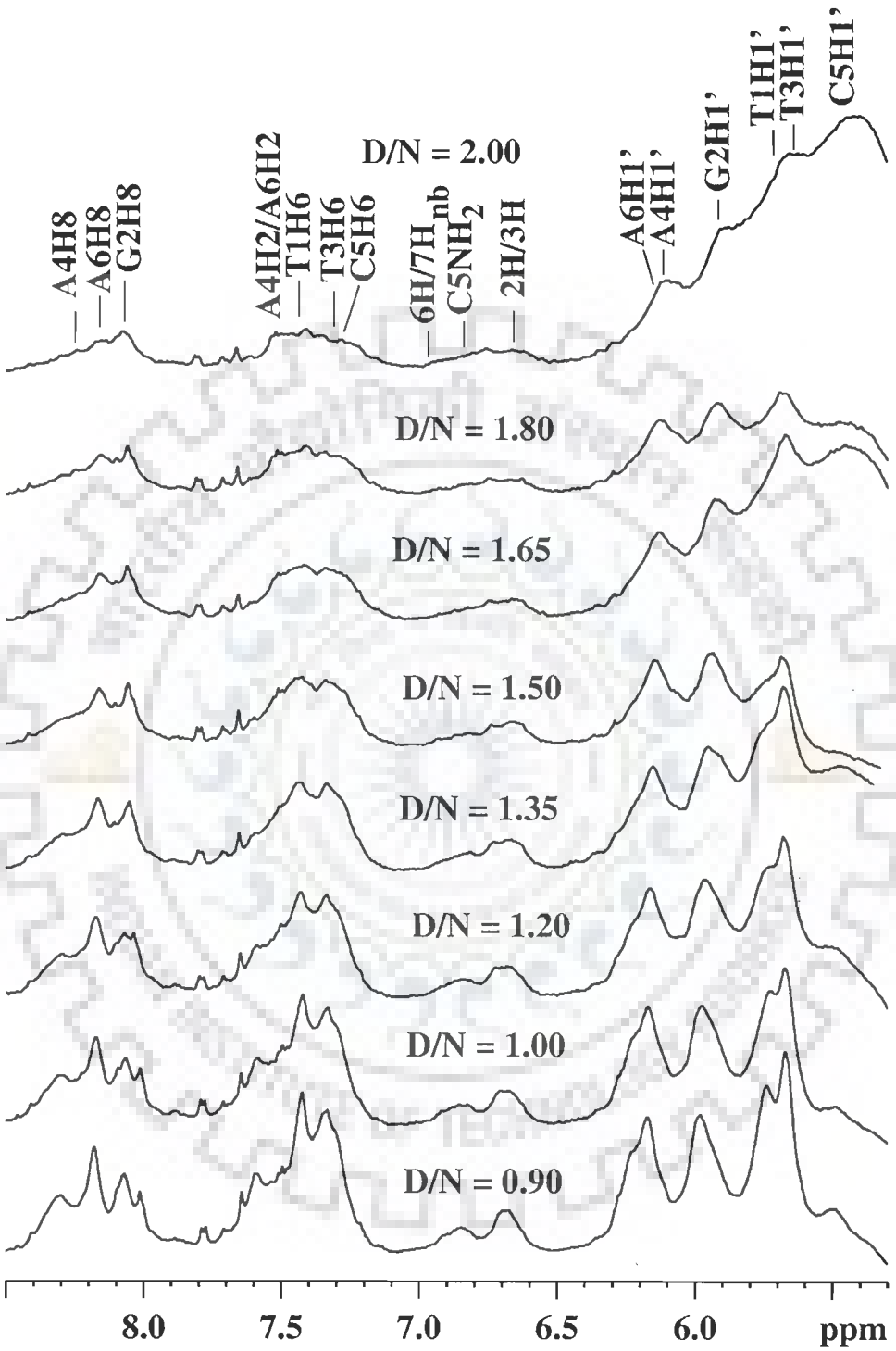
A4H8
A6H8
G2H8
A4H2/A6H2
T1H6
T3H6
C5H6
D/N = 2.00
6H/7H nb
C5NH2
2H/3H
A6H1'
A4H1'
G2H1'
T1H1'
T3H1'
C5H1'
D/N = 1.80
D/N = 1.65
D/N = 1.50
D/N = 1.35
D/N = 1.20
D/N = 1.00
D/N = 0.90
8.0
7.5
7.0
6.5
6.0
ppm

(Fig. 6.5d)

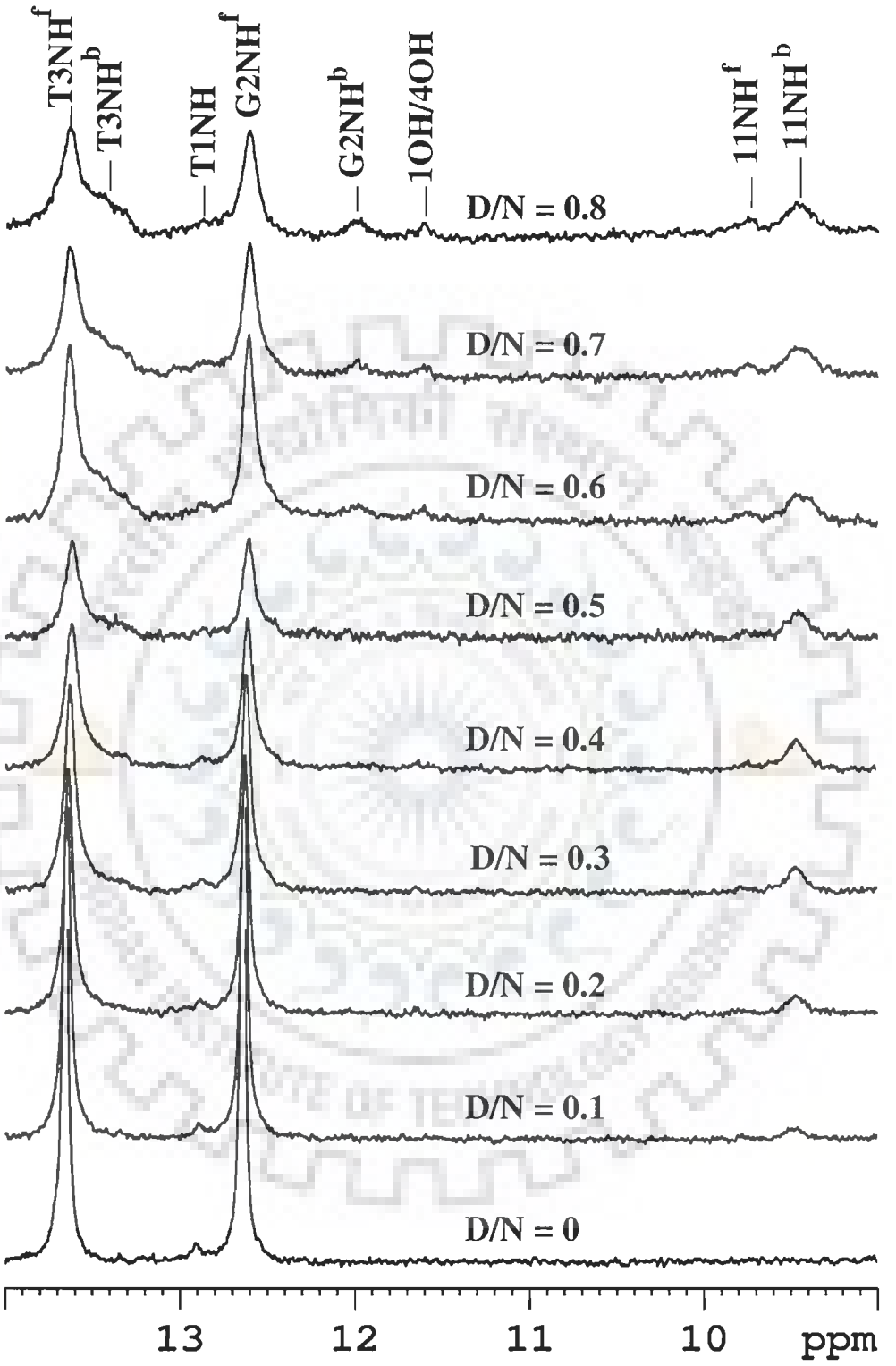
T3NH^f
T3NH^b
T1NH
G2NH^f
G2NH^b
1OH/4OH
11NH^f
11NH^b
D/N = 0.8
D/N = 0.7
D/N = 0.6
D/N = 0.5
D/N = 0.4
D/N = 0.3
D/N = 0.2
D/N = 0.1
D/N = 0
13
12
11
10
ppm

(Fig. 6.5e)

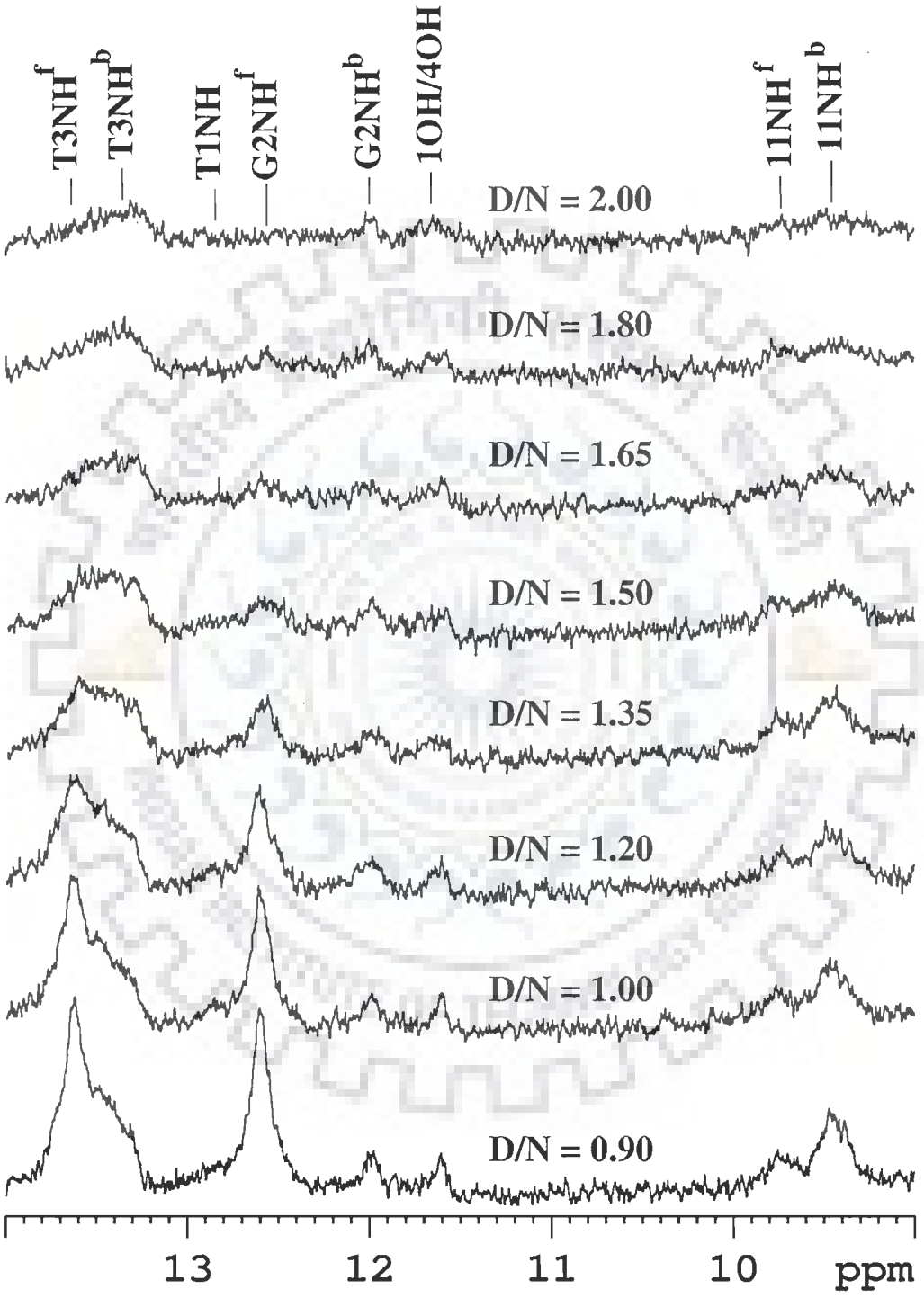
T3NH^f
T3NH^b
T1NH
G2NH^f
G2NH^b
1OH/4OH
11NH^f
11NH^b
D/N = 2.00
D/N = 1.80
D/N = 1.65
D/N = 1.50
D/N = 1.35
D/N = 1.20
D/N = 1.00
D/N = 0.90
13
12
11
10
ppm

(Fig. 6.5f)

Table 6.3: Chemical shift (ppm) of nucleic acid, d-(TGTACA)$_2$, protons in uncomplexed state (δ_f) and that bound to drug (δ_b) at drug (D) to nucleic acid duplex (N) ratio D/N=1.0 at 278 K. Also shown here is the change in chemical shift on binding, $\Delta\delta = \delta_{b(D/N=1.0)} - \delta_f$

Proton	T1			G2			T3			A4			C5			A6		
	δ_b	δ_f	$\Delta\delta$	δ_b	δ_f	$\Delta\delta$	δ_b	δ_f	$\Delta\delta$	δ_b	δ_f	$\Delta\delta$	δ_b	δ_f	$\Delta\delta$	δ_b	δ_f	$\Delta\delta$
H8/H6	7.42	7.42	0.00	8.07	8.10	-0.03	7.35	7.38	-0.03	8.30	8.35	-0.05	7.28	7.35	-0.07	8.17	8.22	-0.05
H1'	5.75	5.83	-0.08	5.98	6.04	-0.06	5.67	5.71	-0.04	6.17	6.22	-0.05	5.49	5.60	-0.11	6.22	6.29	-0.07
H2'	2.01	1.98	+0.03	2.76	2.83	-0.07	2.19	2.20	-0.01	2.75	2.86	-0.11	2.01	1.94	-0.07	2.66	2.69	-0.03
H2"	2.33	2.33	0.00	2.76	2.83	-0.07	2.49	2.50	-0.01	2.75	2.86	-0.11	2.20	2.25	-0.05	2.47	2.49	-0.02
H3'	4.72	4.71	+0.01	4.96	4.97	-0.01	4.91	4.94	-0.03	5.01	5.04	-0.03	4.76	4.77	-0.01	4.70	4.71	-0.01
H4'	4.08	4.09	-0.01	4.11	4.20	-0.09	4.24	4.26	-0.02	4.40	4.43	-0.03	4.08	4.09	-0.01	4.17	4.20	-0.03
H5/H2/CH_3	1.57	1.61	-0.04	-	-	-	1.45	1.54	-0.09	7.52	7.62	-0.10		5.43		7.60	7.62	-0.02
$NH_2{}^b$	-	-	-	7.87	8.00	-0.13	-	-	-	7.85	7.93	-0.08	8.31	8.31	0.00	6.71	6.68	+0.03
$NH_2{}^{nb}$	-	-	-	7.60	7.66	-0.06	-	-	-	6.28	6.41	-0.13	6.85	6.90	-0.05	-	-	-
#NH				12.00	12.60	-0.60	13.42	13.63	-0.21									

observed as separate bound and free species at D/N = 1.0
-ve $\Delta\delta$ indicates upfield shift
+ve $\Delta\delta$ indicates downfield shift

Table 6.4: Chemical shift (ppm), δ^b, of drug protons bound to nucleic acid duplex at drug (D) to nucleic acid (N) ratio D/N = 1.0; that in free state, δ^f (concentration 10 mM); and that in monomeric form, $\delta^{monomer}$ (concentration 10μM) at 275 K. Change in chemical shift, due to binding, that is, $\Delta\delta = \delta^b - \delta^f$ with respect to free drug as well as $\Delta\delta' = \delta^b - \delta^{monomer}$ with respect to the drug in monomeric state are also shown.

Protons	$\delta^b_{(D/N=1)}$	δ^f	$\Delta\delta = \delta^b_{(D/N=1)} - \delta^f$	$\delta^{monomer}$	$\Delta\delta' = \delta^b_{(D/N=1)} - \delta^{monomer}$
6H/7H	6.90	6.93	-0.03	7.39	-0.49
2H/3H	6.66	6.97	-0.31	7.13	-0.47
$11CH_2$	3.44	3.60	-0.16	3.75	-0.31
$12CH_2$	3.27	3.32	-0.05	3.29	-0.02
$13CH_2$	3.27	3.23	+0.04	3.15	+0.12
$14CH_2$	3.86	3.81	+0.05	3.75	+0.11
# 11NH	9.46	9.75	-0.29	10.24	-0.78

observed as separate bound and free species at D/N = 1.0
-ve Δδ indicates upfield shift on binding
+ve Δδ indicates downfield shift on binding

Table 6.5a: Chemical shift (ppm) of nucleotide, d-(TGTACA)$_2$, protons as a function of drug (D) to nucleic acid duplex (N) ratio, D/N, at 275 K. Also shown here is the change in chemical shift on binding, $\Delta\delta = \delta_{(D/N = 2.0)} - \delta_{(D/N = 0)}$

D/N Ratio	T1H1'	G2H1'	T3H1'	A4H1'	C5H1'	A6H1'	T1H6	G2H8	T3H6	A4H8
0.00	5.83	6.04	5.71	6.22	5.60	6.29	7.42	8.10	7.38	8.35
0.10	5.82	6.03	5.70	6.21	5.59	6.28	7.42	8.10	7.38	8.35
0.20	5.82	6.03	5.70	6.21	5.58	6.27	7.42	8.09	7.37	8.34
0.30	5.81	6.02	5.70	6.21	5.58	6.27	7.42	8.09	7.37	8.33
0.40	5.80	6.01	5.69	6.20	5.57	6.26	7.42	8.09	7.36	8.33
0.50	5.79	6.0	5.69	6.19	5.56	6.25	7.42	8.08	7.36	8.32
0.60	5.76	6.0	5.69	6.19	5.52	6.25	7.42	8.08	7.36	8.32
0.70	5.76	6.0	5.67	6.18	5.51	6.24	7.42	8.07	7.35	8.32
0.80	5.75	5.99	5.67	6.18	5.50	6.23	7.42	8.07	7.35	8.32
0.90	5.75	5.98	5.67	6.17	5.50	6.23	7.42	8.07	7.35	8.30
1.00	5.75	5.98	5.67	6.17	5.49	6.22	7.42	8.07	7.35	8.30
1.20	5.75	5.97	5.67	6.10	5.48	6.22	7.43	8.07	7.34	8.30
1.35	5.75	5.95	5.67	6.15	5.48	6.22	7.43	8.06	7.34	8.30
1.50	5.75	5.94	5.67	6.14	5.47	6.22	7.43	8.06	7.34	8.30
1.65	5.75	5.92	5.67	6.13	5.47	6.22	7.43	8.06	7.34	8.30
1.80	5.75	5.91	5.67	6.13	5.47	6.22	7.43	8.06	7.34	8.30
2.00	5.75	5.91	5.67	6.12	5.47	6.22	7.43	8.06	7.34	8.30
$\Delta\delta$	-0.08	-0.13	-0.04	-0.10	-0.13	-0.07	+0.01	-0.04	-0.04	-0.05

D/N Ratio	C5H6	A6H8	G2NH^f	G2NH^b	T3NH^f	T3CH$_3$	T1CH$_3$	A4H2	A6H2
0.00	7.35	8.22	12.64	-	13.65	1.54	1.61	7.62	7.67
0.10	7.35	8.21	12.64	-	13.64	1.53	1.60	7.61	7.66
0.20	7.34	8.21	12.63	-	13.64	1.52	1.60	7.60	7.65
0.30	7.34	8.20	12.63	-	13.63	1.52	1.60	7.59	7.64
0.40	7.33	8.20	12.62	-	13.63	1.51	1.59	7.58	7.64
0.50	7.32	8.20	12.61	-	13.63	1.51	1.59	7.57	7.63
0.60	7.32	8.19	12.61	12.00	13.63	1.51	1.59	7.55	7.61
0.70	7.31	8.19	12.61	12.00	13.63	1.49	1.59	7.54	7.61
0.80	7.30	8.18	12.61	12.00	13.63	1.48	1.58	7.54	7.60
0.90	7.30	8.17	12.60	12.00	13.63	1.47	1.58	7.54	7.60
1.00	7.28	8.17	12.60	12.00	13.63	1.45	1.57	7.52	7.60
1.20	7.28	8.17	12.60	11.99	13.63	1.44	1.57	7.52	7.60
1.35	7.28	8.16	12.60	11.99	13.63	1.44	1.56	7.52	7.60
1.50	7.27	8.16	12.60	11.99	13.63	1.44	1.56	7.52	7.60
1.65	7.27	8.16	12.60	11.99	13.63	1.44	1.56	7.52	7.60
1.80	7.27	8.15	12.60	11.99	13.63	1.44	1.56	7.52	7.60
2.00	7.27	8.15	12.60	11.99	13.63	1.44	1.56	7.52	7.60
$\Delta\delta$	-0.08	-0.07	-0.04	-0.01	-0.02	-0.10	-0.05	-0.10	-0.07

-ve $\Delta\delta$ indicates upfield shift
+ve $\Delta\delta$ indicates downfield shift.

Table 6.5b: Chemical shift (ppm) of drug (mitoxantrone) protons as a function of drug (D) to nucleic acid duplex (N) ratio, D / N, at 275 K. Also shown here is the maximum change in chemical shift due to binding, with respect to drug in free self associated form, δ^{free},(10 mM, 275 K) as well as the drug in monomeric form, $\delta^{monomer}$. $\Delta\delta = (\delta_{D/N=2.0} - \delta^{monomer})$; $\Delta\delta' = (\delta_{D/N=2.0} - \delta^{free})$

D/N Ratio	2H/3H	6H/7H	$11NH^f$	$11NH^b$	$11CH_2$	$12CH_2$	$13CH_2$	$14CH_2$	1OH/4OH
$\delta^{monomer}$	7.13	7.39	10.24	-	3.75	3.29	3.15	3.75	-
δ^{free}	6.97	6.93	9.71	-	3.60	3.32	3.23	3.81	13.19
0.10	6.69	6.93	9.75	9.47	3.48	3.29	3.29	3.88	11.64
0.20	6.69	6.93	9.75	9.47	3.48	3.29	3.29	3.88	11.64
0.30	6.68	6.93	9.75	9.47	3.47	3.28	3.28	3.87	11.63
0.40	6.68	6.92	9.75	9.46	3.47	3.28	3.28	3.87	11.63
0.50	6.68	6.92	9.75	9.46	3.47	3.28	3.28	3.87	11.63
0.60	6.67	6.92	9.75	9.46	3.46	3.28	3.28	3.86	11.62
0.70	6.67	6.91	9.75	9.46	3.46	3.27	3.27	3.86	11.62
0.80	6.67	6.91	9.75	9.46	3.45	3.27	3.27	3.86	11.62
0.90	6.66	6.90	9.75	9.46	3.45	3.27	3.27	3.86	11.62
1.00	6.66	6.90	9.75	9.46	3.44	3.27	3.27	3.86	11.62
1.20	6.66	6.90	9.75	9.46	3.44	3.26	3.26	3.86	11.62
1.35	6.65	6.90	9.75	9.46	3.44	3.26	3.26	3.86	11.62
1.50	6.65	6.90	9.75	9.46	3.44	3.25	3.25	3.86	11.62
1.65	6.65	6.90	9.75	9.46	3.44	3.25	3.25	3.86	11.62
1.80	6.65	6.90	9.75	9.46	3.44	3.25	3.25	3.86	11.62
2.00	6.65	6.90	9.75	9.46	3.44	3.25	3.25	3.86	11.62
$\Delta\delta$	-0.48	-0.49	-0.49	-	-0.31	-0.04	+0.10	+0.11	-
$\Delta\delta'$	-0.32	-0.03	+0.04	-	-0.16	-0.07	+0.02	+0.05	-1.57

-ve $\Delta\delta$ indicates upfield shift
+ve $\Delta\delta$ indicates downfield shift.

Table 6.6a: Chemical shift (ppm) of nucleotide, d-(TGTACA)$_2$, protons as a function of drug (D) to nucleic acid duplex (N) ratio, D/N, at 298 K. Also shown here is the change in chemical shift on binding, $\Delta\delta = \delta_{D/N=2.0} - \delta_{D/N=0.0}$

D/N Ratio	T1H1'	G2H1'	T3H1'	A4H1'	C5H1'	A6H1'	T1H6	G2H8
0.00	5.94	6.05	5.79	6.24	5.79	6.31	7.4	8.08
0.10	5.94	6.04	5.79	6.23	5.79	6.31	7.4	8.07
0.20	5.93	6.03	5.78	6.22	5.78	6.30	7.4	8.07
0.30	5.93	6.03	5.77	6.22	5.77	6.30	7.4	8.06
0.40	5.93	6.02	5.77	6.21	5.77	6.29	7.4	8.06
0.50	5.92	6.01	5.77	6.21	5.77	6.28	7.4	8.05
0.60	5.91	6.01	5.75	6.20	5.75	6.27	7.41	8.05
0.70	5.93	6.00	5.75	6.19	5.75	6.27	7.41	8.04
0.80	5.91	5.99	5.74	6.19	5.74	6.26	7.41	8.04
0.90	5.93	5.98	5.74	6.18	5.74	6.26	7.41	8.03
1.00	5.90	5.97	5.73	6.17	5.73	6.24	7.41	8.03
1.20	5.90	5.96	5.73	6.16	5.73	6.24	7.41	8.02
1.35	5.89	5.95	5.73	6.15	5.73	6.24	7.41	8.00
1.50	5.89	5.93	5.73	6.14	5.73	6.22	7.42	8.00
1.65	5.87	5.92	5.72	6.13	5.72	6.22	7.42	8.00
1.80	5.87	5.92	5.71	6.13	5.71	6.19	7.43	8.00
2.00	5.87	5.90	5.71	6.11	5.71	6.18	7.43	7.98
$\Delta\delta$	-0.07	-0.15	-0.08	-0.13	-0.08	-0.13	+0.03	-0.10

D/N Ratio	T3H6	A4H8	C5H6	A6H8	T3CH3	T1CH3	A4H2	A6H2	C5H5
0.00	7.35	8.33	7.35	8.23	1.58	1.64	7.74	7.77	5.50
0.10	7.35	8.32	7.35	8.23	1.57	1.64	7.72	7.75	5.49
0.20	7.34	8.32	7.34	8.22	1.56	1.64	7.70	7.73	5.47
0.30	7.34	8.31	7.34	8.22	1.55	1.64	7.69	7.72	5.46
0.40	7.33	8.30	7.33	8.21	1.54	1.63	7.67	7.71	5.45
0.50	7.33	8.30	7.33	8.21	1.54	1.63	7.66	7.69	5.43
0.60	7.32	8.29	7.32	8.20	1.52	1.63	7.63	7.66	5.41
0.70	7.32	8.29	7.32	8.20	1.52	1.63	7.63	7.63	5.41
0.80	7.32	8.28	7.32	8.19	1.50	1.62	7.63	7.60	5.38
0.90	7.31	8.28	7.31	8.19	1.48	1.62	7.63	7.58	5.38
1.00	7.31	8.27	7.31	8.18	1.47	1.61	7.63	7.56	5.33
1.20	7.30	8.26	7.30	8.18	1.45	1.61	7.63	7.55	5.33
1.35	7.29	8.26	7.29	8.18	1.41	1.61	7.63	7.54	5.31
1.50	7.28	8.25	7.28	8.16	1.41	1.61	7.63	7.54	5.25
1.65	7.27	8.24	7.27	8.16	1.41	1.61	7.63	7.54	5.25
1.80	7.27	8.23	7.27	8.14	1.41	1.59	7.63	7.54	5.25
2.00	7.26	8.23	7.26	8.14	1.41	1.59	7.63	7.54	5.25
$\Delta\delta$	-0.09	-0.10	-0.09	-0.09	-0.17	-0.05	-0.11	-0.23	-0.25

-ve $\Delta\delta$ indicates upfield shift
+ve $\Delta\delta$ indicates downfield shift.

Table 6.6b: Chemical shift (ppm) of drug (mitoxantrone) protons as a function of drug (D) to nucleic acid duplex (N) ratio, D / N, at 298 K. Also shown here is the maximum change in chemical shift due to binding, with respect to drug in free self associated form, δ^{free},(10 mM, 298 K)

D/N Ratio	2H/3H	6H/7H	11NH[I]	$11CH_2$	$12CH_2$	$13CH_2$	$14CH_2$
δ^{free}	6.83	6.95	9.79	3.69	3.39	3.33	3.93
0.10	6.75	6.87	9.60	3.57	3.38	3.32	3.94
0.20	6.74	6.87	9.59	3.56	3.38	3.32	3.94
0.30	6.72	6.87	9.58	3.55	3.38	3.32	3.93
0.40	6.70	6.87	9.57	3.55	3.38	3.32	3.93
0.50	6.69	6.87	9.57	3.53	3.38	3.32	3.92
0.60	6.67	6.87	9.56	3.53	3.38	3.32	3.92
0.70	6.66	6.87	9.57	3.52	3.38	3.33	3.92
0.80	6.64	6.87	9.55	3.52	3.37	3.33	3.92
0.90	6.64	6.87	9.57	3.52	3.37	3.33	3.91
1.00	6.63	6.87	9.54	3.51	3.37	3.33	3.90
1.20	6.63	6.86	9.54	3.51	3.37	3.33	3.90
1.35	6.62	6.85	9.55	3.51	3.36	3.33	3.90
1.50	6.62	6.84	9.53	3.51	3.36	3.33	3.90
1.65	6.62	6.84	9.53	3.51	3.34	3.33	3.90
1.80	6.62	6.84	9.52	3.49	3.34	3.33	3.89
2.00	6.60	6.83	9.52	3.49	3.34	3.33	3.89
$\Delta\delta = (\delta_{D/N=2.0} - \delta^{free})$	-0.23	-0.12	-0.27	-0.20	-0.05	0.00	-0.04

-ve $\Delta\delta$ indicates upfield shift
+ve $\Delta\delta$ indicates downfield shift.

be that due to monomer ($\delta^{monomer}$) (Manpreet, 2006), as the drug is self–associated at higher concentrations δ^{f}.

The resonances of uncomplexed d–$(TGTACA)_2$ are well resolved. On addition of drug to DNA, new resonance peaks pertaining to drug protons start appearing, which increase in intensity as D / N ratio increases. Sharp resonance peaks are observed up to D / N ~ 0.8. The spectral lines start broadening uniformly at higher ratios indicative of binding of DNA to drug. In uncomplexed d–$(TGTACA)_2$, imino protons T3NH and G2NH appear at 13.65 and 12.64 ppm, respectively. The T1NH resonance observed at

12.91 ppm is almost broadened even at 275 K (Fig. 6.5e and 6.5f), as compared to T3NH and G2NH. This may be attributed to increased fraying at the end of DNA, which leads to a significant exchange of T1NH proton with that of water solvent. On successive addition of mitoxantrone to DNA, additional resonance peaks are observed in this region at 13.42, 12.00, 11.62 ppm at D / N = 1.0 besides the 11 NH peaks at about 9.46 and 9.75 ppm. Since T3NH and G2NH appear at 13.65 and 12.64 ppm in uncomplexed d–$(TGTACA)_2$, accordingly the resonances at 13.63 and 12.60 are designated as $T3NH^f$ and $G2NH^f$, in the d–$(TGTACA)_2$ complexed to mitoxantrone at D / N = 1.0. The 2D NOESY spectra (Fig. 6.8f) showed that pair of protons resonating at 12.60 and 12.00 show cross peaks with each other due to exchange phenomenon expected between free and DNA bound to drug in the solution. Subsequently the 12.60 and 12.00 resonances get assigned as $G2NH^f$ and $G2NH^b$ respectively. The broad resonance at ~13.42 ppm is assigned as $T3NH^b$ based on the exchange correlation observed with $G2NH^b$ (Fig 6.8f).

It is observed that the sharp $T1CH_3$ and $T3CH_3$ peak appearing at 1.61 and 1.54 ppm in the uncomplexed d–$(TGTACA)_2$ show considerable line broadening with increasing D / N, but does not give rise to new upfield signal due to binding as in the case of mitoxantrone binding with d–$(CGTACG)_2$.

The 11NH resonance of the drug appearing at 9.46 ppm increases in intensity with D / N ratio. However in addition, another peak starts appearing at 9.75 ppm (Fig. 6.5e and 5f). These two resonances show chemical exchange cross peak in 2D NOESY spectra (Fig. 6.8f) and both the resonances shows NOE cross peak with $11CH_2$ protons (Fig. 6.8d). Since most of the drug is in bound state in complex having lowest D / N ratio, the resonance peak at 9.46 ppm is assigned to 11NH proton in the bound species, designated

as 11NH^b, while that at 9.75 ppm is the corresponding proton in free state, that is 11NH^f As D / N increases more and more drug exist in free state and the intensity of 9.75 ppm peak increases. This is further corroborated by the fact that the resonance at 9.46 ppm (11NH^b) shows intermolecular NOE crosspeaks with specific nucleic acid protons i.e., A6H4', T1H4', T1CH$_3$, A6H8, T1H6, C5H6 A6H1' and T1H1' (Table 6.9, Fig. 6.8d and 6.8e) whereas the 11NH^f resonance at 9.75 ppm does not give any such intermolecular connectivity.

The existence of two sets of G2NH, T3NH and 11NH (drug) clearly demonstrates that the drug indeed binds to the DNA hexamer and there is exchange of free and bound DNA on NMR time scale at 275 K. Mitoxantrone is shown to have faster dissociation rates for Poly dA–dT than for Poly dG–dC (Krishnamoorthy et al, 1986). Hence the exchange phenomenon between the drug and d-(TGTACA)$_2$ is expected to be faster than that observed with d-(CGTACG)$_2$. Also on binding of mitoxantrone to d–(TGATCA)$_2$, only considerable line broadening is observed with no additional cross peaks due to exchange between the bound and free resonances. It is expected that bound DNA are in fast exchange with the corresponding signals from free DNA to be followed individually at 278 K on NMR time scale.

The change in chemical shift ($\Delta\delta$) of base and H1' protons with D / N ratio are shown in Fig. 6.6 and Table 6.5a (275 K) and Table 6.6a (298 K). The $\Delta\delta$ increases with D / N ratio as more and more DNA oligomer binds to the drug a maximum of 0.13 ppm upfield shift is observed for G2H1' and C5H1' protons at 275 K. The shifts in the base and H1' protons are gradual and small in magnitude. The bound imino protons G2NH^b and T3NH^b are upfield shifted with respect to the corresponding imino protons in free

state (Table 6.3); the shift being 0.60 and 0.21 ppm for G2NH and T3NH, respectively. Such changes may be attributed to stacking or structural changes in complexation, which may be compensatory in nature.

The shift in drug protons on binding is expected to be maximum at low D / N ratio when maximum amount of drug is present in the bound state no significant variation of δ was observed with increasing D / N ratio (Fig. 6.7). The ring protons, 6H / 7H and 2H / 3H, shift upfield substantially by 0.49 and 0.47 ppm with respect to the chemical shift position of drug monomer (i.e., that at 10 μM or lower concentration) in 1:1 drug-DNA complex at 275 K (Table 6.4). The 11NH and $11CH_2$ proton shifts upfield by 0.78 and 0.31 ppm. The shift in the $12CH_2$, $13CH_2$ and $14CH_2$ protons is not significant, it being up to < 0.15 ppm at 275 K. Large upfield shifts in 11NH, 6H/7H and 2H/3H protons on binding demonstrate that aromatic chromophore of mitoxantrone is well stacked with base pairs of DNA and is involved in the interaction. Some of the drug is in free state at D / N = 1, the concentration of which is likely to be in mM range and hence expected to be in self–associated form. Difference in chemical shift, $\Delta\delta = \delta^b - \delta^f$, is 0.29 ppm (upfield) for free and bound species of 11NH proton (Table 6.4). It is noteworthy that 1OH/4OH proton which exchanges with water, appears at 11.62 ppm in the spectra of drug–DNA complex at 275 K. Apparently 1OH/4OH is expected to participate in binding and gets immobilized. The shift observed in resonances of DNA protons is not significant. In fact the change in chemical shift is not a sufficient indicator of the interaction; instead the observed intermolecular short contacts are a direct proof of the structure of a specific drug–DNA complex. Also, the presence of sequential

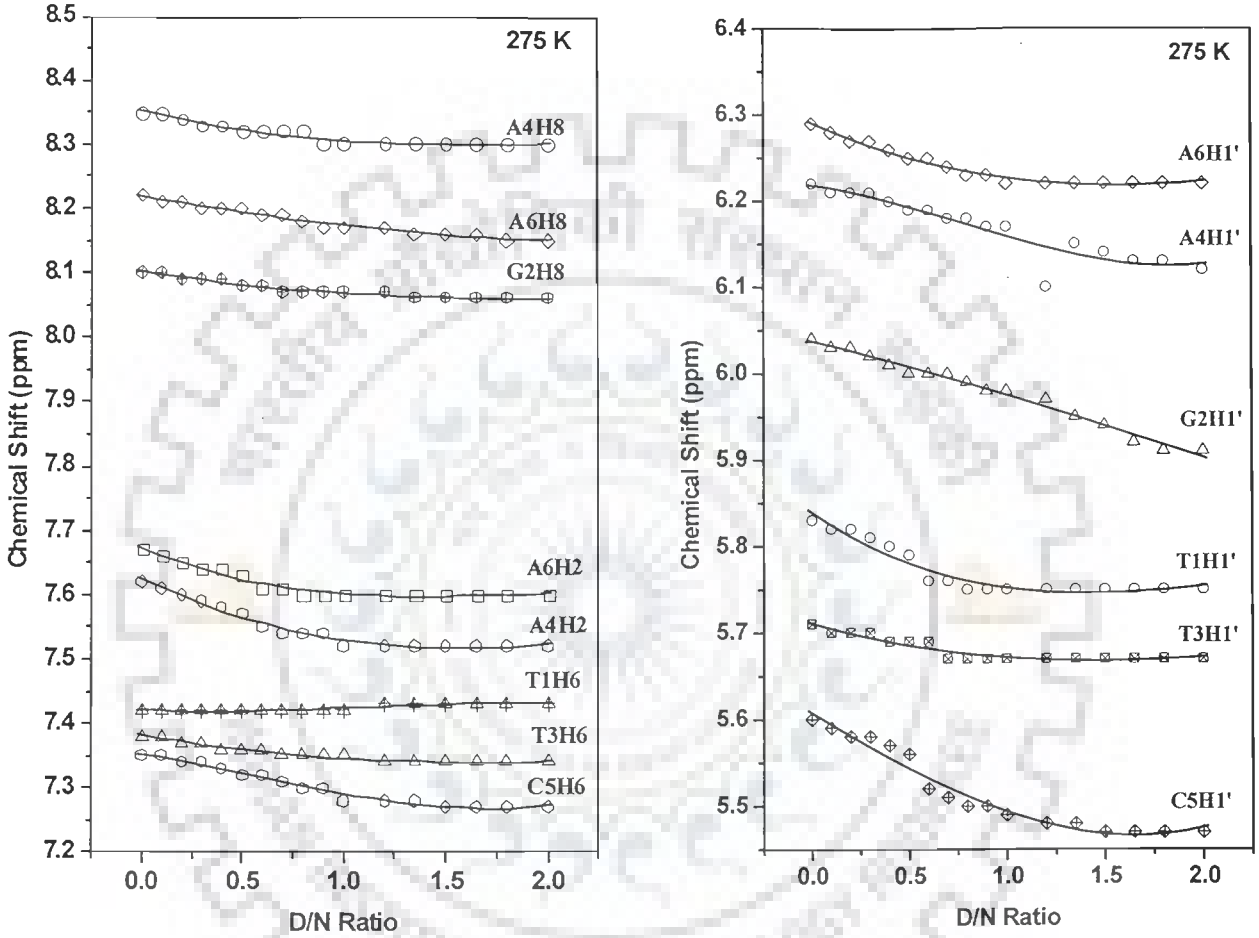

Figure 6.6: Chemical shift of base and H1' protons of d-(TGTACA)$_2$ complexed with mitoxantrone as a function of drug to DNA (D/N) ratio, 275 K

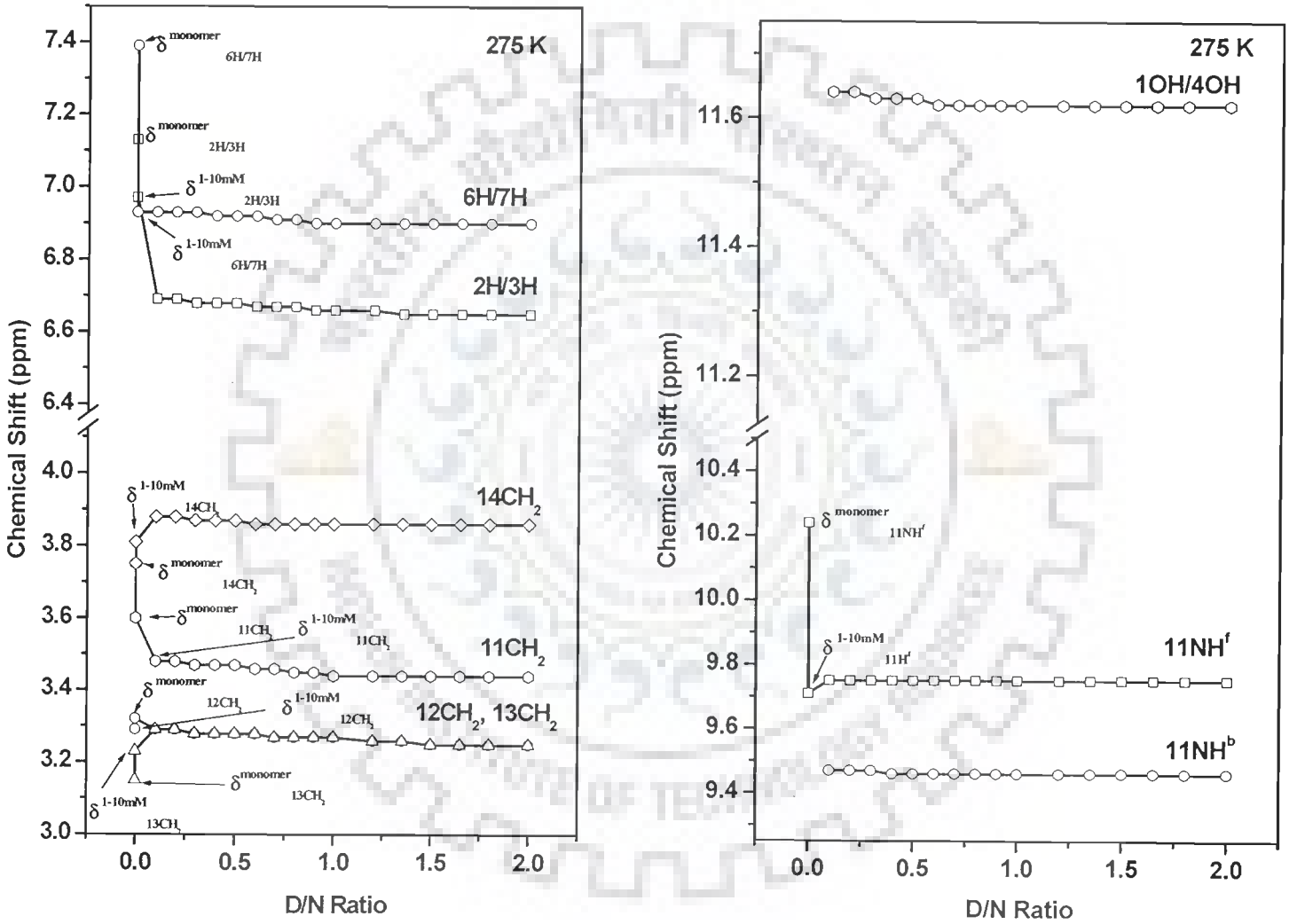

Figure 6.7: ^{1}H Chemical shift of mitoxantrone protons complexed with d-(TGATCA)$_2$ at various D/N ratio, 278 K

connectivity between base to H2'/H2" (discussed further) proves the external mode of binding of the drug to DNA.

6.1.2.2 Structure of the Complex

The 2D NOESY spectra of drug–DNA complex at stoichiometric D / N ratio of 1.0 (Fig. 6.8 a-f) have been investigated extensively at mixing time (τ_m) of 100, 200 and 300 ms at 275 K. The intensities of cross peak have been estimated qualitatively as very strong (ss), strong (s), medium (ws), weak (w), very weakly (ww) intense cross peaks for distances in the range ss 1.8 – 2.5 Å, s 2.5 – 3.0 Å, ws 3.0 – 3.5 Å, w 3.5 – 4.0 Å, ww 4.0 – 5.0 Å, respectively from the spectra recorded at τ_m = 200 ms. The observed NOE for (a) sequential connectivities, (b) intranucleotide connectivities within sugar (c) intranucleotide base to sugar connectivities, and (d) connectivities involving amino and imino protons of base pairs are given in Table 6.7 a-d. The connectivities within the drug molecules are given in Table 6.8. The intermolecular connectivities of drug protons to nucleic acid protons in the complex are given in Table 6.9, respectively. The sequential base (H6/H8)n to (H1')n-1, (H2')n-1, (H2")n-1, (H3')n-1 and base (H6/H8)n-1 connectivities are observed at all base pair steps (Table 6.7a).

The observation of NOE between the imino proton G2NH and the amino proton of the hydrogen bonded partner namely $C5NH_2^b$ in NOESY spectra (Fig. 6.8e), establish Watson–Crick base pairing in G2.C5 base pairs in the duplex. Similarly the observation of a strong NOE between imino proton of thymine, T3NH and A3H2 of adenine residues establish Watson and Crick pairing in T3.A4 base pairs. The sequential connectivity observed between $G2NH^b$ and $T3NH^b$, confirm that the duplex is intact on binding at the T3.A4 base pairs (Fig. 6.8f). All sequential connectivities among adjacent base pairs,

expected for a typical B–DNA structure, are observed (Table 6.7a). This clearly demonstrates that DNA duplex is intact, apparently with no opening of base pairs to accommodate drug chromophore as expected on binding of typical intercalator to DNA molecule. The base sequence d–$(TGTACA)_2$ being self–complementary is responsible for a high symmetry in the NMR spectra, which remains unbroken in the presence of drug. Table 6.8 shows some of the intramolecular NOE connectivities observed within the drug molecule in the drug–DNA complex having D/N = 1.0. It is observed that $11NH^b$ is close to $11CH_2$, $12CH_2/13CH_2$ and 6H/7H protons in the complex. The ring protons 6H / 7H are very close to $11CH_2$ as expected. However, the inter–molecular peaks expected for mitoxantrone dimer i.e., 2H / 3H with $11CH_2$, $12CH_2$, $13CH_2$, $14CH_2$, 6H / 7H protons are missing (Davies et al, 2001b). The drug molecule, though present in millimolar concentration, does not exist as a dimer and is bound as monomer molecule to the DNA.

Table 6.9 gives a list of short intermolecular contacts observed between mitoxantrone and DNA hexamer (Fig.6.8a-e). Since $12CH_2$ and $13CH_2$ overlaps with each other, their proximity to DNA protons cannot be ascertained unambiguously. Intermolecular cross peaks are observed mainly between drug and the terminal T1.A6 base pair of DNA i.e., $11NH^b$–$T1CH_3$, $11NH^b$–T1H6, $11NH^b$–A6H2 , $11NH^b$ –A6H8, $11NH^b$–T1H1', $11NH^b$ – A6H1', 2H/3H – A6H8, 2H/3H –T1H1', 2H/3H –T1H4', $12/13CH_2$–$T1CH_3$, $12/13CH_2$–A6H8, $12/13CH_2$– T1H1' (Table 6.9) which proves that the drug is present at the terminal base pairs of DNA duplex. Also d-$(TGTACA)_2$ does not open to accommodate aromatic chromophore of the mitoxantrone between base pairs, as evidenced by presence of all sequential inter proton connectivities in the two dimensional nuclear overhauser enhancement spectra (Table 6.7a and Fig. 6.8a).

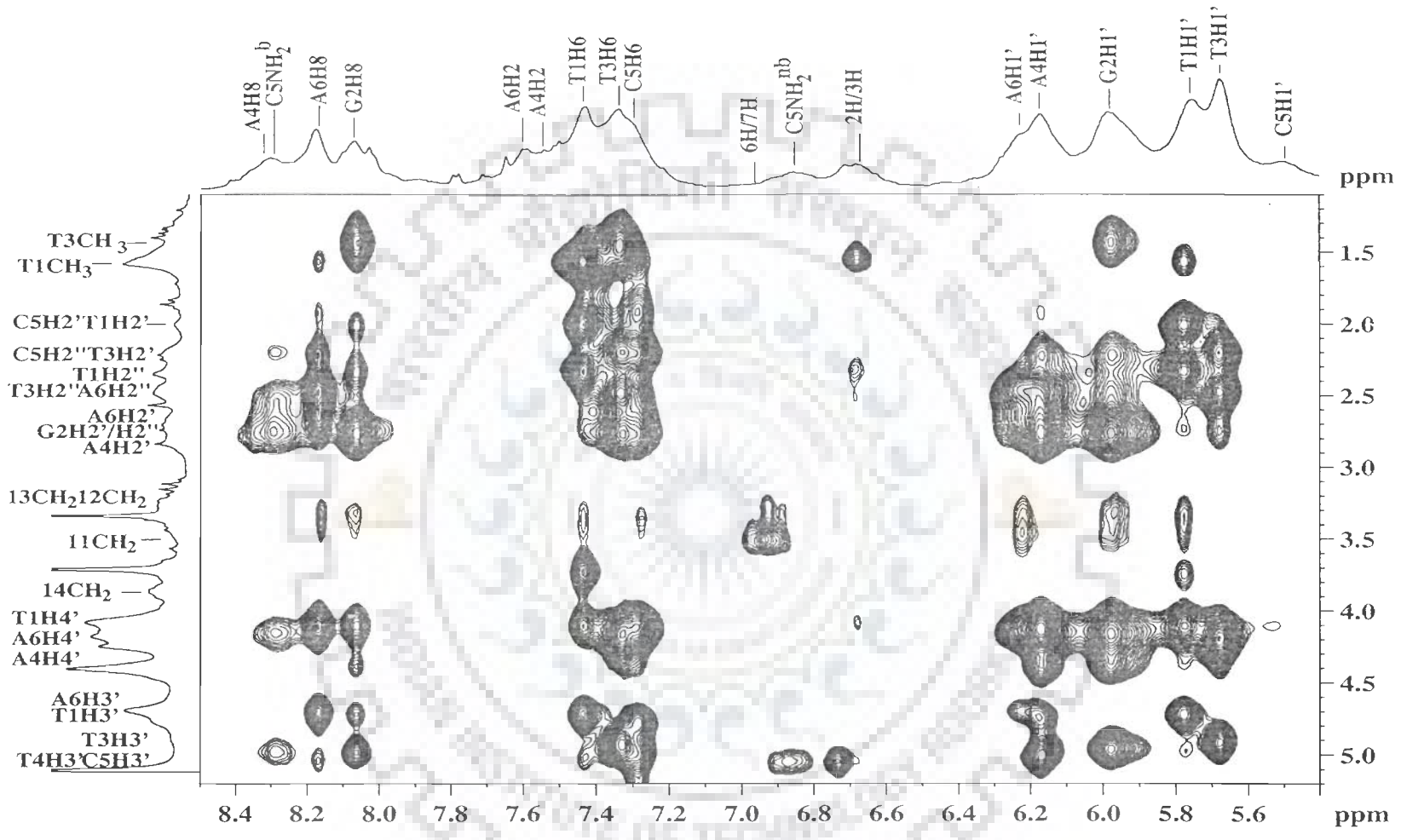

(Fig. 6.8a)

Figure 6.8(a-f): Expansions of various regions of 2D NOESY spectrum of mitoxantrone-d-$(CGTACG)_2$ complex in H_2O at 275 K

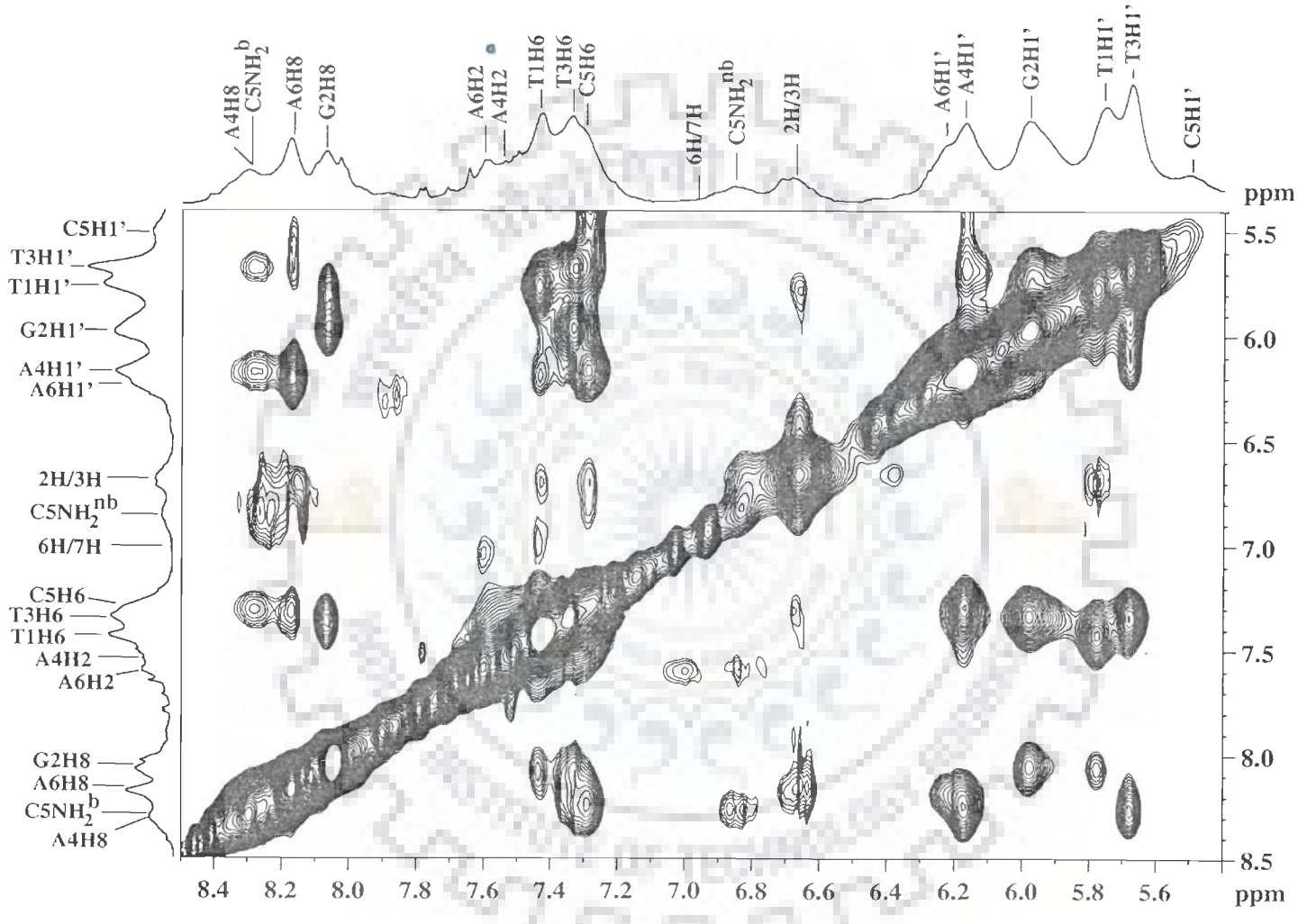
A4H8
C5NH2b
A6H8
G2H8
A6H2
A4H2
T1H6
T3H6
C5H6
6H/7H
C5NH2nb
2H/3H
A6H1'
A4H1'
G2H1'
T1H1'
T3H1'
C5H1'
ppm
8.4
8.2
8.0
7.8
7.6
7.4
7.2
7.0
6.8
6.6
6.4
6.2
6.0
5.8
5.6
5.5
6.0
6.5
7.0
7.5
8.0
8.5

(Fig. 6.8b)

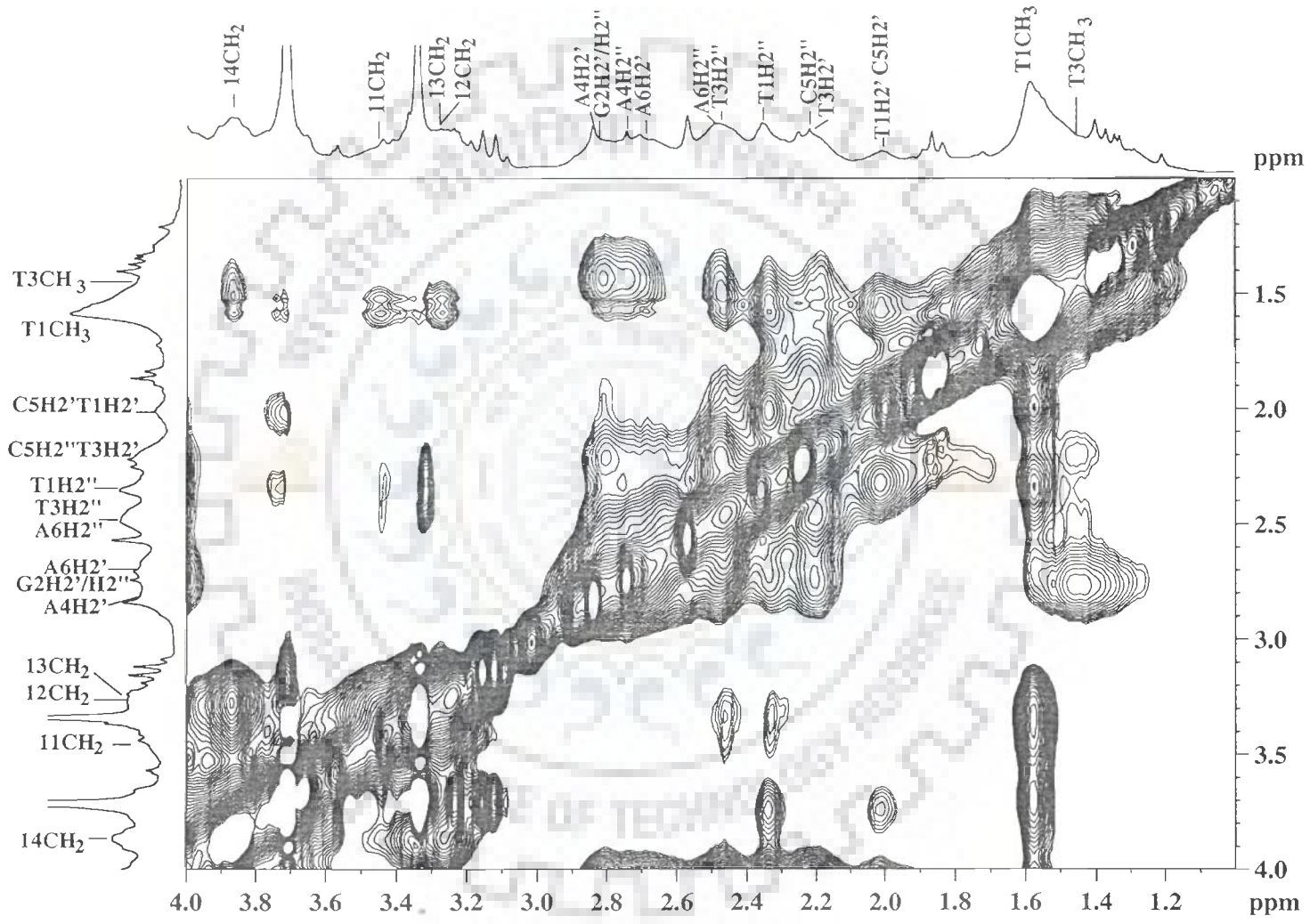
14CH2
11CH2
13CH2
12CH2
A4H2'
G2H2'/H2''
A4H2''
A6H2'
A6H2''
T3H2''
T1H2''
C5H2''
T3H2'
T1H2' C5H2'
T1CH3
T3CH3
ppm
T3CH3
T1CH3
C5H2'T1H2'
C5H2''T3H2'
T1H2''
T3H2''
A6H2''
A6H2'
G2H2'/H2''
A4H2'
13CH2
12CH2
11CH2
14CH2
1.5
2.0
2.5
3.0
3.5
4.0
4.0 3.8 3.6 3.4 3.2 3.0 2.8 2.6 2.4 2.2 2.0 1.8 1.6 1.4 1.2
ppm

(Fig. 6.8c)

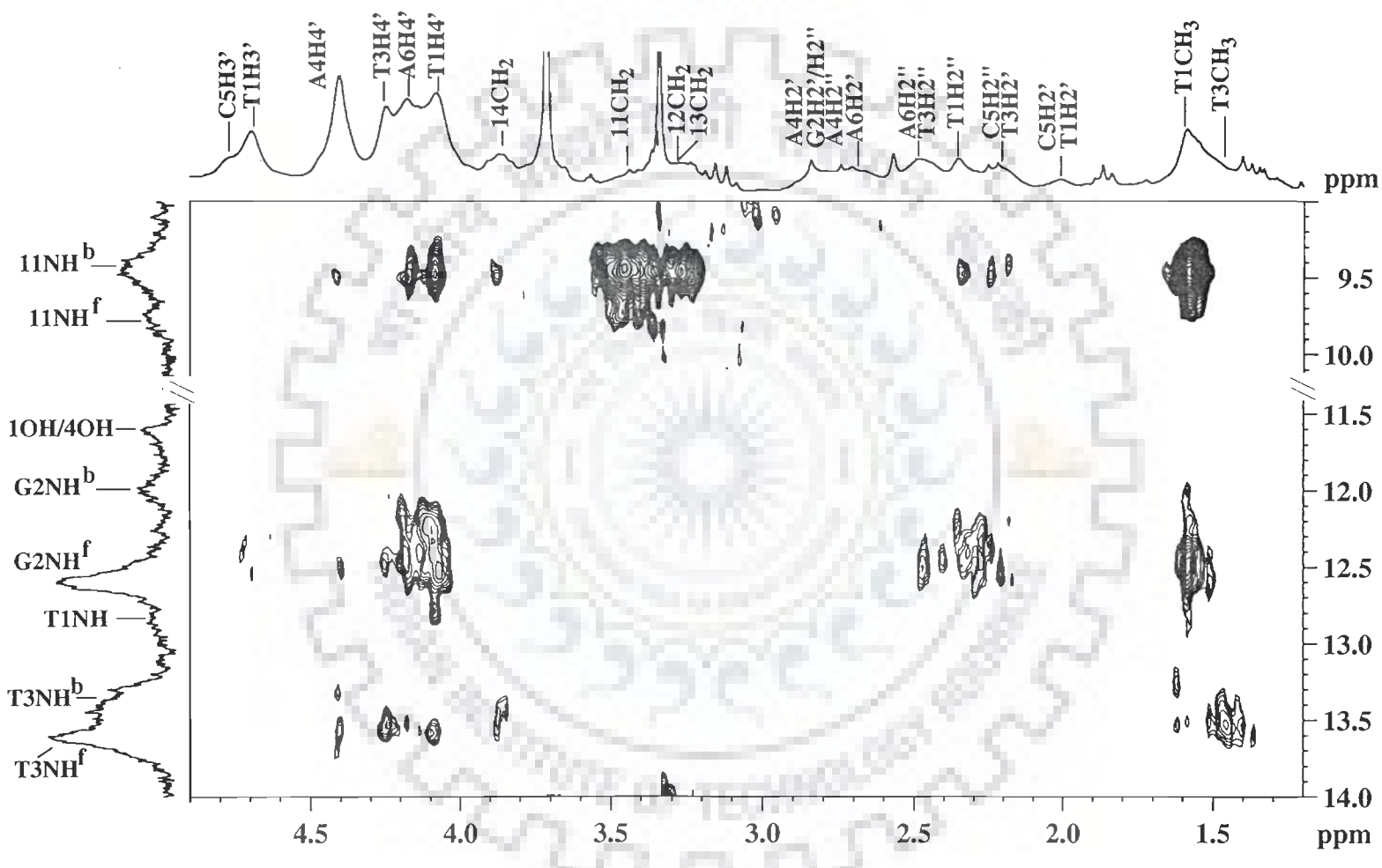
C5H3'
T1H3'
A4H4'
T3H4'
A6H4'
T1H4'
14CH2
11CH2
12CH2
13CH2
A4H2'
G2H2'/H2''
A4H2''
A6H2'
A6H2''
T3H2''
T1H2''
C5H2''
T3H2'
C5H2'
T1H2'
T1CH3
T3CH3
ppm
11NHb
11NHf
1OH/4OH
G2NHb
G2NHf
T1NH
T3NHb
T3NHf
9.5
10.0
11.5
12.0
12.5
13.0
13.5
14.0
4.5
4.0
3.5
3.0
2.5
2.0
1.5
ppm

(Fig. 6.8d)

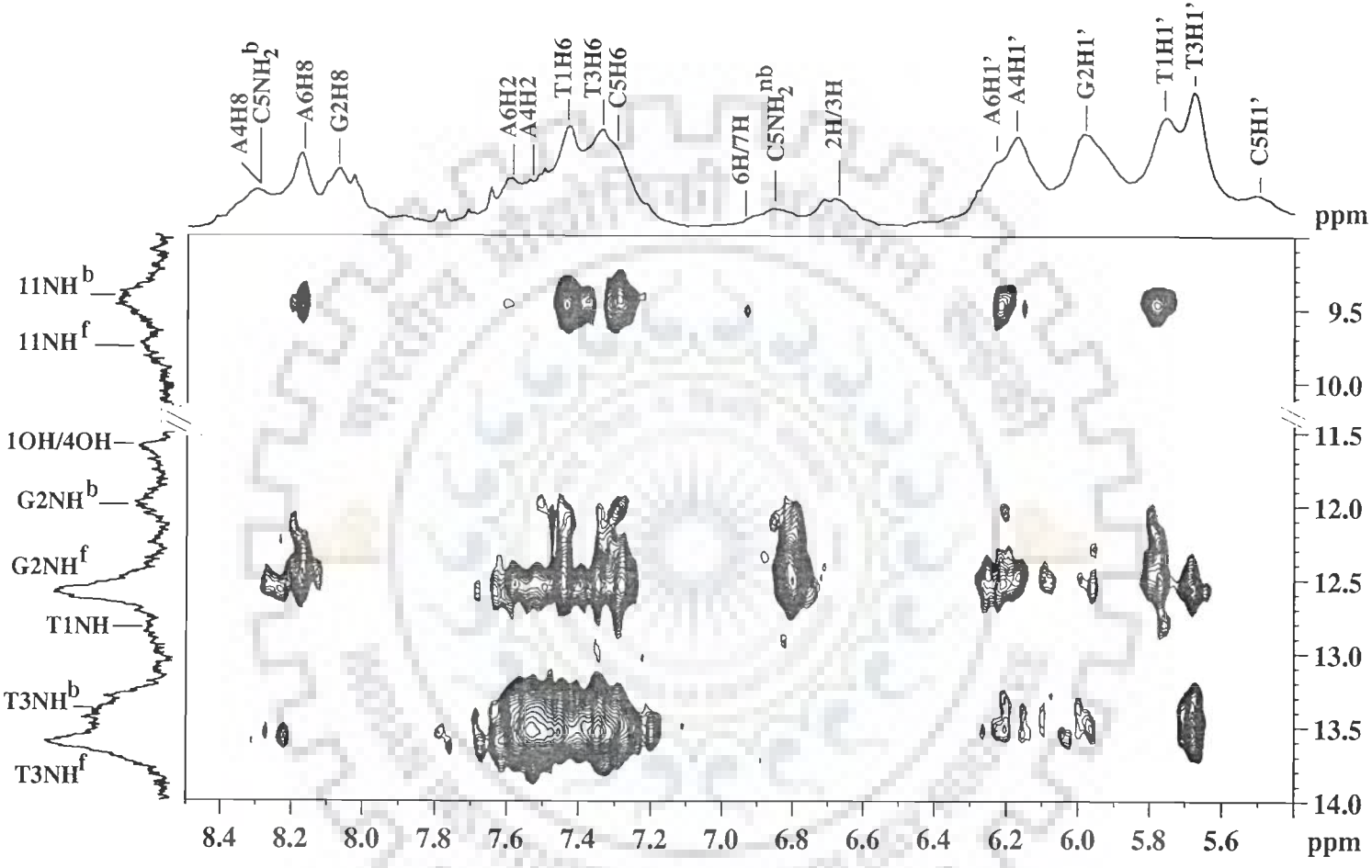
A4H8
C5NH2b
A6H8
G2H8
A6H2
A4H2
T1H6
T3H6
C5H6
6H/7H
C5NH2nb
2H/3H
A6H1'
A4H1'
G2H1'
T1H1'
T3H1'
C5H1'
ppm
11NHb
11NHf
1OH/4OH
G2NHb
G2NHf
T1NH
T3NHb
T3NHf
9.5
10.0
11.5
12.0
12.5
13.0
13.5
14.0
8.4
8.2
8.0
7.8
7.6
7.4
7.2
7.0
6.8
6.6
6.4
6.2
6.0
5.8
5.6
ppm

(Fig. 6.8e)

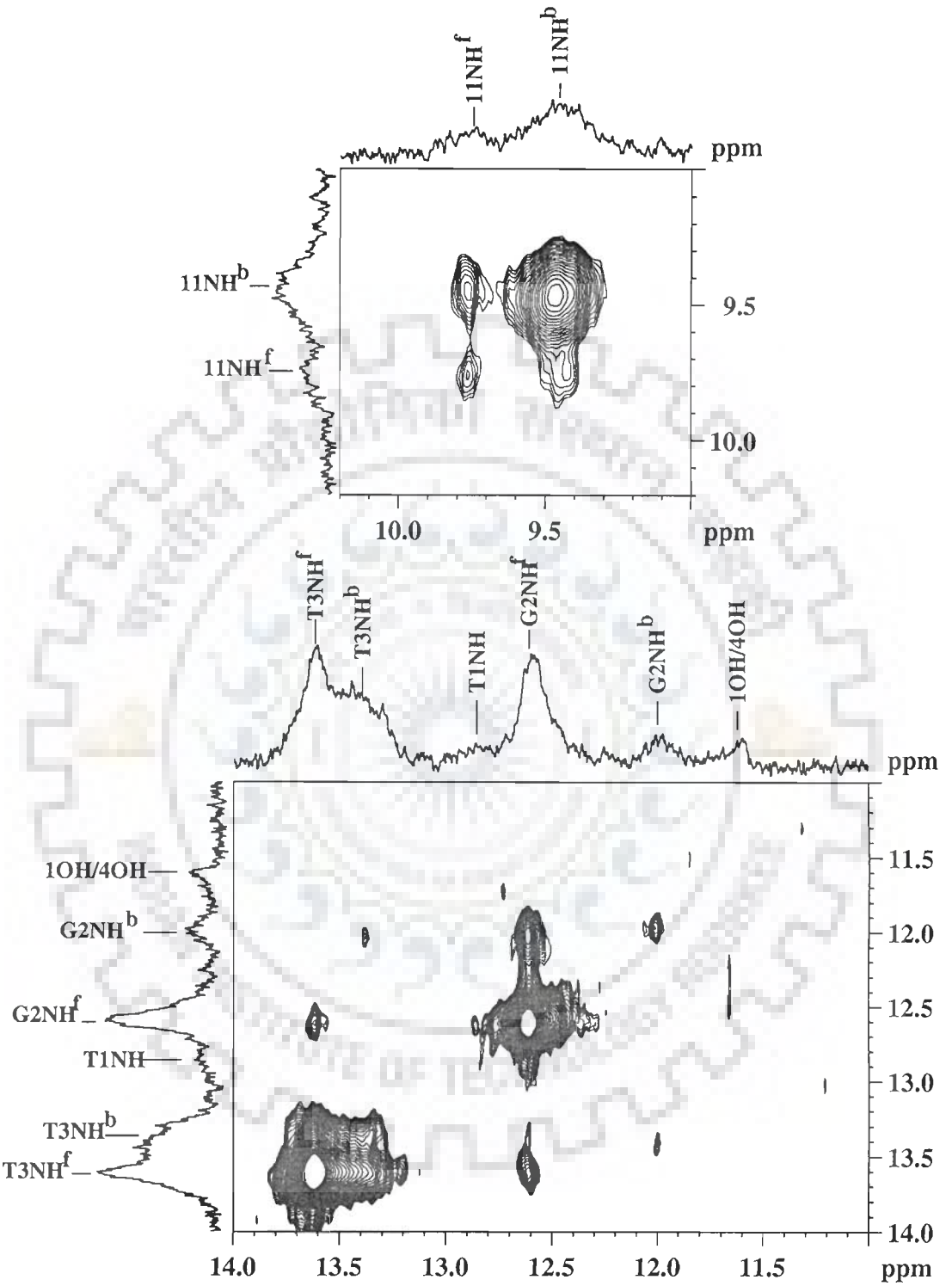
11NH^f
11NH^b
ppm
11NH^b
11NH^f
9.5
10.0
10.0
9.5
ppm
T3NH^f
T3NH^b
T1NH
G2NH^f
G2NH^b
1OH/4OH
ppm
1OH/4OH
G2NH^b
G2NH^f
T1NH
T3NH^b
T3NH^f
11.5
12.0
12.5
13.0
13.5
14.0
14.0
13.5
13.0
12.5
12.0
11.5
ppm

(Fig. 6.8f)

Table 6.7a: Inter residue sequential NOE cross peaks (ds) of nucleotide protons in the drug-DNA complex observed from the NOESY spectra at D/N = 1.0 at 275 K. The very strong (ss), strong (s), medium (ws), weak (w), very weakly (ww) intense cross peaks correspond to distances in the range ss 1.8 – 2.5 Å, s 2.5 – 3.0 Å, ws 3.0 – 3.5 Å, w 3.5 – 4.0 Å, ww 4.0 – 5.0 Å, respectively. Overlap of cross peaks is indicated as o.

Connectivity	Intensity	Connectivity	Intensity	Connectivity	Intensity
T1pG2 Step		T3pA4 step		C5pA6 step	
T1H1'- G2H8	ws	T3H1' - A4H8	ws	C5H1'- A6H8	w
T1H2'-G2H8	w	T3H2' - A4H8	w	C5H2' - A6H8	ww
T1H2"-G2H8	ws	T3H6 - A4H8	ws	C5H2"- A6H8	ws
T1H3'- G2H8	w	T3H2'-A4H2'	s	C5H3'- A6H8	w
T1H6- G2H8	ws			C5H6 - A6H8	ws
G2pT3 step		A4pC5 step			
G2H8 - T3CH_3	ss	A4H1'- C5H6	s		
G2H1' - T3H6	ws	A4H2'- C5H6	o		
G2H2'- T3H6	ss	A4H2"- C5H6	o		
G2H2"- T3H6	ss	A4H3'- C5H6	o		
G2H3'-T3H6	o	A4H8 – C5H6	ws		
G2H8 – T3H6	ws				

Table 6.7b: Intra nucleotide NOE connectivities (di) of sugar protons of nucleic acid in the drug-DNA complex observed from the NOESY spectra at D/N = 1.0 at 275 K. The very strong (ss), strong (s), medium (ws), weak (w), very weakly (ww) intense cross peaks correspond to distances in the range ss 1.8 – 2.5 Å, s 2.5 – 3.0 Å, ws 3.0 – 3.5 Å, w 3.5 – 4.0 Å, ww 4.0 – 5.0 Å, respectively. Overlap of cross peaks is indicated as o.

Cross peak	T1	G2	T3	A4	C5	A6
H1'- H2'	s	o	s	s	-	s
H1'- H2"	s	o	s	o	-	s
H1'- H3'	s	s	ws	s	-	m
H1'- H4'	s	-	-	s	-	ws
H2' - H2"	ss	o	ss	o	o	o
H2'- H3'	ss	ss	-	-	o	s
H2'- H4'	o	o	ws	ss	ws	o
H2"- H3'	o	s	-	s	s	ws
H2"- H4'	o	o	ws	-	o	o
H3'- H4'	ss	o	s	-	s	s

Table 6.7c: Intra nucleotide NOE connectivities (di) of base to sugar protons of nucleic acid in the drug-DNA complex observed from the NOESY spectra at D/N = 1.0 at 275 K. The very strong (ss), strong (s), medium (ws), weak (w), very weakly (ww) intense cross peaks correspond to distances in the range ss 1.8 – 2.5 Å, s 2.5 – 3.0 Å, ws 3.0 – 3.5 Å, w 3.5 – 4.0 Å, ww 4.0 – 5.0 Å, respectively. Overlap of cross peaks is indicated as o.

Cross peak	T1	G2	T3	A4	C5	A6
H8/H6-H1'	s	ws	ws	ws	o	s
H8/H6-H2'	s	ss	s	s	ws	s
H8/H6-H2"	s	ss	s	o	o	s
H8/H6-H3'	ws	ws	ws	w	ws	s
H8/H6-H4'	ws	s	o	-	o	s
CH_3 –H1'	ws	-	-	-	-	-
CH_3-H2'	s	-	o	-	-	-
CH_3-H2'	ws	-	ws	-	-	-

Table 6.7d: NOE connnectivities in the drug – DNA complex at D/N = 1.0 at 275 K. The very strong (ss), strong (s), medium (m), weak (w), very weakly (vw) intense cross peaks correspond to distances in the range ss 1.8 – 2.5 Å, s 2.5 – 3.0 Å, ws 3.0 – 3.5 Å, w 3.5 – 4.0 Å, ww 4.0 – 5.0 Å, respectively in the NOESY spectra. Overlap of cross peaks is indicated as o.

Cross peak	NOE Intensity	Cross peak	NOE Intensity
Intranucleotide (di)		Internucleotide & Inrastrand & Sequential(dps)	
$G2NH^{f}$ – $G2NH^{b}$	ws	$T1NH^{f}$ – $G2NH^{f}$	ww
$G2NH^{f}$ – $G2NH_2^{nb}$	o	$T3NH^{f}$ – $G2NH^{f}$	ws
$T1NH^{f}$ – $T1CH_3$	ww	$T3NH^{f}$ – A4H2	ss
$T3NH^{f}$ – T3H6	ss	$T3NH^{b}$ – A4H2	o
$T3NH^{f}$ – $T3CH_3$	ws	$G2NH^{b}$ – T1H6	w
$A4NH_2^{b}$ –$A4NH_2^{nb}$	ww	$G2NH^{f}$ – $T1CH_3$	ws
$C5NH_2^{b}$ –C5H6	ws	$G2NH^{f}$ – T1H4'	ws
$C5NH_2^{nb}$ –C5H6	ws		
Internucleotide Interstrand & Sequential (dps)		Internucleotide & Interstrand within Base pair (dpi)	
T3NH – $C5NH_2^{b}$	ww	$G2NH^{b}$ – $C5NH_2^{b}$	ww
A4H2 – G2NH	w	$G2NH^{f}$ – $C5NH_2^{b}$	s
A6H2 – G2NH	w	$G2NH^{b}$ – $C5NH_2^{nb}$	o
		$G2NH^{f}$ – $C5NH_2^{nb}$	ss
		T3NH – A4H2	o
		$G2NH^{f}$ – C5H6	s
		$G2NH^{b}$ – C5H6	ww
		T4NH – $C5NH_2^{b}$	ww

Table 6.8: Intensities of NOE cross peaks (di) within the drug molecule in the drug-DNA complex at D/N = 1.0 at 275 K. The very strong (ss), strong (s), medium (ws), weak (w) and very weakly (ww) intense cross peaks refer to distances in the range ss 1.8 – 2.5 Å, s 2.5 – 3.0 Å, ws 3.0 – 3.5 Å, w 3.5 – 4.0 Å, ww 4 – 5 Å, respectively from the NOESY spectra, Overlap of peaks is indicated as o.

Connectivity	Intensity	Uncomplexed drug distances (Å)
$11CH_2$ – 6H/7H	s	2.15
$12CH_2/13CH_2$– 6H/7H	w	2.55
$14CH_2$ –$13CH_2$	ss	2.40
$11NH^f$ – $11CH_2$	w	2.69
$11NH^b$ – $11CH_2$	s	-
$11NH^b$ –$12CH_2/13CH_2$	s	-
$11NH^f$ –$12CH_2/13CH_2$	-	2.83 / 3.08
$11NH^b$ – 6H/7H	ww	3.60-4.70

Table 6.9: Intermolecular NOE connectivities between d-(TGTACA)$_2$ and mitoxantrone in the drug-DNA complex at D/N =1.0 from NOESY spectra at 275 K along with the distances observed in the final rMD structure. The very strong (ss), strong (s), medium (ws) and weakly (w) intense cross peaks correspond to distance of ss 1.8 – 2.5 Å, s 2.5 – 3.0 Å, ws 3.0 – 3.5 Å, w 3.5 – 4.0 Å, ww 4 – 5 Å. Overlap of peaks is indicated as o.

Cross peak	Bound drug D/N=1.0	Distance rMD Model (Å)
11NH^b – T1CH$_3$	s	2.88
11NH^b – T1H6	s	3.01
11NH^b – A6H2	ww	4.21
11NH^b – A6H8	ww	4.74
11NH^b – T1H1'	ws	3.94
11NH^b – A6H1'	ws	4.01
11NH^b – T1CH2''	ww	4.99
11NH^b – A6H4'	w	3.50
11NH^b – T1H4'	ws	3.19
11NH^b – A6H4'	w	3.50
11NH^b – T1H4'	ws	3.19
2H/3H – T1H2"	w	4.00
2H/3H – A6H8	w	5.00
2H/3H – T1H4'	ww	5.02
2H/3H – T1H1'	w	3.32
11CH2 – T1CH3	ws	3.34
11CH$_2$ – A6H2"	w	4.22
11CH$_2$ – T1H2"	w	4.05
12/13 CH$_2$ – T1CH$_3$	ws	3.50
12/13 CH$_2$– A6H8	w	5.00
12/13 CH$_2$ - T1H6	w	4.05
12/13 CH$_2$ – G2H8	w	4.95
12/13 CH$_2$– T1H1'	ws	3.40
12/13 CH$_2$ – A6H2"	ws	3.74
12/13 CH$_2$ – T1H2"	ws	3.47

Since mitoxantrone is shown to have faster dissociation rates for Poly dA–dT than for Poly dG–dC of an order of magnitude (Krishnamoorthy et al, 1986). Throughout the titration only one resonance signal is observed for both DNA and drug protons, with gradual change in chemical shift as the concentration of drug increased, except for T3NH, G2NH of DNA and 11NH of drug. The exchange phenomenon between the bound and free drug is considerably slow as compared to binding with d-$(TGATCA)_2$. Our detailed NMR analysis shows that all the duplex pair peaks, including sequential intra and inter–strand peaks, exist. Thus it may be expected that mitoxantrone binds externally to the DNA duplex, being in close proximity to T1.A6 base pair. All the spectral lines are uniformly broadened on binding as the internal motions are affected and the protons are getting immobilized on binding. 11NH proton of mitoxantrone shows substantial upfield shift, 0.78 ppm on binding. While 6H / 7H and 2H / 3H shift by 0.47 ppm and 0.49 ppm, respectively (Table 6.4). This is indicative of stacking of mitoxantrone chromophore with base pair of DNA. The shift in resonance psoitions of base and H1' protons of DNA are not significant. In fact the change in chemical shift is not a sufficient indicator of the interaction. The direct proof for binding comes from 2D ^{31}P NMR exchange spectra of the complex at with clear exchange is observed between bound and free T1pG2 (Fig. 6.3). The same is also evident in the NH region of ^{1}H NMR spectra (Fig. 6.8f) showing exchange of free and bound G2NH, T3NH and 11NH of drug. The intermolecular cross peaks between drug and the terminal base pair of DNA i.e., $11NH^{b}$–$T1CH_3$, $11NH^{b}$–T1H6, $11NH^{b}$–A6H2 , $11NH^{b}$ –A6H8, $11NH^{b}$–T1H1', $11NH^{b}$ – A6H1', 2H/3H – A6H8, 2H/3H –T1H1', 2H/3H –T1H4', 12/13CH_2–$T1CH_3$, 12/13CH_2– A6H8, 12/13CH_2– T1H1' (Table 6.9) gives direct evidence that the drug is present at the

terminal base pairs of DNA duplex. Also, consecutive base pairs do not open and therefore we conclude that mitoxantrone binds externally to the DNA duplex, in close proximity to T1.A6 base pair. Further, to support this fact, the model of drug-DNA was built using restrained Molecular Dynamics simulations.

6.1.3 Restrained Molecular Dynamics Studies

Attempt had been made to build a model of the drug-DNA complex based on intermolecular (Table 6.9), intramolecular (within drug and within DNA hexamer) NOEs (Tables 6.7a-d). The schematic representation of the initial model of mitoxantrone stacked between two molecules of d-$(TGTACA)_2$ is shown in Fig. 6.9. DNA1 and DNA2 refer to the two hexamer duplex above and below the mitoxantrone chromophore. Distance restraints between atoms involved in the Watson–Crick hydrogen bonding pairs are imposed in the structure calculations based on experimental evidence from NOESY spectra. The final structure obtained after restrained Molecular Dynamics is shown in Fig. 6.10. The stacking interaction of mitoxantrone with respect to base pairs is shown in Fig. 6.11.

Table 6.10 indicates an assessment of refined structures after equilibration (at the end of 25 ps) in terms of energetics including restraint violations energies and root mean square derivative of energy with respect to atomic coordinates. The total potential energy of the final structure is 361 kcal mol^{-1}, which is significantly lower than the corresponding energy of initial model B-DNA structure (3089 kcal mol^{-1}). The forcing potential, which indicates contribution to potential energy due to violations of both experimental distances data, exhibits a decrease from 1841 to 213 kcal mol^{-1} after restrained energy minimization and restrained molecular dynamics. Summary of

experimental restraints and statistical analysis of family of structures generated by restrained molecular dynamics (rMD) is shown in Table 6.11.

Table 6.10: Energy terms (Kcal mol^{-1}) for starting structure and final rMD structure

Structure	Total	Bond	Angle	Dihedral
Initial	3089	208	435	168
Final	361	54	121	-107
	Vdw	Electrostatic	Restraint	
Initial	436	-281	1841	
Final	98	-175	213	

Table 6.11: Summary of Experimental restraints and statistical analysis of final structure generated by restrained molecular dynamics (rMD)

Parameter	
	No. of Distance Restraints
Intra residue	213
Inter residue	56
Inter molecular	25
Average pairwise RMSD	Initial = 0 Final = 0.79
Average residuewise RMSD	T1=0.71, G2=0.95, T3=0.81 A4=0.79, C5=1.04, A6=0.84 Mitoxantrone=0.88

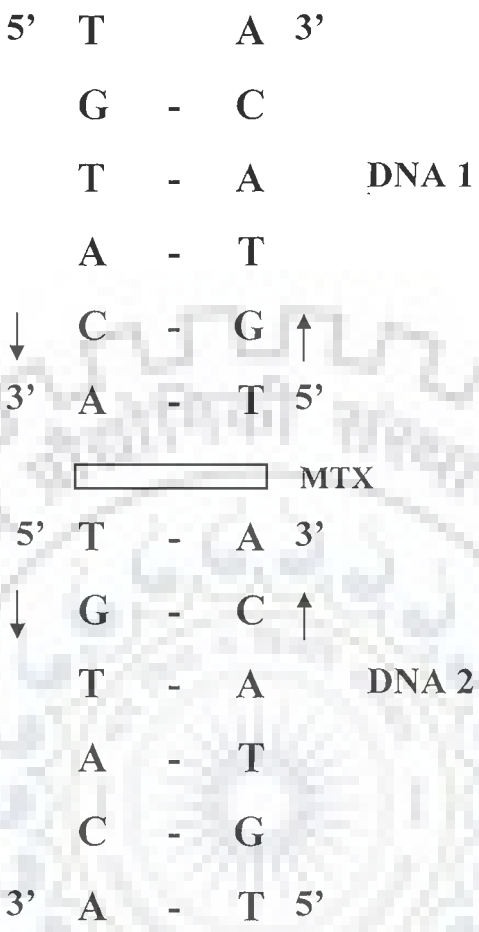

Figure 6.9: Schematic Representation of mitoxantrone (MTX) with d-$(TGTACA)_2$ Complex

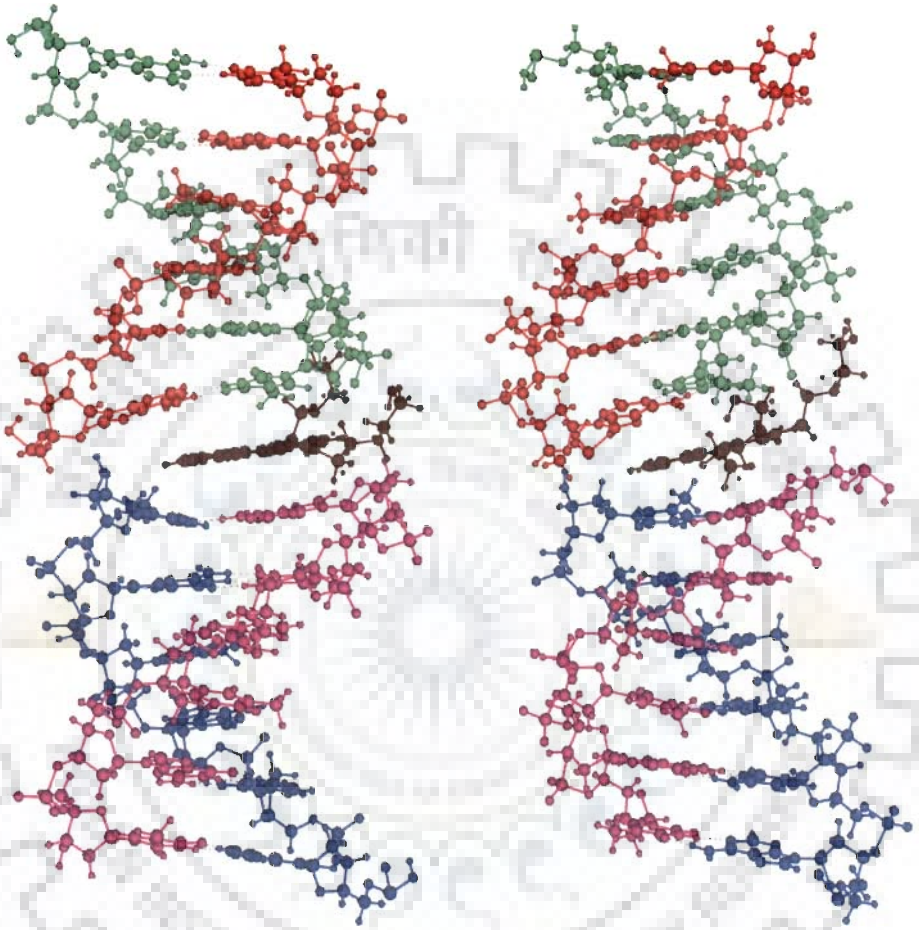

Figure 6.10: The final rMD structure of d-(TGTACA)$_2$-mitoxantrone derived from the NOE data.

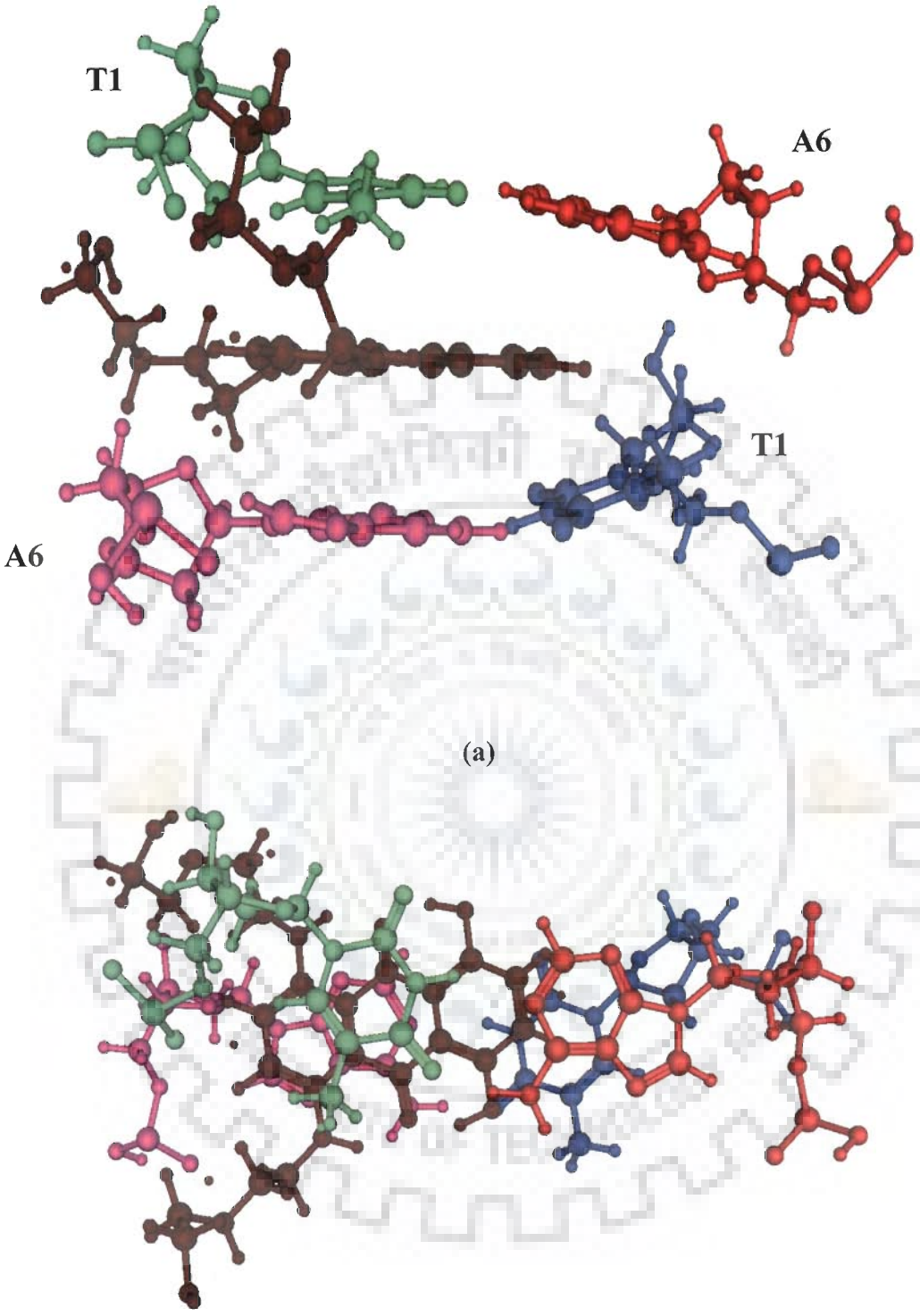

Figure 6.11: Drug-DNA stacking interaction in the intercalation site showing the orientation of the mitoxantrone with respect to base pairs (a) front view (b) top view

All helical parameters, backbone torsional angles, and sugar conformations of the resulting rMD structures were thoroughly analyzed with the program CURVES, version 5.1 (Lavery et al, 1996; Lavery et al, 1989). Plot of the helicoidal parameters as a function of residue position in the duplex is shown in Figure 6.12a-b, along with classical structures of A-DNA and BDNA. The overlap geometry at different base pair steps along the sequence in mitoxantrone - d-$(TGTACA)_2$ is shown in Figure 6.13a-b. In the base pair-axis parameters, the average value of x-displacement is 0.54 Å close to -0.7 Å as seen in canonical B-DNA structures. The average y-axis displacement (dy) is 0.21 Å. The rMD structure display inclination values of ± 2.0° of the average value 11.82°. Among the intra base parameters, the shear (Sx) and stretch (Sy) values do not vary very much from B-DNA values. The stagger (Sz) values lie within ±0.17 Å. Base pair opening lies in the range 3 to 20 for all base pairs.. In regular A-DNA and B-DNA geometries, global values of the inter base pair parameters - shift (Dx), slide (Dy), roll (rho) and tilt (tau) are essentially zero. For rMD structure, the observed shift and slide values are small and do not show any significant variation with the base pair step. The rise per residue (Dz) approximately lies with in the range 3.2-4.0 Å that is standard for B-DNA. The variation of tilt value is ± 12° deviated from the ideal B-DNA value. The twist angle varies between 29° -47°. The backbone torsional angles and glycosidic bond rotation values for the final rMD structure measured using CURVES are shown in Table 6.12. The backbone angles and χ show that the conformation of the structure obtained from rMD is close to that of the B-DNA and not distorted by binding to mitoxantrone. d-$(TGTACA)_2$ sequence has the helical parameters near to standard B-DNA values on binding to mitoxantrone.

Table 6.12: Backbone torsional angles, pseudoratation phase angle and glycosidic bond rotation of the final structure in degrees analyzed using CURVES program.

DNA1		α		β		γ		δ	
Strand I	Strand II	Strand I	Strand II	Strand I	Strand II	Strand I	Strand II	Strand I	Strand II
T1	A12	.....	.....	.....	.....	50.49	51.03	139.42	149.84
G2	C11	-57.21	-61.30	130.48	149.29	50.26	49.05	145.94	141.57
A3	T10	-72.69	-68.49	146.14	147.42	55.74	56.85	137.91	143.03
T4	A9	-71.44	-76.06	176.57	145.27	53.55	56.50	145.76	139.99
C5	G8	-66.65	-78.93	158.53	121.10	57.06	45.71	138.29	138.23
A6	T7	.....	.....	.....	.....	45.45	54.66	152.77	149.27
DNA2									
T1	A12	.....	.....	.....	.....	40.15	53.31	134.23	144.14
G2	C11	-65.73	-79.42	173.79	156.99	62.04	54.11	155.32	139.82
A3	T10	-75.06	-78.55	154.54	179.26	59.59	52.36	135.26	143.46
T4	A9	-72.31	-75.68	176.53	149.29	57.29	60.74	143.87	137.20
C5	G8	-42.65	-67.55	150.83	171.18	49.16	50.10	142.32	144.91
A6	T7	.....	.....	.....	.....	51.26	50.93	149.78	139.37
B-DNA		-63		136		54.0		123	

DNA1		ε		ζ		χ		P	
Strand I	Strand II	Strand I	Strand II	Strand I	Strand II	Strand I	Strand II	Strand I	Strand II
T1	A12	.....	.....	.....	.....	-115.83	-112.63	150.55	176.80
G2	C11	-167.14	-142.26	-93.21	-123.97	-96.61	-111.37	194.81	145.75
A3	T10	-176.70	-171.29	-110.03	-94.67	-114.32	-115.35	146.91	164.02
T4	A9	-174.06	-178.46	-91.89	-107.09	-120.87	-109.15	167.32	147.91
C5	G8	-143.31	-116.14	-127.79	-88.98	-117.88	-94.55	142.00	161.44
A6	T7	.....	.....	.....	.....	-117.92	-90.60	181.87	174.18
DNA2									
T1	A12	.....	.....	.....	.....	-76.29	-132.50	135.48	170.09
G2	C11	-165.73	-139.42	-93.54	-144.08	-89.59	-116.70	164.30	154.59
A3	T10	-175.06	-178.45	-109.14	-91.24	-114.77	-111.61	143.57	164.91
T4	A9	-172.31	-175.68	-93.99	-113.41	-113.47	-118.43	164.51	144.57
C5	G8	-142.65	167.55	-131.54	-93.21	-110.79	-97.81	147.05	160.02
A6	T7	.....	.....	.....	.....	-112.87	-116.52	176.60	149.78
B-DNA		-169		-108		-105		162	

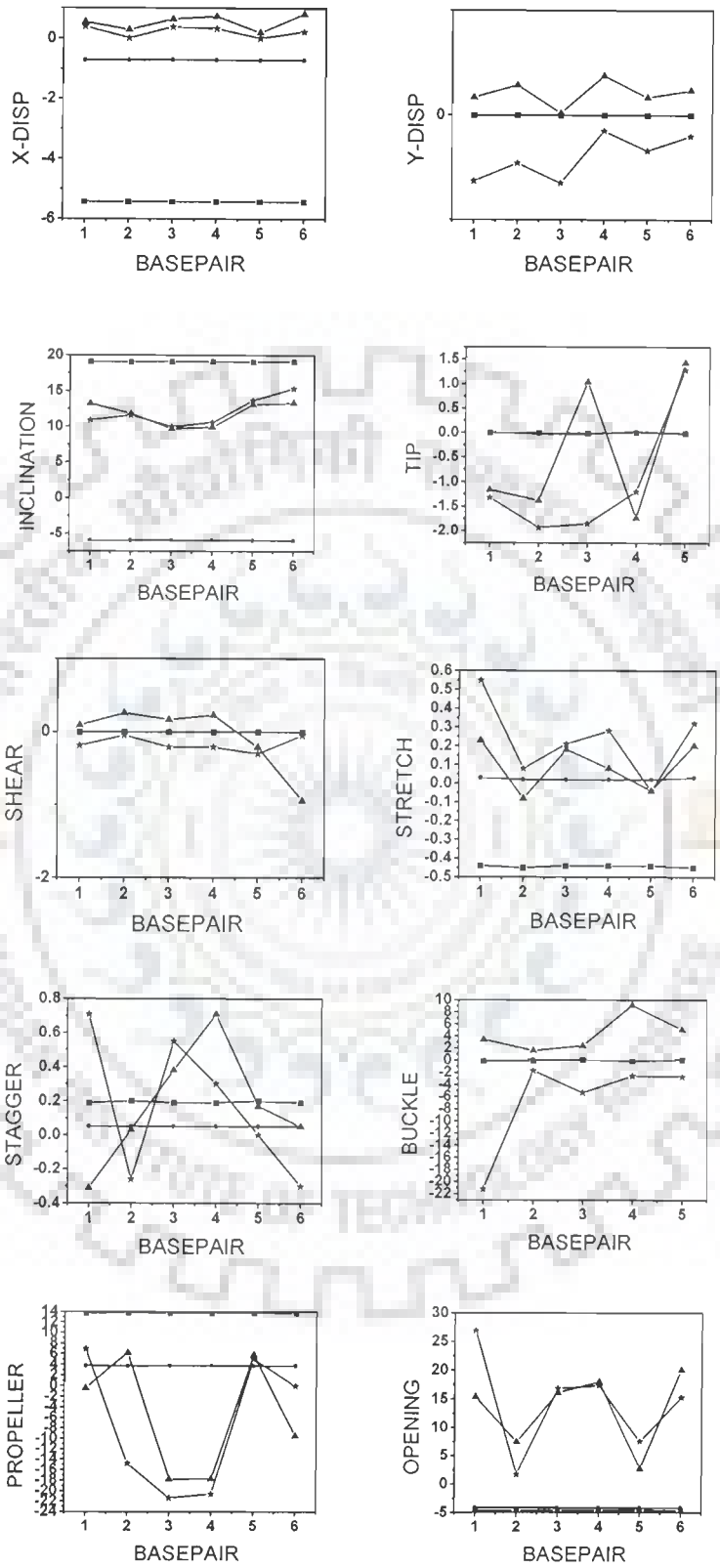
X-DISP
BASEPAIR
Y-DISP
BASEPAIR
INCLINATION
BASEPAIR
TIP
BASEPAIR
SHEAR
BASEPAIR
STRETCH
BASEPAIR
STAGGER
BASEPAIR
BUCKLE
BASEPAIR
PROPELLER
BASEPAIR
OPENING
BASEPAIR

(Fig. 6.12a)

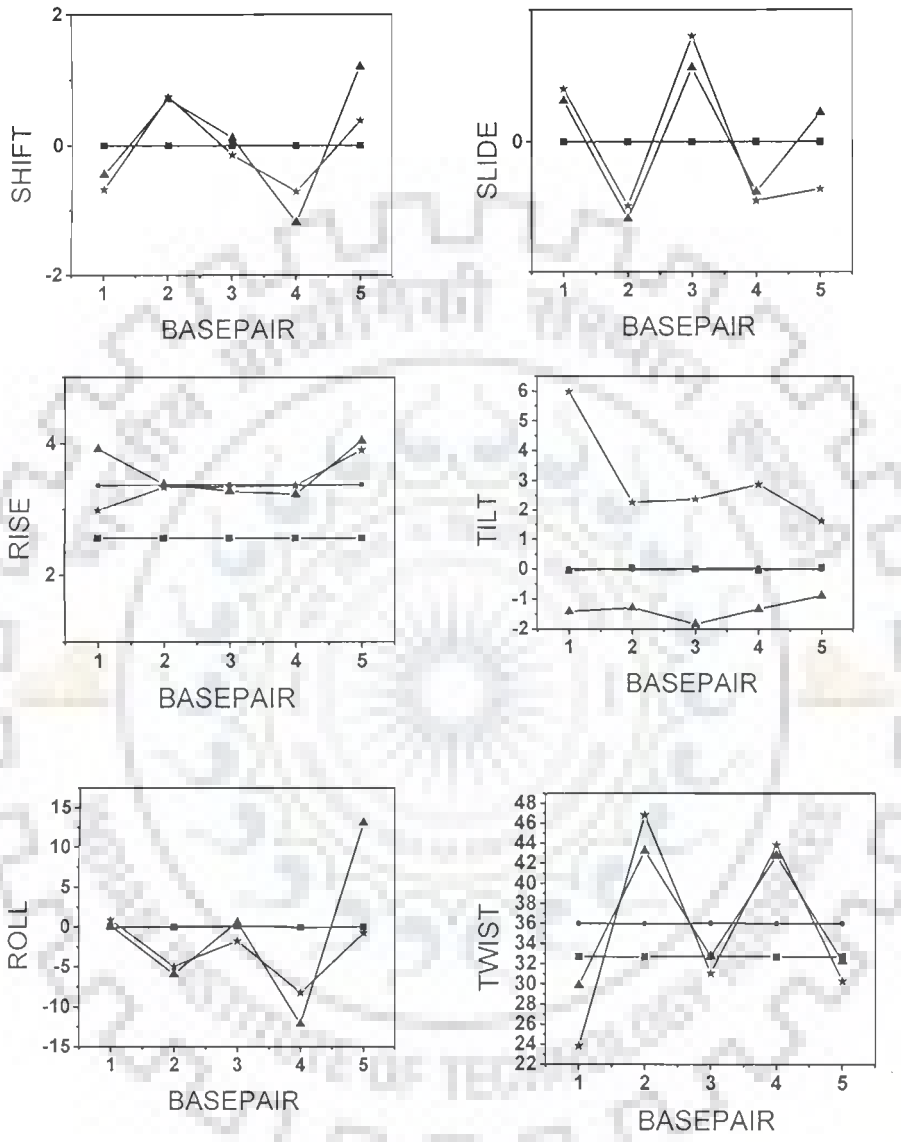

(Fig. 12b)

Figure 6.12: Helical parameters for d-(TGTACA)$_2$ complexed with mitoxantrone calculated for structure obtained by restrained molecular dynamics simulation, simulation (DNA1 - ▲; DNA2 - ★) canonical A-DNA (■) and B-DNA (●) (a) Global Base pair – axis and base – base parameters (b) Global inter-base pair parameters

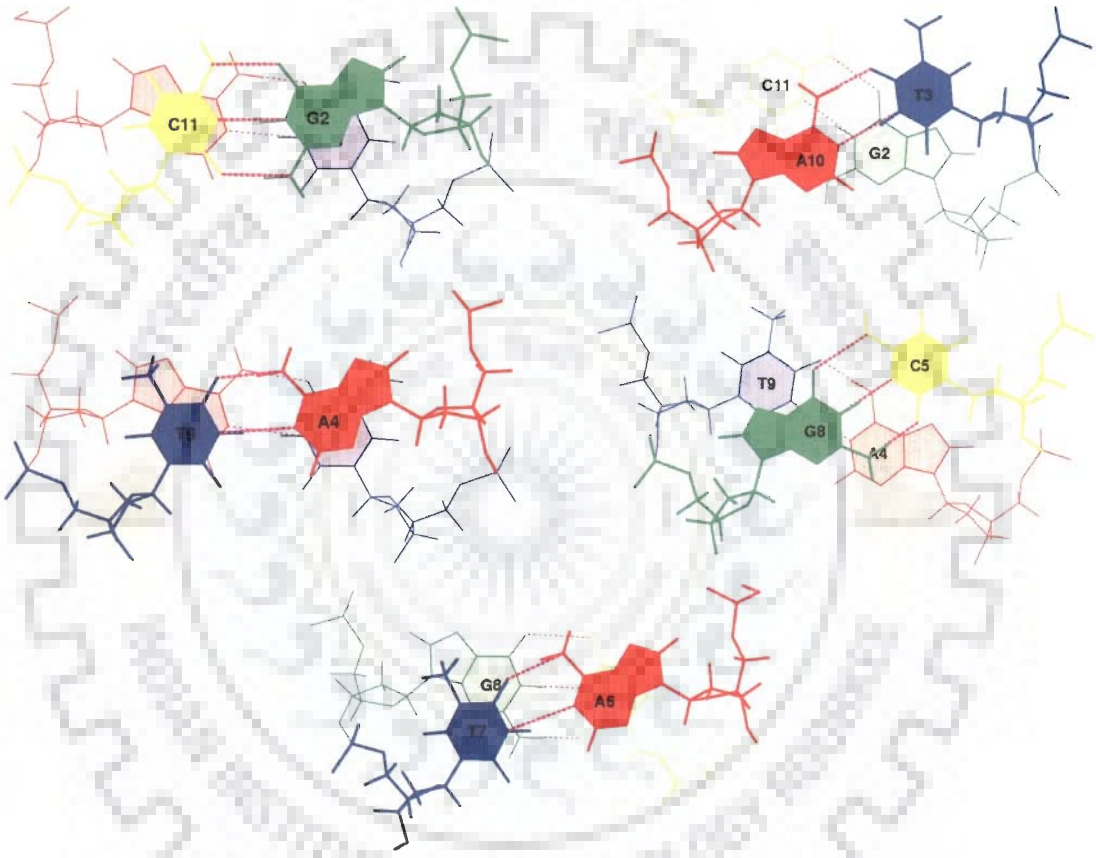

(Fig. 6.13a)

Figure 6.13: Overlap of base pairs at different base pair steps in d-(TGTACA)$_2$-mitoxantrone complex showing stacking interactions (a) DNA 1 (b) DNA 2.

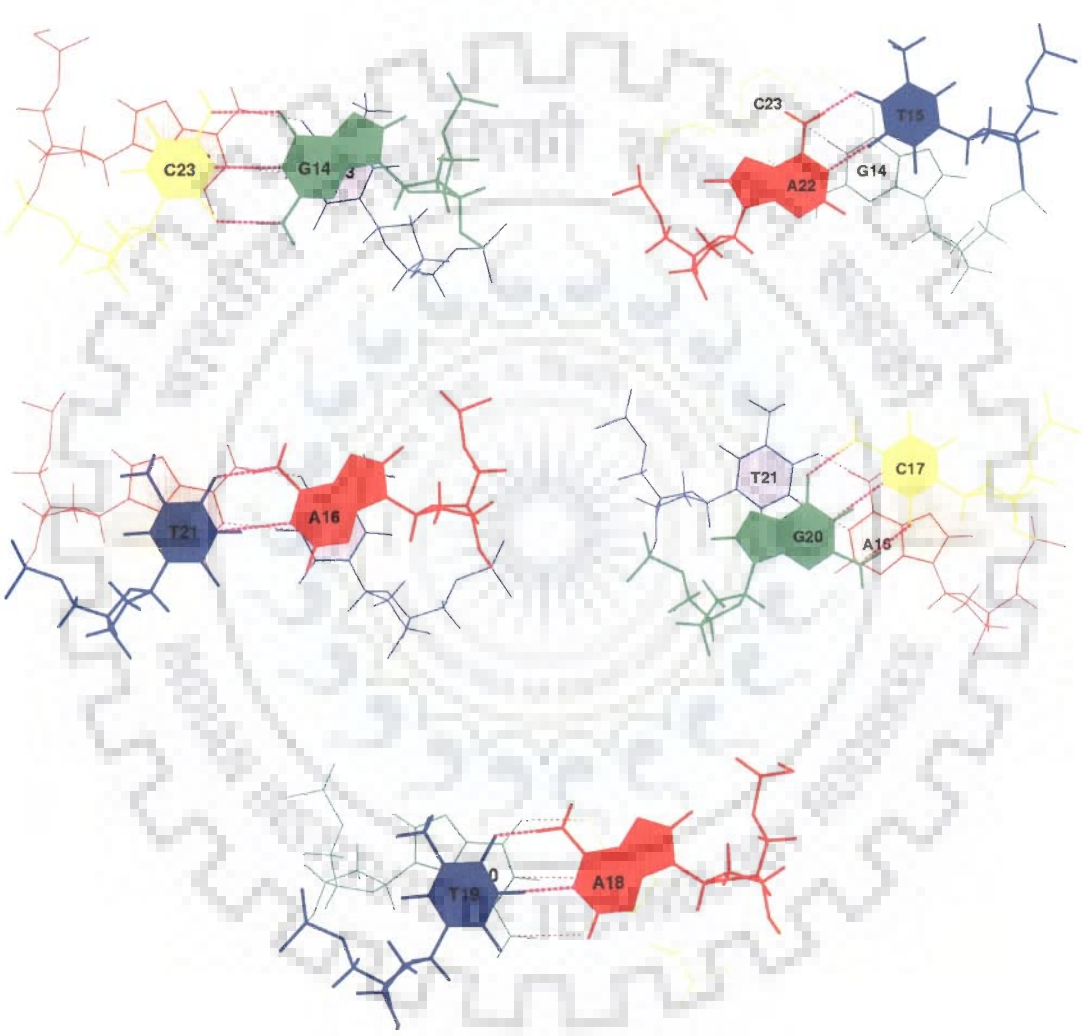

(Fig. 6.13b)

6.2 CONCLUSIONS

Titration studies show that addition of mitoxantrone to DNA hexamer does not cause the ^{1}H as well as ^{31}P resonances to drift continuously. The T3NH, G2NH resonance lines, instead gives rise to new set of broad signals upfield at the expense of the intensities of the free resonances. 2D ^{31}P NMR exchange spectrum shows strong exchange correlation between bound and free T1pG2 resonance at stoichometric ratio of 0.5. The bound T1pG2 resonance is 1.15 ppm downfield shifted with respect to its free resonance. The significantly large downfield shift may be attributed to local drug–induced distortions at T1pG2 step leading to change in phosphate backbone conformation from gauche, gauche (α = -60°, ζ = -90°) to gauche, trans (α = -60°, ζ = -180°). 11NH proton adjacent to aromatic chromophore of drug gives two set of signals corresponding to bound and free forms. The existence of two sets of G2NH, T3NH and 11NH (drug) clearly demonstrates that the drug thus indeed binds to the DNA hexamer and there is exchange of free and bound DNA on NMR time scale at 275 K. Mitoxantrone is shown to have faster dissociation rates for Poly dA–dT than for Poly dG–dC of an order of magnitude (Krishnamoorthy et al, 1986). Hence the exchange phenomenon between the drug and d-$(TGTACA)_2$ is expected to be faster than that observed with d-$(CGTACG)_2$. Several intermolecular contacts observed are close to T1.A6 base pair. $11NH^b$ gives close contacts with $T1CH_3$, T1H6, A6H2, A6H8, T1H1' and A6H1'. 2H/3H is close to A6H8 as well as with T1H1' and T1H4'. Similarly $12/13CH_2$ gives close contacts with $T1CH_3$, A6H8 and T1H1'. Mitoxantrone protons ($11NH^b$, $12CH_2/13CH_2$ and 2H/3H) are simultaneously close to T1 and A6 residue protons of DNA which are located on opposite sides of the base pair. Such NOE connectivities are possible only if mitoxantrone

aromatic chromophore binds externally to the terminal base pairs of DNA. Also, 2D NOESY spectra show the presence of all internucleotide sequential connectivities between non-exchangeable protons, which suggests that drug, is binding externally to the hexamer sequence. Also, throughout the titration only one resonance signal is observed for both DNA and drug protons, with gradual and small change in chemical shift as the concentration of drug increased. Mitoxantrone binds externally to d-$(TGTACA)_2$ with the aromatic chromophore stacking with T1.A6 base pairs leading to large upfield shifts in 6H / 7H, 2H / 3H and particularly 11NH protons ($\Delta\delta \sim 0.78$ ppm upfield). It is evident from the sequential connectivities that the base pairs do not open up to accommodate the aromatic anthraquinone chromophore like typical intercalators, such as ethidium bromide, daunomycin, adrimycin, actinomycin. Apparently drug is binding externally to the hexamer sequence in a specific orientation which gives rise to the observed NOEs. Mitoxantrone binds externally to the DNA duplex, in close proximity to T1.A6 base pair.

Chapter 7

Comparative results of mitoxantrone complexed with d-(TGATCA)$_2$, d-(CGTACG)$_2$ and d-(TGTACA)$_2$

Phosphorus-31 and proton Nuclear Magnetic Resonance spectroscopy followed by restrained Molecular Dynamics simulations were used to study conformation of mitoxantrone–DNA complexes with DNA hexamer sequences, d–(TGATCA)$_2$, d–(CGTACG)$_2$ and d–(TGTACA)$_2$. ^{31}P-^{31}P NOESY exchange studies of complexes reveal separate bound and free ^{31}P signals in some of the phosphorus signals. T1pG2 signal in complex with d–(TGTACA)$_2$ is downfield shifted up to ~ 1.15 ppm and may be attributed to local drug–induced distortions leading to change in phosphate backbone conformation from gauche, gauche (α = -60°, ζ = -90°) to gauche, trans (α = -60°, ζ = -180°). All other ^{31}P signals in the complexes studied shift to a much lesser extent, by about 0.2-0.5 ppm. Maximum shift due to binding was observed at the interaction site in all three complexes. Comparision with similar dug-DNA complexes of mitoxantrone also show that chemical shift of the ^{31}P resonances is not affected significantly, $\Delta\delta$ < 0.35 ppm (Lown et al, 1985b; Kotovych et al, 1986). Berberine and pyridopurine, which are known to bind externally to DNA also do not affect chemical shift of any of the ^{31}P resonances significantly ($\Delta\delta$ < 0.2 ppm) (Mazinni et al, 2003; Favier et al, 2001). On the other hand, complexes of daunomycin, adriamycin and morpholinodoxorubicin reported in literature (Mazzini et al., 1988; Ragg et al., 1988), shows that stretching of DNA backbone by drug intercalation causes large downfield shift (upto 1.5 ppm) of the phosphates at intercalation or adjacent site.

Since ^{31}P chemical shifts are related to backbone stretching (change in torsional angle ζ) and O-P-O bond angles, it may be inferred that mitoxantrone distorts each of the DNA on binding to it in a unique way. Thus the changes are specific and bear the signature of sequence of bases to which it binds.

11NH proton adjacent to aromatic chromophore of drug gives two set of signals corresponding to bound and free forms in d-$(CGTACG)_2$ and d-$(TGTACA)_2$. It is 0.1 -0.3 ppm upfield shifted in the complexes studied. The aromatic protons 2H/3H and 6H/7H show significant upfield shift on drug binding, maximum being 0.52 ppm for 2H/3H in d-$(CGTACG)_2$ complex.

There is a slow exchange on NMR time scale between free and bound species as exhibited by separate bound and free resonance for DNA protons – TNH, GNH, TCH_3 and 11NH of mitoxantrone for d-$(CGTACG)_2$ and d-$(TGTACA)_2$. Whereas for d-$(TGATCA)_2$, only one resonance signal is observed for both DNA and drug protons, with gradual change in chemical shift as the concentration of drug increased. It is suggested the signals are in fast exchange regime and the observed resonance is considered to be an average of free and bound proton. Mitoxantrone is shown to have faster dissociation rates for Poly dA–dT than for Poly dG–dC (Krishnamoorthy et al, 1986).

Several intermolecular contacts observed between drug and DNA protons confirm the proximity of drug chromophore to terminal base pair in all complexes. T1.A6 base pair in d-$(TGTACA)_2$ and d-$(TGTACA)_2$ and C1.G6 in case of d-$(CGTACG)_2$. Mitoxantrone protons 2H/3H, 11NH, $12CH_2/13CH_2$ are simultaneously close to protons which are located on opposite sides of terminal base pair. Such NOE connectivities are

possible only if mitoxantrone aromatic chromophore binds externally to the terminal base pairs of DNA, preferably stacked between two molecules of DNA. The presence of intra base pair, sequential inter base pair and all sequential intramolecular NOE connectivities expected in standard B–DNA geometry confirms that the DNA duplex is intact in all three complexes with apparently no opening of base pairs to accommodate drug chromophore as generally observed with drug intercalation. Conformational analysis of the final rMD structure shows DNA hexamer in complexed state adopts a conformation close to that of canonical B–DNA structure. The key features of mitoxantrone interaction with the three hexamer sequences studied are shown in Table 7.1

Table: 7.1: Key features of interaction of mitoxantrone with d-$(TGATCA)_2$, d-$(CGTACG)_2$ and d-$(TGTACA)_2$

Feature	d-$(TGATCA)_2$	d-$(CGTACG)_2$	d-$(TGTACA)_2$
Change in ^{31}P chemical shift	T1pG2 maximum downfield shifted (0.26 ppm)	C1pG2 maximum downfield shifted (0.40 ppm)	T1pG2 maximum upfield shifted (1.15 ppm)
Exchange Phenomenon	Fast exchange – only one average signal observed for DNA and drug protons	Slow exchange – separate free and bound signal observed for T3NH, G2NH, G6NH, $T3CH_3$ and 11NH (drug)	Slow exchange – separate free and bound signal observed for T3NH, G2NH and 11NH (drug)
Drug-DNA intermolecular close contacts	2H/3H, 6H/7H, $11CH_2$, $12CH_2/13CH_2$ and 11NH gives close contacts with T1 and A6 residues	11NH, 1OH/4OH, $12CH_2$ / $13CH_2$ and $14CH_2$ gives close contacts with C1 and G6 residues	11NH, $12CH_2/13CH_2$ and 2H/3H gives close contacts with T1 and A6 residues
Sequential NOE connectivities	all intramolecular sequential observed	all intramolecular sequential observed	all intramolecular sequential observed
Conformational analysis	Mitoxantrone binds externally to T1.A6 base pair	Mitoxantrone binds externally to C1.G6 base pair	Mitoxantrone binds externally to T1.A6 base pair

The present ^{1}H and ^{31}P NMR studies on mitoxantrone with d-$(TGATCA)_2$, d-$(CGTACG)_2$ and d-$(TGTACA)_2$ complexes clearly demonstrate that the mitoxantrone chromophore does not intercalate between base pairs in the three drug-DNA complexes studied. This is in contrary to transcriptional assay and electron microscopic studies on mitoxantrone binding with DNA. Since mitoxantrone has two long side chains having seven torsional angles hence large degrees of freedom, it may orient in different ways under different experimental conditions such as Drug/DNA concentration, DNA sequence, pH, salt concentration, etc. Thus the interaction of mitoxantrone with DNA may be much more specific than that for classical intercalators e.g. daunomycin and adriamycin. The difference in distortions induced in DNA due to binding will affect the manner in which mitoxantrone binds to topoisomerase-II enzyme and form ternary complex of drug-enzyme-DNA. This eventually shifts DNA cleavage-religation equilibrium action of topoisomerase II towards cleavage and causes multiple DNA strand breaks which are responsible for the anticancer action. Mitoxantrone on binding to DNA induce alterations in backbone conformation which are base sequence specific. The conformational features evidenced by intermolecular NOEs also bear the signature of DNA sequence which suggests that the drug may be more suitable for specific oncogene sequences. The exact way of binding to DNA is expected to influence its further binding to topoisomerase and hence a specific molecular basis of action.

References

1. Abraham R. J., Mobli M. and Smith R. J. 1H chemical shifts in NMR. Part 20 - Anisotropic and steric effects in halogen substituent chemical shifts (SCS), a modelling and ab initio investigation. Magn. Reson. Chem., 2004, 42, 436-444.
2. Adams A., Guss J. M., Denny W. A., and Wakelin L.P.G. Crystal structure of the topoisomerase–II poison 9–amino–[N–(2–dimethylamino)ethyl]acridine–4–carboxamide bound to the DNA hexanucleotide $d(CGATCG)_2$. Implications for structure–activity relationships of acridinecarboxamide topoisomerase poisons. Nucleic Acids Research, 2002, 30, 719–725.
3. Alberts D.S., Griffith K.S., Goodman G.E., Herman T.S and Murray E; (1980) Phase I clinical investigation of 1, 4–dihydroxy–5, 8 bis[(2[(2hydroxyethyl) amino]ethyl]amino]]–9,10–anthracenedione dihydrochloride (NSC 301739), a new anthracenedione. Cancer Res., 1980, 40, 1516–1518.
4. Almond P., Cutbush S. D., Islam S. A., Kuroda R., Neidle S., Gandecha B. M. and Brown J. R. Nucleic acid binding drugs. VIII. Structures of 1-[2-(diethylamino)ethylamino]anthracene-9,10-dione, $C_{20}H_{22}N_2O_2$ (I) and 1,5-bis[2-(diethylamino)ethylamino]anthracene-9,10-dione, $C_{26}H_{36}N_4O_2$ (II), models for antitumour drugs. Acta. Cryst. 1983, C38, 627-630.
5. Altona C. and Sundaralingam, M. Conformational analysis of the sugar ring in nucleotides and nucleosides. A new description using pseudo–rotation. J. Am. Chem. Soc., 1972, 94, 8205–8212.
6. Anderson, J. E., Ptashne, M., & Harrison, S.C. Structure of the bacteriophage 434 repressor-operator complex. Nature, 1987, 326, 846-852.
7. Arcamone F. Doxorubicin: In "Anticancer Antibiotics". Academic Press, New York, 1981.
8. Arcamone F., Penco S. In "Anthracyclines and anthracediones based anticancer agents". (Eds. Lown J.W.), Elsevier, New York, 1988.
9. Askirka V.F., Maskevich A.A., Stepuro V.I. and Maskevich S.A. Luminescent properties of mitoxantrone In different microsurroundings. Journal of Applied Spectroscopy, 2004, 71 (1), 42-47

10. Babayan Yu. S., Sngryan A.E., Kazaayran, Avetisyan M. G., Sogomonyan L.R. and Garibyan D. V. Interactions of antitumor drugs mitoxantrone and Ametantrone with DNA as Determined from the Changes in Circular Dichorism Spectra. Molecular Biophysics, 1998, 43, 398–402.

11. Bailly C., Rouier S., Bernier, Jean–Luc.and Waring M. J. DNA recognition by two mitoxantrone analogues: Influence of the hydroxyl groups. FEBS letters, 1986, 379, 269–272.

12. Balaji V. N., Dixon J. S., Smith D. H., Venkataraghavan R. and Murdock K. C. Design of anticancer drugs using modeling techniques. Annals of the New York Academy of Sciences, 1985, 439, 140–161.

13. Barthwal R., Monica, Awasthi P., Srivastava N., Sharma U., Kaur M. and Govil G. Structure of DNA hexamer sequence d-CGATCG by two-dimensional Nuclear Magnetic Resonance Spectroscopy and Restrained Molecular Dynamics. J. Biomol. Struct. Dyn., 2003, 21, 407– 423

14. Barthwal R., Awasthi P., Monica, Kaur M., Sharma U., Srivastava N., Barthwal S. K. and Govil G. Structure of DNA Sequence d–TGATCA by two–dimensional Nuclear Magnetic Resonance Spectroscopy and Restrained Molecular Dynamics. J. Structural Biology, 2004, 148, 34– 50.

15. Barthwal R., Prashansa A., Tripathi A. N., Sharma U., Jagannathan N. R. and Govil G. Structural elucidation of 4'-epiadriamycin by nuclear magnetic resonance spectroscopy and comparison with adriamycin and daunomycin using quantum mechanical and restrained molecular dynamics approach. Arch Biochem Biophys. 2008, 474, 48-64.

16. Becke A.D. Density functional thermochemistry. III. The role of exact exchange. J. Chem. Phys., 1993, 98, 5648-5652

17. Bell D.H. Characterization of fluorescence of the antitumor agent, mitoxantrone. Biochemica et Biophysica., 1989, 949, 132–137.

18. Bhattacharya D. and Bansal M. Groove width and depth of B–DNA structure depend on local variations in slide. J. Biomol. Struct. Dyn., 1992, 10, 213–216.

19. Birlirakis N. and Perly B. One and two–dimensional ^{1}H NMR investigations of the inclusion of the anti–cancer drug mitoxantrone in cyclomaltooligosaccharides. Carbohydrate Research, 1992, 235, C1–C4.

20. Bodenhausen G., Freeman R. and Turner D.L. Suppression of artifacts in two–dimensional spectroscopy. J. Magn. Reson., 1977, 27, 511–514.

21. Bodhenhausen, et al. Phys. Rev. Lett. 38, 1977, 1116–1119.

22. Boelens R, Scheek R. M., Dijkstra K. and Kaptein R. Sequential assignment of imino and amino proton resonances in 1H NMR spectra of oligonucleotides by 2D NMR spectroscopy. Apllication to a lac operator fragment. J. Magnetic Resonance.1985, 62, 378-386.

23. Bonnadonna G. and Monfardini S. Cardiac toxicity of daunorubicin. Lanclet. 1969, 1, 837–854.

24. Callandine, C. R. Mechanics of sequence-dependent stacking of bases in B-DNA. J.Mol. Biol. 1982, 161, 343-352.

25. Cances M. T., Mennucci B. and Tomasi J. A new integral equation formalism for the polarizable continuum model: theoretical background and applications to isotropic and anisotropic dielectrics. J. Chem. Phys., 1997, 107, 3032

26. Capranico G., De Isabella P., Tinelli S., Bigioni M. & Zunino F. (1994) Similar sequence specificity of mitoxantrone and VM–26 stimulation of in vitro DNA cleavage by mammalian DNA topoisomerase II. Biochemistry 32, 3038–3046.

27. Casanovas J., Namba A. M., Leon S., Aquino G. L. B., Silva G. V. J. D., Aleman, C. J. Org. Chem., 2001, 66, 3775.

28. Celda V., Widmer H., Leupin W., Chazin W., Denny A. and Wuthrich K. Conformational studies of d-$(AAAAATTTTT)_2$ using constraints from nuclear overhauser effects and from quantitative analysis of the cross peak fine structures in two-dimensional ^{1}H Nuclear Magnetic Resonance spectra. Biochemistry, 1989, 28, 1462.

29. Chaires J. B., Dattagupta N. and Crothers M. Self association of Daunomycin Biochemistry, 1982, 21, 3927–3932.

30. Chen K. X., Gresh N., and Pullman B. A theoretical investigation on the sequence selective binding of mitoxantrone to double–stranded tetranucleotides. J. Biomol. Struct. Dyn. 1985, 3, 445–466.

31. Chen T. K., Fico R. and Canellakis E. S. Diacridine, Bifunctional Intercalators. Chemistry and Antitumor Activity. J. Med. Chem. 1979, 21, 868–874

32. Chen K. X., Gresh N. and Pullman B. A theoretical investigation on the sequence selective binding of mitoxantrone to double–stranded tetranucleotides. Nucleic Acids Res. 1986, 14, 3799–3812.

33. Cheng C. C. and Zee–Cheng R. K. Y. The design synthesis and development of new class of potent antineoplastic anthraquiones. In "Progress in Medicinal Chemistry" (Eds. Ellis, G.P.; West, G. B.,) Elsevier, Amsterdam), 1983.

34. Clore G. M. and Gronenborn A. M. Probing the three–dimensional structures of DNA and RNA oligonucleotides in solution by nuclear Overhauser enhancement measurements. FEBS Letts., 1985, 179, 187–198.

35. Collier D. A. and Neidle S. Synthesis, Molecular modeling, DNA binding and antitumor properties of some substituted amido anthraquinones. J. Med. Chem. 1988, 1, 847–857.

36. Colombo D., Ferraboschi P., Ronchetti F. and Toma L., Stereochemical analysis of the 3α- and 3β-hydroxy metabolites of tibolone through NMR and quantum-chemical investigations. An experimental test of GIAO calculations. Magn. Reson. Chem, 2002, 40, 581-588

37. Cornbleet M. A., Stuart–Harris R. C., Smith I. E., Coleman R. E., Rubens R. D., McDonald, M., Mouridsen H. T., Rainer H., Oosterom A. T. and Smyth .J Mitoxantrone for the treatment of advanced breast cancer: single–agent therapy in previously untreated patients. Eur J Cancer Clin Oncol., 1984, 20, 1141–1146.

38. Cotter F.E. Br. J. Clin. Pract., 1988, 42, 207; Ehninger, G., Schuler, U., Proksch, B., Zeller K. P. and J. Blanz, Clin. Pharmacokinet., 1990, 18, 365; Arlin, Z., Case, D. C., Moore, J., Wiernik, P., Feldman, E., Saletan, S., Desai, P., Sia, L. and. Cartwright, K. Leukemia, 1990, 4, 177; Faulds, D., Balfour, J. A., Chrisp P. and Langtry, H. D. Drugs, 1991, 41, 400; Armitage, O.J. Oncology, 2002, 16, 490

39. Davies D. B., Djimant L. N. and Veselkov A. N. ^{1}H NMR investigation of self–association of aromatic drug molecules in aqueous solutions. J. Chem. Soc., Faraday Trans., 1996, 92, 383–390

40. Davies D. B., Pahomov V. I. and Veselkov A. N. NMR Determination of the conformational and drug binding properties of the DNA heptamer d–(GpCpGpApApGpC) in aqueous solution. Nucleic Acids Research, 1997, 25, 4523–4531.

41. Davies D. B, Veselkov D. A., Djimant L. N. and Veselkov A. N. Hetero–association of caeffine and aromatic drugs and their competitive binding with DNA oligomer. Eur. Biophys. J., 2001a, 30, 354–356.

42. Davies D. B., Veselkov D. A., Evstigneev M. P. and Veselkov A. N. Self–association of the antitumour agent novatrone (mitoxantrone) and its hetero–association with caffeine. J Chem Soc Perkin Trans., 2001b, 2, 61–67.

43. Derome A.E. In "Modern NMR techniques for Chemistry Research". Volume 6, Pergamon Press, Oxford U.K. 1987.

44. Di Marco A., Arcamone F. and Zunino F. In "Antibiotics". (Eds. Corcoran J.W. and Hahn I.E.) Springer–Verlag, Berlin, 1974. 101–108.

45. Dickerson, R. E. Base sequence and helix structure variation in B and A DNA. J. Mol. Biol. 1983, 166, 419-441.

46. Dronberger U., Flemming J. and Fritzsche H. Structure determination and analysis of helix parameters in the DNA decamer d–$(CATGGCCATG)_2$ Comparison of results from NMR and crystallography. J. Mol. Biol. 1998, 284, 1453–1463.

47. Favier A., Blackledge M., Simmone J. P., Crouzy S., Dabouis V. and Gueiffier A., Dominique M, and Debouzy J.C, Solution structure of 2–(–[(1, 2–e] purin–4–yl) amino–ethanol intercalated in the DNA duplex d–$(CGATCG)_2$. Biochemistry, 2001, 40, 8717–8726.

48. Feigon J., Wright, J. M., Leupin, W., Denny, W. A. and Kearns, D.R. Use of two–dimensional NMR in the study of double–stranded decamer. J. Amer. Soc., 1982, 104, 5540–5541.

49. Feofanov A., Sharonov S., Kudelina I., Fleury F., Nabiev I. Localization and molecular interactions of mitoxantrone within living K562 cells as probed by confocal spectral imaging analysis. Biophys J. 1997, 73, 3317–3327

50. Fox K. R., Waring M. J., Brown J. R. and Neidle S., FEBS Letters, 1986, 202, 289-294.

51. Foye W. O., Vajragupta O. and Sengupta S. K. DNA–binding specificity and RNA polymerase inhibitory activity of bis(aminoalyl)anthraquinones and bis(methylthio)vinylquinolinium iodides. J. Pharm. Sci., 1982, 71, 253–257.

52. Frederick C. A., Williams L. D., Ughetto G., Van der Marel G. A., Van Boom J. H., Rich A. and Wang A. H. J. Structural Comparison anticancer drug–DNA complex: Adriamycin and Daunomycin. Biochemistry, 1990, 29, 2538–2549.

53. Gabbay E. J., Grier D., Fingerie R. E., Reimer R., Levy R., Pearce S.W. and Wilson W. D. Interaction specificity of the anthracyclines with deoxyribonucleic acid. Biochemistry, 1976, 15, 2062–2070.

54. Gatto B., Zagatto G., Sissi C., Cera C., Uriate E., Palu G., Caparnici G., and Palumbo M. Peptidyl Anthraquinones as potential Antineoplastic Drugs: Synthesis, DNA Binding, Redox cycling and Biological activity. J. Med. Chem. 1996, 39, 3114–3122.

55. Gochin M. Zon G. and James. T.L. Two dimensional COSY and two dimensional NOE spectroscopy of $d(AC)_4$, $d(GT)_4$: Extraction of structural constraints. Biochemistry, 1990, 29, 11161.

56. Gaussian 03. Frisch M. J., Trucks G. W., Schlegel H. B., Scuseria G. E., Robb M. A., Cheeseman J. R., Montgomery J. A., Jr., Vreven T., Kudin K. N., Burant J. C., Millam J. M., Iyengar S. S., Tomasi J., Barone V., Mennucci B., Cossi M., Scalmani G., Rega N., Petersson G. A., Nakatsuji H., Hada M., Ehara M., Toyota K., Fukuda R., Hasegawa J., Ishida M., Nakajima T., Honda Y., Kitao O., Nakai H., Klene M., Li X., Knox J. E., Hratchian H. P., Cross J. B., Bakken V., Adamo C., Jaramillo J., Gomperts R. R., Stratmann E., Yazyev O., Austin Cammi A. J., Pomelli R. C., Ochterski J. W., Ayala P. Y., Morokuma K., Voth G. A., Salvador P., Dannenberg J. J., Zakrzewski V. G., Dapprich S., Daniels A. D.,. Strain M. C., Farkas O., Malick D. K., Rabuck A.

D., Raghavachari K., Foresman J. B., Ortiz J. V., Cui Q., Baboul A., G. Clifford S., Cioslowski J., Stefanov B. B., Liu G., Liashenko A., Piskorz P., Komaromi I., Martin R. L., Fox D. J., Keith T., Al-Laham M. A., Peng C. Y., Nanayakkara A., Challacombe M., Gill P. M. W., Johnson B., Chen W., Wong M. W., Gonzalez C. and Pople J. A., , Gaussian Inc., Wallingford CT, 2004.

57. Giessner–Prettre C. and Pullman B. On the atomic or "local" contributions to proton chemical shifts due to the anisotropy of the diamagnetic susceptibility of the nucleic acid base. Biochem. Biophys. Res. Commun., 1976, 578–581.

58. Gorenstein, D. G., Kar, D. ^{31}P chemical shifts in phosphate diester monoanions. Bond angle and torsional angle effects, Biochem. Biophys. Res. Commun. 1975, 65, 1073.

59. Gorenstein, D. G., Luxon, B. A., and Findlay, J. B. The torsional potential for phosphate diesters The effect of geometry optimization in CNDO and ab initio molecular orbital calculations, Biochim Biophys. Acta, 1977, 475, 184.

60. Gorenstein, D. G., in "Phosphorus-31 NMR: Principles and Applications" (D. G Gorenstein ed.) p.7. Academic Press, Orlando, Florida, 1984.

61. Gorenstein D.G. ^{31}P NMR of DNA Spectroscopic methods for analysis of DNA. Methods in Enzymology, 1992, 211, 254–285.

62. Gorenstein D.G. Conformation and dynamics of DNA and protein–DNA complexes by ^{31}P NMR. Chem. Rev. 1994, 94, 1315–1338.

63. Gresh N., and Kahn P. H. Theoretical design of novel, 4 base pair Selective derivatives of mitoxantrone. J. Biomol. Struct. Dyn., 1985, 1141–1159.

64. Gresh N. and Phillippe H. K. Theoretical Design of a Bistetrapeptide Derivative of Mitoxantrone targetted towards the double stranded hexanucleotide d–$(GCCGGC)_2$. J. Biomol. Struct. Dyn., 1991, 8, 827–844.

65. Gronenborn A. M. and Clore G. M. Investigation of the solution structure of short nucleic acid fragments by means of nuclear overhauser enhancements measurements. Prog. NMR Spec., 1985, 17, 1–32.

66. Gunther U. L., Ludwig C., and Ruterjans H; NMRLAB-Advanced NMR data processing in MATLAB. J. Magn. Reson., 2000, 145, 201.

67. Hilbers C. W. and Patel D. J. Proton Nuclear Magnetic resonance investigations of the Nucleation and Propogation Reactions associated with the helix–coil transition of d–ApTpGpCpApT in H_2O. Biochemistry, 1975, 12, 2656–2660.

68. Horn D. E., Michael S. L., Amy J. F. and Gray E. Synthesis of symmetrically substituted 1, 4– bis [(aminoalkyl) amino]–5, 8–Dimethylanthracene–9,10–diones. ARIKOV, 2000, 1, 876–881.

69. Hosur R. V., Ravikumar M., Roy K. B., Kunn T. Z. and Miles H. T. and Govil G. In 'Magnetic resonance in Biology and medicine. (Eds. Govil, G. Khetrpal C. L. and Saran, A.) Tata Mc Graw Hill, New Delhi, 1985.

70. Hosur, R.V., Ravikumar M., Chary K.V.R., Sheth A., Govil G., Tan-Zu-Kunn and Miles H.T. solution structure of d-GAATTCGCAATTC by 2D NMR: A new approach to determination of sugar geometries in DNA segments. FEBS Letts., 1986, 205, 71.

71. Hosur R.V., Govil G. and Miles H.T. Application of two–dimensional NMR spectroscopy in the determination of solution conformation of nucleic acids. Magn. Reson. Chem., 1988, 26, 927–944.

72. Hunter C.A. Sequence-dependent DNA Structure: The role of base stacking interactions. J. Mol. Biol., 1993, 230, 1025.

73. Isabella P. D., Palumbo M., Sissi C., Carenini N., Caparnicao G., Menta E., Oliva A., Speneli S., Krapcho A.P., Guillani F.C., and Zunino F. Physiochemical properties, cytotoxic Activity and Topoisomerase Inhibition of 2, 3 Diaza–Anthracenediones. Biochem. Pharmacology, 1997, 53, 161–169.

74. Isabella P. D., Palumbo M., Sissi C., Carenini N., Caparnicao G., Menta E., Carenini N., Oliva A., Speneli S., Krapcho A. P., Guillani F. C., and Zunino F. Topoisomerase II DNA cleavage stimulation, DNA binding Activity, cytotoxicity, and physiochemical properties of 2–aza and 2–aza oxide– anthracene dione derivatives.Molecular Pharmacology, 1995, 30, 30–38.

75. Islam S. A., Neidle S., Gandecha B. M., Partridge M., Patterson L.H. and Brown J.R. Comparative computer graphics and solution studies of the DNA interaction of substituted anthraquinones based on doxorubicin and mitoxantrone. J. Med. Chem., 1985, 28, 857–864.

76. Jeener J. Paper presented at the AMPERE International summer school, Borsko, Polje, Yugoslavia, 1971.

77. Kapuscinski J., Darzynkiewicz Z., Traganos F. and Melamed M. R. Interactions of a new antitumor agent 1, 4–dihydroxy–5,8–bis [[2–[hydroxyethyl) amino]–ethyl] amino]–9,10 anthracenedione, with nucleic acids. Biochem. Pharmacol., 1981, 30, 231–240.

78. Kapuscinski J. and Darzynkiewicz Z. Interactions of antitumor agents ametantrone and mitoxantrone (novantrone) with double–stranded DNA. Biochem. Pharmacol., 1985, 34, 4203–4213

79. Kapuscinski J. and Darzynkiewicz Z. Relationship between the pharmacological activity of antitumor drugs ametantrone and mitoxantrone (Novatrone) and their ability to condense nucleic acids. Proc. Natl. Acad. Sci., USA, 1986, 83, 6303–6306.

80. Karplus M. Contact electron–spin coupling of nuclear magnetic moments. J. Chem. Phys., 1959, 30, 11–15.

81. Karplus M. Vicinal protons coupling in nuclear magnetic resonance. J. Am. Chem. Soc., 1963, 85, 2870–2871.

82. Keeler J. and Neuhaus D. Comparison and evaluation of methods for two–dimensional NMR spectra with absorption mode line shape. J. Magn. Reson., 1985, 63, 454–472.

83. Khetrapal C. L., Kunwar A. C., Tracey A. S. and Diehl P. Nuclear Magnetic Resonance Studies in Lyotropic Liquid Crystals, NMR: Basic Principles and Progress, 9, 1975, Berlin-Heidelberg-New York, Springer.

84. Kohn W. and Sham L. Self-Consistent Equations Including Exchange and Correlation Effects. J. Phys. Rev., 1965, 140, A1133-A1138

85. Kohn W., Becke A. D. and Parr R. G. Density Functional Theory of Electronic Structure J. Phys. Chem., 1996, 100, 12974.

86. Kolodziejczyk P. and Suillerot A. G. Circular dichroism study of the interaction of mitoxantrone. Ametantrone and their Pd (II) complexes with deoxyribonucleic acid. . Biochimica et Biophysica Acta., 1987, 926, 249–257.

87. Konopa J. In Molecular Aspects of Chemotherapy (Borowski E, & Shugar, D Eds.) 1988, pp. 83–94. Pergamon Press, New York, NY.

88. Kotovych G., Lown J. W and Tong P. K. High field ^{1}H and ^{31}P NMR studies on the binding of the anticancer agent mitoxantrone to d–[CpGpApTpCpG)$_2$. J Biomol Struct Dyn., 1986, 4, 111–125.

89. Krishnamoorty C. R., Yen, Shau–Fong., Smith J. C., William J. W. and Wilson W. D. Stopped flow kinetics analysis of the interaction of anthraquinone anticancer drugs with calf–thymus DNA, Poly[d(G–C).Poly[d–(G–C) and Poly[d(A–T). Poly[d–(A–T). Biochemistry, 1986, 25, 5933–5940.

90. Kupka T., Pasterna G., Jaworska M., Karali A. and Dais P. GIAO NMR calculations for carbazole and its *N*-methyl and *N*-ethyl derivatives. Comparison of theoretical and experimental ^{13}C chemical shifts. Magn. Reson. Chem. 2000, 38 (3), 149-155.

91. Labauowski J. and Andzeln J. Density Functional Methods in Chemistry, Springer-Verlag, New york, 1991.

92. Lampert H., Mikenda W., Karpfen A. and Kahlig H. NMR Shieldings in Benzoyl and 2-Hydroxybenzoyl Compounds. Experimental versus GIAO Calculated Data J. Phys. Chem. A 1997, 101, 9610.

93. Lancelot G. and Paquet F. In: G.A. Webb, Editor, Annual Reports on NMR Spectroscopy, Elsevier Science Ltd. 2003 pp. 170

94. Lavery R., Sklenar H., Zakrzewska K. and Pullman B. The flexibility of the nucleic acids: (II). The calculation of internal energy and applications to mononucleotide repeat DNA. J. Biomol. Struct. Dyn. 1986, 3, 989–1014.

95. Lavery R. Junctions and bends in nucleic acids: a new theoretical modelling approach. In Structure and Expression 3 (Eds. Olson, W.K., Sarma, M.H., Sarma, R.H. & Sundaralingam, M.), Adenine Press, New York. 1988, 191– 211.

96. Lavery R. and Sklenar H. The definition of generalized helicoidal parameters and of axis curvature for irregular nucleic acids. J. Biomol. Struct. Dyn., 1988, 6, 63–91.

97. Lavery R. and Sklenar J. Defining the Structure of Irregular Nucleic Acids: Conventions and Principles. J. Biomol. Struct. Dyn., 1989, 6, 655–667.

98. Lavery R. and Sklenar H. CURVES 5.1. Helical analysis of irregular nucleic Acids. Laboratory of Theoretical Biology. CNRS, Paris, 1996.

99. Lee C., Yang W. and Parr R. G. Development of the Colle-Salvetti correlation-energy formula into a functional of the electron density. Phys. Rev. B, 1988, 37, 785-789.

100. Lee B. S. and Dutta P. K. Optical Spectroscopic Studies of the Antitumor Drug 1, 4 – Dihydroxy,–5,8–bis[[2–[(2–hydroxyethyl)amino]ethyl] amino]–9,10–anthracenedione (Mitoxantrone). J. Phy. Chem., 1989, 93, 5665–5672.

101. Leonard G. A., Hambley T. W., Mc Auley Hecht K., Brown T., and Hunter W. N. Anthracycline DNA interactions at unfavourable base pair triplet binding sites: Structures of d–(CGGCCG) / daunomycin and d–(TGGCCA) / adriamycin complexes. Acta. Cryst. 1993, D49, 458–467.

102. Lerman L. S. Structural considerations in the interaction of DNA with acridines. J. Mol. Biol., 1961, 3, 18–30.

103. Lown J. W. Hanstock C. C., Bradley, R. D. and Douglas G. S. Interactions of Antitumor agents Mitoxantrone and Deoxyribonucleic Acids studied by electron Microscopy. Molecular Pharmacology, 1983, 25, 178–184.

104. Lown J. W. Hanstock C. C., Bleackley, R. C., Imbach, J. L. Rayner, B. and Vasseur, J. Synthesis and complete ^{1}H assignment and conformations of the self complemetary hexanucleotide d–$(CpGpApTpCpG)_2$ and its fragment by high field NMR. Nucleic Acids Research, 1984, 12, 2519–2526.

105. Lown J. W., Morgan A. R., Shau–Fong, Yen., Wang Y. H. and Wilson W. D Characterization of binding of the anticancer agents mitoxantrone and ametantrone and related structures to deoxyribonucleic acids. Biochemistry, 1985a, 24, 4028–4035.

106. Lown J. W. and Hanstock C. C. High field ^{1}H–NMR analysis of the 1:1 intercalation complex of the antitumor agent mitoxantrone and the DNA duplex [d(CpGpCpG)]. J. Biomol. Struc. Dyn., 1985b, 2, 1097–1106.

107. Marion D. and Wuthrich K. Application of phase sensitive two–dimensional correlated spectroscopy (COSY) for measurement of ^{1}H–^{1}H spin coupling constant in proteins. Biochem. Biophys. Res. Comm., 1983, 113, 967–974.

108. Martin R. B. Comparisons of Indefinite Self–Association Models. Chem Rev., 1996, 96, 3043–3064.

109. Manpreet Kaur, Structural studies of anticancer drug mitoxantrone and its complex with DNA, Ph.D. Thesis, 2006.

110. Mazerski J., Martelli S. and Borowski E. The geometry of intercalation complex of antitumor mitoxantrone and ametantrone with DNA: Molecular dynamics Simulations, Acta Biochimica Polonica, 1998, 45, 1–11.

111. Mazzini S. Mondelli R. and Ragg E. Structure and dynamics of intercalation complexes of Anthracyclines with d–$(CGATCG)_2$. 2D ^{1}H and ^{31}P NMR investigations. J. Chem. Soc. Perkin Trans. 2, 1998 1983–1991.

112. Mazzini S., Bellucci M. C. and Mondelli R. Mode of binding of cytotoxic alkaloid Berberine with the double Helix Oligonucletide d–$(AAGAATTCTT)_2$. Bioorganic and Medicinal Chemistry, 2003, 11(4), 505–514.

113. Moore M. H., Hunter W. N., Langlois d' Estaintot B. and Kennard O. DNA–drug interactions. The crystal structure of d–CGATCG complexed with daunomycin. J. Mol. Biol , 1989, 206, 693–705.

114. Mujeeb A., Kerwin S. M., Kenyon G. L. and James T. L. Solution structure of conserved DNA sequence from the HIV–I genome: Restrained molecular dynamics simulations with distance and torsion angle restraints derived from the two–dimensional NMR spectra, Biochemistry, 1993, 32, 13419–13431.

115. Murdock K. C., Child R.G., Fabio P.F., Angier R.B., Wallace T.E., Durr F.E. and Citarella R.V. Antitumor Agents.1, 4 Bis–[aminoalkyl) amino]–9,10 anthracenedione J. Med. Chem, 1979, 22, 1024–1030.

116. Neidle S. and Waring M.J. Molecular Aspects of Anti-cancer Drug Action, Macmillan, London, 1983.

117. Ott, J. and Eckstein, F. Phosphorus-31 NMR spectral analysis of the dodecamer d(CGCGAATTCGCG), Biochemistry, 1985, 24, 2530

118. Panousis C. and Phillips D.R. DNA sequence specificity of Mitoxantrone. Nucleic Acids Research, 1994, 22, 1342–1345.

119. Panousis C., Kettle A. J. and Phillips D. R. Oxidative metabolism of mitoxantrone by human neutrophil enzyme myeloperoxide. Biochemical Pharmacology, 1994, 48, 2223–2226.

120. Panousis C. and Phillips D. R. DNA sequence specificity of Mitoxantrone. Nucleic Acids Research, 1994, 22, 1342–1345.

121. Panousis C., Ketttle A. J. and Phillips D. R. Myeloperoxidase oxidizes mitoxantrone to metabolites which bind covalenly to DNA and RNA. Anti–Cancer Drug Design, 1995, 10, 593–605.

122. Parker B. S., Cullinane C. and Phillips D. R. Formation of DNA adducts by formaldehyde–activated mitoxantrone. Nucleic Acids Research, 1999, 27, 2918–2923.

123. Parker B. S., Cutts S. M., Cullinane C. and Phillips D. R. Formaldehyde activation of mitoxantrone yields CpG and CpA specific DNA adducts. Nucleic Acids Research, 2000, 28, 983–989.

124. Parker B. S., Buley T., Evinson B, Cutts S. M., Neumann G. M., Iskander M. N., Phillips D. R. Molecular understandings of mitoxantrone–DNA adduct formation: Effect of cytosine methylation and flanking sequences. J Biol. Chem., 2004, 279, 18814–18823.

125. Parr R. G., Yang W. Density Functional Theory of Atoms and Molecules, Oxford University Press Inc., New York, 1989.

126. Patel D. J. Peptide antibiotic dinucleotide interactions. Nuclear Magnetic Resonance investigations of complex formation between actinomycin D and d–pGpC in aqueous solution. Biochemistry, 1974, 13, 2388–2395.

127. Patel D. J. and Canuel L. L., Ethidium bromide-$(dC–dG–dC–dG)_2$ complex in solution: intercalation and sequence specificity of drug binding at the tetranucleoitide duplex level. .Proc. Natl. Acad. Sci. USA., 1976, 73, 3343-3347.

128. Patel D. J. d–CpGpGpC and d–GpGpCpC self–complementary duplexes: NMR studies of the Helix–coil transition. Biopolymers, 1977, 16, 1635–1636.

129. Patel D.J. Helix-coil transition of the dG-dC-dG-dC self-complementry duplex and complex formation with daunomycin in solution. Biopolymers, 1979, 18, 553.

130. Patel D. J. Kolowski S. A. and Rice J. A. Hydrogen bonding, overlap geometry, and sequence specificity in anthracycline antitumor antibiotic: DNA complexes in solution. Proc. Natl. Acad. USA. 1981, 78, 3333–3337.

131. Patel D. J. Kolowski S. A. and Rich A. Right handed and left handed DNA: Studies of B–and Z–DNA by proton nuclear Overhauser effect and P–NMR. Proc. Natl. Acad. USA, 1982, 79, 1413–1417

132. Paul Charlesworth (Chapter 3 thesis) http://chemistry.mtu.edu/~pcharles/RESEARCH/thesis/ch03/Homepage.html)

133. Piantini U., Sorensen O. W. and Ernst R. R. Multiple quantum filters for elucidating NMR networks. J. Am. Chem. Soc., 1982, 104, 6800–6801.

134. Prashansa Agrawal, Drug-DNA interactions by spectroscopic and molecular modeling techniques, Ph.D. Thesis, 2007.

135. Pullay P. and Hinton J. F. Encyclopedia of Nuclear Magnetic Resonance. Willey: New York, 1995, 4334.

136. Ragg E., Mondelli R., Battistini C., Garbesi A. and Colonna F. P. ^{31}P NMR study of daunorubicin–d–(CGTACG) complex in solution: Evidence of the intercalation sites. FEBS Letts. 1988, 236, 231–234.

137. Rajeshwari M. R. Tryptophan Intercalation in G, C containing Polynucleotides: Z to B conversion of Poly [d(G-5MC)] in low salt induced by a tetrapeptide. J. Biomol. Struct. & Dyn., 1996, 14, 25-30.

138. Rao M. V. R., Atreyi M. and Kumar A. Interaction of antitumor agent mitoxantrone with Poly[d (G–C)}– A Circular dichroic study. Indian Journal of Biochemistry and Biophysics, 1989, 26, 5–8

139. Redfield A. G., Kunj S. and Ralph E. K. Dynamic range in Fourier transform proton magnetic resonance. J. Magn. Reson., 1975, 19, 114–116.

140. Rehn C. Pindur U. Monatshefte Fur Chemie, 1996, 127, 631-644

141. Reid B.R., Banks K., Flynn P. and Nerdal W. NMR distance measurement in DNA duplex: Sugar and bases have the same correlation times. Biochemistry, 1989, 28, 10001–10007.

142. Reszka K., Hartley J. A., Kolodziejcyk P. and Lown J. W. Interaction of the peroxidase derivative of mitoxantrone with nucleic acids. Evidence for covalent binding of 14C labeled drugs. Biochem. Pharmacol. 1989, 38, 4253–4260.

143. Riahi S., Ganjali M. R., Dinarvand R., Karamdoust S., Bagherzadeh K. and Norouzi P., A Theoretical Study on Interactions Between Mitoxantrone as an Anticancer Drug and DNA: Application in Drug Design, Chem. Biol. Drug. Des. 2008; 71: 474–482

144. Roche C., Berowitz D., Sulkowski G. A., Danishefsky S. J. and Crothers D. M. Binding affinity and site selectivity of daunomycin analogues. Biochemistry, 1994, 33, 926–935.

145. Rosenberg L. S., Carvlin M. J. and Krugh T. R.antitumor agent mitoxantrone binds cooperatively to DNA: Evidence for heterogeneity in DNA conformation. Biochemistry . 1986, 25, 1002–1008.

146. Saenger, W. Principles of Nucleic Acid Structure, Springer-Verlag, New York. 1984

147. Schmitz U., Sethson I., Egan W. M. and James T. L. Solution structure of a DNA octamer containing the pribnov box via restrained molecular dynamics simulations with distance and torsion angles derived from two–dimensional nuclear magnetic resonance fitting. J. Mol. Biol., 1992, 227, 510–531.

148. Schroeder, S.A., Roongta, V., Fu, J. M., Jones, C. R. and Gorenstein, D. G. Sequence-dependent variations in the ^{31}P NMR spectra and backbone torsional angles of wild-type and mutant Lac operator fragments. Biochemistry, 1989, 28, 8292–8303.

149. Searle M. S., Hall J. G., Denny W. A. and Wakelin L. P. G. NMR studies of the interaction of the antibiotic nogalamycin with the hexadeoxyribonucleotide duplex d (5'–GCATGC)$_2$. Biochemistry, 1988, 27, 4340–4349.

150. Singh M.P., Joseph T., Kumar S., Bathini Y. and Lown J. W. Synthesis and Sequence –Specific DNA binding of a Topoisomerase Inhibitory Analog of Hoechst 33258 designed for altered base and sequence recognition. Chem. Res. Toxicol. 1992, 5, 597-607.

151. Sissi C., Moro S., Zagatto G., Ellis M., Krapcho A. P., Menta E. and Palumbo M. Binding of bis–substituted 2–aza–anthracenedione regioisomers to DNA: effects of the relative poisoning of the side chains. Anti cancer Drug Design, 1999, 14, 265–274.

152. Skladanowski A. and Knopa J. Relevance of the interstrand DNA croslinking induced by the anthracyclines for their biological activity. Biochem. Pharmacology, 1994, 47, 2279–2287.

153. Skladanowski A., Konopa J. Mitoxantrone and ametantrone induce interstrand cross-links in DNA of tu-mour cells. Brit. J. Cancer. 82 (7), 2000, 1300-1304.

154. Smith I. E. Mitoxantrone (novantrone): A review of experimental and early clinical studies. Cancer Treat Rev., 1983, 10, 103–115.

155. Smith P. J., Morgan S. A., Fox M. E. and Watson J.V. Mitoxantrone–DNA binding and the induction of topoisomerase II associated DNA damage in multi–drug resistant small cell lung cancer cells. Biochem. Pharmacol., 1990, 40, 2069–2078.

156. States D. J., Haberkorn R. A. and Reuben D. J. A two–dimensional nuclear overhauser experiment with pure absorption phase in four quadrants. J. Magn. Reson., 1982, 48, 286.

157. Stejskal E. O. and Tanner J. E., Spin Diffusion Measurements: Spin Echoes in the Presence of a Time-Dependent Field Gradient. J. Chem. Phys., 1965, 42, 288–292.

158. Sundaralingam M. Stereochemistry of nucleic acids and their constituents. Allowed and preferred conformations of nucleosides, nucleoside mono–, di–, tri–, tetraphosphates, nucleic acids and polynucleotides Biopolymers, 1969, 7, 821–860.

159. Tanious F. A., Jenkins T. C., Neidle S. and Wilson W. D. Substituent position dictates the intercalative DNA–Binding mode for anthracene 9, 10–dione antitumor drugs, Biochemistry, 1992, 31, 11632–11640.

160. Tarasiuk J., Tkaczyk–Gobis K., Stefanska B., Dzeieduszycka M., Priebe W., Martelli S., Borowski E. The role of structural factors of anthraqinone compounds

and their quinone–modified analogues in NADH dehydrogenase–catalysed oxygen radical formation. Anti–cancer Drug Design, 1998, 13, 923–939.

161. Traganos F., Evenson D. P., Staianco–Coico L., Darzynkiewicz Z & Melamed M. R. Action of dihydroxyanthraquinone on cell cycle progression and survival of variety of cultured mammalian cell. Cancer Res. 1980, 40, 671–681.

162. Trotta E., D'Ambrosio, E., Ravagnan, G. and Maurizio, P. Simulations and Different binding Mechanisms of 4', 6–diamino–2–phenylindole to DNA hexamer d–$(CGATCG)_2$ A ^1H NMR study. J. Biol. Chem., 1996, 271, 27608–27614.

163. Veselkov A. N., Evstigneev M. P., Vysotski S., Veseklov D. A., and Davies D. B; Thermodynamic analysis of interaction of antibiotic mitoxantrone with tetranucleotide 5'–d (TpGpCpA) in aqueous solution based on ^1H NMR spectroscopy data. Biofizika., 2002, 47, 432–438.

164. Wang A. H. J., Ughetto G., Quigley G. J., and Rich A. Interaction between anthracycline antibiotic and DNA: Molecular structure of daunomycin complexed to d–CpGpTpApCpG at 1.2 Å resolution. Biochemistry, 1987, 26, 1152–1153.

165. Wang H., Pin Yang P., Tian Y., Zhang Z., and Zhao C; Experimental antitumor activity of the Ce (IV)–Mitoxantrone complex and its interaction with Deoxyribonucleic Acid. J. Inorg. Chem., 1997, 68, 117–121.

166. Waring M. J; Complex formation between ethidium bromide and nucleic acids. Journal of Molecular Biology, 1965, 13, 269–82.

167. Wehenkel A., Fernandez P., Bellinzoni M., Catherinot V., Barilone N., Labesse G., Jackson M., Alzari P.M. FEBS Letters, 2006, 580, 3018.

168. William J. W., Hanstock C. C., Bradley R. D., and Scraba D. G; Molecular Pharmacology, 1983, 20, 178–184.

169. Wilson W. D. and Jones R. L. Interaction of actinomycin D, ethidium, quinacrine daunorubicin, and tetralysine with DNA: ^{31}P NMR chemical shift and relaxation investigation. Nucleic Acids. Res., 1982, 10, 1399-1410.

170. Wüthrich K. Resonance assignments and structure determination in nucleic acids. In NMR of Proteins and Nucleic Acids Wiley Interscience, New York. 1986.

171. Yang P., Wang H., Gao F., and Yang B; Antitumour Activity of the Cu (II)–mitoxantrone and its interaction with deoxyribonucleic acid. J. Inorg. Chem., 1996, 62, 137–145.

172. Yang X. L., Robinson H., Gao Y. G. and Wang A.H.J. Binding of macrocyclic bisacridine and ametantrone to CGTACG involves similar unusual intercalation platforms. Biochemistry, 2000, 39, 10950–10957.

173. Zaggatto G., Moro S., Uriatte E., Ferrazzi E., Palu G. and Palumbo M; Amido analogues of mitoxantrone: Physico chemical properties, molecular modeling cellular effects and antineoplastic potential. Anticancer Drug Design, 1997, 12, 99–112.

174. Zaggatto G., Supino R., Favini E., Moro, S. and Palumbo M; New 1, 4 anthracence–9, 10 dione derivatives as potential anticancer agents. IL Farmaco, 2000, 55, 1–5.

175. Zee–Cheng R. K. Y., Mathew A. E., Northcutt R. V. and Cheng, C.C. Structural Modification Study of Mitoxantrone (DHAQ). Chloro–Substituted Mono–and Bis [(aminoalkyl)amino] anthraquinones. J. Med. Chem., 1987, 30, 1682–1686.

176. Zhang Y. Z., Patterson Y. and Roder H. Rapid amide proton exchange rates in peptides and proteins measured by solvent quenching and two dimensional methods. Protein Sci., 1995, 4, 804–814.